

MODELING OF TRANSIENT HEAT PIPE OPERATION

Final Report

NASA GRANT NAG-1-392

Submitted to

**National Aeronautics and Space Administration
Langley Research Center
Hampton, Virginia 23665**

**NASA Technical Officer
Charles J. Camarda
Mail Stop 396**

By

**Gene T. Colwell
Georgia Institute of Technology
George W. Woodruff School of Mechanical Engineering
Atlanta, Georgia 30332**

Period Covered

August 19, 1983 through December 31, 1988

Submitted

January 15, 1989

SUMMARY

Mathematical models and an associated computer program have been developed for heat pipe startup from the frozen state. The models have been checked against previously published analytical and experimental data. Agreement is relatively good for most situations examined.

When a liquid metal heat pipe is started by introducing heat to one end while cooling the other, internal working fluid dynamics may greatly affect temperature distributions and fluid properties within the pipe as well as the overall conductance of the pipe. For example, if the working fluid is initially frozen, during startup melting will occur in the capillary structure and the vapor will experience free molecular, choked, and continuum flow at various times. These changing internal conditions generally make the heat pipe relatively slow to transport energy from heated to cooled ends and very large radial and axial temperature gradients may develop.

The present work uses finite element formulations of the governing equations written for each heat pipe region for each operating condition experienced during startup from a frozen state. In the shell, energy transport is by conduction only. In the capillary structure, conduction and heat of fusion are considered. In the vapor region different sets of governing equations are utilized for regions undergoing free molecular, choked and normal continuum flow. The various models were checked against analytical and experimental data available in the literature for three specific types of operation. For example the models used to predict melting in the capillary structure were checked against analytical results previously published for melting in a corner region.

Computation using the methods developed in the present work were made for

a space shuttle reentry mission where a heat pipe cooled leading edge was used on the wing. This wing had a sodium heat pipe built into the wing near the leading edge. Charles J. Camarda of NASA Langley Research Center made experimental measurements of startup behavior for such a heat pipe. Results computed in this work compared well with Camarda's data.

TABLE OF CONTENTS

Page

LIST OF TABLES

LIST OF ILLUSTRATIONS

LIST OF SYMBOLS

Chapter

| | | |
|-------|---|----|
| I. | INTRODUCTION | 1 |
| 1.1 | Statement of the problem | |
| 1.2 | Description of heat pipe operation | |
| 1.3 | Literature review | |
| II. | MODELING OF STARTUP | 13 |
| 2.1 | Introduction | |
| 2.2 | Mathematical model development | |
| 2.2.1 | Transition temperature | |
| 2.2.2 | Heat pipe shell and capillary structure with working fluid | |
| 2.2.3 | Analysis of the vapor flow | |
| III. | NUMERICAL MODEL DEVELOPMENT FOR PHASE CHANGE | 29 |
| 3.1 | Introduction | |
| 3.2 | Mathematical model | |
| 3.3 | Description of numerical formulations | |

| | | |
|-------|---|-----|
| 3.3.1 | Finite element formulation | |
| 3.3.2 | Time stepping scheme | |
| IV. | VAPOR FLOW DYNAMICS IN HEAT PIPES | 43 |
| 4.1 | Introduction | |
| 4.2 | Similarity solution for a semiporous channel | |
| 4.2.1 | Governing differential equations | |
| 4.2.2 | Similarity transformations | |
| 4.2.3 | Solution of equation | |
| 4.3 | Compressible vapor flow analysis | |
| 4.3.1 | Formulation of differential equations | |
| V. | COMPUTATIONAL PROCEDURES | 57 |
| 5.1 | Transient conduction equation with phase change | |
| 5.2 | Compressible vapor flow | |
| 5.3 | Coupling vapor flow effect | |
| 5.4 | Overall computational procedures | |
| VI. | RESULTS AND DISCUSSION | 66 |
| 6.1 | Transient conduction and phase change | |
| 6.1.1 | Temperature of a semi-infinite body | |
| 6.1.2 | Convection and radiation boundary conditions | |
| 6.1.3 | Phase change of sodium | |
| 6.2 | Compressible vapor flow | |
| 6.3 | Heat pipe startup | |
| 6.4 | Simulation of reentry heating environment | |
| VII. | CONCLUSIONS AND RECOMMENDATIONS | 130 |
| 7.1 | Conclusions | |
| 7.2 | Recommendations | |

APPENDICES

| | |
|---|-----|
| A. ELEMENT MATRICES | 134 |
| B. LISTING OF THE COMPUTER PROGRAM | 140 |
| C. SAMPLE INPUT DATA | 187 |
| D. THERMAL PROPERTIES OF SODIUM | 190 |
| E. THERMAL PROPERTIES OF HASTELLOY X AND STAINLESS STEEL | 193 |
| REFERENCES | 195 |

LIST OF TABLES

| Table | Page |
|---|------|
| 1.1 Heat pipe working fluids from Ref.[6] | 5 |
| 6.1 Description of heat pipes | 78 |

LIST OF ILLUSTRATIONS

| Figure | | Page |
|--------|---|------|
| 1.1 | Components and principles of operation of a conventional heat pipe | 3 |
| 2.1 | Schematic diagram of a heat pipe cooled leading edge | 14 |
| 2.2 | Transition temperature for sodium as a heat pipe working fluid . | 18 |
| 2.3 | Simplified cross-section A-A of Figure 2.1 | 19 |
| 2.4 | Heat pipe vapor flow limits and corresponding Reynolds numbers | 24 |
| 3.1 | Control volume \bar{V} | 31 |
| 3.2 | Variations of properties near the phase change temperature | 33 |
| 3.3 | Two-dimensional solution domain | 35 |
| 4.1 | Schematic diagram of a semiporous channel | 45 |
| 4.2 | Velocity profiles for wall injection in a semiporous channel | 49 |
| 4.3 | Velocity profiles for wall suction in a semiporous channel | 50 |
| 4.4 | Variations of friction, momentum and energy factors, with wall Reynolds number | 52 |
| 5.1.a | Algorithm flowchart | 59 |
| 5.1.b | Algorithm flowchart | 60 |
| 6.1 | Finite element mesh for the transient conduction heat transfer problem | 67 |
| 6.2 | Semi-Infinite domain temperature distributions | 68 |
| 6.3 | Comparison of convection and radiation boundary conditions ... | 70 |
| 6.4 | Two-dimensional mesh used to represent a corner region; 242 elements, 144 nodes | 71 |

| | | |
|------|--|----|
| 6.5 | Solidification of sodium in a corner region; position of the interface at different times | 73 |
| 6.6 | Comparison of axial variation of vapor pressures | 76 |
| 6.7 | Comparison of axial variation of vapor temperatures | 77 |
| 6.8 | Axial variation of vapor temperature, pressure, velocity, and density at an operating temperature of 773 K | 80 |
| 6.9 | Axial variation of vapor temperature for various heat inputs ... | 81 |
| 6.10 | Axial variation of vapor pressure for various heat inputs | 82 |
| 6.11 | Axial variation of Mach number for various heat inputs | 83 |
| 6.12 | Axial variation of vapor temperature, pressure, velocity, and density at the sonic limit condition for operation temperature of 773 K | 84 |
| 6.13 | Axial variation of vapor temperature, pressure, velocity, and density at an operating temperature of 808 K | 86 |
| 6.14 | Axial variation of vapor temperature, pressure, velocity, and density at the sonic limit condition for an operating temperature of 808 K | 87 |
| 6.15 | Axial variation of vapor temperature for various heat inputs .. | 88 |
| 6.16 | Axial variation of vapor pressure for various heat inputs | 89 |
| 6.17 | Axial variation of Mach number for various heat inputs | 90 |
| 6.18 | Distribution of heat input to the evaporator and condenser | 92 |
| 6.19 | Axial variation of vapor temperature, pressure, velocity, and density for nonuniform heat input shown in Figure 18.a | 93 |
| 6.20 | Axial variation of vapor temperature, pressure, velocity, and density for nonuniform heat input shown in Figure 18.b | 94 |
| 6.21 | Comparison of the two cross-sections | 96 |
| 6.22 | Normalized heating distribution | 98 |
| 6.23 | Heat input at the stagnation point | 99 |

| | | |
|------|--|-----|
| 6.24 | Heat flux distribution on a leading edge model | 100 |
| 6.25 | Two-dimensional mesh used to represent a heat pipe cooled leading edge; 138 elements, 96 nodes | 101 |
| 6.26 | Temperature of a heat pipe cooled leading edge | 102 |
| 6.27 | Location of phase change of sodium | 104 |
| 6.28 | Position of continuum flow front | 105 |
| 6.29 | Temperature history of three locations in the heat pipe | 106 |
| 6.30 | Temperature distribution at the different locations in wall | 108 |
| 6.31 | Temperature distribution at the surface | 109 |
| 6.32 | Temperature distribution at the interface | 110 |
| 6.33 | Average vapor temperature variation during startup | 112 |
| 6.34 | Axial variation of vapor temperature, pressure, velocity, and density at $t = 1140$ sec. | 113 |
| 6.35 | Computed temperature distribution for uncooled and cooled leading edge; $t = 1450$ sec. | 114 |
| 6.36 | Heat input at the stagnation point for reentry simulation | 116 |
| 6.37 | Heat flux distribution on a leading edge model for reentry simulation | 117 |
| 6.38 | Two-dimensional mesh used to represent a heat pipe cooled leading edge for reentry simulation; 80 elements, 63 nodes | 118 |
| 6.39 | Temperature of a heat pipe cooled leading edge for reentry simulation | 119 |
| 6.40 | Location of phase change of sodium for reentry simulation | 120 |
| 6.41 | Position of continuum flow front for reentry simulation | 121 |

| | | |
|------|--|-----|
| 6.42 | Temperature history of three locations in the heat pipe for reentry simulation | 123 |
| 6.43 | Temperature distribution at interface between shell and capillary structure for reentry simulation | 124 |
| 6.44 | Temperature distribution at the interface for reentry simulation | 125 |
| 6.45 | Temperature distribution at the different locations in wall for reentry simulation | 126 |
| 6.46 | Average vapor temperature variation during startup for reentry simulation | 127 |
| 6.47 | Axial variation of vapor temperature, pressure, velocity, and density at $t = 503$ seconds for reentry simulation | 128 |
| 6.48 | Computed temperature distribution for uncooled and cooled leading edge of reentry simulation; $t = 700$ seconds | 129 |
| A.1 | Three-node, linear, triangular element with global coordinates | 135 |

LIST OF SYMBOLS

| | |
|--------------|---|
| a | condensation or evaporation coefficient |
| A | area |
| A_c | cross-section area of the vapor space |
| c_p | specific heat |
| C | volumetric heat capacity |
| D | height of the vapor space |
| E_f | energy factor |
| f | dimensionless stream function |
| $f_i(x)$ | functions which describe the curvatures of the wing section |
| F | friction factor |
| Fo | Fourier number |
| h | enthalpy |
| h_{cr} | heat transfer coefficient |
| h_f | enthalpy of saturated liquid |
| h_{fg} | latent heat of vaporization |
| H | enthalpy per unit volume |
| H_{ls} | latent heat of phase change |
| k | number of nodes assigned to the element |
| K | thermal conductivity |
| K_n | Knudsen number |
| l | direction cosine |
| L | total length of heat pipe |
| ΔL_i | side length of element |
| m | number of elements at the interface |

| | |
|------------|---|
| \dot{m} | rate of condensation or evaporation per unit area |
| M | molecular weight |
| M_f | momentum factor |
| n | unit outward normal direction |
| N_i | shape function |
| P | pressure |
| \dot{Q} | heat input rate |
| \ddot{Q} | heat input rate per unit area |
| R | solution domain |
| R_g | thermal resistance |
| R_u | universal gas constant |
| Re_o | wall Reynolds number |
| S_i | interface position |
| S | chordwise direction |
| t | time |
| T | temperature |
| T_m | temperature of phase change |
| T_o | initial temperature |
| T_s | specified surface temperature |
| T_∞ | reference temperature |
| U | X - component of velocity |
| $U^*(0)$ | average velocity at $X = 0$ |
| v | specific volume of vapor |
| v_f | specific volume of saturated liquid |
| v_g | specific volume of saturated vapor |
| V | average velocity at cross section |

| | |
|-----------|---------------------------|
| V^* | Y - component of velocity |
| \bar{V} | control volume |
| V_o | velocity at porous wall |
| W | width of the vapor space |
| X | coordinate direction |
| X_q | quality of vapor |
| Y | coordinate direction |

Greek symbols

| | |
|---------------|---|
| α | thermal diffusivity |
| β | $\sigma \epsilon LT^3 / K$ |
| γ | ratio of specific heats |
| ϵ | porosity of wick |
| ε | emissivity |
| λ | length of mean free path |
| μ | dynamic viscosity |
| ν | kinematic viscosity |
| ρ | density |
| σ | Stefan-Boltzmann constant |
| ψ | angle used to identify chordwise location |
| τ | shear stress |
| φ | stream function |
| ω | dimensionless length coordinate |

Subscripts

| | |
|----|---------------------|
| 1 | heat pipe shell |
| 2 | capillary structure |
| 21 | old phase |

| | |
|----|------------------------|
| 22 | new phase |
| a | adiabatic section |
| c | condenser |
| cr | convection |
| e | evaporator |
| f | liquid state |
| g | vapor state |
| i | index |
| o | liquid-vapor interface |
| r | radiation |
| x | X direction |
| y | Y direction |

Superscripts

| | |
|-----|--|
| * | transition from free molecular to continuum flow |
| (e) | element |

CHAPTER I

INTRODUCTION

1.1 Statement of the problem

Since the heat pipe concept was first introduced independently by Gaugler[1] in 1942 and Grover[2] in 1963, theoretical and experimental studies have been underway to understand and develop heat pipe technology. Most theoretical studies concern certain portions of the heat pipe, such as the evaporator, condenser, capillary structure, and vapor flow region. The overall performance of the entire heat pipe, including the thermal behavior along the heat pipe wall and capillary structure, vapor flow dynamics, and the various types of boundary conditions on the evaporator and condenser surfaces have received less attention. However, the steady state characteristics of heat pipe performance at low temperatures and under normal operating conditions are relatively well understood, and heat pipes have been successfully applied in various fields.

Little research has been done on the transient case. Transient behavior of heat pipes have been experimentally and numerically studied for low temperatures and working fluids with high vapor density by Chang and Colwell[3,4,5].

Recently, use of the heat pipe has been considered as a means of reducing the peak temperature and alleviating the thermal gradients at the leading edges of reentry vehicles and hypersonic aircraft, and in nuclear reactors. In these applications, the rate of heat transfer may be large, and the range of operating temperatures broad, from ambient to high temperature, so that liquid metal, which is in the solid state at ambient temperature, may be used as the working fluid. Under these conditions, the working fluid in the capillary structure may be in the solid or liquid state,

or may be freezing or thawing, with some liquid and some solid present. The vapor flow may be free molecular, continuum, choked, or some combination of these. No complete research has been reported on this subject.

The primary objective of this research is to investigate analytically the performance of an entire heat pipe with metallic working fluid during startup from a frozen state. To accomplish this goal, a mathematical model has been developed, and a numerical solution technique tested to predict the transient temperature distributions along the heat pipe, and the optimal heat transfer rate.

1.2 Description of heat pipe operation

Many scientists and engineers have observed the phenomenon of surface tension in nature and tried to understand, formulate, and apply it for improving human life. Among many natural phenomena, the action of surface tension can raise liquid against a gravity force within a small vertical tube or gauze with a portion immersed in liquid. This capillary action can transport liquid through suitable materials without using external power. When phase change takes place from one state to another, the change of enthalpy is rapid, and the difference between enthalpies of two states is large. Therefore a large amount of energy may be absorbed or released depending on the direction of phase change, and without a large temperature gradient. These two phenomena are utilized in a heat pipe.

A heat pipe consists mainly of a shell as the container, a capillary structure or wick to transport liquid by using surface tension, and a vapor space to provide vapor passage as shown in Figure 1.1. Heat pipe shells have been made of stainless steel, copper, nickel alloys, hastelloy, et cetera. Wire screen, fiber glass, porous metal, and woven cloth have been used as capillary structures. Narrow grooves cut lengthwise in the interior pipe wall have also served as a capillary structure. The capillary

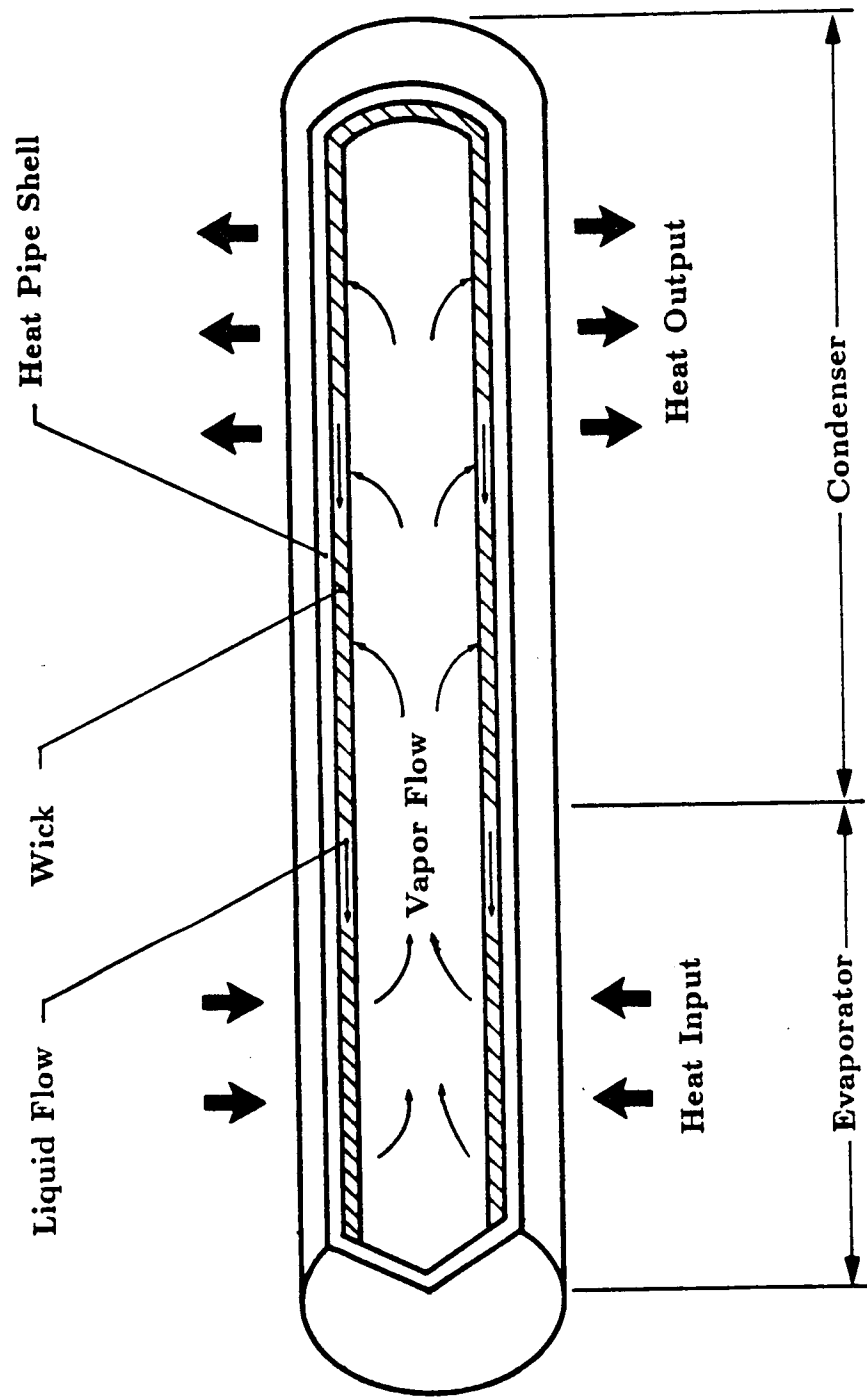


Figure 1.1. Components and principles of operation of a conventional heat pipe.

structure is saturated by the working fluid in the liquid state, and the vapor space is occupied by the working fluid in the vapor state. Heating and/or cooling devices are applied to the outer surface of the heat pipe shell. In the longitudinal direction, the heat pipe consists of an evaporator and a condenser.

Heat added to the evaporator is transferred to the working fluid by conduction and causes vaporization of the working fluid at the surface of the capillary structure. Vaporization causes the local vapor pressure in the evaporator to increase and vapor to flow towards the condenser thereby transporting the latent heat of vaporization. Since energy is extracted at the condenser, the vapor transported through the vapor space is condensed at the surface of the capillary structure, releasing the latent heat. The radius of curvature of the meniscus in the capillary structure of the evaporator is decreased and that in the condenser is increased. This difference in radii between the two sections creates the pumping force that transports the liquid from the condenser to the evaporator through the capillary structure. This process continues so long as no extreme heat fluxes are encountered.

Hence, in a heat pipe energy is transported by utilizing phase change of the working substance instead of a large temperature gradient and without external power. Also, the amount of energy transferred through a small cross-section is much larger than that by conduction or convection. Heat pipes may be operated over a broad range of temperatures by choosing an appropriate working fluid, as shown in Table 1.1[6].

However, this useful device has some operating limitations such as the sonic limit, the capillary limit, the entrainment limit, and the boiling limit. When any of these limitations is encountered, the capillary structure may dry out leading to failure of the heat pipe. In addition to these limitations, when liquid metal is used as the working fluid, startup difficulty may take place due to possible solid state of

Table 1.1 Heat pipe working fluids from Ref.[6]

| Medium | Melting point (°C) | Boiling point at atmos. press. (°C) | Useful range (°C) |
|-----------|--------------------------|---|----------------------|
| Helium | - 272 | - 269 | - 271 - - 269 |
| Nitrogen | - 210 | - 196 | - 203 - - 160 |
| Ammonia | - 78 | - 33 | - 60 - 100 |
| Freon 11 | - 111 | 24 | - 40 - 120 |
| Pentane | - 130 | 28 | - 20 - 120 |
| Freon 113 | - 35 | 48 | - 10 - 100 |
| Acetone | - 95 | 57 | 0 - 120 |
| Methanol | - 98 | 64 | 10 - 130 |
| Ethanol | - 112 | 78 | 0 - 130 |
| Heptane | - 90 | 98 | 0 - 150 |
| Water | 0 | 100 | 30 - 200 |
| Toluene | - 95 | 110 | 50 - 200 |
| Mercury | - 39 | 361 | 250 - 650 |
| Cesium | 29 | 670 | 450 - 900 |
| Potassium | 62 | 774 | 500 - 1000 |
| Sodium | 98 | 892 | 600 - 1200 |
| Lithium | 179 | 1340 | 1000 - 1800 |

the working fluid and extremely low vapor density.

1.3 Literature review

The heat pipe is a highly effective device for transporting heat between a source and a sink. Since Gaugler[1] received a patent on the heat pipe concept applied to a refrigeration system and Grover[2] referred to a "heat pipe" in a patent filed for the United States Atomic Energy Commission in 1963, scientists and engineers have been developing heat pipe technology. The first paper which described the basic principle of operation of a heat pipe was published by scientists at the Los Alamos National Laboratory[7] in 1964. They built two heat pipes with water and sodium as the working fluids for an initial qualitative experiment. Work at Los Alamos[8,9] continued actively, emphasizing space applications for the transfer of very high heat fluxes between two components and for the elimination of temperature gradients over relatively large areas. For high temperature applications, lithium and silver were tested as the working fluid at 1300°C and 2000°C, respectively. For the first actual flight test, a stainless steel heat pipe with distilled water as the working fluid operated successfully. At this stage, research on heat pipes was also conducted in England and Italy[6].

Cotter[10] developed the general basic theory for making certain quantitative calculations of heat pipe behavior. This analysis was confined to right circular cylinders of large length-to-diameter ratio and emphasized the vapor flow. Uniform injection or suction were assumed for a steady state condition. The axial transport of energy was modeled with the vapor flow carrying the latent heat of vaporization while neglecting axial conduction and radiation in the vapor space. After this pioneering effort, several books[6,11,12] were published which describe the basic theory of conventional heat pipe operation at steady state and low temperature.

Busse[13] studied the pressure drop in laminar vapor flow in a long, cylindrical heat pipe. The vapor density was assumed to be constant. The Navier-Stokes equations were simplified by a boundary layer approximation and solved by approximating the axial velocity component as a polynomial of the fourth power of the radius, with a correction function which varied only in the flow direction.

Levy[14,15] used a one-dimensional approach in solving the vapor flow problem, taking into account compressibility, shear stress at the liquid-vapor interface and the vapor dissociation-recombination reaction. The analytical results indicated that the shear stress is the most important factor, which reduces the maximum rate of heat transfer from that based on the sonic limit.

Brovalsky et al.[16] described the vapor flow for alkali-metals by using averaged equations of motion over the cross-section. Compressibility and friction at the liquid-vapor interface were considered. Momentum and energy factors, and the friction factor were evaluated based on theoretical data available for incompressible vapor flow in a channel with porous walls. The comparison of numerical results with available experimental data indicated a maximum discrepancy of 10 %. The temperature drop along the heat pipe was also observed.

Bankston and Smith[17] studied the fluid dynamics of the vapor flow at three different Reynolds numbers; 0.01, 4, and 1000. The Navier-Stokes equations for steady, incompressible, laminar vapor flow in a cylindrical heat pipe were solved by a finite difference method in which the dependent variables were transformed to the stream function and the vorticity. Inflow and outflow boundary conditions were described at the wall as blowing and suction through a porous wall pipe, but no thermodynamic change of phase was actually employed in the analysis. Their results show that vapor flow in the condenser is more complex than that in the evaporator, and that the vapor pressure varies not only in the axial, but also in the

radial direction for large Reynolds numbers.

A numerical analysis of steady two dimensional heat and mass transfer in the vapor-gas region of a gas loaded heat pipe was made by Tien and Rohani[18]. In this study, the radial component of velocity at the wall was determined by writing an energy balance equation at the liquid-vapor interface. Numerical results show that considerable pressure variations in the axial direction exist for large heat fluxes, due to friction at the liquid-vapor interface. Thus, a temperature drop in the axial direction occurs and vapor pressure variations play a significant role in overall performance of the heat pipe.

Vapor flow dynamics in a flat plate heat pipe with asymmetric boundary conditions was studied by Ooijen and Hoogendoorn[19]. The numerical study was confined to two-dimensional, steady state, laminar and incompressible flow. From computational results, velocity profiles were plotted in the evaporator and condenser for wall Reynolds numbers of 2, 10, and 50, and were compared with parabolic Poiseuille profiles for three locations. Flow reversal was observed, and similarity did not exist for high wall Reynolds numbers in the condenser section. For small Reynolds numbers, the pressure drop is similar to the Poiseuille flow model. However, for high wall Reynolds number, the large difference in velocity profiles in the condenser section causes a higher pressure drop than that resulting from the Poiseuille model. Good agreement was observed between experimental and computational results for nitrogen gas.

Ismail and Murcia[20] studied combined liquid and vapor flow in a tube with a porous wick. Governing equations for the flow of viscous incompressible fluid were solved using the separation of variables with known evaporation or condensation rates. For the case of small Reynolds number, analytical results were obtained.

Demichele[21] investigated the two-dimensional, steady state and compressible

flow problem by using an integral transformation of the general compressible flow equation introducing stream tubes which can be thought of as a set of concentric nozzles. For each stream tube equations were derived with a different initial condition. Numerical solutions predicted velocity, pressure, and temperature profiles. Effects of viscous terms on pressure recovery were deemed to be important.

Compressible, transient and axisymmetric Navier-Stokes equations were numerically solved to derive a friction coefficient expression to be used in one-dimensional heat pipe vapor models by Bowman[22]. The equation for the friction coefficient was expressed in terms of local axial Reynolds number, Mach number, pipe aspect ratio and radial Reynolds number. The one-dimensional model with the friction coefficient showed good agreement with experimental results.

Overall thermal performance of a heat pipe at steady state was studied theoretically and experimentally, by Sun and Tien[23,24]. In the analysis, a simple conduction model was developed for a single-component heat pipe in one dimension with uniform saturated vapor temperature and uniform mass injection or suction. Axial wall temperature distributions were predicted. Theoretical predictions were compared with measured results for gas-loaded heat pipes and good agreement was reached.

As the digital computer was developed numerical techniques were used to solve more complicated models. The simple conduction model developed by Sun and Tien was extended by Kuramae[25] to transient heat pipes with time varying thermal loads. In this model, the temperature was assumed to vary only in the axial direction for the wall but in both the axial and radial directions for the wick structure. It was assumed that the vapor temperature was dependent on time but uniform in space. A numerical method was used to solve the governing equations and the calculated axial temperatures were compared with typical experimental results.

Experimental and numerical studies were conducted for transient operating characteristics of low temperature heat pipes by Chang and Colwell[3,4,5]. The computational model assumed that two-dimensional conduction in the heat pipe shell and wick are the dominant heat transfer modes. A lumped mass model was used for a combination of vapor space and central composite slab wick. Thermal resistance at the liquid-vapor interface and along the vapor space was neglected. To provide boundary conditions at the interface between the heat pipe wall and the vapor space, the vapor region was modeled assuming that the vapor temperature was a function of time only. A finite-difference method was used to predict performance.

Cotter[26] described three basic transient modes for heat pipe startup. A frontal startup mode was observed when the vapor density is so low that the molecular mean free path exceeds the diameter of the vapor passage. In this mode of startup, the vapor in the hot zone is in continuum flow and that in the cold zone is in free molecule flow. A large temperature gradient is developed and decreases with time. Eventually, an isothermal steady state could be reached.

Ivanovskii et al.[11] carried out experimental studies of the temperature distribution along the length of a sodium heat pipe in which the working fluid was in the solid state at ambient temperature. The temperature distributions were measured with the aid of a movable microthermocouple placed directly in the vapor channel. Ivanovskii observed three simultaneous flow regimes in the condensation zone for intense heat removal in a pipe operating at the sonic heat transfer limit: continuum vapor flow at the start of the condensation zone and intermediate and free molecular regimes further on.

Neal[27] investigated the successful startup of a heat pipe with water as the working fluid. The water in the condenser was initially frozen, but that in the evaporator remained in the liquid phase. Experimental results showed that a large

temperature gradient developed along the heat pipe length with increasing time and even for a small heat flux the heat pipe failed to start up.

Shlosinger[28] studied the startup behavior of low temperature heat pipes with the water initially frozen. With a heat input of 15 watts, the heat pipe working fluid melted without wick dryout and normal operation began after approximately one hour. Use of an auxilliary heat pipe which had a working fluid with a lower melting point greatly improved the startup of the primary heat pipe without local overheating and the transient period was reduced.

Deverall et al.[29] made a series of tests to study the startup problem with water and metallic heat pipes. They described the transient behavior of heat pipe startup based on their experiments. With the working fluid in the solid state, startup was possible, but was highly dependent on the heat rejection rate at the condenser. For successful startup, the heat rejection rate at the condenser had to be low enough to enable the heat to melt the working fluid in the condenser, and allow liquid to return through the wick structure before the evaporator was depleted of fluid. Heat rejection by radiation is a self-compensating system and automatically controls the heat rejection rate. Therefore, startup difficulties were not normally encountered under these conditions. Another method suggested to aid the startup of a heat pipe was the addition of a small amount of inert noncondensable gas which has a result similar to that of radiation.

Camarda[30] investigated the performance of a heat pipe cooled leading edge, experimentally and analytically. In the analysis, it was assumed that the temperature was uniform throughout the continuum flow region and the melting process of the working fluid was neglected. Temperatures were calculated by a lumped system method which used a volumetric heat capacity per unit length of heat pipe. Rates of continuum vapor region growth, which were predicted using simple energy

balances, were compared with experimental results.

Most experimental studies[27,28,29] attempted simply to see if it was possible to obtain successful startup from the frozen state. It has been noted that startup difficulties are normally encountered when the working fluid is initially in the solid phase. No analytical studies which include the effects of phase change of the working fluid and vapor flow dynamics have been reported, and further more, comprehensive and qualitative research on startup from the frozen state has not been carried out experimentally and numerically.

CHAPTER II

MODELING OF STARTUP

2.1 Introduction

The use of heat pipes is being considered as a means of reducing the peak temperature and large thermal gradients at leading edges of reentry vehicles and hypersonic aircraft, and in nuclear reactors[31,32]. In the basic cooling concept, the heat pipe, which is a highly effective heat transport device, covers the leading edge, a portion of the lower wing surfaces, and a portion of the upper wing surface. Aerodynamic heat is mainly absorbed at the leading edge, and transported through the heat pipe to the upper and lower wing surfaces, where it is rejected by thermal radiation and convection. Once fully operational, the near isothermal heat pipe virtually eliminates temperature gradients and reduces peak temperatures.

A previous feasibility study[31] of heat pipes for this application recommends a rectangular cross-section for the heat pipe based on weight per unit surface area of heat pipe cooling structure and fabrication considerations. A schematic diagram of the physical model based on results presented in reference[31] is shown in Figure 2.1.

Previous experimental observations[26-32] suggest the following sequence of events during heat pipe startup from the frozen state. Initially, the working fluid is in the solid state and the vapor density is extremely low, so that free molecular flow conditions prevail throughout the vapor space. The input flux over the evaporator starts to melt the frozen substance in this region, while the heat transport from the hot zone to the adjacent zone proceeds quite slowly via axial conduction through working fluid and capillary structure, while heat transfer in the vapor is almost

ORIGINAL PAGE IS
OF POOR QUALITY

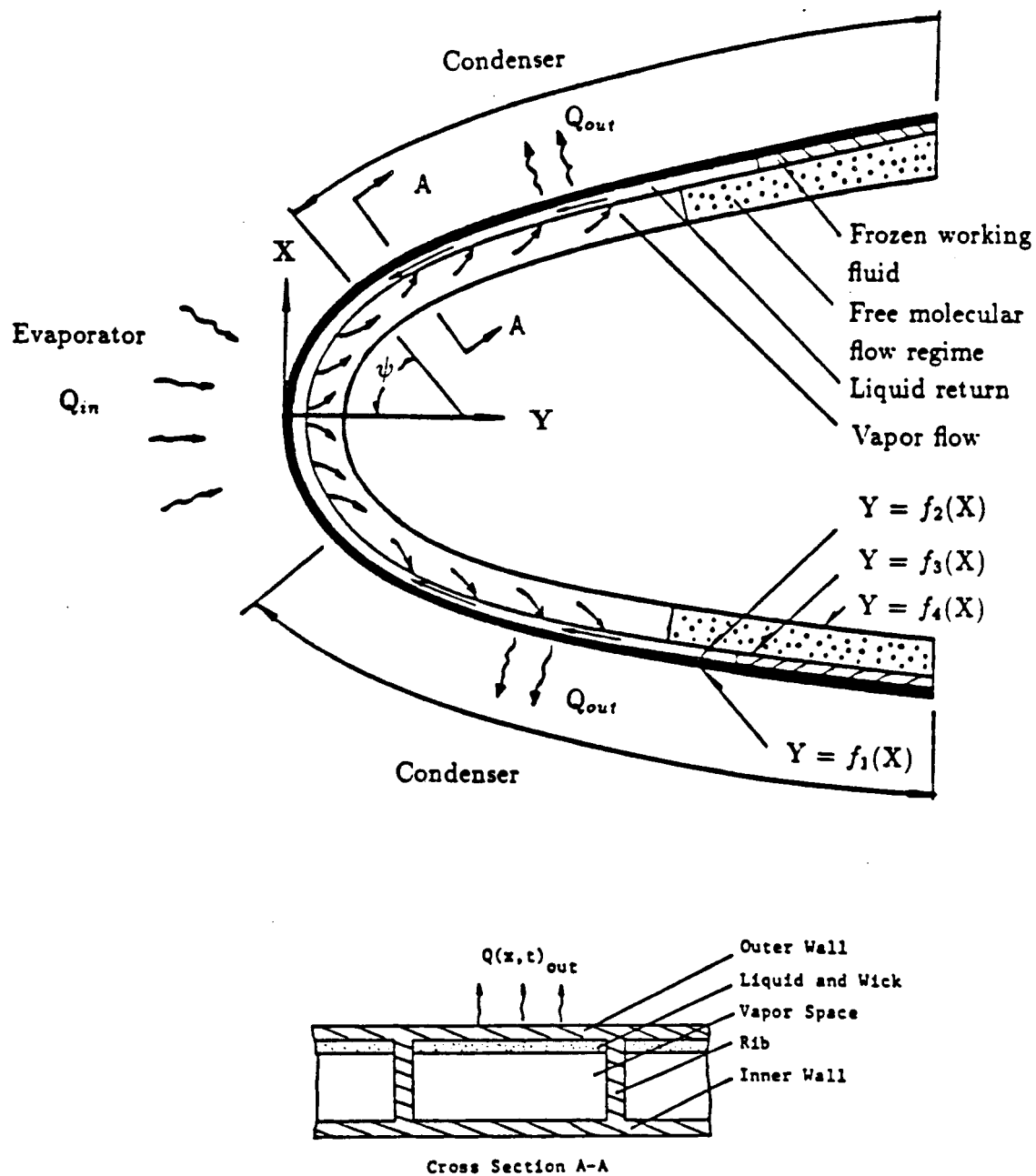


Figure 2.1. Schematic diagram of a heat pipe cooled leading edge.

negligible.

When energy is continuously added to the evaporator, the frozen working fluid in the evaporator is melted, so that evaporation can take place at the liquid-vapor interface and vapor flows into the condenser section due to the large pressure gradient. Vapor therefore freezes on the inner surface of the frozen working fluid in the cold zone and the vapor-solid interface temperature increases until the melting temperature is reached. During this stage, energy is mainly transferred as latent heat owing to vaporization in the heated zone, and condensation and freezing in the cooled zone. The vapor flow may be choked at the exit of the evaporator because of very low pressure in the cold zone.

This process continues until the frozen working fluid is completely melted and the continuum flow regime reaches the end of the heat pipe, at which time liquid returned to the evaporator is sufficient for normal transient operation. Eventually the heat pipe may reach a steady state condition. As suggested, during the startup of the heat pipe from a frozen state, the behavior of vapor flow may be divided into three distinct phases for convenience of analysis.

Phase I: Vapor flow in the heat pipe is in free molecular condition through the vapor space.

Phase II: In the vapor space, a region of continuum flow is established in the heated zone and a continuum flow front moves toward the heat pipe cooled end. Vapor flow may be choked at the end of the evaporator.

Phase III: Continuum flow exists over the entire heat pipe length in the vapor region and the sonic limit is not encountered.

2.2 Mathematical model development

On the basis of experimental observations, basic governing equations are written to determine the startup, transient, and steady state performance of a heat pipe which has initially frozen alkali-metal as the working fluid. These equations can be coupled by several types of boundary conditions on the heat pipe surface, such as specified temperature, heat flux, convection and radiation boundary conditions. The boundary condition at the liquid-vapor interface depends on the three phases of vapor flow dynamics mentioned in section 2.1.

2.2.1 Transition temperature

Continuum flow in the vapor space is considered to be established when the mean free path, λ , is substantially less than the minimum dimension, D , of the vapor flow passage, e.g.,

$$K_n \equiv \frac{\lambda}{D} \leq 0.01 \quad (2.1)$$

From kinetic theory of gases[33], the dynamic viscosity and the mean molecular velocity can be expressed as

$$\mu = 0.5\rho\lambda V \quad (2.2)$$

$$V = \sqrt{\frac{8R_u T}{\pi M}} \quad (2.3)$$

Eliminating the mean free path from Equations(2.1) and (2.2) yields the temperature of the vapor space corresponding to the given mean free path,

$$T^* \geq \frac{\pi}{2 \times 10^{-4}} \frac{M}{R_u} \left(\frac{\mu}{\rho D} \right)^2 \quad (2.4)$$

where ρ is the density of the vapor, μ is the dynamic viscosity of the vapor, R_u is the universal gas constant, and M is the molecule weight.

Iterations are required to obtain a value of T^* due to the temperature dependence of properties. Figure 2.2 illustrates the transition temperature, T^* , from free molecular to continuum flow as a function of minimum vapor passage for sodium. When the temperature of the vapor space is greater than that calculated by Equation(2.4), continuum flow is assumed to be established in the vapor space.

2.2.2 Heat pipe shell and capillary structure with working fluid

Unlike the case of a conventional cylindrical heat pipe, aerodynamic heating for the heat pipe shown in Figure 2.1 will cause the highest temperature to occur at the outer shell of the heat pipe. Thus, to simplify the analysis, it is assumed that the inner shell is sufficiently thin to neglect its thermal resistance and capacitance. Furthermore, the following additional assumptions are made. The thicknesses of the heat pipe and the rib are assumed to be much smaller than the width and therefore temperature gradients would be developed primarily in the chordwise direction during heat pipe startup. Therefore, the rib may be neglected in the analysis. Also, the heat pipe is assumed to be symmetric about the stagnation line so that the upper half section of the heat pipe only is considered. Hence, a two-dimensional model is considered for mathematical formulation. A simplified cross section is shown in Figure 2.3.

The unsteady, two-dimensional conduction equation is applied to the heat pipe shell and the capillary structure to evaluate the temperature distributions under

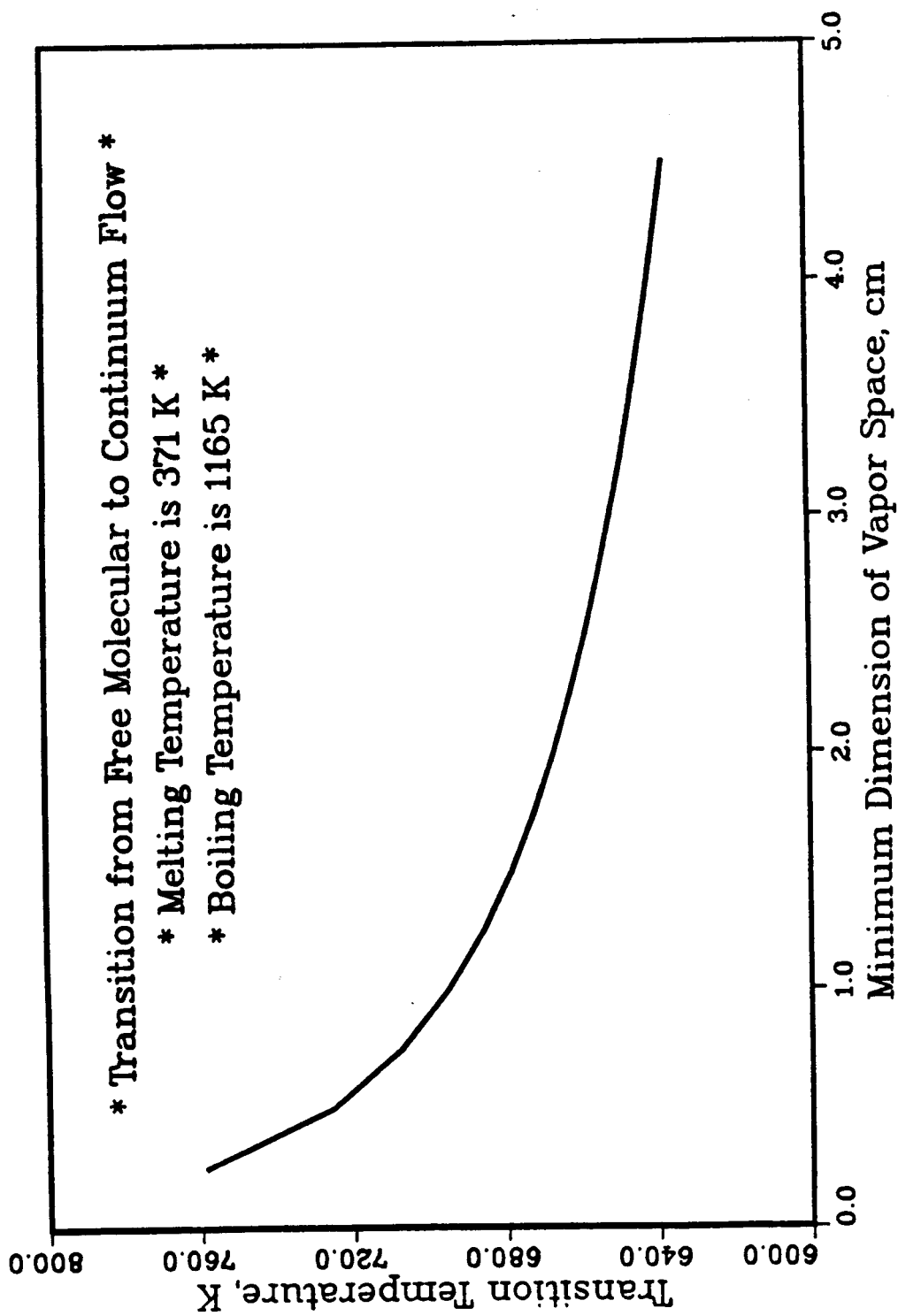


Figure 2.2. Transition temperature for sodium as a heat pipe working fluid.

ORIGINAL PAGE IS
OF POOR QUALITY

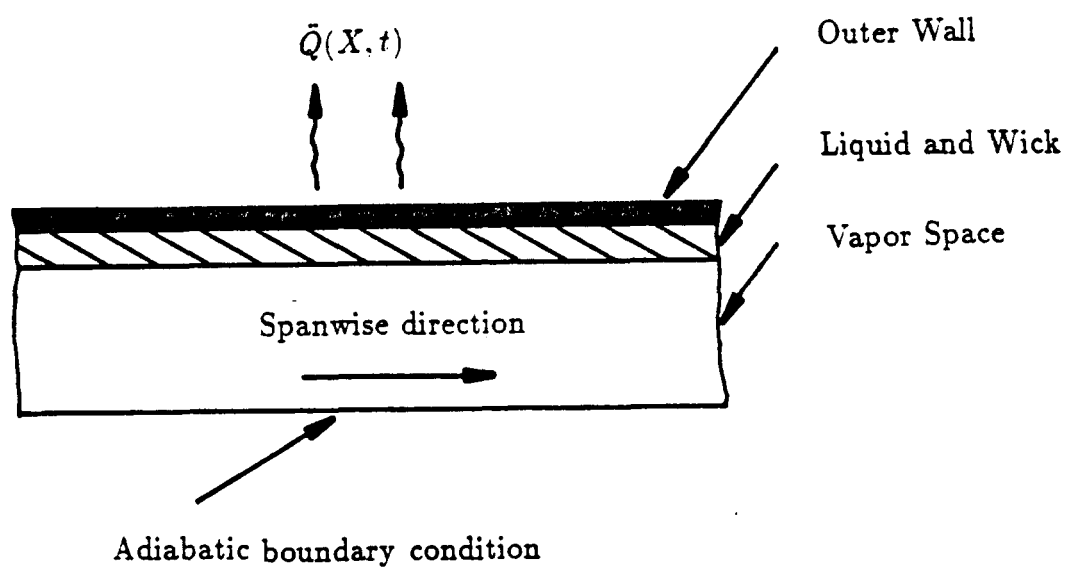


Figure 2.3. Simplified cross-section A-A of Figure 2.1.

the following assumptions:

1. The heat transferred through the wick and working fluid is by conduction only since liquid flow velocity is very low, liquid layer is thin and thermal conductivity is very high;
2. The presence of the wick structure does not affect the melting of the working substance, and melting occurs over a small, finite temperature range, ΔT , around the melting temperature;
3. Boundary conditions at the liquid-vapor interface are subject to the phases of vapor flow dynamics noted in section 2.1.
4. Radiation heat transfer at the liquid-vapor interface is neglected based on the small thermal emissivity of liquid sodium[34].

The governing equations and boundary conditions for the heat pipe shell and capillary structure with working fluid are expressed in one form:

$$C_i \frac{\partial T_i}{\partial t} = \frac{\partial}{\partial X} \left(K_i \frac{\partial T_i}{\partial X} \right) + \frac{\partial}{\partial Y} \left(K_i \frac{\partial T_i}{\partial Y} \right) , \quad i = 1, 2 \quad (2.5)$$

$$T_i = T_0 \quad \text{for } t < 0 \quad (2.6)$$

$$K_1 \frac{\partial T_1}{\partial n} = \ddot{Q}(X, t) \quad \text{at } Y = f_1(X) \quad \text{for } 0 \leq \psi \leq \psi_e \quad (2.7)$$

$$-K_1 \frac{\partial T_1}{\partial n} = h_{cr}(T_1 - T_{cr}) + \sigma \epsilon (T_1^4 - T_r^4) \quad \text{at } Y = f_1(X) \quad \text{for } \psi_e \leq \psi \leq \psi_c \quad (2.8)$$

$$T_1 = T_2 \quad \text{and} \quad K_1 \frac{\partial T_1}{\partial n} = K_2 \frac{\partial T_2}{\partial n} \quad \text{at } Y = f_2(X) \quad \text{for } 0 \leq \psi \leq \psi_c \quad (2.9)$$

$$\frac{\partial T_i}{\partial S} = 0, \quad i = 1, 2 \quad \text{at} \quad \psi = 0 \quad \text{and} \quad \psi = \psi_c \quad (2.10)$$

where the subscripts 1 and 2 denote the heat pipe shell and the capillary structure, n represents the unit outward normal direction, and S_d represents the chordwise direction.

In X - Y coordinates

$$K \frac{\partial T}{\partial n} = K \frac{\partial T}{\partial X} l_x + K \frac{\partial T}{\partial Y} l_y \quad (2.11)$$

where l_x and l_y are the direction cosines between the surface outward normal, n , and the X and Y axes, respectively.

2.2.3 Analysis of the vapor flow

Analysis of the vapor flow is necessary to provide the boundary condition at the liquid-vapor interface when continuum flow is established in part of the vapor space. However, the behavior of the vapor flow as mentioned in section 2.1 is very complicated due to the extremely small vapor density of the metallic working fluid at low vapor pressure, and the large pressure gradient in the chordwise direction. Limits on vapor flow are encountered, and considerable thermal resistance exists at the liquid-vapor interface due to phase change of the working fluid. The case of a flat plate heat pipe with asymmetrical boundary conditions shown in Figure 2.3 is considered for the vapor flow passage.

2.2.3.1 Evaporation and condensation

From kinetic theory, a significant thermal resistance exists at the liquid-vapor interface for liquid metal[35] and this resistance increases with decreasing vapor

pressure. This means that the difference between the vapor temperature and the interface temperature is not negligible. At the interface, interphase mass transfer has been stated from the viewpoint of kinetic theory as a net molecular flux which is the difference between the rate of arrival of molecules from the vapor space towards the interface and vice-versa. While condensation is proceeding, the arrival rate of molecules exceeds the departure rate. During evaporation, the reverse is true, and during the equilibrium state, the net molecular flux is zero. Hence, evaporation and condensation are modeled by using an expression for the net rate derived from the kinetic theory of gases[36]:

$$\dot{m}_o = \left(\frac{2a\epsilon}{2-a} \right) \sqrt{\frac{M}{2\pi R_u}} \left[\frac{P_f}{\sqrt{T_f}} - \frac{P_g}{\sqrt{T_g}} \right] \quad (2.12)$$

where a is the condensation or evaporation coefficient which is assumed to be unity, ϵ is the porosity of the wick, \dot{m}_o is the rate of condensation or evaporation per unit area, M is the molecular weight, R_u is the universal gas constant, P_f and T_f are the pressure and temperature, respectively, at the interface, and P_g and T_g are the pressure and temperature of the vapor, respectively.

2.2.3.2 Limitations of vapor flow

After continuum flow is established in the vapor space, because of the low density of vapor at low pressure and the large pressure gradient, the vapor flow is choked at the end of the evaporator, even for a low heat flux, just as it is at the throat of a convergent nozzle for large pressure gradient. This sonic limit is the first among several limitations encountered, and the performance of the heat pipe is restricted until the vapor temperature increases accordingly until the velocity of the vapor leaving the evaporator is less than the sonic velocity.

The expression for the sonic limit[15,29] in terms of flow conditions at the beginning of the evaporator, from an energy balance on a control volume enclosing the entire evaporator, is:

$$Q_s = \frac{\rho_o A_c h_{fg} \sqrt{\gamma R_u T_o}}{\sqrt{2(\gamma + 1)M}} \quad (2.13)$$

where A_c is the cross-section area of the vapor space, h_{fg} is the enthalpy of vaporization, γ is the ratio of specific heats, M is the weight of a molecule, R_u is the universal gas constant, T_o is the vapor temperature at the beginning of the evaporator and ρ_o is taken as the saturation density corresponding to T_o . Experimental verification of Equation(2.13) has been made by Kemme[37] for sodium, potassium and cesium heat pipes.

Figure 2.4 shows the sonic limit, the entrainment limit[12] and the axial Reynolds number for a heat pipe which has a cross-sectional area of 0.55 cm^2 , hydraulic radius of 0.32 cm , 100 mesh screen wick, and sodium as the working fluid. The type of limitation restricting performance of a heat pipe is determined by which limitation has the lowest value at the temperature under consideration. Thus, the first limit encountered is the sonic limit, as shown in Figure 2.4. However, when the actual chordwise heat transfer required is below these limits, no limits are encountered.

2.2.3.3 Modeling of vapor flow during phase II

Even though some of the working substance is in the liquid state, the transition temperature from free molecular flow to continuum flow is much greater than the melting temperature, so that the vapor flow is assumed to be free molecular during phase I, and an adiabatic boundary condition is applicable at the interface. However, during phase II, a region of continuum flow is assumed to be established in the

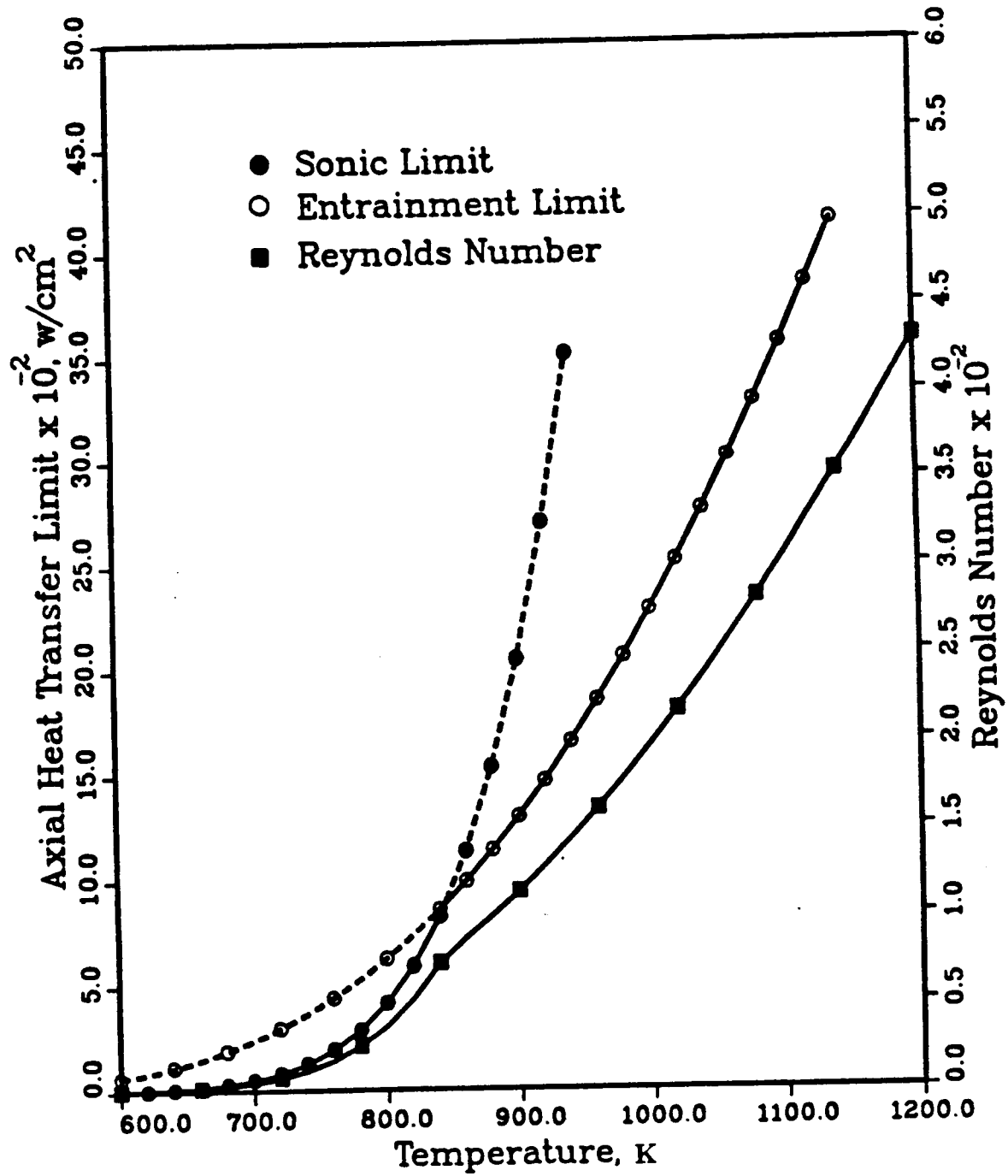


Figure 2.4. Heat pipe vapor flow limits and corresponding Reynolds numbers.

adjacent vapor space when the interface temperature is greater than the transition temperature, while in the cold zone the vapor is still in free molecular flow. The continuum flow region grows until it reaches the end of the heat pipe. The temperature in the region of free molecular flow remains unchanged except in the vicinity of the continuum flow region. Therefore, an imaginary plane, which is adiabatic and normal to the liquid-vapor interface, is assumed to divide the two vapor flow regions at the point of the transition temperature, and the dividing plane moves toward the cooled end of the heat pipe as the location of the transition temperature at the interface moves.

In the continuum flow region, energy is mainly transported as latent heat of the working fluid, and variations of temperature and pressure in the chordwise direction are significant. Even though continuum flow exists in the vapor space, the vapor pressure is low and the pressure gradient in the chordwise direction is large, so the heat transfer is limited by the choked flow condition, and supersonic vapor flow and a shock front[6,11,23,29] may occur in the condenser.

In this research, the overall performance of a heat pipe is of more interest than details of one portion, and as noted, the ultimate heat transfer rate in the axial direction is limited by the sonic limit. Thus, the vapor flow during phase II may be approximated, without losing generality and accuracy, by evaluating the sonic limit properly. In order to evaluate the sonic limit, the total heat input to the vapor space, which can be obtained by applying Equation(2.12) to the element adjacent to the continuum flow region, is equated to the sonic limited transport from Equation(2.13) as follows:

$$\sum_{i=1}^{m_e} 2\epsilon \sqrt{\frac{M}{2\pi R_u}} \left[\frac{P_{fi}}{\sqrt{T_{fi}}} - \frac{P_g}{\sqrt{T_g}} \right] \Delta L_i W = \frac{\rho A_c \sqrt{\gamma R_u T_g}}{\sqrt{2(\gamma + 1)M}} \quad (2.14)$$

where A_c is the cross-section area, ΔL_i is the length of the element, m_e is the number of elements at the interface in the evaporator, and W is the width of the vapor space. From Equation(2.14), the uniform vapor temperature can be computed by iteration. This vapor temperature may be lower than true vapor temperature at the beginning of the evaporator, but at this stage the variation of density with temperature and the density itself is very small, so that the variation of sonic limit with respect to temperature is also small, as shown in Figure 2.4. Thus, the heat flux at the liquid-vapor interface and the sonic limit can be obtained by solving Equations(2.12) and (2.13), respectively, with the vapor temperature obtained from Equation(2.14). This method may be used until the vapor flow state reaches phase III.

2.2.3.4 Vapor flow during phase III

In this stage, the entire working fluid is completely melted and continuum flow exists throughout the vapor space. However, the heat pipe has not reached the desired operating condition and the density of the vapor is still small, so that compressibility should be considered. The amount of energy stored in the vapor space is negligible. The Reynolds number in Figure 2.4 is the maximum value corresponding to a given temperature and the diameter of the vapor space. When the actual heat transfer required is below these limits, no limits are encountered. A model[30] test, in which a thermal history for space shuttle reentry heating was simulated, showed that the typical maximum heat pipe operating temperature is about 940 K. At this temperature, the maximum Reynolds number is 1200. A study of the effect of mass injection and suction, and/or chordwise pressure gradients on flow transition from laminar to turbulent flow in the vapor space of a heat pipe, was conducted by Bowman[22]. His results showed that mass injection and pressure

drops in the evaporator correspond to those for laminar flow for axial Reynolds number up to 10^6 . For the condenser, transition of flow is observed at a Reynolds number of 12,000. Even though the Reynolds number depends on the geometry of the heat pipe and the actual heat transfer rate, the results cited from the previous study show that the vapor flow may be assumed laminar. Also, it was observed that the vapor reaches the steady state quickly, while the thermal response of the heat pipe wall and wick progresses slowly. It was recommended that a steady state model can be employed for the vapor flow.

Thus, quasi-steady, compressible, one-dimensional laminar flow in the vapor space is considered. For purposes of formulating the mass, momentum, and energy equations in one-dimensional form, the velocity is taken to be the average velocity, which is approximated by the velocity distributions based on the similarity solutions of semiporous channels. In addition, friction at the liquid-vapor interface, variations of vapor quality, and momentum and energy factors are similarly calculated. The vapor is evaporated at the interface with mass injection rate per unit area, \dot{m}_o . It is assumed that this vapor flows inward with a normal component of velocity only, and joins the chordwise vapor flow.

Mass, momentum and energy balances in the chordwise direction, with the assumptions noted, yield:

$$D \frac{d}{dS} (\rho V) = \dot{m}_o \quad (2.15)$$

$$\frac{dP}{dS} + \frac{d}{dS} (M_f \rho V^2) = -\frac{F \rho V^2}{8D} \quad (2.16)$$

$$D \frac{d}{dS} \left[\rho V \left(h + \frac{E_f V^2}{2} \right) \right] = \dot{m}_o \left(h_o + \frac{V_o^2}{2} \right) \quad (2.17)$$

where D is the height of the vapor space, h is the vapor enthalpy and h_o is the vapor enthalpy at the interface.

A friction factor F for the surface is written as

$$F = \frac{8\tau_g}{\rho V^2} \quad (2.18)$$

Momentum and energy factors, M_f and E_f , respectively, are expressed as

$$M_f = \frac{1}{DV^2} \int_0^D U^2 dy \quad (2.19)$$

$$E_f = \frac{1}{DV^3} \int_0^D U^3 dy \quad (2.20)$$

Normal velocity of the vapor at the interface is expressed in terms of the heat transfer rate and latent heat of vaporization as follows:

$$V_0 = \frac{\dot{Q}}{h_{fg}\rho_o A_o} \quad (2.21)$$

where \dot{Q} is the heat input rate at the interface, ρ_o is the density for the interface temperature and A_o is the interface area.

CHAPTER III

NUMERICAL MODEL DEVELOPMENT FOR PHASE CHANGE

3.1 Introduction

Transient and nonlinear heat transfer problems having phase change have been encountered in many engineering fields, and pose inherent difficulties for analytical and numerical solutions, because the interface between the new and old phase is moving with time, and properties such as conductivity, specific heat, and density are discontinuous at the phase change region.

The fundamental feature of these phase change problems was given attention and was solved analytically by Lamé and Clapeyron in 1831, Stefan in 1891, and Newmann in 1912. Since then, many scientists have introduced analytical methods of solution of phase change problems to a number of idealized problems involving semi-infinite or infinite regions, subject to simple boundary and initial conditions. A brief discussion of these methods is presented by Ozisik[38]. A large number of numerical solutions of phase change problems were made possible by the availability of high speed digital computers. The finite element method has been used for nonstructural problems since the procedure was first proposed by Zienkiewicz and Cheung[39]. The solution process is now well established for linear situations, but relatively little work has been reported for nonlinear problems.

The Galerkin weighted residual method is used here to derive finite element formulations. Since the governing differential equations are highly nonlinear due to the temperature dependence of the thermophysical properties, a three time level difference scheme which was proposed by Dupont et al.[40] is utilized to allow a direct evaluation of the properties at an intermediate time level, thereby eliminating

iterations within each time step. However, this scheme is not self-starting, so the implicit method with Newton-Raphson iteration is used for the first few time steps.

3.2 Mathematical model

For the system, having an arbitrary control volume \bar{V} and control surface area A , the general principle of conservation of energy implies that whatever energy enters the system must either leave the system across the boundary or cause a change in the energy within the system. With no work, mass transfer, nor energy generation sources, the net rate of change of the total energy within the system must equal to the net rate of energy entering the system due to heat transfer across the control surface area. This statement can be expressed in mathematical form as follows:

$$\frac{\partial}{\partial t} \int_{\bar{V}} \rho h d\bar{V} = \int_A K \nabla T \cdot \vec{n} dA \quad (3.1)$$

where ρ is the density, h is the specific enthalpy, K is the thermal conductivity, ∇T is the gradient of temperature and \vec{n} is the unit outward normal to the surface as shown in Figure 3.1.

For a single phase region, the fixed control volume is independent of time, and the divergence theorem is used to convert the surface integral to a volume integral. Therefore, Equation(3.1) can be written

$$\int_{\bar{V}} \frac{\partial}{\partial t} (\rho h) d\bar{V} = \int_{\bar{V}} \nabla \cdot (K \nabla T) d\bar{V} \quad (3.2)$$

The volume may be chosen so small as to remove the integral, and the specific enthalpy can be replaced by the expression for the specific heat and temperature. Equation(3.2) is then reduced for an arbitrary small volume \bar{V} as follows:

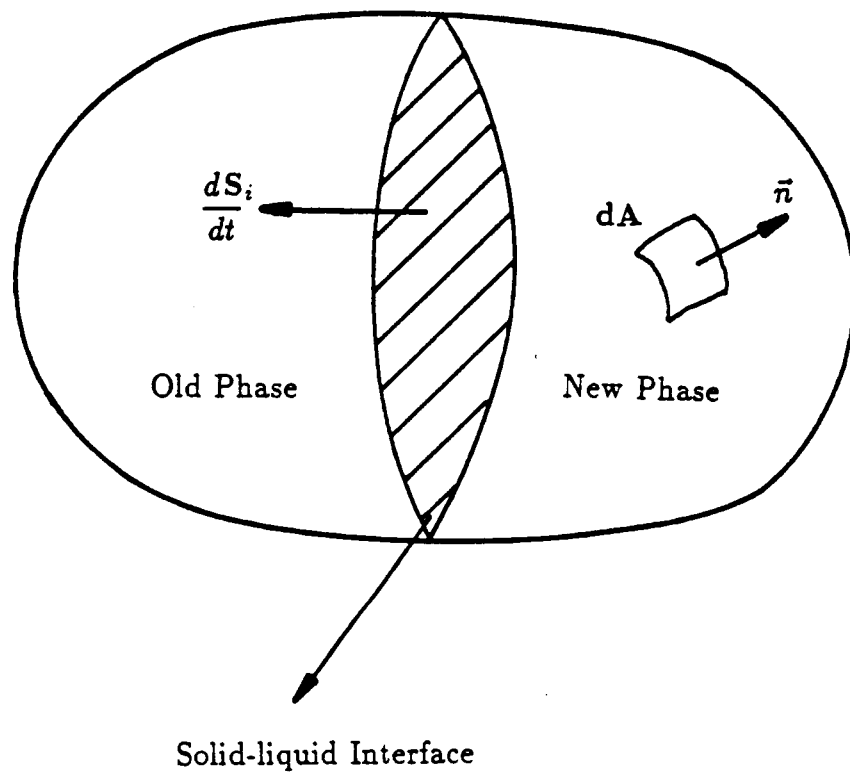


Figure 3.1. Control volume \bar{V} .

$$\rho c_p \frac{\partial T}{\partial t} = \nabla \cdot (K \nabla T) \quad (3.3)$$

This equation can be applied to the solid and liquid regions when the motion of the liquid due to the change of the density is neglected. However, the properties of the material are discontinuous at the interface as shown in Figure 3.2, so that a single equation cannot describe the phase change phenomenon. Hence, a problem with the phase change of a substance is mathematically described as follows:

$$C_{21} \frac{\partial T_{21}}{\partial t} = \nabla \cdot (K_{21} \nabla T_{21}) \quad \text{for old phase} \quad (3.4)$$

$$C_{22} \frac{\partial T_{22}}{\partial t} = \nabla \cdot (K_{22} \nabla T_{22}) \quad \text{for new phase} \quad (3.5)$$

with initial condition

$$T_{21} = T_0 \quad (3.6)$$

Boundary conditions are, for $i = 1, 2$,

$$T_{2i} = T_s, \quad \text{on } A_1 \quad (3.7)$$

$$-K_{2i} \nabla T_{2i} = \ddot{Q} \quad \text{on } A_2 \quad (3.8)$$

$$-K_{2i} \nabla T_{2i} = h_{cr}(T_{2i} - T_{cr}) \quad \text{on } A_3 \quad (3.9)$$

$$-K_{2i} \nabla T_{2i} = \beta_r(T_{2i} - T_r) \quad \text{on } A_4 \quad (3.10)$$

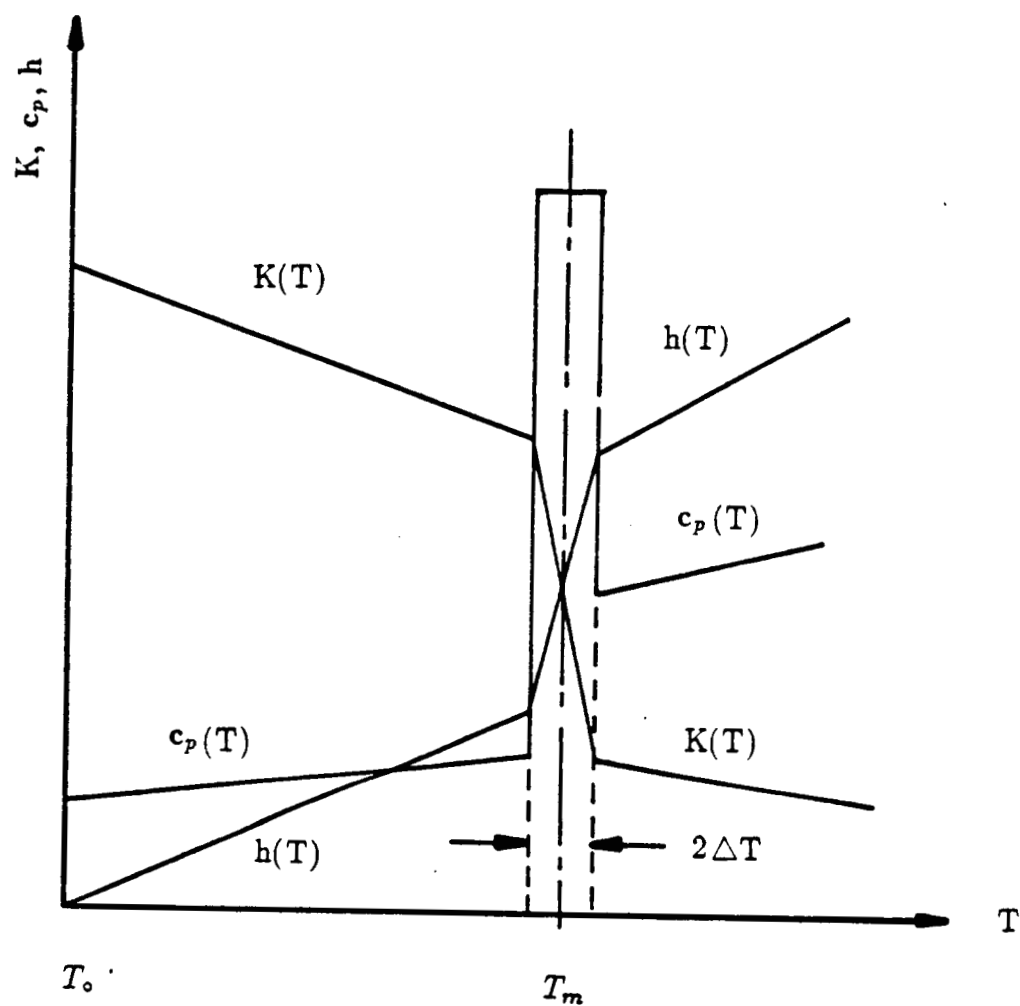


Figure 3.2. Variations of properties near the phase change temperature.

where $\beta_r = \sigma\epsilon(T_{2i}^2 + T_r^2)(T_{2i} + T_r)$ and coupling conditions at the interface are

$$T_{21} = T_{22} = T_m \quad (3.11)$$

$$K_{21} \frac{\partial T_{21}}{\partial n} - K_{22} \frac{\partial T_{22}}{\partial n} = H_{ls} \frac{dS_i}{dt} \quad (3.12)$$

where h_{cr} is the heat transfer coefficient, H_{ls} is the latent heat of a phase change, S is the interface position, T_m is the temperature of the phase change, ϵ is the emissivity, and σ is the Stefan-Boltzmann constant.

3.3 Description of numerical formulations

3.3.1 Finite element formulation

The Galerkin weighted residual method is used to derive finite element formulations. Within each element, the unknown function T may be approximated at any time t by the relationship

$$T(x, y, t) = \sum_{i=1}^k N_i(x, y) \cdot T_i(t) \quad (3.13)$$

where k is the number of nodes assigned to the element, T_i are the discrete nodal values of T , and N_i are the shape functions.

To derive the element equations for differential Equation(3.3) and their boundary conditions, the solution domain R in two dimensions, as shown in Figure 3.3, is divided into m linear triangular elements of k nodes each. Application of the Galerkin method to Equation(3.3) yields

$$\int_{R^{(e)}} N_i \left[\frac{\partial}{\partial X} \left(K \frac{\partial T^{(e)}}{\partial X} \right) + \frac{\partial}{\partial Y} \left(K \frac{\partial T^{(e)}}{\partial Y} \right) - C \frac{\partial T^{(e)}}{\partial t} \right] dX dY = 0 \quad (3.14)$$

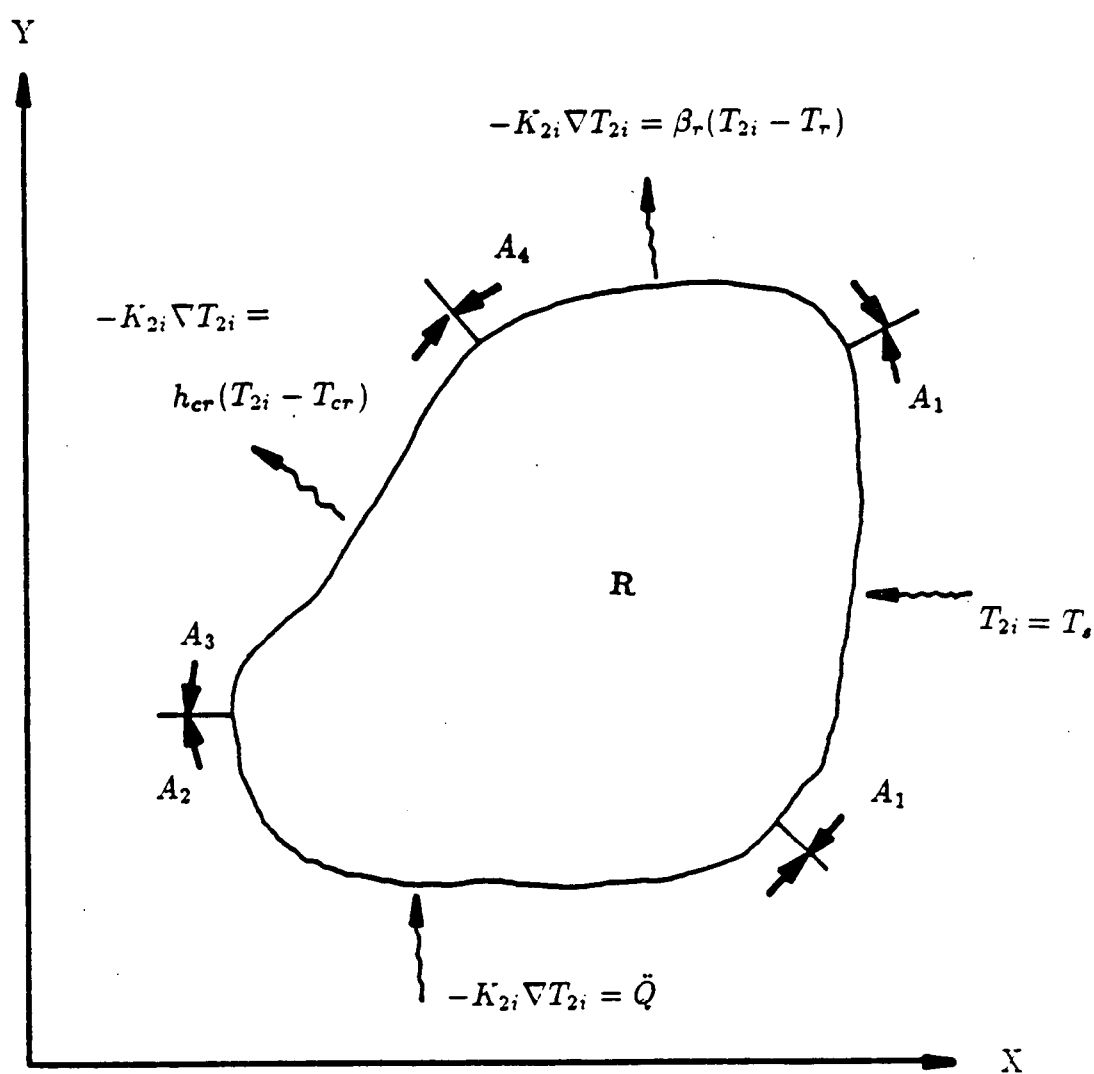


Figure 3.3. Two-dimensional solution domain.

where N_i are the shape functions which are conveniently chosen as weighting functions in the Galerkin method.

To reduce the order of the derivatives in the equation above and to introduce the influence of the boundary conditions, the second order derivatives are integrated by parts

$$\begin{aligned} \int_{R^{(e)}} N_i \left[\frac{\partial}{\partial X} \left(K \frac{\partial T^{(e)}}{\partial X} \right) + \frac{\partial}{\partial Y} \left(K \frac{\partial T^{(e)}}{\partial Y} \right) \right] dX dY = \\ - \int_{R^{(e)}} \left[\frac{\partial N_i}{\partial X} \left(K \frac{\partial T^{(e)}}{\partial X} \right) + \frac{\partial N_i}{\partial Y} \left(K \frac{\partial T^{(e)}}{\partial Y} \right) \right] dX dY \\ + \int_{A^{(e)}} N_i \left[\left(K \frac{\partial T^{(e)}}{\partial X} \vec{i} + K \frac{\partial T^{(e)}}{\partial Y} \vec{j} \right) \cdot \vec{n} \right] dS \end{aligned} \quad (3.15)$$

where \vec{i} is the unit vector in the X direction, \vec{j} is the unit vector in the Y direction, and \vec{n} is the outward unit vector normal to the surface, which coincides with the boundary to the solution domain. For the surfaces(or sides) of the elements contained within the solution domain, the surface integrals cancel out by continuity of heat flux when the element equations are assembled into the global system of equations. Only those surfaces of elements which coincide with the boundary to the solution domain, and do not have a specified temperature at the boundary, contribute to the surface integral.

The surface integral can be expressed as the sum of integrals over the external surfaces A as follows:

$$\begin{aligned} \int_{A^{(e)}} N_i \left[\left(K \frac{\partial T^{(e)}}{\partial X} \vec{i} + K \frac{\partial T^{(e)}}{\partial Y} \vec{j} \right) \cdot \vec{n} \right] dS = \\ \int_{A_2} \tilde{Q} N_i dS - \int_{A_3} h_{cr}(T^{(e)} - T_{cr}) N_i dS - \\ \int_{A_4} \beta_r(T^{(e)} - T_r) N_i dS \end{aligned} \quad (3.16)$$

Substitution of Equations(3.15) and (3.16) into Equation(3.14) results in the following expression

$$\begin{aligned} \int_{R(\epsilon)} \left[\frac{\partial N_i}{\partial X} \left(K \frac{\partial T^{(\epsilon)}}{\partial X} \right) + \frac{\partial N_i}{\partial Y} \left(K \frac{\partial T^{(\epsilon)}}{\partial Y} \right) + N_i C \frac{\partial T^{(\epsilon)}}{\partial t} \right] dX dY = \\ \int_{A_2} \bar{Q} N_i dS - \int_{A_3} h_{cr} (T^{(\epsilon)} - T_{cr}) N_i dS - \int_{A_4} \beta_r (T^{(\epsilon)} - T_r) N_i dS \end{aligned} \quad (3.17)$$

After substituting the expression for unknown function $T^{(\epsilon)}$ into Equation (3.17), the resulting element equation is expressed as

$$\begin{aligned} \int_{R(\epsilon)} K \left(\frac{\partial N_i}{\partial X} \frac{\partial N_j}{\partial X} + \frac{\partial N_i}{\partial Y} \frac{\partial N_j}{\partial Y} \right) T_j dX dY + \int_{R(\epsilon)} \left(C N_i N_j \dot{T}_j \right) dX dY + \\ \int_{A_3} h_{cr} N_i N_j T_j dS + \int_{A_4} \beta_r N_i N_j T_j dS = \\ \int_{A_2} \bar{Q} N_i dS + \int_{A_3} h_{cr} N_i T_{cr} dS + \int_{A_4} \beta_r N_i T_r dS \end{aligned} \quad (3.18)$$

Finally, the assembly of the nonlinear transient element equations can be expressed in matrix form as follows:

$$[C]\{\dot{T}\} + \left[[K_c] + [K_h] + [K_r] \right] \{T\} = \{F_q\} + \{F_h\} + \{F_r\} \quad (3.19)$$

where

$$[C] = \int_{R(\epsilon)} C N_i N_j dX dY \quad (3.19.1)$$

$$[K_c] = \int_{R(\epsilon)} K \left(\frac{\partial N_i}{\partial X} \frac{\partial N_j}{\partial X} + \frac{\partial N_i}{\partial Y} \frac{\partial N_j}{\partial Y} \right) dX dY \quad (3.19.2)$$

$$[K_h] = \int_{A_3} h_{cr} N_i N_j dS \quad (3.19.3)$$

$$[K_r] = \int_{A_4} \beta_r N_i N_j dS \quad (3.19.4)$$

$$[F_q] = \int_{A_2} \ddot{Q} N_i dS \quad (3.19.5)$$

$$[F_h] = \int_{A_3} h_{cr} N_i T_{cr} dS \quad (3.19.6)$$

$$[F_r] = \int_{A_4} \beta_r N_i T_r dS \quad (3.19.7)$$

3.3.2 Time stepping scheme

The finite element method is now firmly established to investigate transient field problems governed by parabolic equations. However, the time derivative has usually been approximated by the finite difference method. Thus, a finite element discretization in space is coupled with finite difference approximation in time.

3.3.2.1 Implicit method

Let t^r denote a typical time in the response so that $t^{r+1} = t^r + \Delta t$ where Δt is the time increment, and an intermediate time t_θ within each time step may be expressed as

$$t_\theta = t^r + \theta \Delta t, \quad 0 \leq \theta \leq 1 \quad (3.20)$$

Then, Equation(3.19) at t_θ is given as

$$[C]\{\dot{T}\}_\theta + [K]\{T\}_\theta = \{F\} \quad (3.21)$$

A first-order Taylor expansion in time is used,

$$\{T\}^r = \{T\}_\theta - \frac{d}{dt}\{T\}_\theta(\theta \Delta t) \quad (3.22)$$

and the following approximation for $\{\dot{T}\}$ is introduced.

$$\frac{d}{dt}\{T\}_\theta = \left(\{T\}^{r+1} - \{T\}^r\right)/\Delta t \quad (3.23)$$

Substitution of Equation(3.23) into Equation(3.22) yields

$$\{T\}_\theta = (1 - \theta)\{T\}^r + \theta\{T\}^{r+1} \quad (3.24)$$

Finally, substitution of the expressions for $\{T\}_\theta$ and $\{T\}_\theta$ into Equation(3.21) gives

$$\left(\frac{[C]}{\Delta t} + \theta[K]\right)\{T\}^{r+1} = \left(\frac{[C]}{\Delta t} - (1 - \theta)[K]\right)\{T\}^r + \{F\} \quad (3.25)$$

Since the values of $[C]$, $[K]$, and $\{F\}$ depend on $\{T\}_\theta$, a choice from among the values $\theta = 0, 1/2, 2/3$, and 1 , respectively, yields Euler forward-difference, Crank-Nicolson center-difference, Galerkin, and fully implicit backward-difference formulations. The fully implicit backward-difference scheme is unconditionally stable and predicts a smooth decay.

3.3.2.2 Explicit methods

The implicit method is much more stable than the explicit method, but requires an iteration within each time step. To avoid iteration, a three level scheme proposed by Lees[41] was used by Comini et al.[42-46] and Morgan et al.[47]. Oscillations have been observed in certain instances, so a slightly modified form was used to improve stability.

Another three level scheme is referred to as the Dupont three level scheme. Hogge[48] demonstrated its overall performance to be superior in accuracy and

stability to other time stepping schemes in solving the one-dimensional homogeneous equation.

Thomas et al.[49] compared several time integration schemes such as the Lees scheme, the Dupont scheme, and the Crank-Nicolson method. He concluded that the Dupont three level scheme was clearly superior to that of Lees in both accuracy and stability, and temperature-dependent terms should be evaluated using $\{T\}^{r+1}$ instead of $\{T\}^{r+\frac{1}{2}}$. With the use of Dupont method, Equation(3.21) can be approximated as follows:

$$\left(\frac{3}{4}[K] + \frac{[C]}{\Delta t}\right)\{T\}^{r+2} = \frac{[C]}{\Delta t}\{T\}^{r+1} + \frac{[K]}{4}\{T\}^r + \{F\} \quad (3.26)$$

The Equation(3.26) allows the explicit evaluation of $\{T\}^{r+2}$ without iteration, provided that $\{T\}^{r+1}$ and $\{T\}^r$ are known. However, this scheme is not self-starting, so that $\{T\}^{r+1}$ at the first time step may be calculated by using the implicit method.

3.3.2.3 Latent heat evaluation schemes

The principal difficulties in the analysis of the phase change problem are that the variation of the heat capacity is very severe at the interface, as shown in Figure 3.2. The position of the moving interface is not known a priori and the shape may be multi-dimensional. Thus, physically realistic approximation techniques must be used to overcome these difficulties. It is convenient to divide them into two groups, based on the choice of grids.

In the first group, the moving mesh technique continuously tracks the location of the interface by deforming the grid system to maintain the finest mesh in the vicinity of the critical phase change region. This technique may be limited to very simple geometries. In the second group, a fixed grid technique can avoid tracking

down the position of the moving interface, but the interface is generally at an unknown location between nodes. Many different types of methods are available with the fixed grid system. The first method uses the enthalpy as a dependent variable along with the temperature, and may be referred to as the enthalpy method[50]. Since two dependent variables are used, the system of algebraic equations are solved by iteration.

The second method treats the latent heat effect accompanying a change of phase in terms of a temperature-dependent specific heat, or with the use of an enthalpy function. These methods avoid the moving interface difficulty so that instead of continuously tracking down the position of the moving interface, the same numerical scheme for conduction heat transfer without phase change is equally applicable to the phase change region. Then, the position of the interface can be easily determined by linear interpolation of nodal temperatures.

When temperature approaches the phase change temperature, the heat capacity tends to the Dirac delta function, and cannot be satisfactorily represented across the peak by any smooth function. Frivik and Comini[42] proposed a technique based on the integral of the heat capacity with respect to temperature

$$H = \int_{T_{\infty}}^T C dT \quad (3.27)$$

This is a smooth function of temperature in the phase change zone. Therefore, the enthalpy rather than the heat capacity is interpolated in a element as follows:

$$H = \sum_{i=1}^k N_i(x, y) H_i(t) \quad (3.28)$$

where H_i are the enthalpy values at nodal points.

From definition, the heat capacity can be expressed as

$$C = \frac{dH}{dT} \quad (3.29)$$

Thus, the values of the heat capacity can be approximated by evaluating the gradient of enthalpy with respect to temperature. Defining the direction n to be normal to the interface line, Equation(3.29) is expressed as

$$\begin{aligned} C &= \left(\frac{\partial H}{\partial n} / \frac{\partial T}{\partial n} \right) \\ &= \left(\frac{\partial H}{\partial X} l_{nx} + \frac{\partial H}{\partial Y} l_{ny} \right) / \left(\frac{\partial T}{\partial n} \right) \end{aligned} \quad (3.30)$$

where

$$\begin{aligned} l_{nx} &= \frac{\partial T}{\partial X} / \frac{\partial T}{\partial n} \\ l_{ny} &= \frac{\partial T}{\partial Y} / \frac{\partial T}{\partial n} \\ \frac{\partial T}{\partial n} &= \left[\left(\frac{\partial T}{\partial X} \right)^2 + \left(\frac{\partial T}{\partial Y} \right)^2 \right]^{\frac{1}{2}} \end{aligned}$$

Hence, for the entire element, the final expression of the heat capacity proposed by Del-Giudice et al.[51] is given as

$$C = \left[\frac{\partial H}{\partial X} \frac{\partial T}{\partial X} + \frac{\partial H}{\partial Y} \frac{\partial T}{\partial Y} \right] / \left[\left(\frac{\partial T}{\partial X} \right)^2 + \left(\frac{\partial T}{\partial Y} \right)^2 \right] \quad (3.31)$$

CHAPTER IV

VAPOR FLOW DYNAMICS IN HEAT PIPES

4.1 Introduction

Analysis of the hydrodynamics of vapor flow in heat pipes with metallic working fluids indicates considerable difficulties at low vapor pressure, due to the extremely small vapor densities. Even for relatively small heat transfer rates, vapor velocity in the chordwise direction can be very large, accelerated towards sonic velocity because viscous action causes pressure and density to decrease. Additional heat input causes choking at the condenser inlet. Such behavior makes it necessary to include vapor compressibility and viscous action in mathematical models. The vapor pressure drop due to friction cannot be recovered completely in the condenser section. Thus, the temperature distributions along the length of the heat pipe are not isothermal, and thermal resistance in the vapor region is significant. Studies of the distributions of temperature, pressure, and velocity in the vapor passage along the length of a heat pipe are essential for an evaluation of the maximum heat transfer rates and prediction of correct heat pipe performance.

Reviews of the literature on hydrodynamic processes in vapor flow of cylindrical heat pipes made by Tien[52] and Ivanovskii et al.[11] indicate that no completely detailed investigation has been presented thus far. Moreover, experimental measurements of pressure and velocity for metallic working fluids have not been reported.

An analysis of the steady, compressible, one-dimensional, laminar flow of sodium vapor is presented for the case of a flat plate-type heat pipe with asymmetrical boundary conditions. In addition, shear stress at the liquid-vapor interface,

variations of vapor quality, and momentum and energy factors are considered. A similarity solution for a semiporous channel is used to provide the velocity profile at cross sections.

4.2 Similarity solution for a semiporous channel

4.2.1 Governing differential equations

A sketch of the geometry for a semiporous channel is given in Figure 4.1. The following assumptions are made: that the fluid flow is incompressible and laminar, and that the properties of the fluid are constant. The width of the channel is assumed much greater than the height. Therefore, two-dimensional flow is considered. Fully developed flow is assumed in the channels. A constant injection or suction velocity is used. With these assumptions, the Navier-Stokes equations for two-dimensional, steady state, incompressible, laminar flow are written as

$$U \frac{\partial U}{\partial X} + V^* \frac{\partial U}{\partial Y} = -\frac{1}{\rho} \frac{\partial P}{\partial X} + \nu \left[\frac{\partial^2 U}{\partial X^2} + \frac{\partial^2 U}{\partial Y^2} \right] \quad (4.1)$$

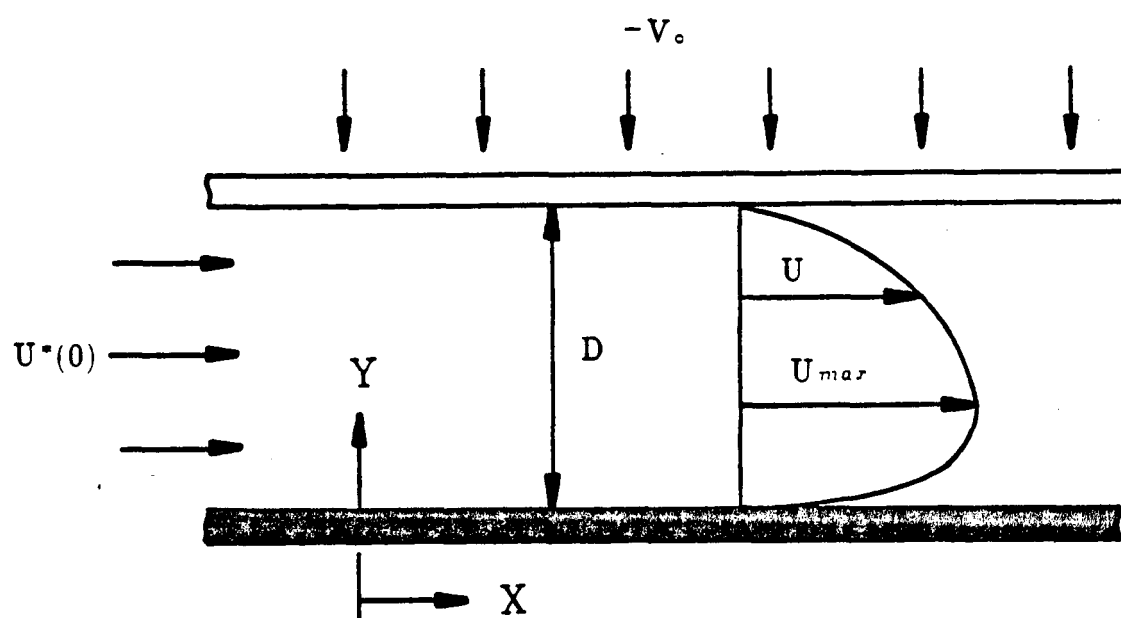
$$U \frac{\partial V^*}{\partial X} + V^* \frac{\partial V^*}{\partial Y} = -\frac{1}{\rho} \frac{\partial P}{\partial Y} + \nu \left[\frac{\partial^2 V^*}{\partial X^2} + \frac{\partial^2 V^*}{\partial Y^2} \right] \quad (4.2)$$

and the continuity equation is

$$\frac{\partial U}{\partial X} + \frac{\partial V^*}{\partial Y} = 0 \quad (4.3)$$

Boundary conditions used on the channel surfaces are

$$U = 0, \quad \text{and} \quad V^* = 0 \quad \text{at } Y = 0 \text{ (solid wall)} \quad (4.4)$$



$-V_o$: Injection, depicted.

V_o : Suction.

Figure 4.1. Schematic diagram of a semiporous channel.

$$U = 0, \quad \text{and} \quad V^* = V_0 \quad \text{at } Y = D \text{ (porous wall)} \quad (4.5)$$

4.2.2 Similarity transformations

The governing equations can be transformed into total differential equations by the use of a dimensionless length coordinate, ω , and a dimensionless function, f , which automatically satisfies the continuity equation. The new variables[53] are defined as

$$\omega = \frac{Y}{D} \quad (4.6)$$

$$f(\omega) = \frac{\varphi}{DV} \quad (4.7)$$

where $V(X) = U^*(0) - \frac{V_0 X}{D}$ and $U^*(0)$ is the average velocity at $X = 0$.

Then, the local velocity can be expressed by the new variables as follows:

$$U = \frac{\partial \varphi}{\partial Y} = V f' \quad (4.8)$$

$$V^* = -\frac{\partial \varphi}{\partial X} = V_0 f \quad (4.9)$$

Use of Equations(4.1), (4.2), and (4.6) to (4.9) gives

$$-\frac{1}{\rho} \frac{\partial P}{\partial X} = V \left[\frac{V_0}{D} (f f'' - f')^2 - \frac{\nu}{D^2} f''' \right] \quad (4.10)$$

$$-\frac{1}{\rho} \frac{\partial P}{\partial \omega} = V_0 \left[V_0 f f' - \frac{\nu}{D} f'' \right] \quad (4.11)$$

Since the right side of Equation(4.11) is a function of ω only, differentiating with respect to X yields

$$\frac{\partial^2 P}{\partial X \partial \omega} = 0 \quad (4.12)$$

On taking the derivative with respect to ω , applying Equation(4.12), and integrating, Equation(4.10) becomes

$$Re_o \left[(f')^2 - f f'' \right] + f''' = -A \quad (4.13)$$

where $Re_o = \frac{V_o D}{\nu}$ and $A = -\frac{D^2}{\nu \rho} \frac{\partial P}{\partial X}$

The transformed boundary conditions are written as

$$f' = f = 0 \quad \text{at } \omega = 0 \text{ (solid wall)} \quad (4.14)$$

$$f' = 0, f = 1 \quad \text{at } \omega = 1 \text{ (porous wall)} \quad (4.15)$$

4.2.3 Solution of equation

Differential Equation(4.13) together with the associated boundary conditions, constitutes a nonlinear boundary value problem with the parameter Re_o . Since this governing equation is no longer partial differential equation, it can be solved numerically by the Runge-Kutta integration method. However, the number of boundary conditions is not enough to solve Equation(4.13). Therefore, for each specified Re_o , the value of A and $f''(0)$ are guessed to solve a system of the first order differential equations. Then, at $\omega = 1$ (porous wall), the calculated values of f' and f are

compared with the given boundary conditions. When both values are not acceptable, other values are used until the convergent tolerance is satisfied. When wall Reynolds numbers for suction are greater than 13, separation occurs on the solid wall. Similarity solutions are valid for wall Reynolds numbers up to 13. Hence, the equation is solved for wall Reynolds numbers ranging from -30 to 13 .

A comparison of the present results with those found in the literature[53,54], which use the perturbation method for small Reynolds numbers and a different numerical scheme, verifies the accuracy of this numerical solution.

The velocity profiles for the suction and injection sections are shown in Figures 4.2 and 4.3. Asymmetric boundary conditions cause the velocity profiles to be asymmetric. For injection, $Re_o < 0$, the location of the maximum velocity shifts from the center of the channel toward the solid wall. Thus, injection increases friction at the solid wall, and decreases friction at the porous wall. As wall Reynolds numbers increase, the degree of shifting is large, although the general shape is changed little. For suction, $Re_o > 0$, the location of the peak velocity shifts toward the porous wall. Hence, suction increases friction at the porous wall and decreases friction at the solid wall. Unlike injection, separation for suction appears around a wall Reynolds number of 13. The velocity profiles change considerably with wall Reynolds number. In general, friction for the semiporous channel is larger than that for the impermeable channel.

Results[19] from two-dimensional, incompressible, Navier-Stokes equations for a flat plate heat pipe show similar velocity profiles. In the evaporator, the velocity profiles retain similarity for a wall Reynolds number of 50, which is the highest value tested. However, back flow was observed near the end of the condenser for a wall Reynolds number of 10. For a wall Reynolds number of 50, back flow was observed in the entire condenser section.

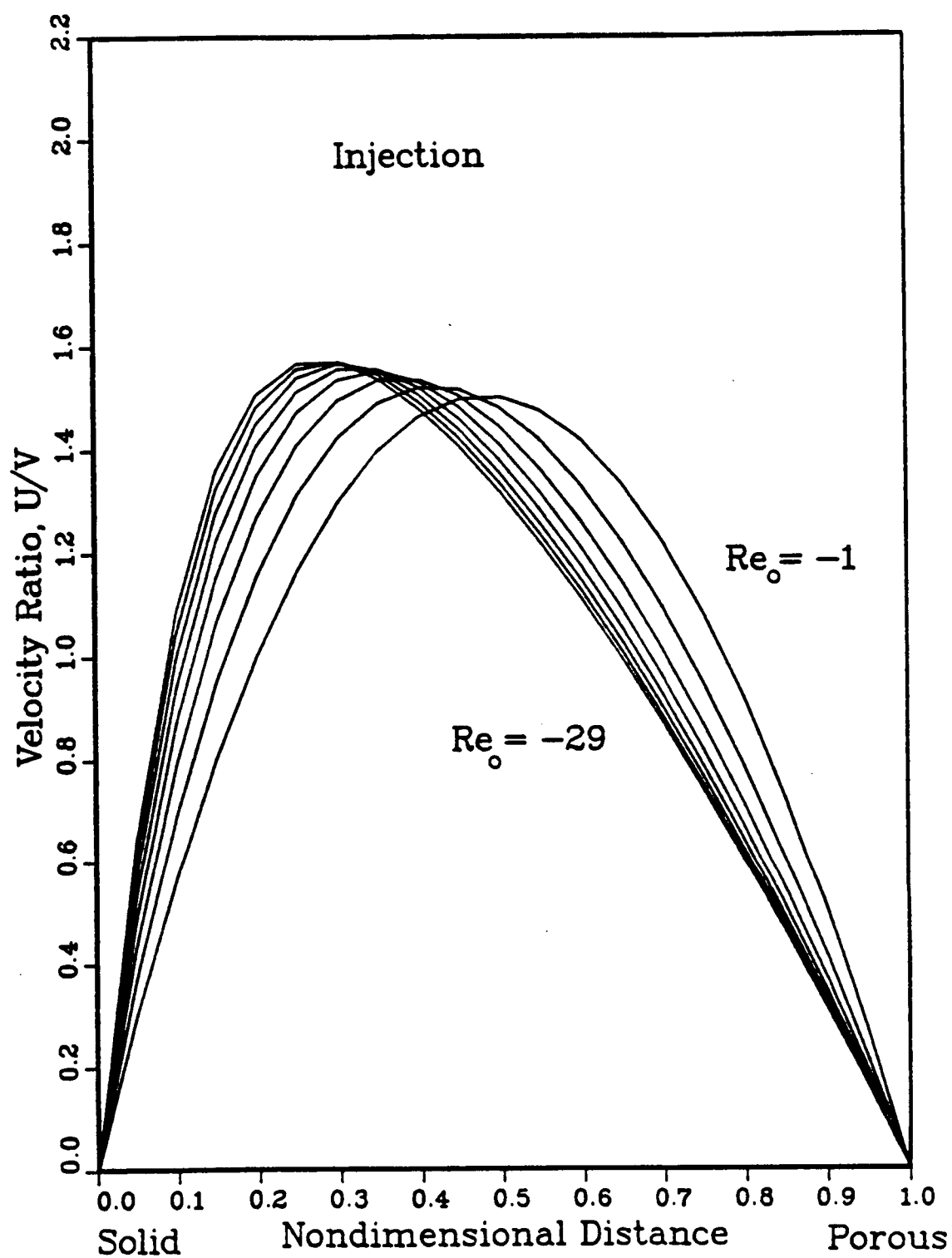


Figure 4.2. Velocity profiles for wall injection in a semiporous channel.

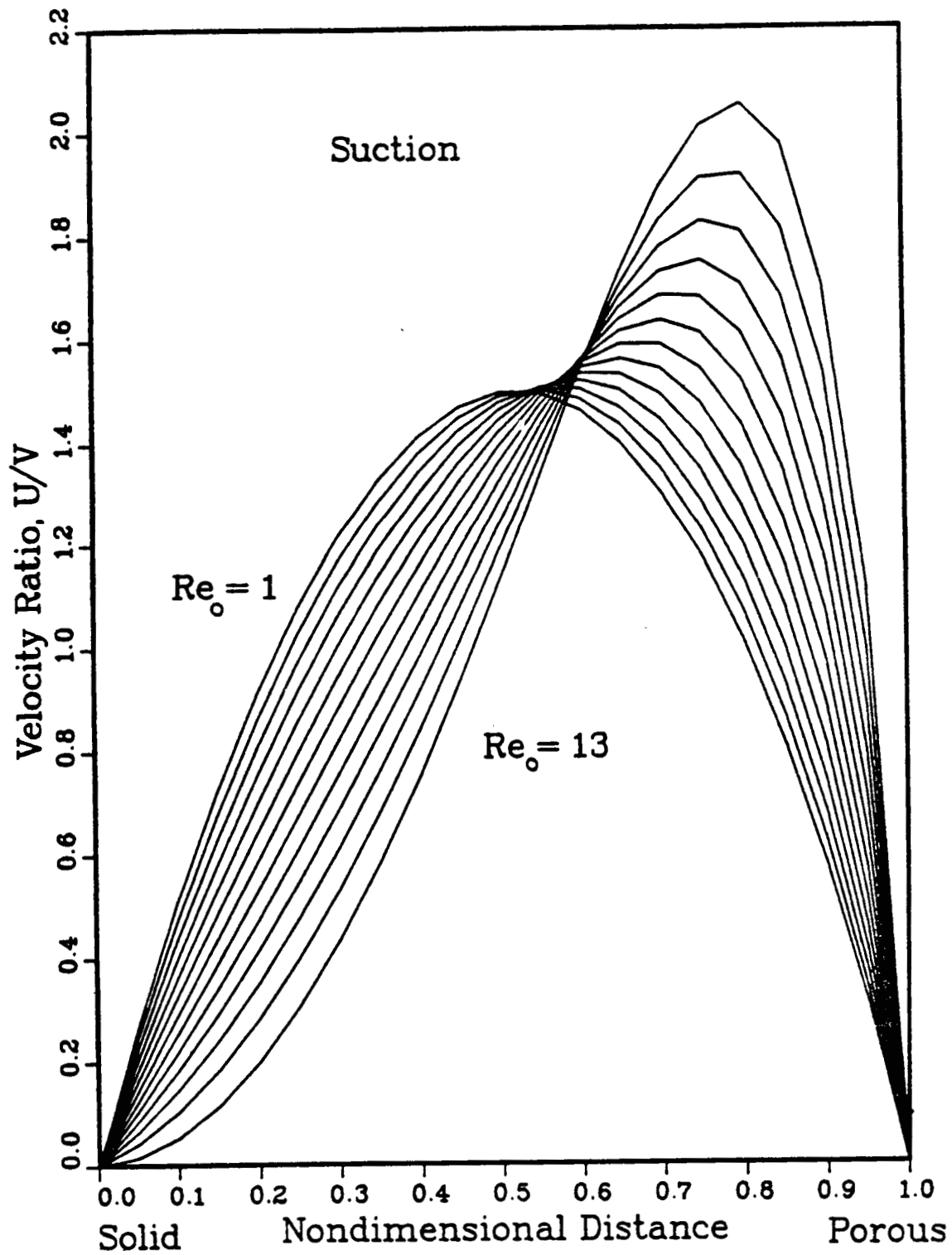


Figure 4.3. Velocity profiles for wall suction in a semiporous channel.

4.3 Compressible vapor flow analysis

Steady, compressible, one-dimensional, laminar flow in a heat pipe is considered. The principal governing equations for mass, momentum, and energy are formulated by using the average velocity as described in Chapter 2. This velocity is approximated from velocity distributions based on the similarity solution of semiporous channels. Shear stress at the interface, and the momentum and energy factors are similarly calculated and shown in Figure 4.4.

The fluid in the vapor passage of the heat pipe is assumed to be a mixture of liquid and monatomic vapor. Thus, the quality of the vapor is considered. The specific volume v and the enthalpy h are expressed as

$$v = v_f + X_q \times (v_g - v_f) \quad (4.16)$$

$$h = h_f + X_q \times h_{fg} \quad (4.17)$$

The specific volume of the saturated vapor can be approximated by

$$v_g = \frac{R_u T}{P M} \quad (4.18)$$

Also, the temperature and pressure are related by the Clausius-Clapyron equation:

$$\frac{dP}{P} = \frac{h_{fg} M}{R_u} \frac{dT}{T^2} \quad (4.19)$$

where h_{fg} is the enthalpy of vaporization, v_f and v_g are the specific volume of saturated liquid and vapor, respectively, and X_q is the vapor quality.

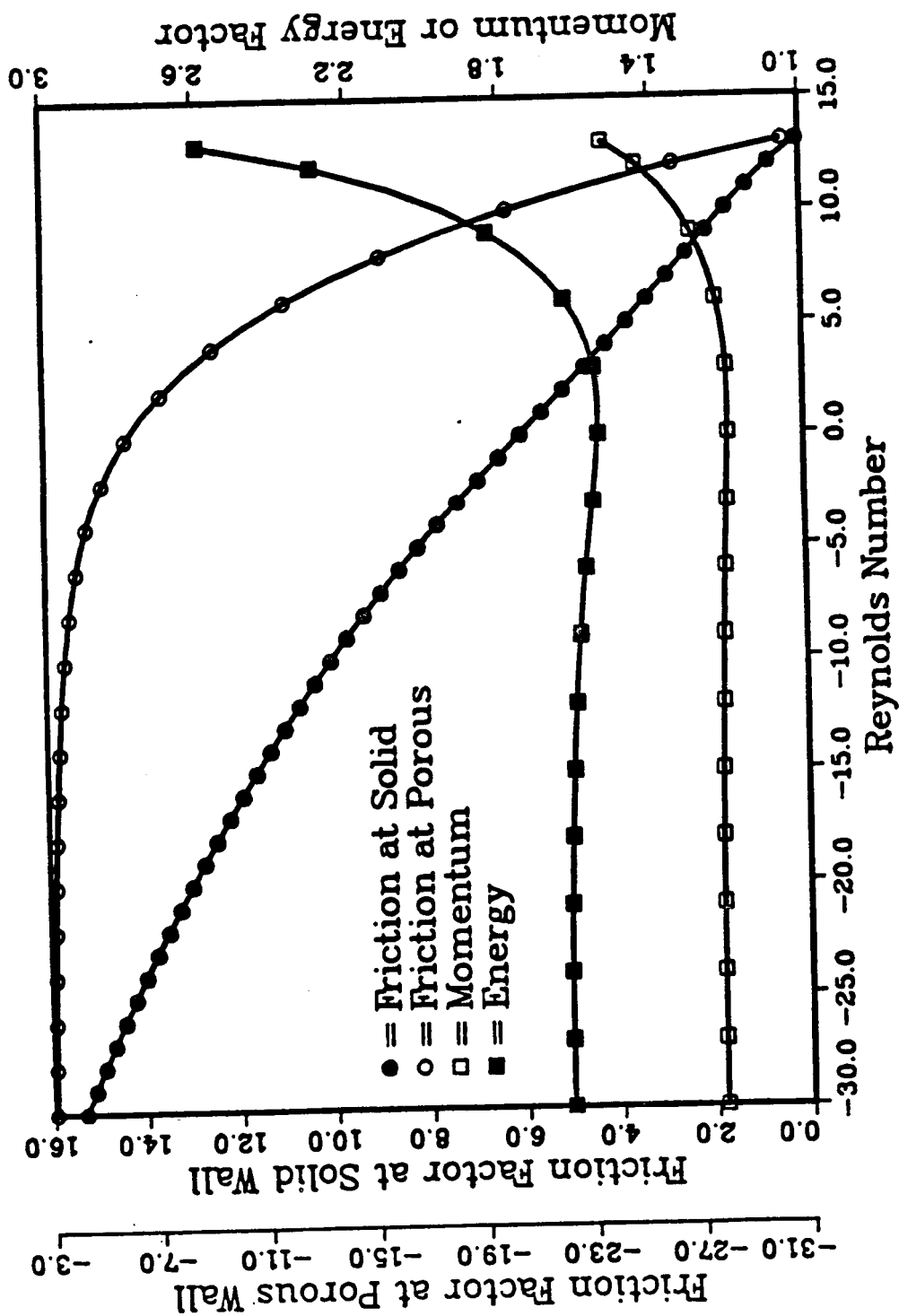


Figure 4.4. Variations of friction, momentum and energy factors, with wall Reynolds number.

4.3.1 Formulation of differential equations

Bankston and Smith[17] showed that variation of the momentum and energy factors with axial distance and radial Reynolds number is very small except near the end of the heat pipe. Figure 4.4 shows that both M_f and E_f are nearly independent of the radial Reynolds number except near separation. These results are taken from the similarity solution for semiporous channels. Therefore, it is assumed that the derivatives of M_f and E_f with respect to chordwise distance are equal to zero. In addition, assuming v_f and h_{fg} are constant quantities, and combining Equations(2.15) through (2.21) and Equations(4.16) through (4.19) yields the chordwise gradients for the density, quality, velocity, pressure, and temperature.

4.3.1.1 Density

The differentiation of Equation(4.18) with respect to S gives

$$\frac{dv_g}{dS} = -\frac{v_g}{P} \frac{dP}{dS} + \frac{v_g}{T} \frac{dT}{dS} \quad (4.20)$$

Substitution of Equation(4.19) into the equation above yields

$$\frac{dv_g}{dS} = \frac{v_g}{P} \left[\frac{R_u T}{h_{fg} M} - 1 \right] \frac{dP}{dS} \quad (4.21)$$

The derivative of the mixture specific volume in the S-direction is written as

$$\frac{dv}{dS} = \frac{dv_f}{dS} + (v_g - v_f) \frac{dX_q}{dS} + X_q \left[\frac{dv_g}{dS} - \frac{dv_f}{dS} \right] \quad (4.22)$$

With the prescribed assumption for v_f , substitution of Equation(4.21) into Equation(4.22) results in

$$\frac{dv}{dS} = (v_g - v_f) \frac{dX_g}{dS} + \frac{v_g X_g}{P} \left[\frac{R_u T}{h_{fg} M} - 1 \right] \frac{dP}{dS} \quad (4.23)$$

The derivative of specific volume and density are related as follows:

$$\frac{d\rho}{dS} = -\frac{1}{v^2} \frac{dv}{dS} \quad (4.24)$$

From Equations(4.23) and (4.24), the expression for density in differential form can be written as

$$\frac{d\rho}{dS} = -\frac{1}{v^2} \left[(v_g - v_f) \frac{dX_g}{dS} + \frac{v_g X_g}{P} \left(\frac{R_u T}{h_{fg} M} - 1 \right) \frac{dP}{dS} \right] \quad (4.25)$$

4.3.1.2 Quality

From Equation(4.23), the quality gradient is expressed as

$$\frac{dX_g}{dS} = \frac{1}{(v_g - v_f)} \left[\frac{dv}{dS} + \frac{v_g X_g}{P} \left(1 - \frac{R_u T}{h_{fg} M} \right) \frac{dP}{dS} \right] \quad (4.26)$$

Substitution of Equation(4.24) and the equations for conservation of mass, Equation(2.15), and momentum,Equation(2.16), into Equation(4.26) yields

$$\begin{aligned} \frac{dX_g}{dS} = \frac{v^2}{(v_g - v_f) V^2} \left\{ \left[-\frac{1}{M_f} + \frac{V^2 X_g v_g}{P v^2} \left(1 - \frac{R_u T}{h_{fg} M} \right) \right] \frac{dP}{dS} - \frac{F V^2}{8 D v M_f} \right\} \\ - \frac{v^2}{(v_g - v_f)} \frac{2 \dot{m}_o}{DV} \end{aligned} \quad (4.27)$$

4.3.1.3 Velocity

The equation for conservation of mass,Equation(2.15), can be expressed as follows:

$$\frac{dV}{dS} = \frac{v\dot{m}_o}{D} + \frac{V}{v} \frac{dv}{dS} \quad (4.28)$$

Substitution of Equation(4.23) into the expression above gives

$$\frac{dV}{dS} = \frac{v\dot{m}_o}{D} + \frac{V(v_g - v_f)}{v} \frac{dX_g}{dS} + \frac{VX_g}{P} \frac{v_g}{v} \left(\frac{R_u T}{h_{fg} M} - 1 \right) \frac{dP}{dS} \quad (4.29)$$

4.3.1.4 Pressure

With the previously mentioned assumptions, substitution of the energy Equation(2.17) into the momentum Equation(2.16) yields

$$\frac{dP}{dS} - \frac{M_f \rho}{E_f} \frac{dh}{dS} - \frac{M_f \dot{m}_o}{E_f V D} \left(h - h_o - \frac{E_f V^2}{2} - \frac{V_o^2}{2} \right) = - \frac{F \rho V^2}{8D} \quad (4.30)$$

In order to obtain an expression for the derivative of the vapor enthalpy, differentiation of Equation(4.17) is taken with respect to S, and Equation(4.19) is substituted:

$$\frac{dh}{dS} = h_{fg} \frac{dX_g}{dS} + \frac{c_p R_u}{h_{fg} M} \frac{T^2}{P} \frac{dP}{dS} \quad (4.31)$$

After the expressions for the derivative of the enthalpy and quality are substituted into Equation(4.29), the pressure gradient can be expressed as follows:

$$\frac{dP}{dS} = \frac{-\frac{M_f \dot{m}_o}{E_f V D} \left[2h_{fg} + \frac{v_g - v_f}{v} \left(h_o - h + \frac{E_f V^2}{2} + \frac{V_o^2}{2} \right) \right] - \frac{1}{E_f} \frac{h_{fg}}{v} \frac{F}{8D} - \frac{v_g - v_f}{v^2} \frac{F V^2}{8D}}{\frac{v_g - v_f}{v} + \frac{1}{E_f} \frac{h_{fg}}{V^2} - \frac{M_f}{E_f} \frac{h_{fg} X_g}{P} \frac{v_g}{v^2} \left(1 - \frac{R_u T}{h_{fg} M} \right) - \frac{M_f}{E_f} \frac{v_g - v_f}{v^2} \frac{c_p R_u}{h_{fg} M} \frac{T^2}{P}} \quad (4.32)$$

4.3.1.4 Temperature

The temperature gradient is derived from the Clausius-Clapyron equation, Equation(4.19), as follows:

$$\frac{dT}{dS} = \frac{R_u T^2}{h_{fg} M P} \frac{dP}{dS} \quad (4.33)$$

CHAPTER V

COMPUTATIONAL PROCEDURES

5.1 Transient conduction equation with phase change

The algorithm proceeds similarly to most finite element method procedures. First, the element data are generated by a grid generation program. This data consists of the coordinates of the nodal points of each element, by element, and the properties and boundary conditions for each element. Based on this data, the capacitance matrices, $[C]$, and the conductance matrices, $[K_c]$, related to the time derivative of nodal temperatures and conduction, are calculated for each element. The conductance matrices, $[K_h]$ and $[K_r]$, and the vectors $\{F_q\}$, $\{F_h\}$, and $\{F_r\}$ for specified surface heating, convection, and radiation boundary conditions, are computed only for elements having the boundary conditions above. These boundary conditions may be time dependent, so these matrices and vectors must be evaluated based on the appropriate temperatures. For an implicit time step, the iteration scheme is such that temperatures are initially assumed, and the proper value of θ is chosen to obtain stable and accurate results. In this study, $\theta = \frac{1}{2}$ or 1 is used, so iterations are required within each time step. However, for an explicit time step, such as the Dupont scheme, the element temperatures for the previous step are involved in obtaining the matrices and vectors related to the boundary conditions. Then, these element matrices and vectors are assembled into the global matrices for the entire solution domain, and the full set of equations may be written in matrix form as

$$[AM]\{T\} = \{RM\} \quad (5.1)$$

where $[AM]$ represents the banded coefficient matrix, $\{T\}$ denotes a column matrix of unknown temperatures, and $\{RM\}$ is the column matrix of constants. If temperatures are specified on some boundary surfaces, these boundary conditions must be incorporated into the global matrices as described in reference[55].

Once the global matrices have been assembled, they are solved by using Choleski decomposition. Choleski's method[56] has the advantage of being simpler and easier to implement than other elimination methods. It may also be used to advantage for storage in the computer by overlaying the upper and lower triangular matrices in the same storage location($[AM]$ matrix).

The system of Equations(3.25) for the implicit method or (3.26) for the explicit method is then marched forward in time. Among the various iteration schemes, the Newton-Raphson method is used for the implicit method because of its fast convergence. For the explicit method, iteration is not required, but it is not a self-starting scheme, so the implicit method is employed for the first few time steps. When temperatures at two previous time steps are known, the explicit method can be marched forward. The algorithm flowchart is shown in Figure 5.1.a.

5.2 Compressible vapor flow

The five dependent variables: density, quality, velocity, pressure, and temperature, are coupled by differential Equations(4.25), (4.27), (4.29), (4.32), and (4.33), which are first order, nonlinear, ordinary differential equations. A computer code has been written to numerically solve these equations simultaneously using the Runge-Kutta integral method, which needs only proper boundary conditions for

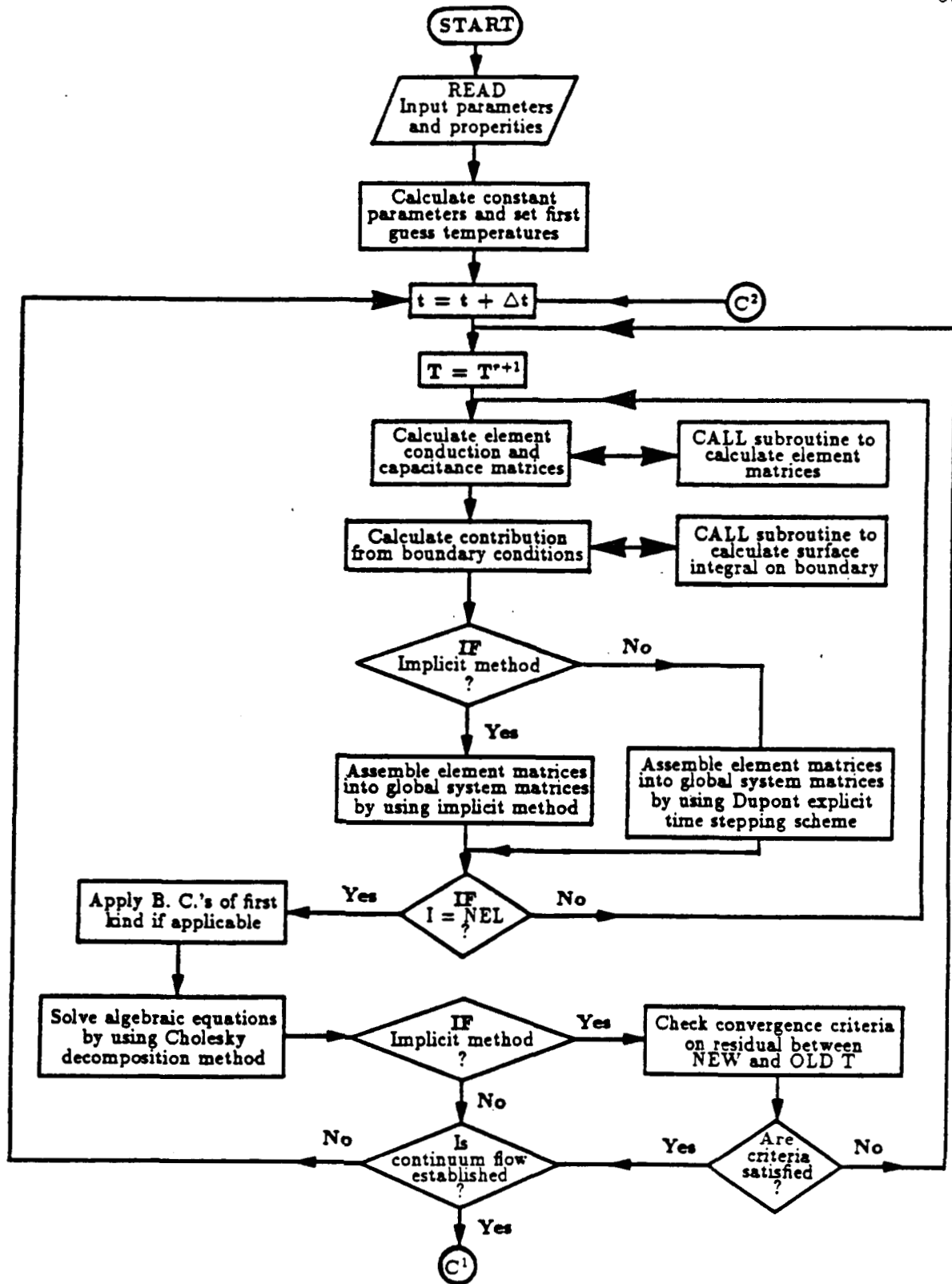


Figure 5.1.a Algorithm flowchart.

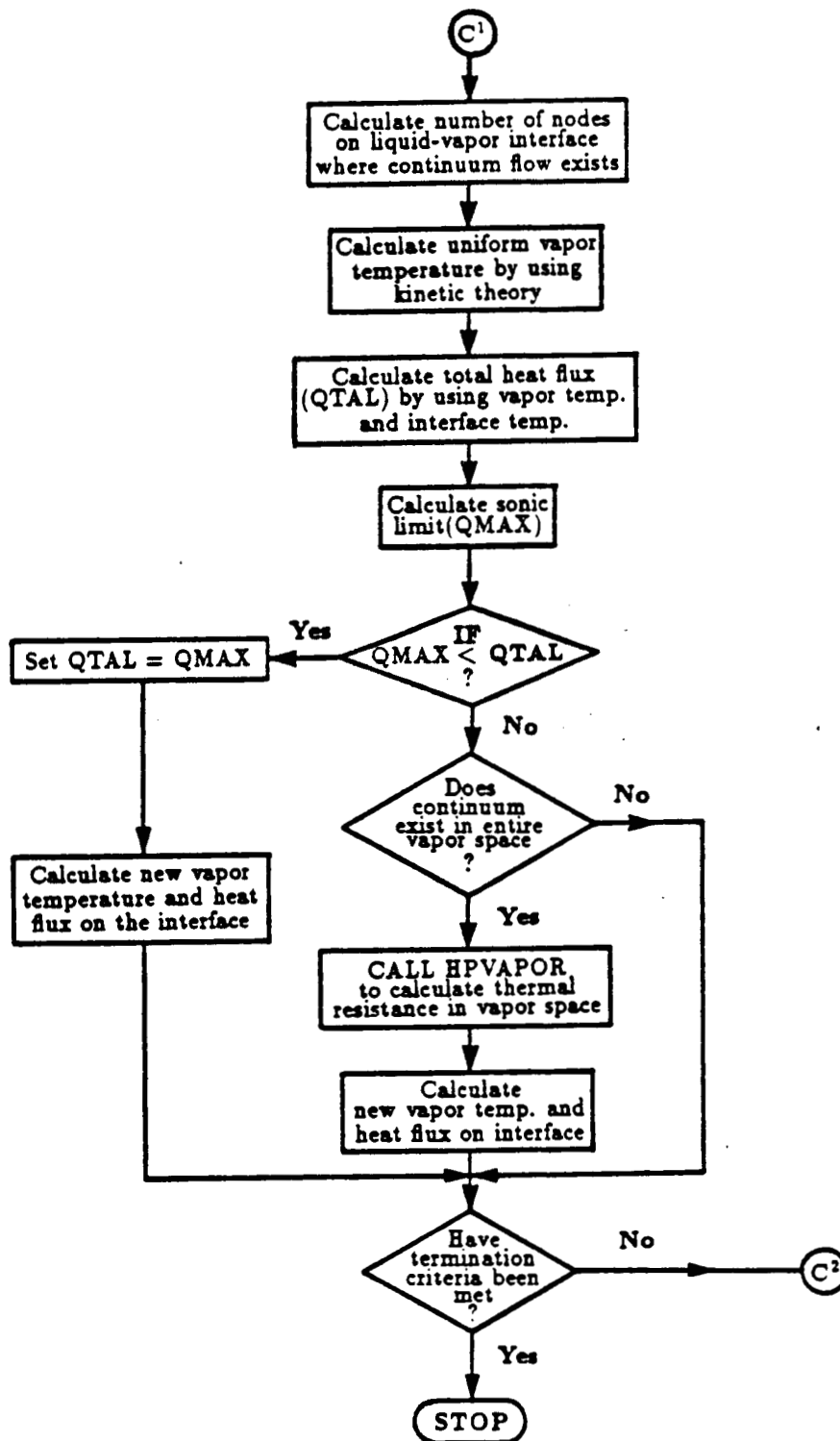


Figure 5.1.b Algorithm flowchart.

ORIGINAL PAGE IS
OF POOR QUALITY

the first step of integration.

Since the velocity term appears in the denominator of Equation(4.32), the physical boundary condition for velocity cannot be used directly. To avoid this problem, proper boundary conditions at the upstream end of the evaporator are determined for initiating all calculations as follows: a new boundary condition for the velocity is determined a short distance away from the beginning of the evaporator, assuming incompressible and saturated vapor flow at the temperature corresponding to the heat pipe operating temperature. Saturation pressure is used for the pressure. Since the velocity is small at this point close to the upstream end of the evaporator, boundary conditions determined this way are realistic. The differential equations are solved using these boundary conditions.

5.3 Coupling vapor flow effects

When the Mach number is less than about 0.2, compressibility is neglected, and friction effects at the interface may be negligible due to the low velocity of the vapor. Thus, most studies of heat pipe performance[5,23-25] assumed that the temperature is uniform throughout the vapor space. This approximation eliminates difficulties encountered in solving the vapor flow dynamics, and gives simple results for low operating temperatures with small heat fluxes. When the vapor temperature is uniform in the vapor space, no thermal resistance exists, so a maximum amount of energy can be transferred through the vapor space for a given operating condition.

The energy stored in the vapor space is negligible due to low density, so the energy entering the evaporator is equal to the that leaving the condenser. Equation(2.12), which describes evaporation and condensation, is applied to every element at the interface, and the energy balance in the vapor space is:

$$\sum_{i=1}^{m_e} \left[\frac{P_{fi}}{\sqrt{T_{fi}}} - \frac{P_g}{\sqrt{T_g}} \right] \Delta L_i = \sum_{i=1}^{m_c} \left[\frac{P_{fi}}{\sqrt{T_{fi}}} - \frac{P_g}{\sqrt{T_g}} \right] \Delta L_i \quad (5.2)$$

where m_e is the number of elements at the interface in the evaporator, m_c is the number of elements in the condenser, and ΔL_i is the side length of an element at the interface. Equation(5.2) can be solved by iteration to obtain the uniform vapor temperature, as long as the temperature at the interface is known. The heat flux at the interface is evaluated using Equation(2.12) with known temperatures.

However, when liquid metal is used as the working fluid, and the heat flux applied to the surface is large, the velocity of the vapor is large, so the temperature drop in the vapor space should be considered. The temperature drop in the vapor region implies that the thermal resistance allows less energy to be transferred from the evaporator to the condenser. Thus, the evaporator temperature is higher, and the condenser temperature is lower, than in the uniform vapor temperature case.

When vapor flow dynamics is coupled with the heat pipe shell and capillary structure at the interface, the governing equations are solved simultaneously with unknown boundary conditions at the interface. Iterations are required for every time step until both results match at the interface. This method may yield accurate results, but in general consumes much computational time, due to iteration. Also convergence may not be reached. Hence, an approximation method is employed to eliminate these difficulties.

Instead of simultaneously solving governing equations for both regions, governing equations for the vapor region are separately solved with a given heat flux, so that the temperature drop, ΔT_g , can be obtained. The thermal resistance, R_g , in the vapor space may then be evaluated from Equation(5.3):

$$Q = \frac{\Delta T_g}{R_g} \quad (5.3)$$

In order to obtain the thermal resistance, the total heat flow rate is needed. But without solving both governing equations, the heat flow rate is also unknown. Thus, the known heat flow rate at the previous time step is used, and the heat flow rate evaluated at the present time step is used at the next time step.

Coupling of the evaporator and condenser sections becomes very difficult when vapor temperature changes along the length of the vapor section. An approximate coupling method is used here which accounts for thermal resistance in the vapor region but which uses a constant vapor temperature. Since the total heat transfer rate through the vapor space, which is computed by using Equation(2.12), is the same as the heat input at the liquid-vapor interface in the evaporator or heat output at the interface in condenser, a certain fictitious layer, which has the same thermal resistance as that evaluated in the vapor space, may be placed at the liquid-vapor interface. Thus, the temperature at the new interface in the evaporator is lower than that at the true interface, due to the resistance in the fictitious layer, and vice-versa for the condenser. With this coupling technique the heat fluxes are correct throughout the pipe and vapor thermal resistance is taken into account.

In order to compute the uniform vapor temperature, the temperatures at the new interface are used for $T_{f,i}$ in Equation(5.2), and the heat flux at the interface is calculated by using Equation(2.12) with the uniform vapor temperature and the temperatures at the new interfaces. This heat flux then serves as the boundary condition at the liquid-vapor interface when solving the governing equations for the heat pipe shell, capillary structure, and vapor flow at the next time step. By using this approximation scheme, iterations can be excluded, while vapor flow effects are

retained.

5.4 Overall computational procedures

Since the working fluid of the heat pipe is initially in the solid state and the wick structure is saturated, the transient conduction equation is applied to the heat pipe shell and wick structure. The variable heat flux and radiation boundary condition are considered on the outside surface of the heat pipe. The adiabatic boundary condition is used at the liquid-vapor interface, due to the vacuum in the vapor space, until the nodal temperatures at this interface are greater than the transition temperature (700 K). The implicit method is used for the first ten time steps, and then the explicit method is employed using a time step of 10 seconds.

When the temperatures of the first two nodes at the liquid-vapor interface are greater than 700 K, Equation(5.2) is solved for the vapor temperature by using the Newton-Raphson method. Then, the heat fluxes are calculated using Equation(2.12) with the known interface and vapor temperatures. These heat fluxes are to be used as boundary conditions at the interface for the next time step. However, the adiabatic boundary condition is still applicable for the rest of the interface. From then on, a small time step is used to obtain stable startup. These procedures continue until the heat transport in the chordwise direction is less than the sonic limit.

When the sonic limit is encountered, the total heat transport through the vapor space should equal the sonic limit, and Equation(2.14) is solved for the vapor temperature. The heat fluxes at the interface in the evaporator are calculated by using this vapor temperature and the nodal temperatures at the interface. Then the heat fluxes for the condenser are evaluated in proportion to nodal temperatures which are greater than 700 K. Again, these heat fluxes are used to solve the transient

conduction equation for the heat pipe shell and wick structure. This scheme is effective until the entire vapor space achieves continuum flow and the heat transport in the chordwise direction is less than the sonic limit.

When the sonic limit is not encountered, Equations(4.25), (4.29), (4.32), and (4.33), which are first order, nonlinear, ordinary differential equations for compressible vapor flow dynamics, are solved to evaluate the thermal resistance in the vapor space, as stated in section 5.3. This computational scheme is used until the desired operating temperature, or the steady state condition, is reached. Figures 5.1.a and 5.1.b schematically shown the computational procedures.

Since any implicit scheme is excluded, except the first few steps to provide initial conditions for the explicit method, time steps are gradually decreased from 0.5 seconds to the order of milli-seconds to maintain a stable condition at the liquid-vapor interface. The computer code is successively tested against the given physical model by following these procedures.

CHAPTER VI

RESULTS AND DISCUSSION

6.1 Transient conduction and phase change

To verify the finite element formulation and algorithm, computed numerical solutions are compared with available solutions, such as analytical and other approximate solutions.

6.1.1 Temperature of a semi-infinite body

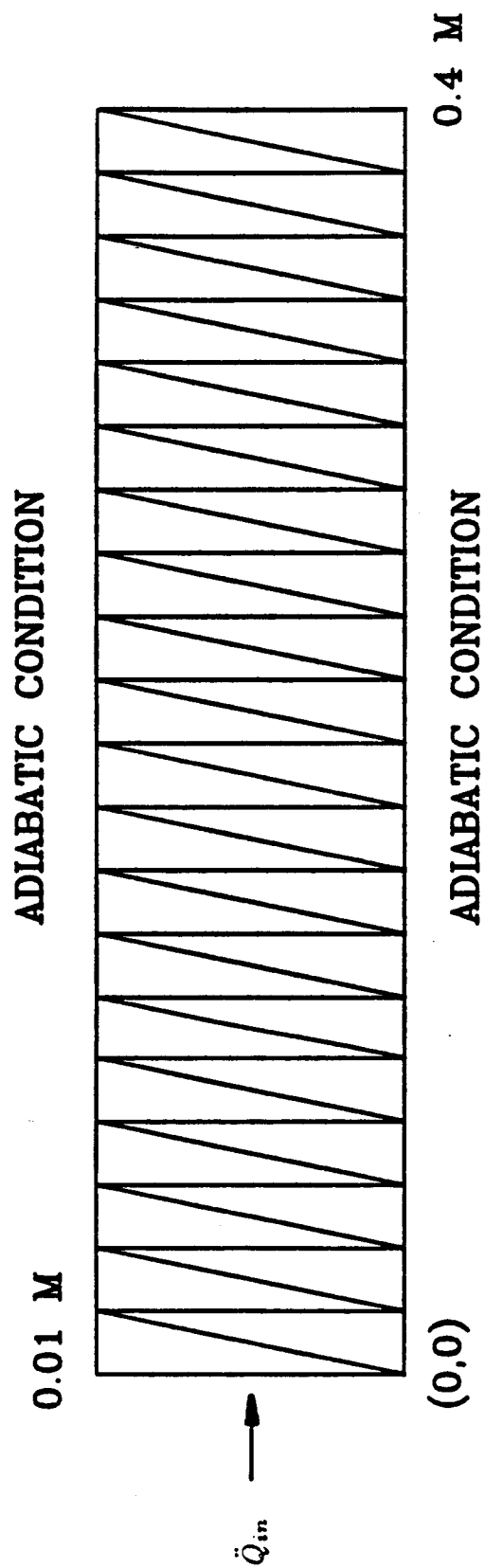
This case involves pure conduction of heat, without phase change, over a semi-infinite body. It is solved as a two-dimensional problem, shown in Figure 6.1. Adiabatic boundary conditions are assumed throughout, but at the surface ($X = 0$), the constant heat flux ($\ddot{Q} = 100kW/m^2$) is imposed to heat the surface while the initial sodium temperature of 293 K is uniform. The conductivity and specific heat are assigned constant values for sodium.

The exact solution to this problem was given by Luikov[57] as

$$T(X,t) = \frac{2\ddot{Q}}{K} \sqrt{\alpha t} \left[\frac{1}{\sqrt{\pi}} \exp\left(\frac{-X^2}{4\alpha t}\right) - \frac{X}{2\sqrt{\alpha t}} \operatorname{erfc}\left(\frac{X}{2\sqrt{\alpha t}}\right) \right] + T_0 \quad (6.1)$$

where $\alpha = \frac{K}{\rho c_p}$

For the numerical solution, an explicit time stepping scheme is used with an implicit method for starting. A time step of 5 seconds is used, and numerical calculations are terminated as the temperature of the last node starts to change from the initial temperature. Numerical results are compared to the analytical solution in Figure 6.2. The results yield excellent agreement.



$$K = 93.0 \text{ W/m K}$$

$$C = 2.57 \times 10^6 \text{ J/m}^3 \text{ K}$$

Figure 6.1. Finite element mesh for the transient conduction heat transfer problem.

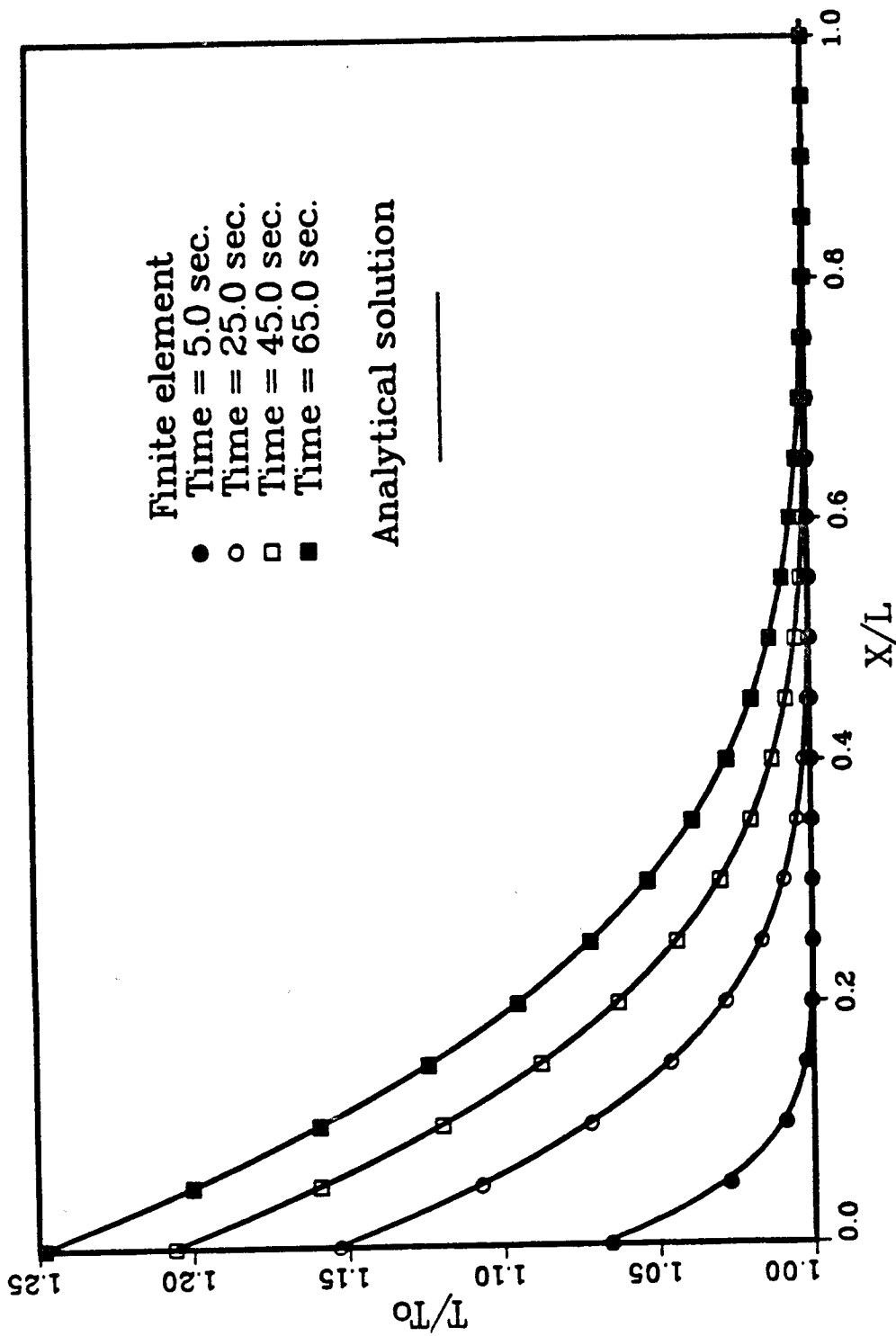


Figure 6.2. Semi-Infinite domain temperature distributions.

6.1.2 Convection and radiation boundary conditions

This example tests the ability of the numerical method to handle convection and radiation boundary conditions. The same grid system shown in Figure 6.1 is used, but the boundary condition on the surface at $X = 0$ is replaced. For a Biot number of 1.0, three different cases are examined. First, only a convection boundary condition ($\beta = 0.0$) is applied to the surface, and an initial temperature of 1650 K is used. Next, convection and radiation boundary conditions ($\beta = 1.0$) are applied to the surface with the same initial temperature. Finally, an initial temperature of 2650 K, which is greater than the previous two cases, is used for $\beta = 4.0$. In these tests, phase change is not involved, and the properties of sodium are used for specific heat and conductivity.

An analytical solution for this case is not available except for one having only a convection boundary condition, so the numerical results are compared with probability solutions which Sheikh and Sparrow[58] found for the same cases. As shown in Figure 6.3, temperatures at the boundary surface and opposite end are plotted versus time. The results show good agreement.

6.1.3 Phase change of sodium

In this example, sodium is used as the phase change material for two-dimensional region as shown in Figure 6.4. An initial temperature of 393 K is used. The ratio of diffusivities of solid and liquid phases is assumed to be one to compare with the existing solution. Boundary conditions ($T_s = 293$ K) of the first kind are imposed on the surfaces. Since specified temperature boundary conditions are suddenly imposed on the surface, the temperature gradient in this region is infinite, which causes unstable conditions. This difficulty may be eliminated by introducing

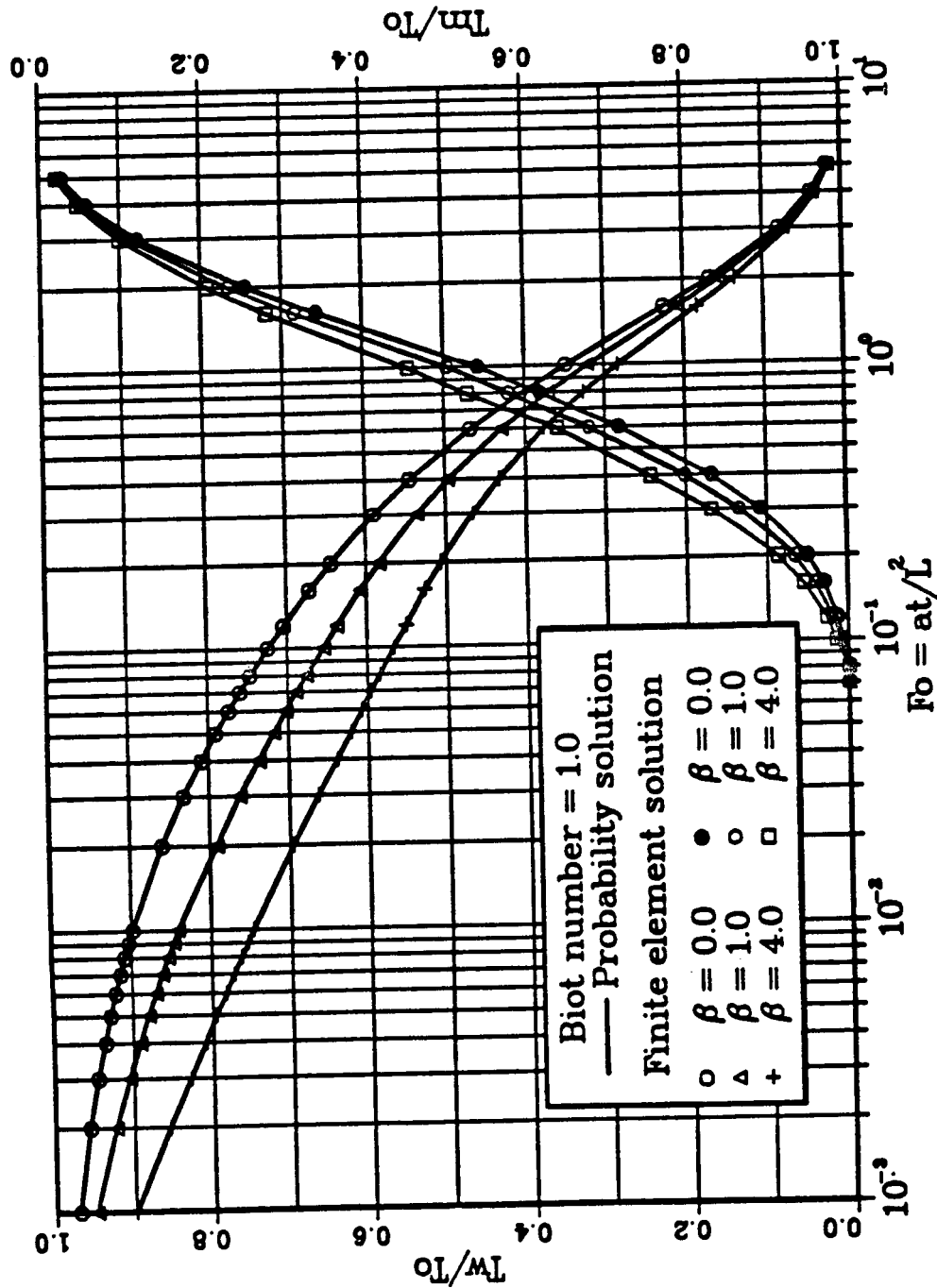


Figure 6.3. Comparison of convection and radiation boundary conditions.

ORIGINAL PAGE IS
OF POOR QUALITY

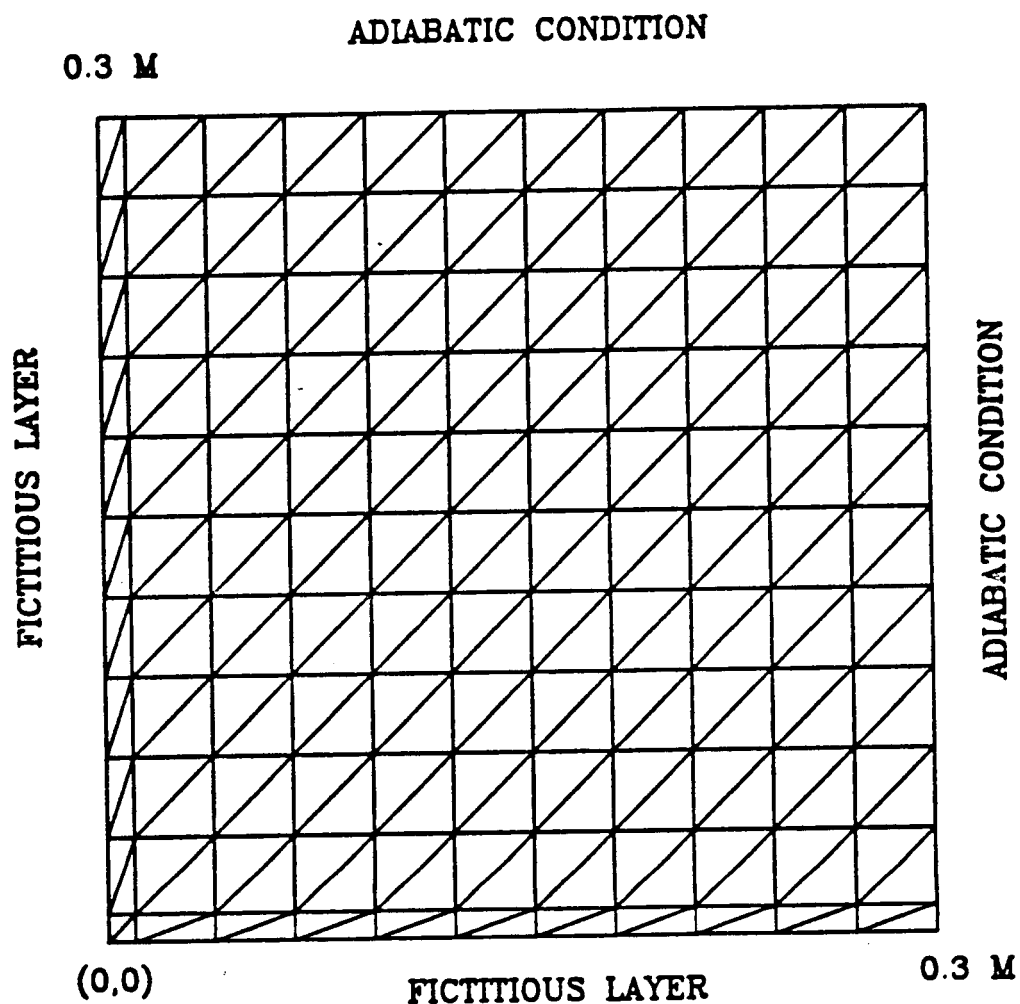


Figure 6.4. Two-dimensional mesh used to represent a corner region: 242 elements,
144 nodes.

a layer of fictitious elements with negligible thermal storage capacity and very high conductivity, such that the temperature gradient at this region artificially becomes finite. For this purpose, numerical values of the thermophysical properties of the fictitious layer are chosen as follows:

$$\rho c_p = 1.26 \times 10^4 J/m^3 K$$

$$K = 4.19 \times 10^3 W/mK$$

Two different time stepping schemes, the fully implicit method and the explicit method, are employed to compare the computational time and results. A time step of 5 seconds is used. For the two-dimensional case, the position of the interface is compared with an approximate solution given by Rathjen and Jiji[59]. This solution assumes that the ratio of diffusivities of solid and liquid is unity, and that the interface at points beyond three times of the one-dimensional interface in X and Y directions is the same as the one-dimensional interface position. Both numerical solutions for explicit and implicit methods are directly compared with the approximate solution, and good agreement is obtained for early time steps, as shown in Figure 6.5. As time passes, the position of the interface given by numerical results advances further than for the approximation, and the interface lines obtained from the approximate are not perpendicular to the boundary surface. According to assumptions made by Rathjen and Jiji, adiabatic boundary conditions for the approximate solution can be located beyond the present solution domain at certain time steps. However, the numerical calculations use adiabatic boundary conditions, so that all heat is used for phase change, while the approximate solution does not match the same boundary condition within the solution domain. This explains why the positions of the two interfaces are different.

Numerical results predicted by the explicit method using an implicit scheme for

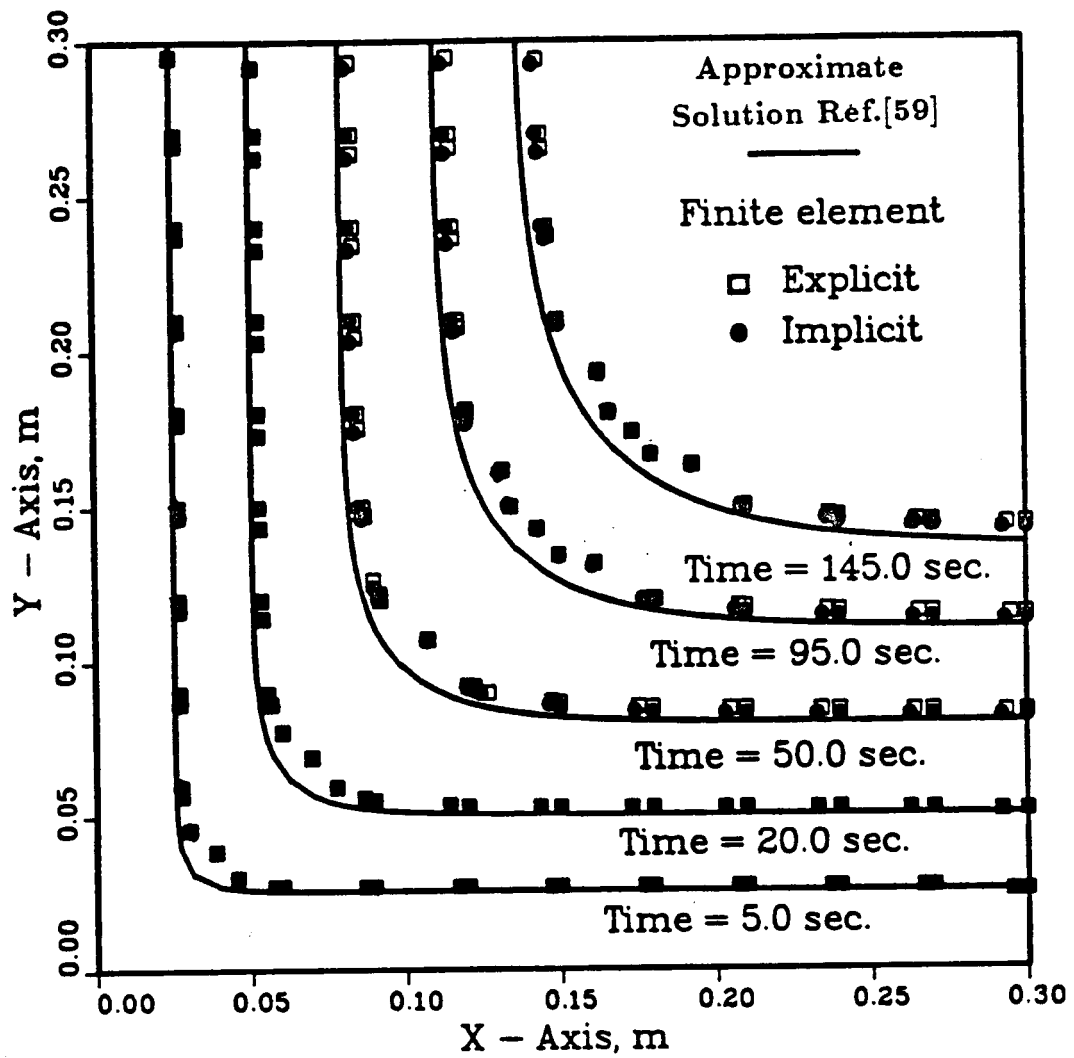


Figure 6.5. Solidification of sodium in a corner region: position of the interface at different times.

a few initial time steps are close to those of the fully implicit scheme and the explicit method consumes much less computational time, since iterations are eliminated.

Even though the numerical solutions do not exactly match the approximate solutions, because of different boundary conditions, general trends in the numerical results and the usefulness of the explicit time stepping scheme are verified.

6.2 Compressible vapor flow

To test the differential formulations and algorithm for vapor flow, the numerical solutions are compared to other numerical results[18] for cylindrical heat pipes with sodium as the working fluid, since data for a flat plate heat pipe are not available. The two-dimensional mass, momentum, and energy conservation equations, which were transformed in terms of the stream function, vorticity and enthalpy, were solved numerically. The dimensions of this cylindrical heat pipe are: total length of 0.6 m, evaporator length of 0.2 m, condenser length of 0.3 m, and inside radius of 0.0086 m. Since variation of temperature and pressure in the axial direction for low heat input is small, two different operating conditions are selected. One has an operating temperature of 818 K with a uniformly distributed heat input of 610 watts. Another has an operating temperature of 841 K with a heat input of 1265 watts.

To match the results for the rectangular heat pipe to that for the cylindrical heat pipe, the rectangular cross-section of the vapor space is modeled such that the cross-section area is the same as for the cylinder, and the hydraulic radius is close to the radius of cylinder. Also, the same heat input is applied to yield the same velocity and a similar Reynolds number in the axial direction, and the same length for each section is used. The wall Reynolds number at the condenser must be less than 14 to use the results of the similarity solution. Therefore, two different cross

sections are chosen. For high heat flux, the wall Reynolds number cannot be less than 14 so that a square of 0.0152 m is used and comparison is made only for the evaporator and adiabatic sections. For low heat flux, the cross section is chosen such that the wall Reynolds number at the condenser is close to the allowable maximum value. Thus, the cross section is rectangular with a width of 2.11 cm and a height of 1.1 cm, resulting in a wall Reynolds number of 13.4 in the condenser. Even though the two models do not match exactly, the effect of vapor flow may be simulated using these models.

One-dimensional numerical results of the flat plate heat pipe are compared with published two-dimensional numerical data for cylindrical heat pipes as shown in Figures 6.6 and 6.7. Pressure and temperature drops for the one-dimensional case are a little greater than those for the two-dimensional case, but overall agreement is good. For high heat flux, pressure variation with axial position is somewhat different for the two cases, but the total pressure drops are nearly the same. Temperature profiles agree well. Thus, as shown in Figures 6.6 and 6.7, one-dimensional differential formulations yield valuable results. The difficulties of solving two-dimensional governing equations are avoided.

To investigate various vapor effects, two other heat pipes with sodium as the working fluid were selected for analysis. One has an adiabatic section, the other does not. Dimensions of the heat pipes are shown in Table 6.1. Different operating temperatures were chosen so that temperature effects could be evaluated. For each operating temperature, various heat fluxes were considered. Since the similarity solutions used are valid only while wall Reynolds numbers are less than 14, the maximum heat flux on the condenser is chosen to satisfy this condition.

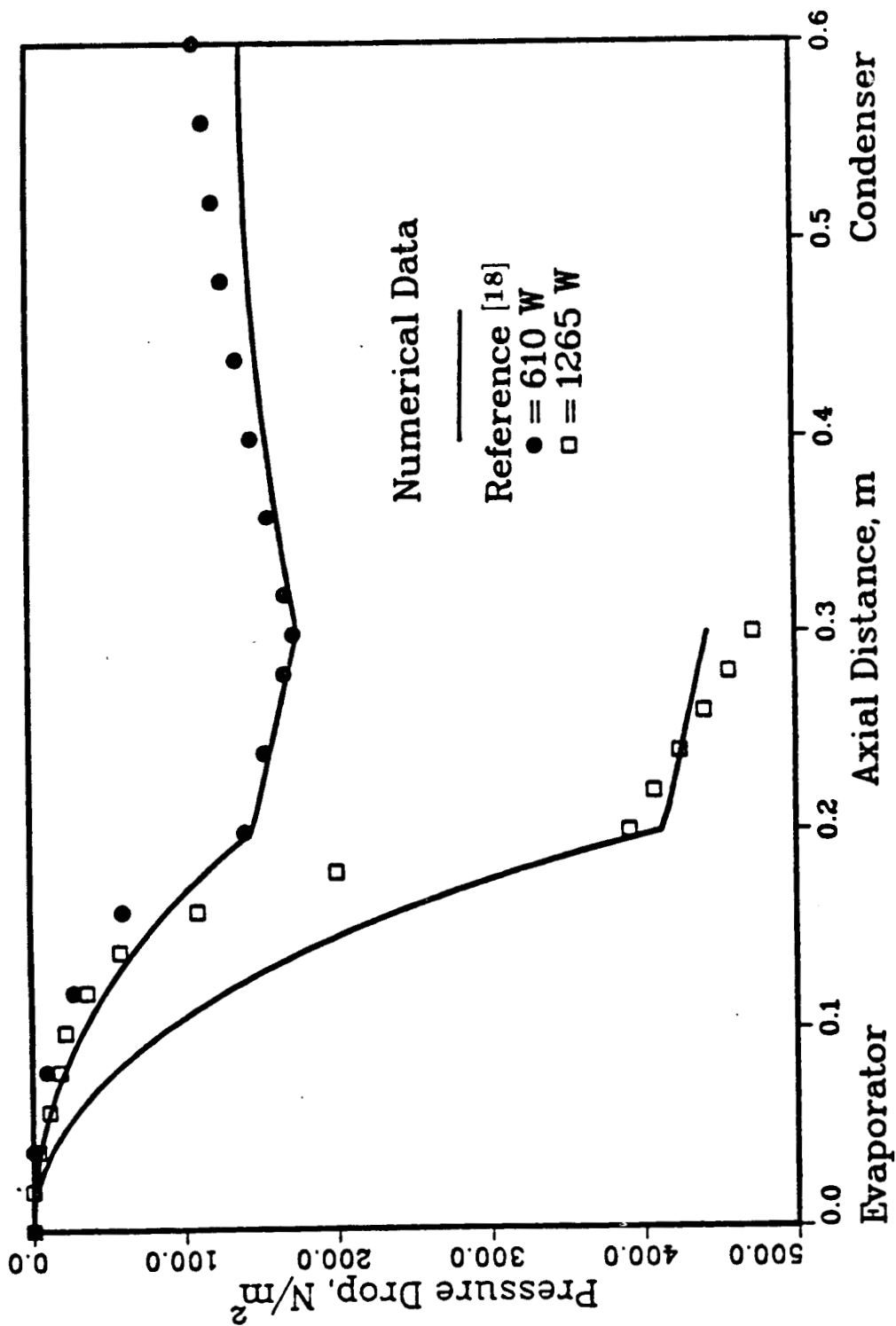


Figure 6.6. Comparison of axial variation of vapor pressures.

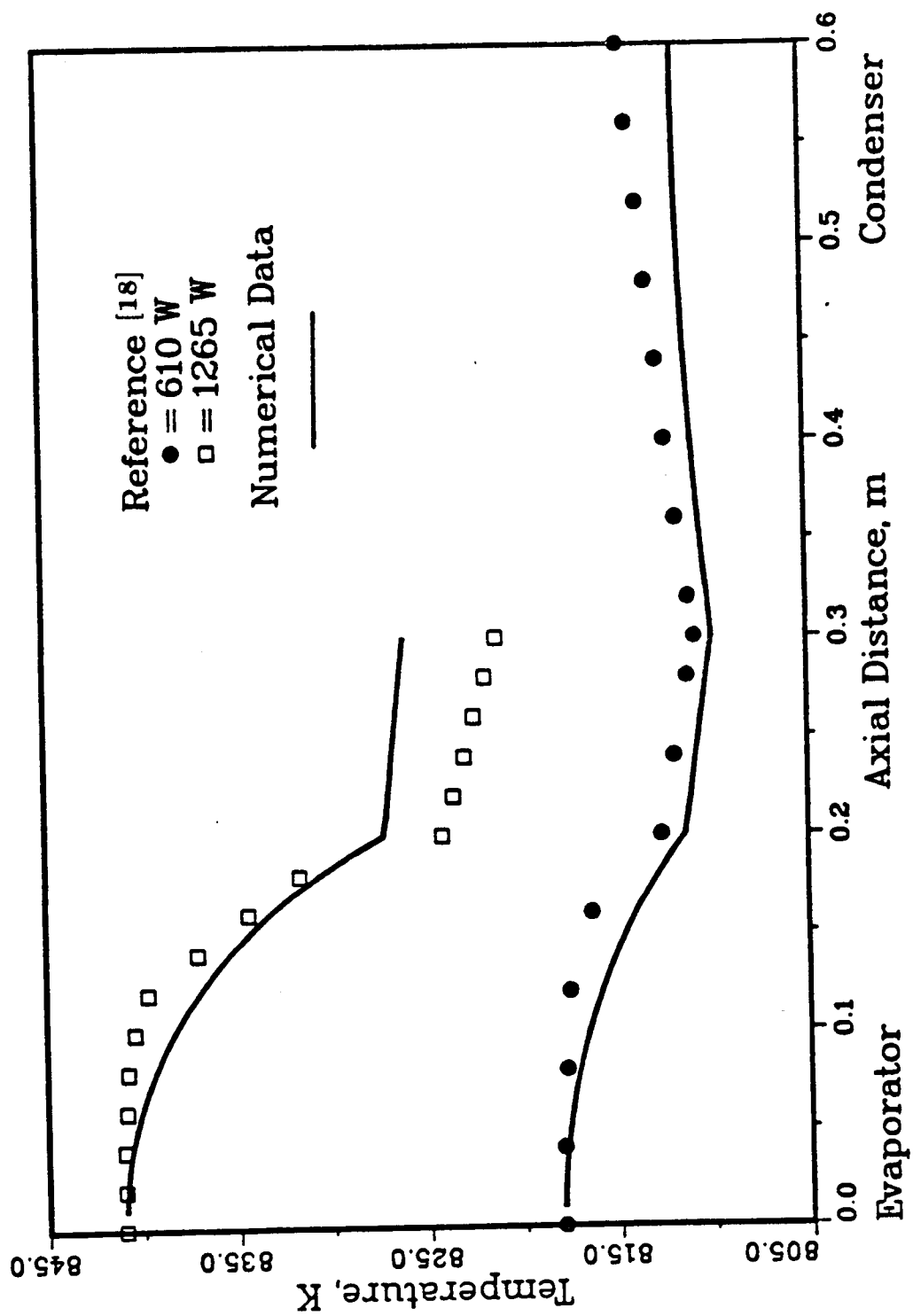


Figure 6.7. Comparison of axial variation of vapor temperatures.

Table 6.1. Description of heat pipes

| Dimension | 773 K | 808 K |
|--------------------------|-------|-------|
| L_e (cm) | 8.0 | 20.0 |
| L_a | 0.0 | 10.0 |
| L_c | 22.0 | 30.0 |
| D | 1.33 | 1.35 |
| W | 1.33 | 1.72 |
| A_o (cm ²) | 10.64 | 34.4 |

Figure 6.8 shows solutions for axial variation of vapor temperature, pressure, velocity, and density, as obtained from Equations(4.25), (4.27), (4.29), (4.32), and (4.33). An operating temperature of 773 K and a uniformly distributed heat transfer rate of 200 watts were used. Momentum equation(2.16) implies that variation of pressure in the axial direction depends on the relation between the contributions of inertia and friction. Thus, the pressure of the vapor in the evaporator falls sharply along the vapor passage due to friction and acceleration of the flow caused by the injection of mass. The corresponding temperature also drops sharply about 5.5 K. Since the density of sodium vapor is relatively low at low temperatures, the velocity is correspondingly large in order to transfer the required mass. Results show that the maximum Mach number reaches 0.3 at the exit of the evaporator.

In the condenser, extraction of mass tends to increase pressure because of decreasing velocity while friction tends to decrease pressure. Therefore, pressure cannot recover completely due to friction loss. Even though some temperature recovery is achieved in the condenser, the temperature at the end of the condenser is about 4.2 K less than that at the beginning of the evaporator. Figures 6.9, 6.10, and 6.11 show variations of temperature, pressure, and Mach number, respectively, corresponding to five different heat fluxes. At an operating temperature of 773 K, larger heat input leads to greater pressure and temperature drops, and to a higher Mach number. When the Mach number exceeds about 0.2, variation of the Mach number is large, due to expansion of the vapor. For heat inputs of 50 and 100 watts, the vapor can be assumed to be isothermal.

Figure 6.12 shows that heat transfer is limited to about 351 watts, because velocity at the end of the evaporator approaches the sonic velocity at this heat input.

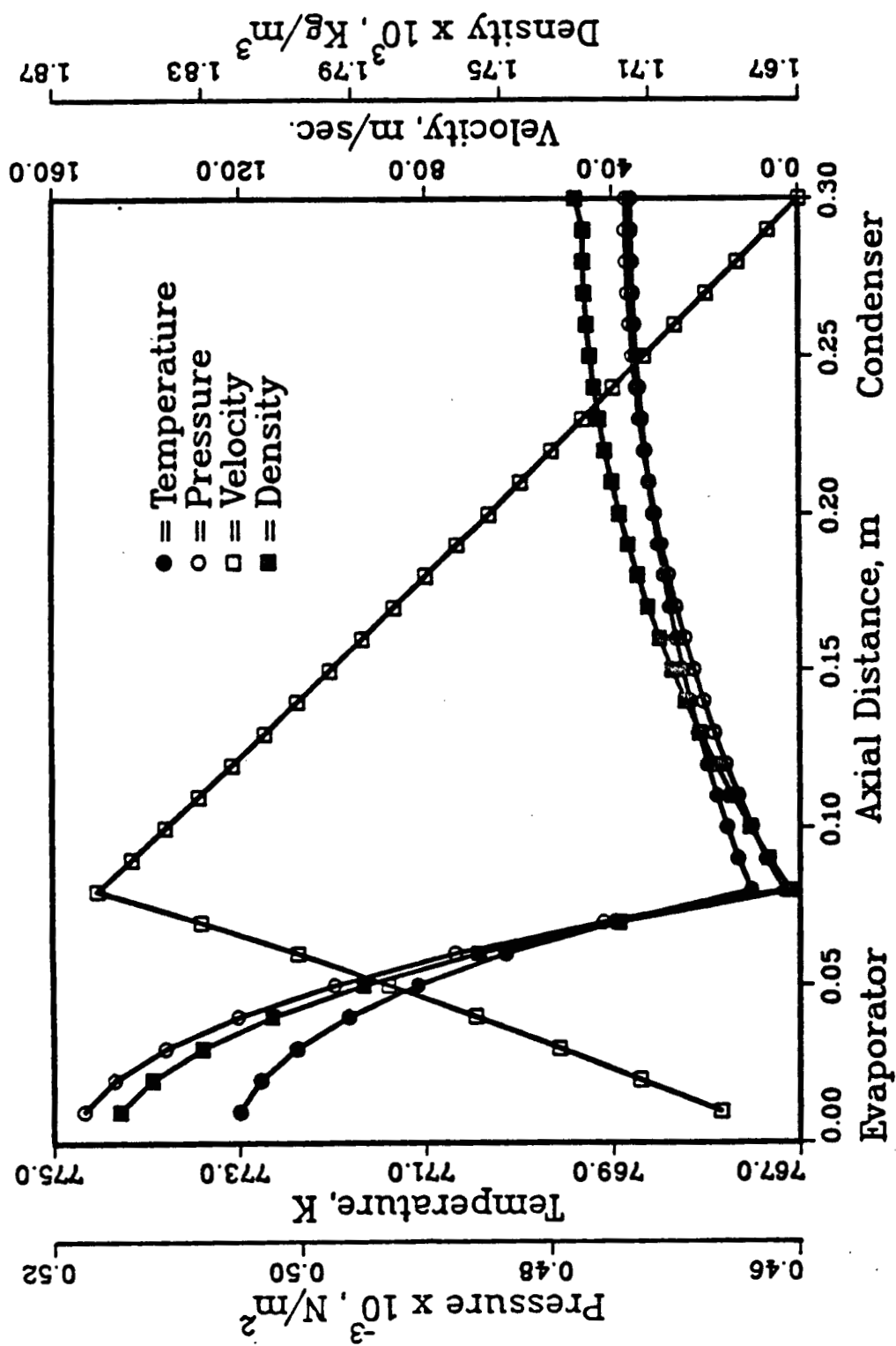


Figure 6.8. Axial variation of vapor temperature, pressure, velocity, and density at an operating temperature of 773 K.

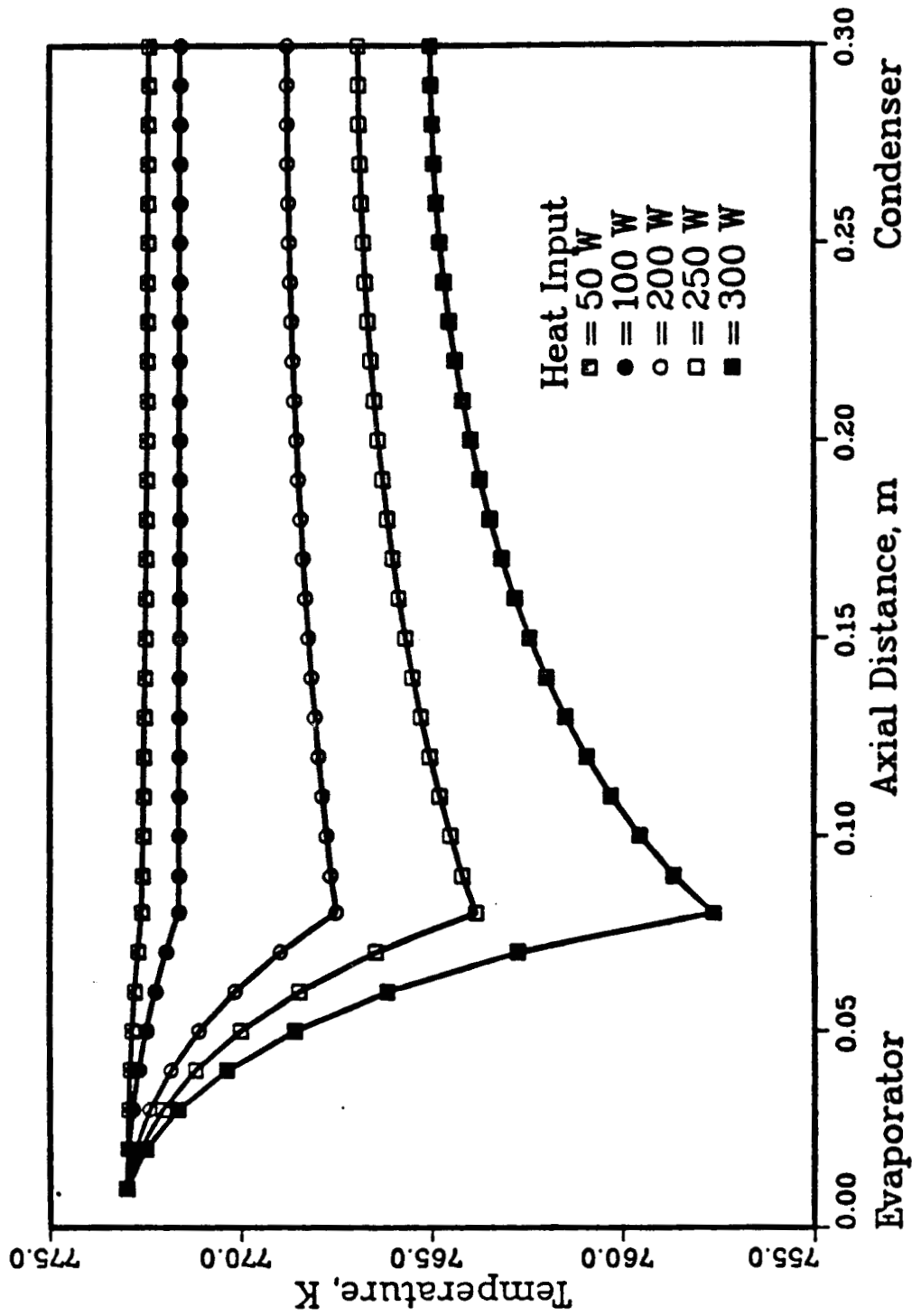


Figure 6.9. Axial variation of vapor temperature for various heat inputs.

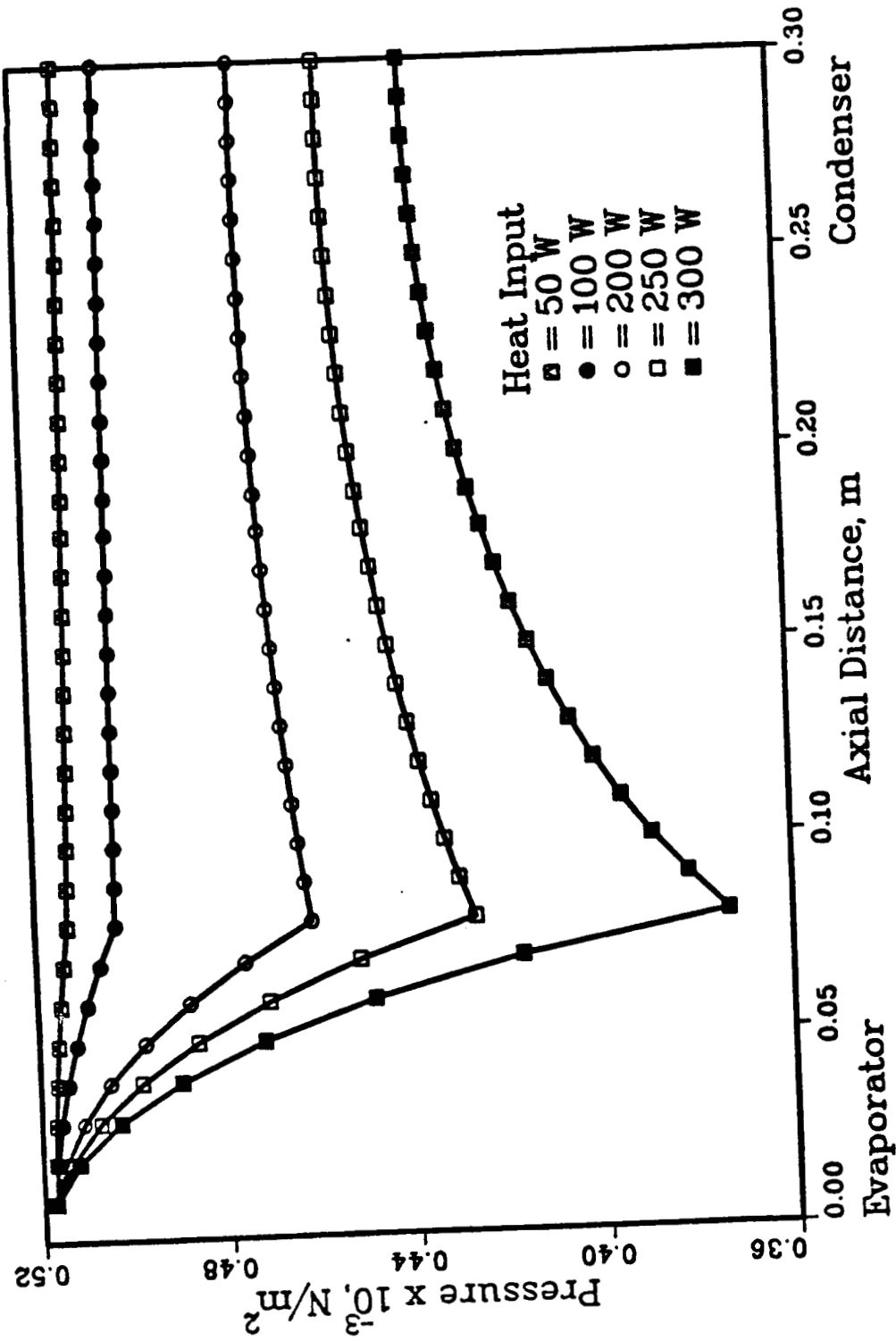


Figure 6.10. Axial variation of vapor pressure for various heat inputs.

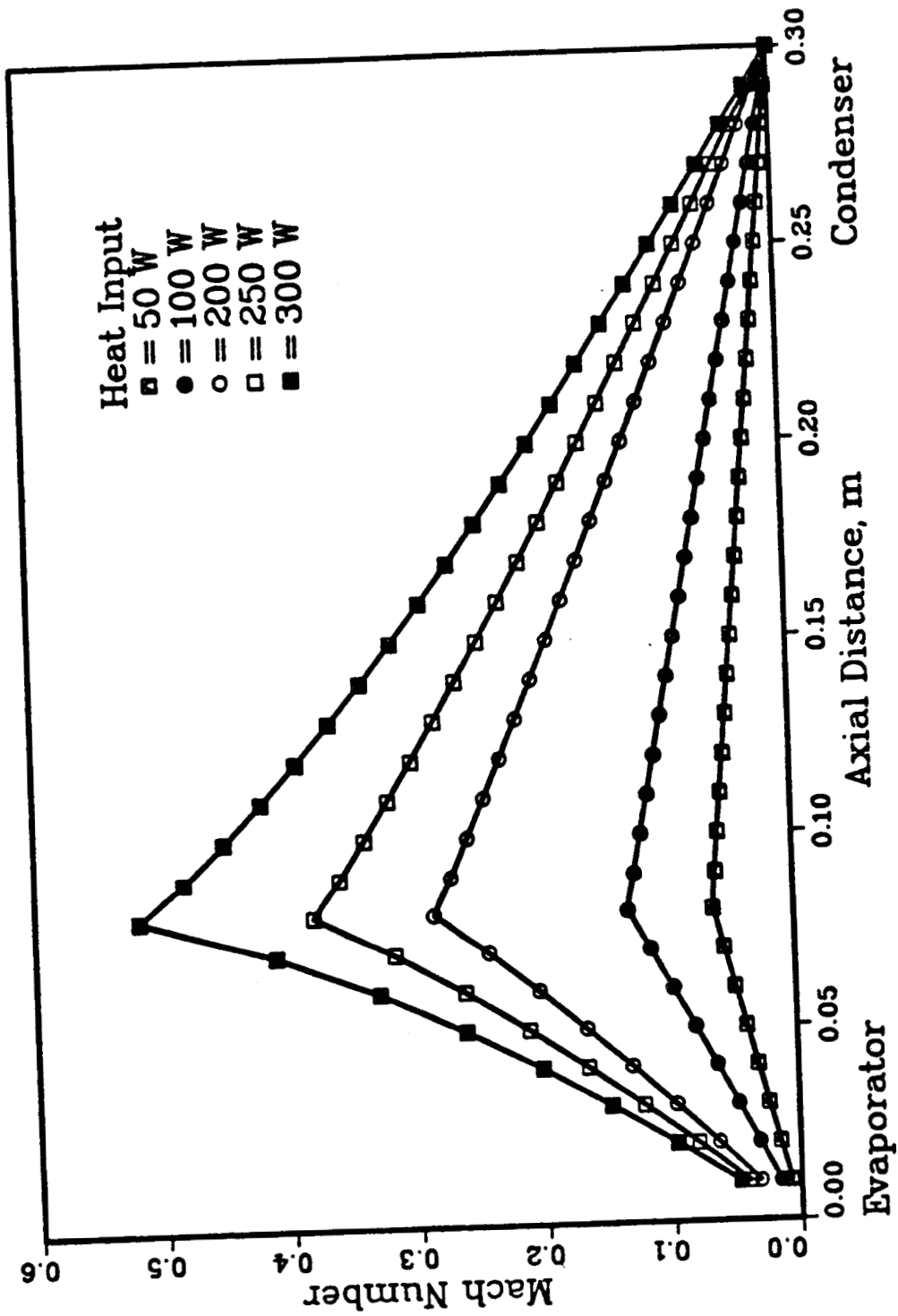


Figure 6.11. Axial variation of Mach number for various heat inputs.

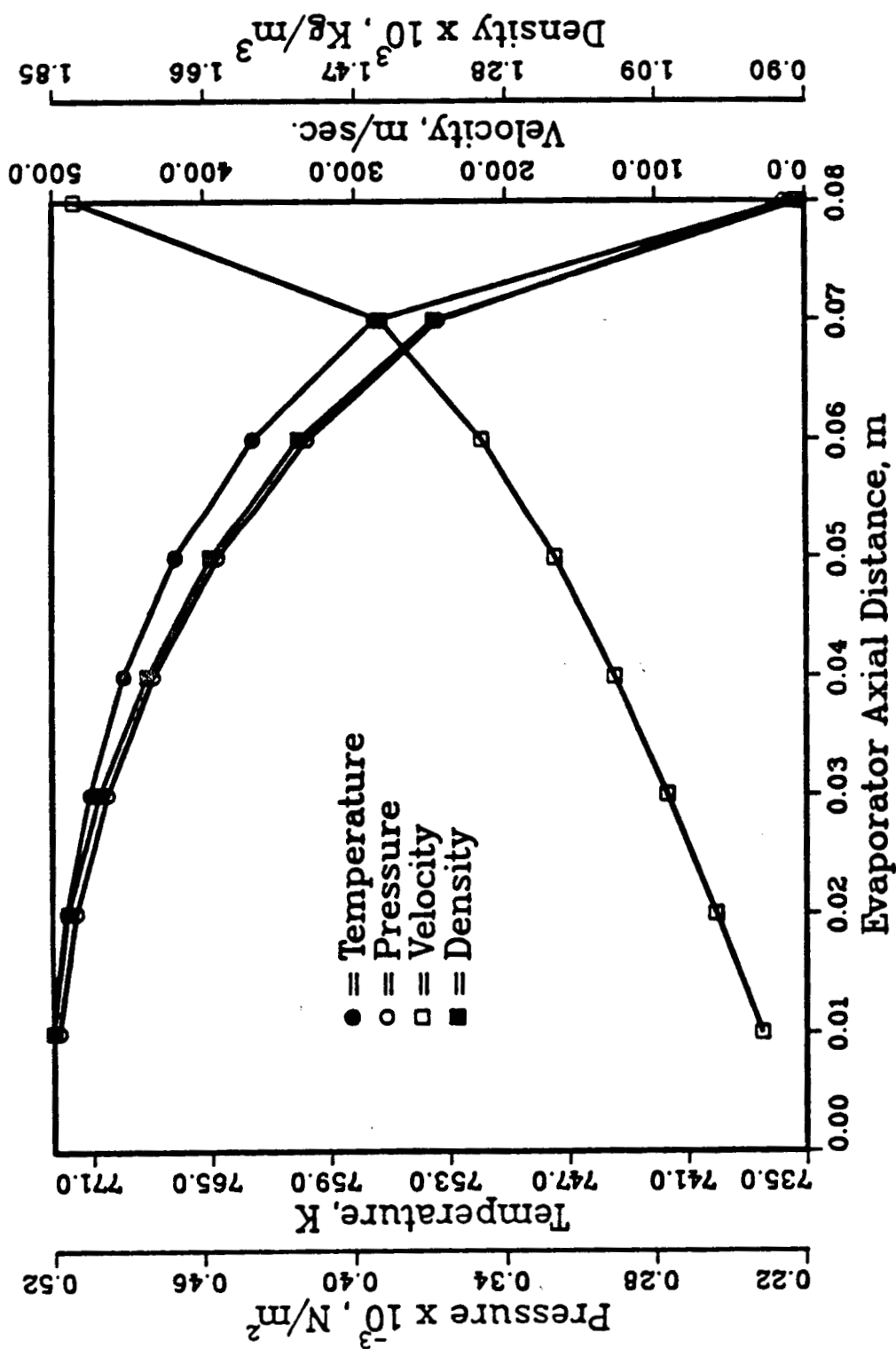


Figure 6.12. Axial variation of vapor temperature, pressure, velocity, and density at the sonic limit condition for operation temperature of 773 K.

Figure 6.13 presents axial variation of vapor temperature, pressure, velocity, and density at an operating temperature of 808 K, with a uniformly distributed heat input rate of 350 watts. For this case, the operating temperature is 35 K higher, but the pressure and density are twice as high as for 773 K. Thus, velocities are small and the maximum Mach number is only about 0.2. This leads to a small pressure drop, with a corresponding temperature drop of about 2 K. Even though the heat input is twice as much as for 773 K, a comparison of temperature drops suggests that the pressure and temperature drops depend mainly on the operating temperature.

In the adiabatic section, there is no mass injection or extraction. Hence, pressure simply decreases due to friction, and the velocity increases very little. The contribution of the adiabatic section is the addition of pressure and temperature drops such that, for a high Mach number at the exit of the evaporator, maximum heat transfer rate is reduced considerably. Figure 6.14 shows this phenomenon. A heat input of 865 watts results in a Mach number of 0.7 at the exit of the evaporator. Then, the vapor is accelerated in the adiabatic section, so that velocity of the vapor approaches sonic velocity at the end of this section.

As expected, in the condenser section the pressure and temperature are partially recovered, but the degree of recovery is small due to the small vapor velocity and large friction loss in the longer condenser. Numerical results show that temperature recovery is only 0.6 K. Variations of temperature, pressure, and Mach number corresponding to six different heat fluxes at an operating temperature of 808 K are presented in Figures 6.15, 6.16, and 6.17, respectively. For heat input up to 200 watts, pressure recovery is not observed. This implies that the pressure drop due to friction in the condenser may exceed the value of the inertial contribution. However, total pressure drops are small, so that the vapor can be assumed isothermal.

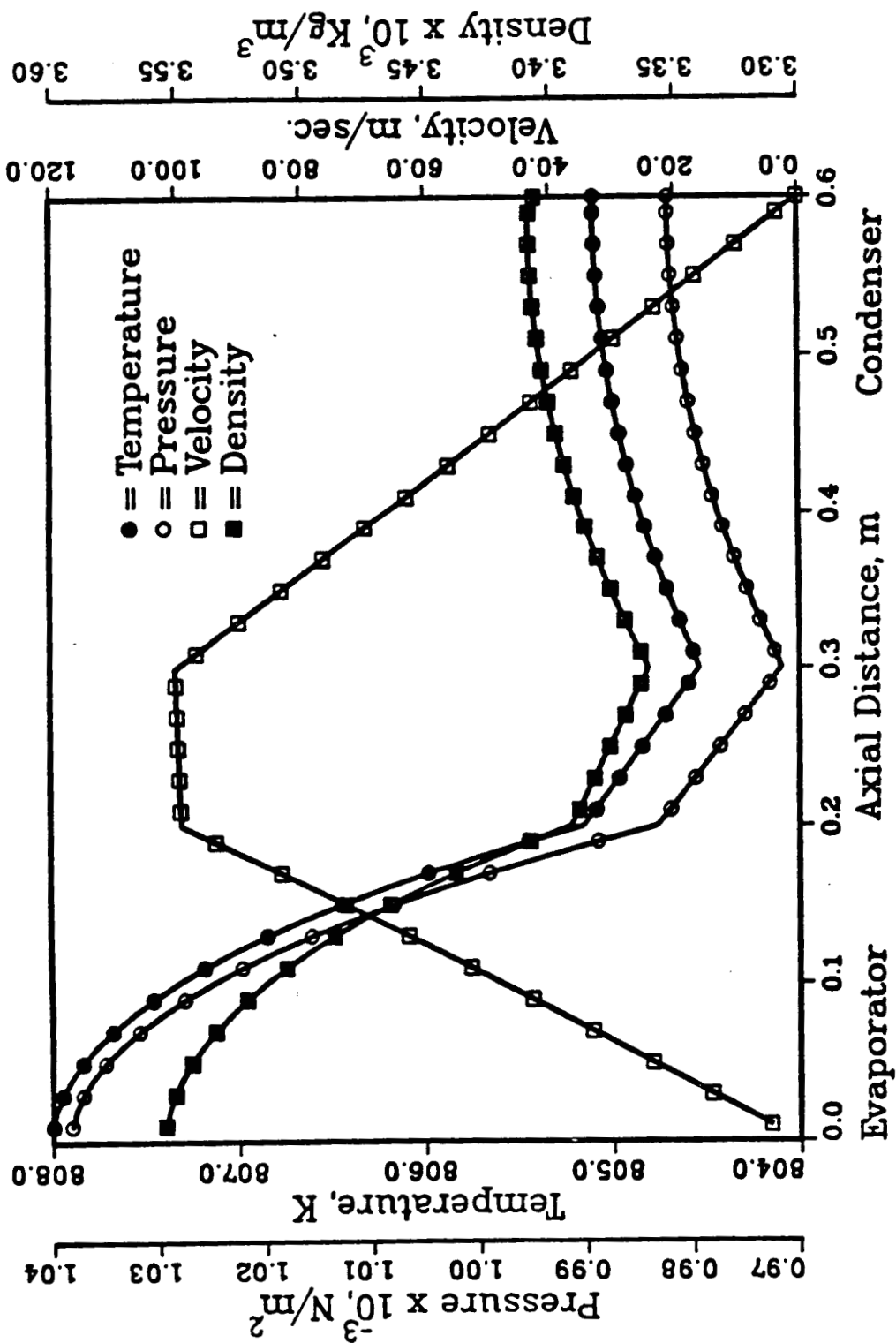


Figure 6.13. Axial variation of vapor temperature, pressure, velocity, and density at an operating temperature of 808 K.

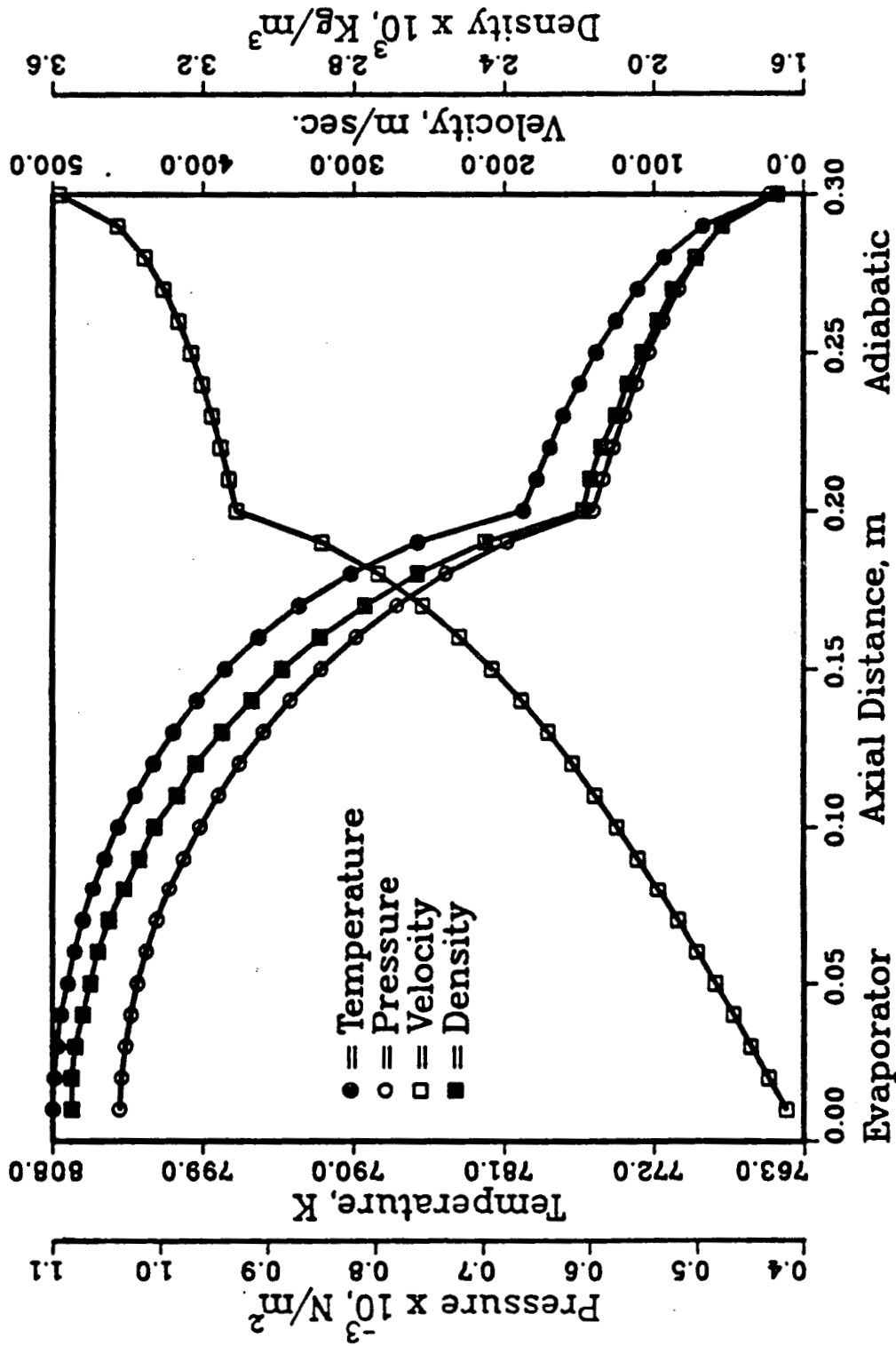


Figure 6.14. Axial variation of vapor temperature, pressure, velocity, and density at the sonic limit condition for an operating temperature of 808 K.

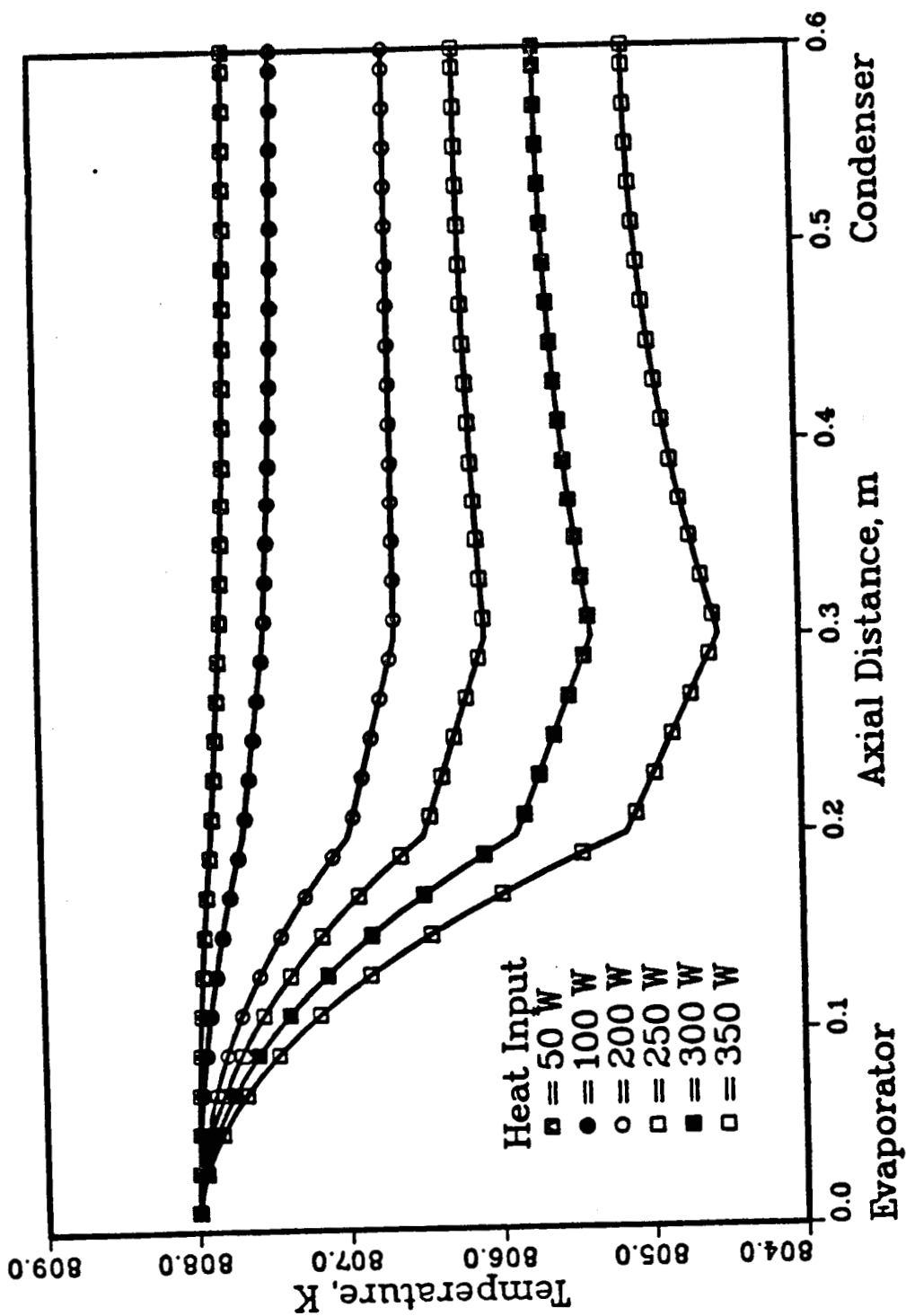


Figure 6.15. Axial variation of vapor temperature for various heat inputs.

ORIGINAL PAGE IS
OF POOR QUALITY

89

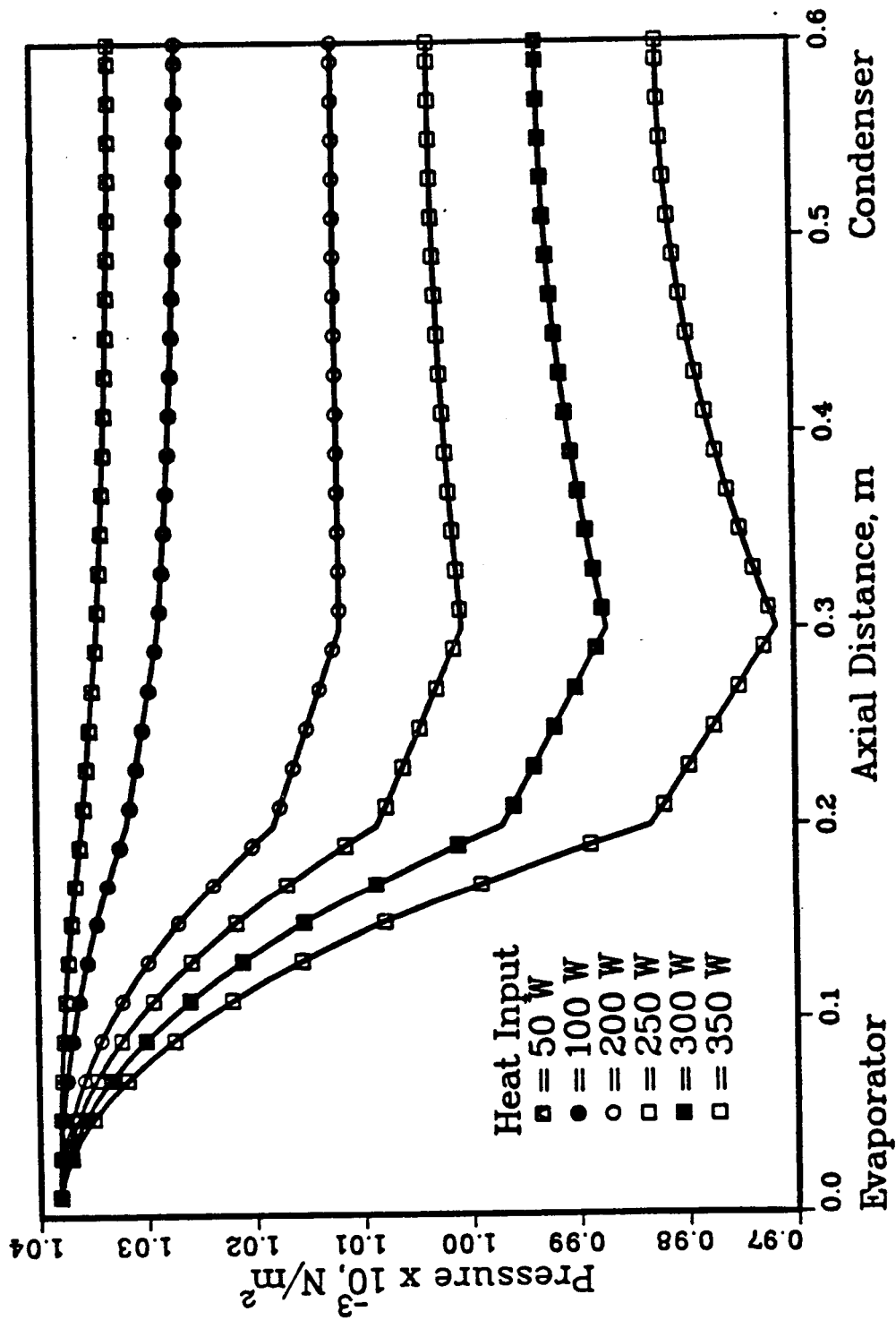


Figure 6.16. Axial variation of vapor pressure for various heat inputs.

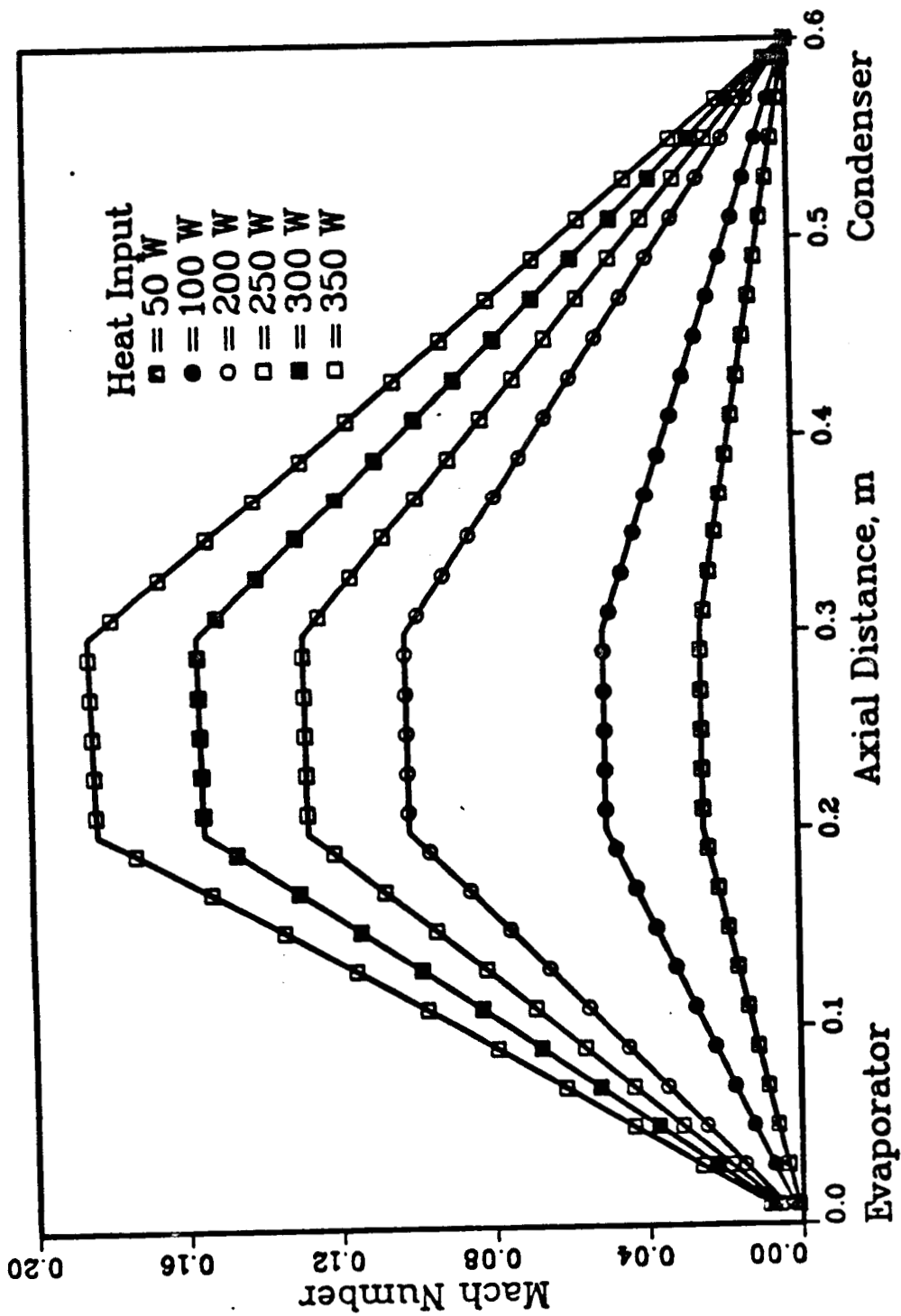
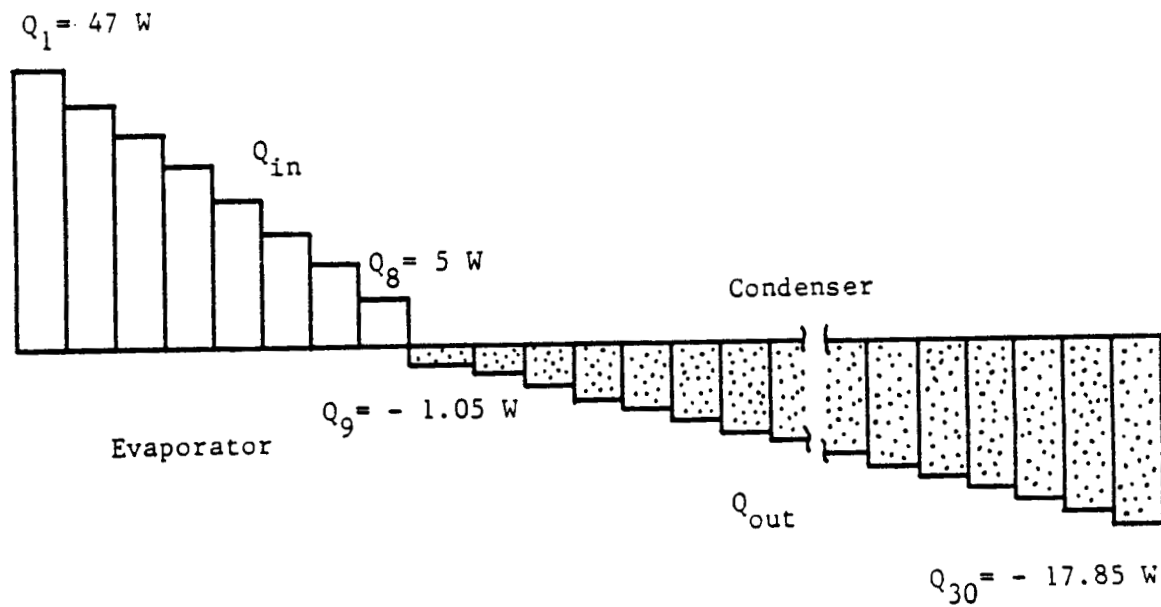


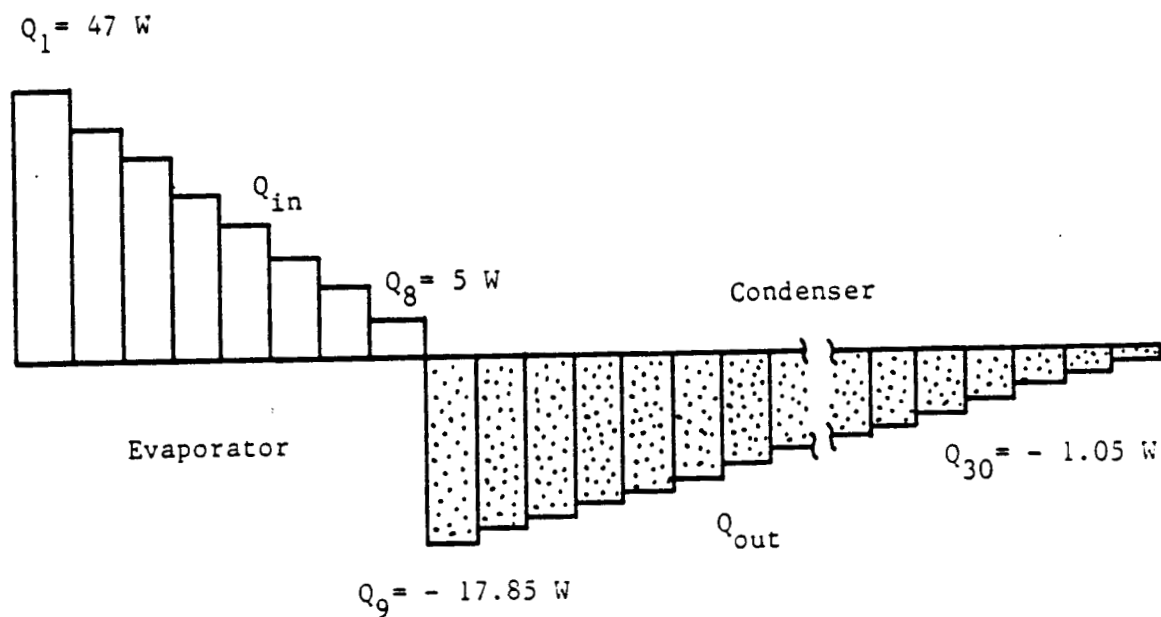
Figure 6.17. Axial variation of Mach number for various heat inputs.

Figure 6.18 shows the distribution of nonuniform heat flux on the evaporator length of 8 cm and condenser in another case studied numerically. Axial variations of vapor temperature, pressure, velocity and density corresponding to the distribution shown in Figure 6.18.a, are presented in Figure 6.19. At a short distance from the beginning of the condenser, the slight heat extraction causes that the axial variation of the vapor velocity is small. Thus, the friction effect in this region is dominant. The minimum temperature and pressure appear in the condenser, instead of at the exit of the evaporator. As heat extraction increases, the absolute value of axial variation of velocity increases and the vapor velocity decreases. The pressure is recovered gradually. In Figure 6.20, corresponding to the distribution shown in Figure 6.18.b, temperature and pressure are recovered immediately from the beginning of the condenser, due to large heat extraction. As expected, axial variations of temperature, pressure, velocity, and density depend on distribution of heat input.

In summary, the degree of pressure recovery depends mainly on the heat flux, operating temperature, and length of the condenser. The higher the heat flux, the lower the operating temperature and the shorter the condenser, the greater the pressure recovery. However, for this case, the pressure drop in the evaporator can be large enough so that the heat pipe is not entirely isothermal. Since experimental data is not available, quantitative comparison cannot be achieved. However, comparison of the general behavior of the present results with published data[15,18] gives qualitative agreement.



(a)



(b)

Figure 6.18. Distribution of heat input to the evaporator and condenser.

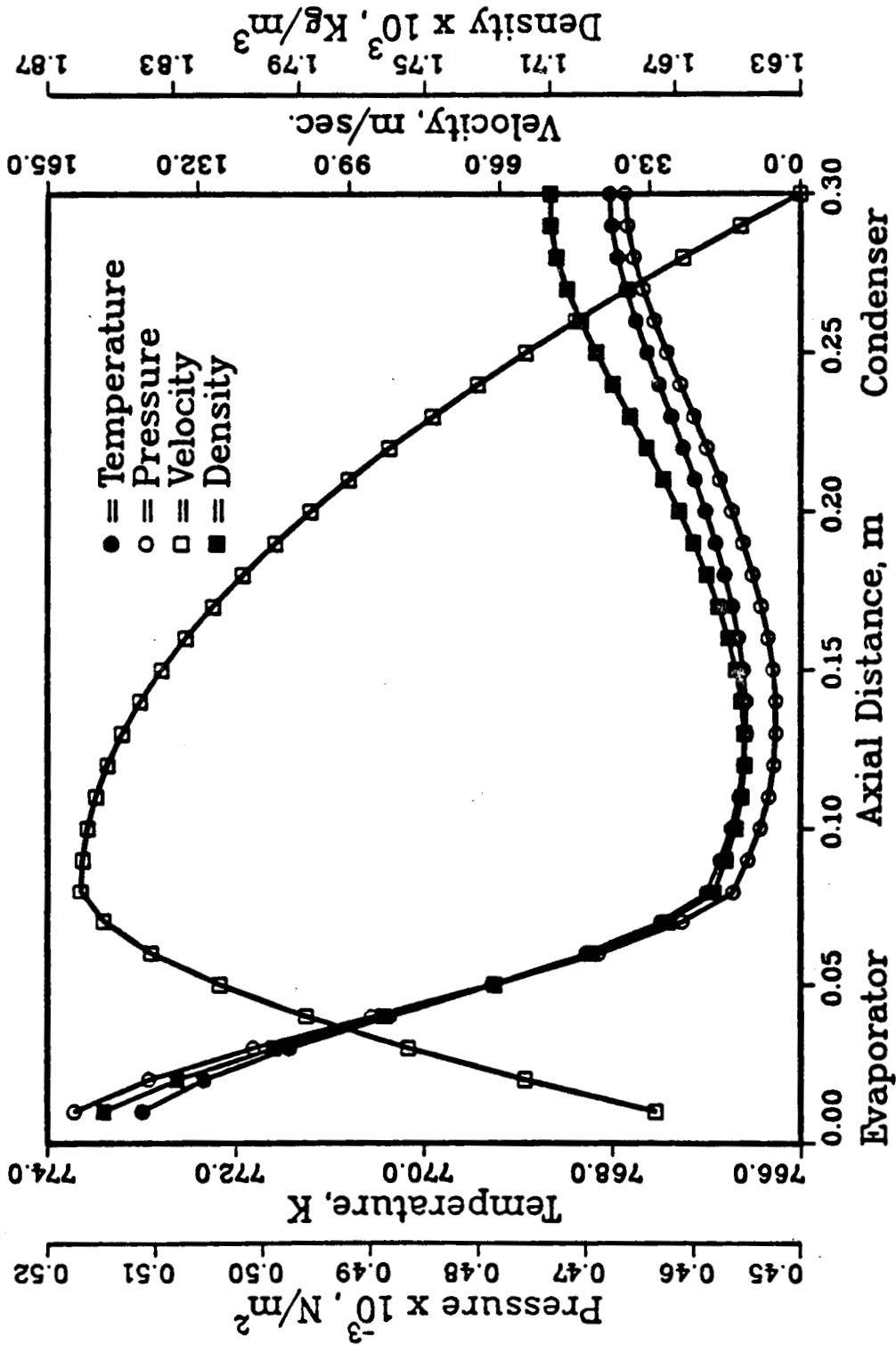


Figure 6.19. Axial variation of vapor temperature, pressure, velocity, and density for nonuniform heat input shown in Figure 18.a.

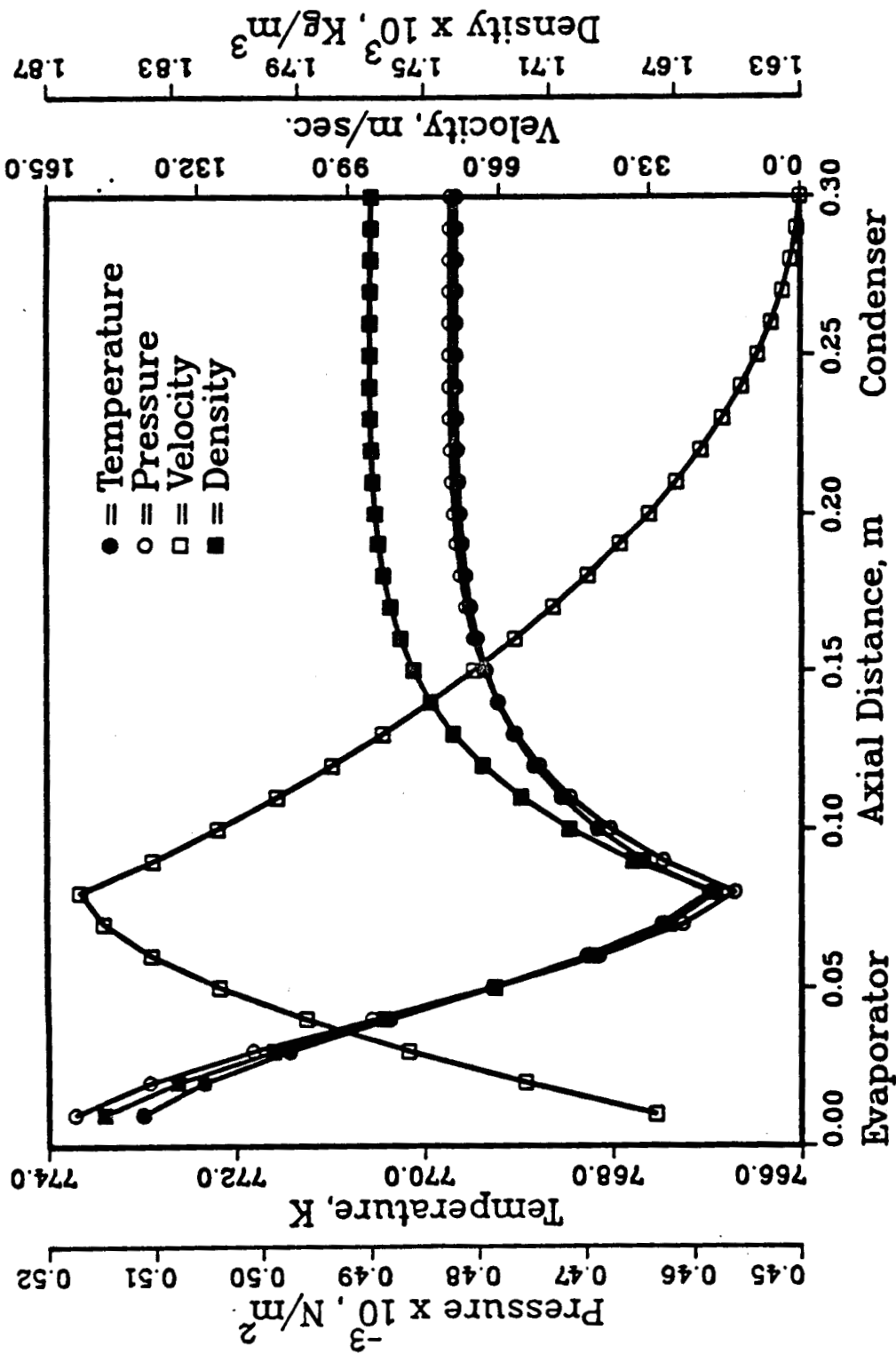


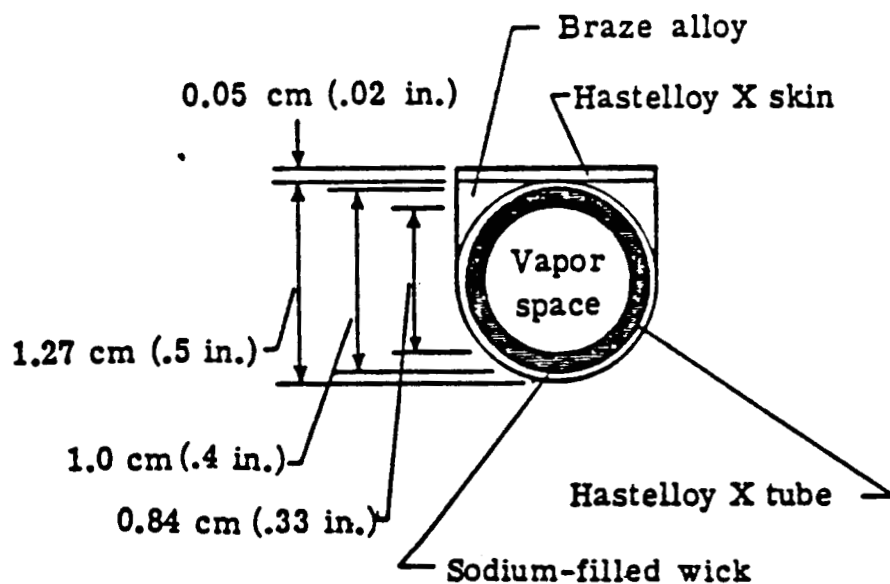
Figure 6.20. Axial variation of vapor temperature, pressure, velocity, and density for nonuniform heat input shown in Figure 18.b.

ORIGINAL PAGE IS
OF POOR QUALITY

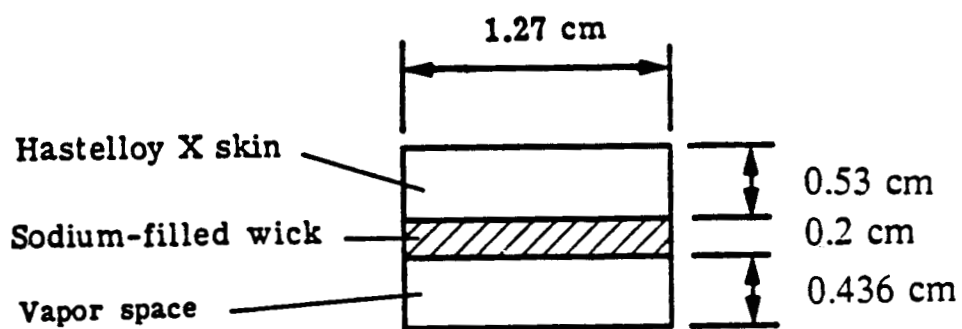
6.3 Heat pipe startup

To verify the model developed for heat pipe cooled leading edges, computed numerical results are compared to Camarda's experimental results[30]. The shape of the cross-section of Camarda's model is different from that of the model under consideration. However, the rectangular cross-section used in this research is modeled such that the cross-section areas occupied by the heat pipe shell, the capillary structure, and the vapor space are the same as for Camarda's experiment. A comparison of these two cross-sections is shown in Figure 6.21. The surface area where the heat flux is applied for the model is chosen to be identical to that of the experiment so that the width and length of the heat pipe are identical, but the thicknesses of the components of the two heat pipes are different. The thickness is much smaller than other dimensions, and the temperature drop at the cross-section is small compared to that in the axial direction, so the effects of the difference in thicknesses are minimal. Effects of energy storage and fusion of the working fluid in the heat pipe shell and the capillary structure are the same, and the effect of vapor flow dynamics may be simulated. Since the minimum dimension of the vapor space is different, due to the different thickness of the heat pipe, the transition temperature, which is evaluated based on the dimension of the vapor space, is not identical. However, this temperature determines the boundary condition at the liquid-vapor interface. Therefore, to simulate Camarda's case, the inner diameter of the circular heat pipe is used to calculate the transition temperature.

The material of each component used in the computation is the same as in the experiment, except that the braze alloy is assumed to be Hastelloy X to simplify computations in the heat pipe shell. Properties of the materials are varied with temperature during numerical calculation.



Camarda's heat pipe [30]



Computational model

Figure 6.21. Comparison of the two cross-sections.

Heat distribution on the heat pipe surface as used in the model is based on a normalized distribution[30] is shown in Figure 6.22 and heat input at the stagnation point is shown in Figure 6.23. Actual heat distribution due to aerodynamic heating is shown in Figure 6.24. In addition to aerodynamic heating, a radiation boundary condition is used to extract energy from the entire heat pipe surface, so that the net rate affects the heat pipe internal operation. The section which has a net positive rate is considered the evaporator, and the section with the net negative rate is the condenser.

Figure 6.25 shows the two-dimensional grid system, dimensions, boundary conditions, and materials used to represent a leading edge. It is assumed that the temperature of the heat pipe is initially the ambient temperature, which is below the melting point of the sodium working fluid. A temperature of 700 K is used for transition from free molecular to continuum flow.

An explicit method with a few implicit initial steps is used as the time stepping scheme. Until continuum flow is established in the vapor space, a constant time step of 10 seconds is used. This time is gradually decreased, due to the increasing heat input on the external surface.

Figure 6.26 shows a comparison of numerical and experimental results at various times. Since measured temperatures were not surface temperatures but the temperatures at intermediate points, numerical data at the interface between the heat pipe shell and capillary structure are used for comparison. Since most of the energy which is transferred by conduction through the heat pipe shell and capillary structure in the axial direction is added near the stagnation point, temperature at that point increases rapidly and a large temperature gradient is established in the heat pipe during startup. This implies that the heat pipe is not effective, due to the extremely small vapor density, for about the first 450 seconds. Temperatures in

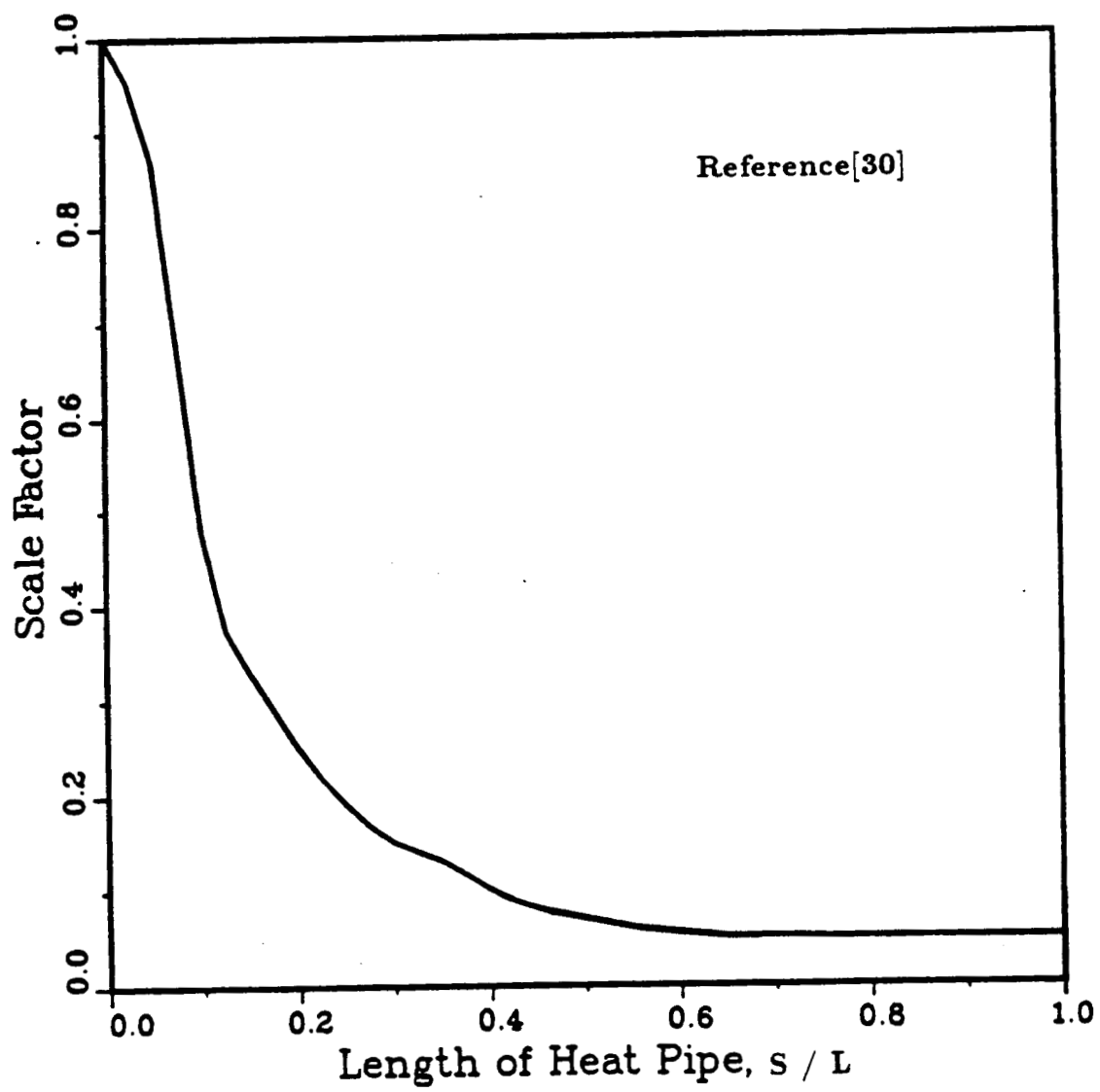


Figure 6.22. Normalized heating distribution.

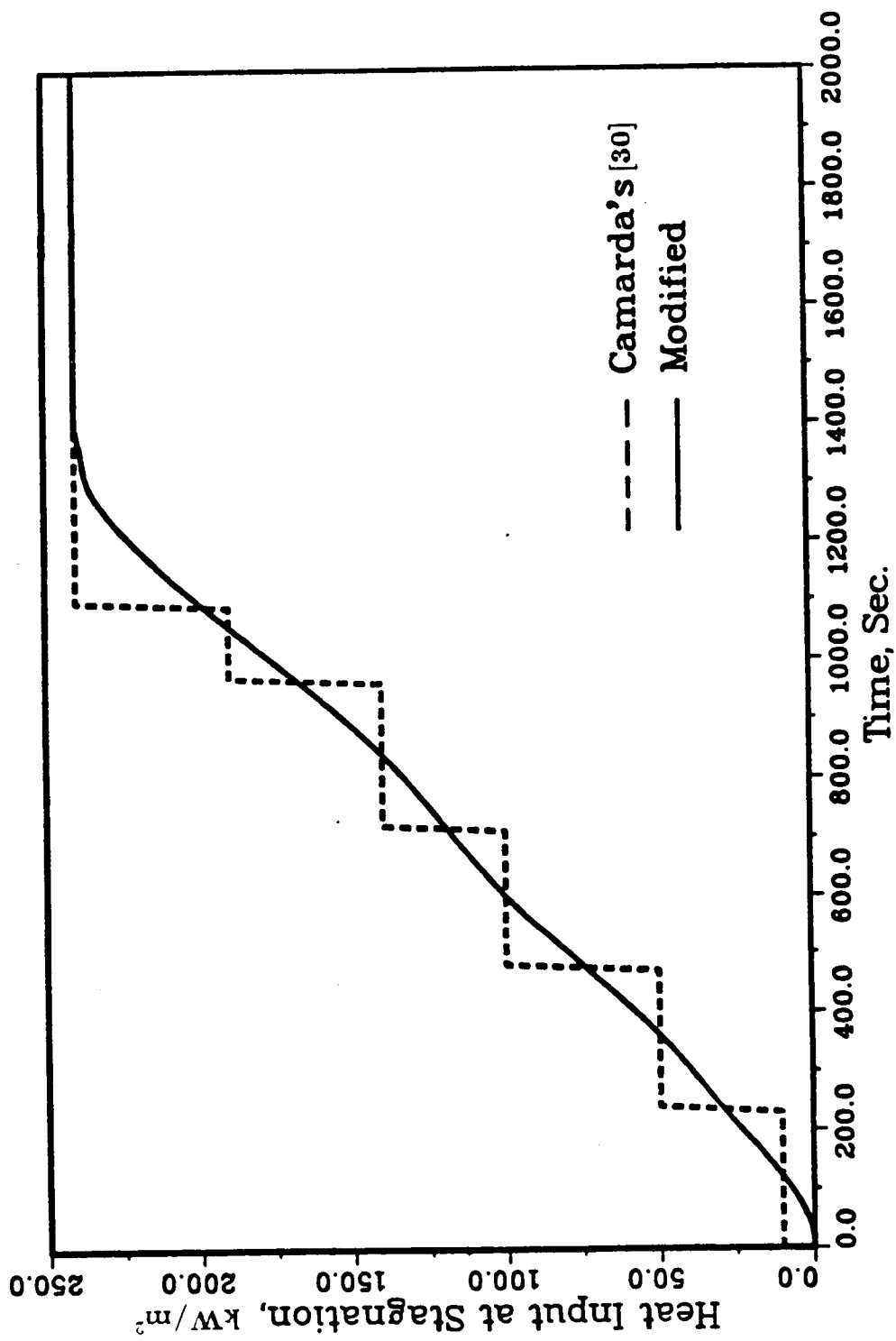


Figure 6.23. Heat input at the stagnation point.

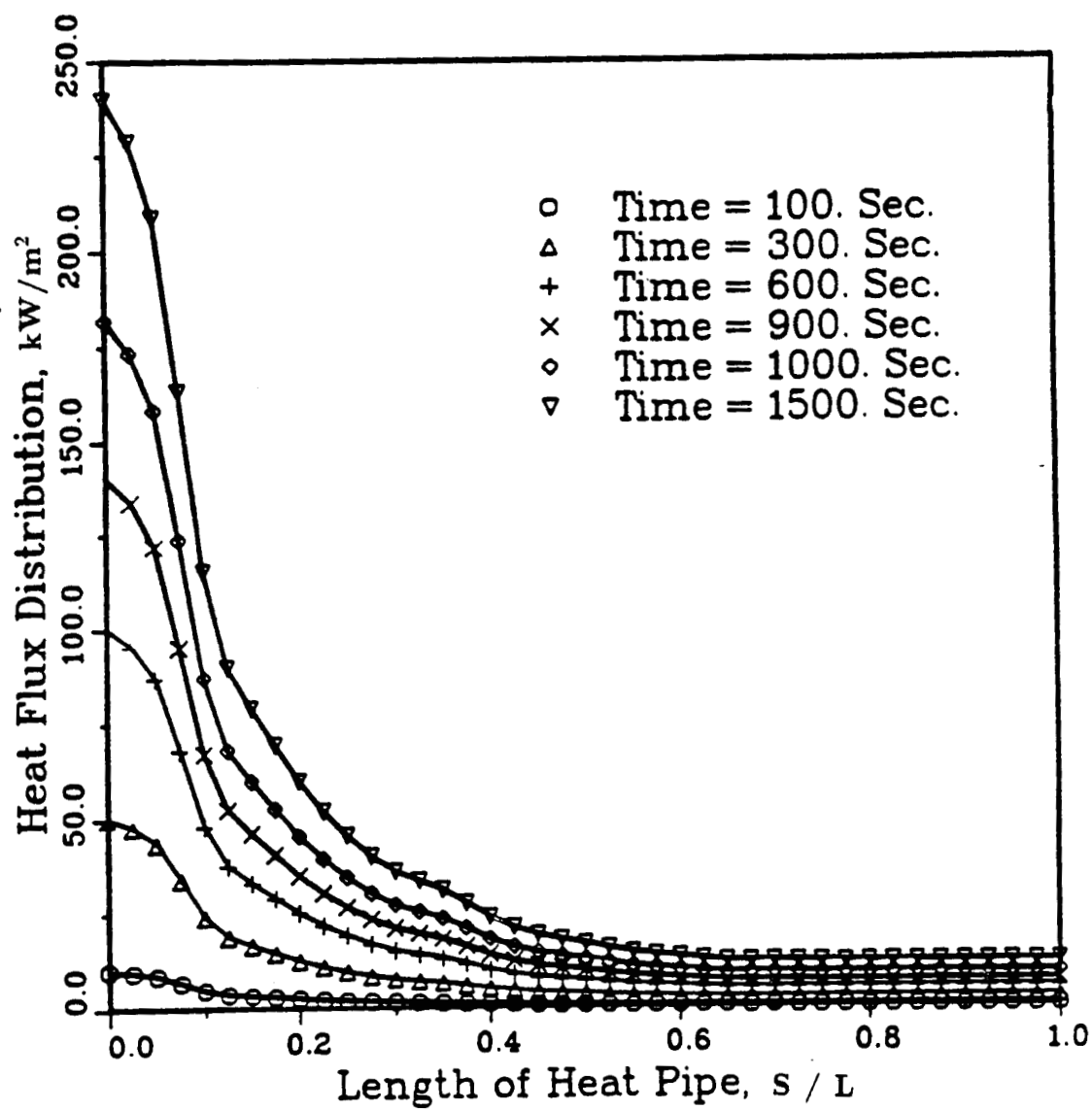


Figure 6.24. Heat flux distribution on a leading edge model.

Variable heat flux and radiation boundary condition($T_r = 293\text{ K}$)

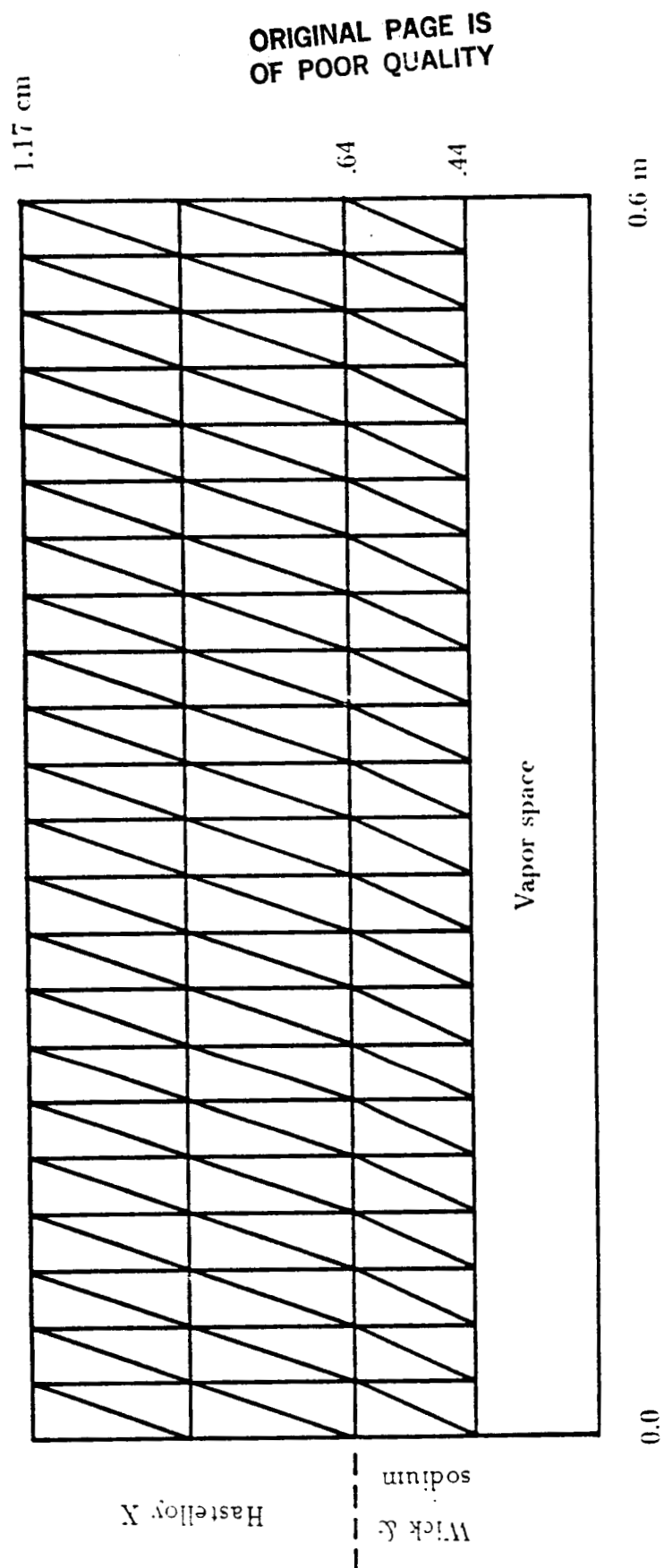


Figure 6.25. Two-dimensional mesh used to represent a heat pipe cooled leading edge; 138 elements, 96 nodes.

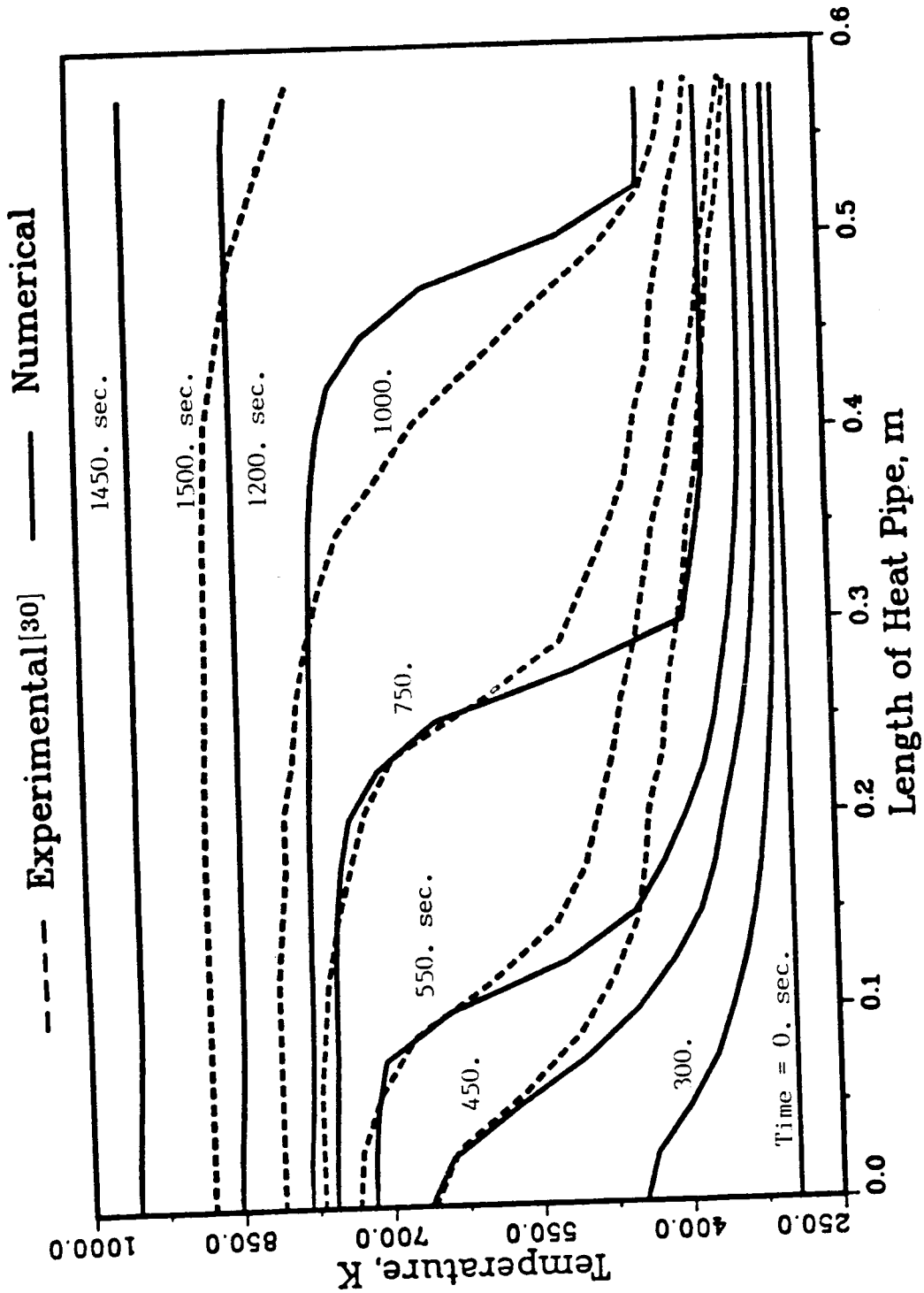


Figure 6.26. Temperature of a heat pipe cooled leading edge.

the rest of the heat pipe are not much different from the initial condition. At 550 seconds, temperature at the stagnation point is greater than the transition temperature and the temperature gradient in the region adjacent to this point begins to decrease. This means that a continuum flow region is established in the vapor space, so that energy is mainly transported via latent heat transport. However, as shown in Figures 6.27 and 28, most of the working fluid is in the frozen state, and free molecule flow prevails in most of the vapor space. With time, the continuum flow region is expanded, so that at about 750 seconds, two-fifths of the device performs as a heat pipe. The rest of the heat pipe still behaves like a solid bar in which heat is transported only by conduction, even though the working fluid is melted over the entire length. Between the two flow regions, a large temperature gradient exists, where the continuum flow front is located. This front moves down toward the cool end of the heat pipe. At 1000 seconds, most of the heat pipe is active, except near the end of the condenser section. About 100 seconds later, continuum flow exists in the entire vapor space as shown in Figure 6.28. Until this moment, the sonic limit is encountered due to the large temperature gradient in the vapor space. Therefore, maximum heat transport in the vapor space is equal to the sonic limit. However, the expression used for the sonic limit excludes friction effects at the interface, so that the sonic limit is overestimated. Thus, at a time of 1000 seconds, temperature near the stagnation point is less than that found in experiments, and the continuum flow front is advanced further. After a time of 1200 seconds, the heat pipe becomes isothermal, but due to increasing heat input the temperature increases until the system reaches a steady state at a later time.

Figure 6.29 shows temperature history of the heat pipe at three different locations in the axial direction. When a part of the vapor space has free molecular flow, most of the heat input is used to heat up the condenser section, so that the temper-

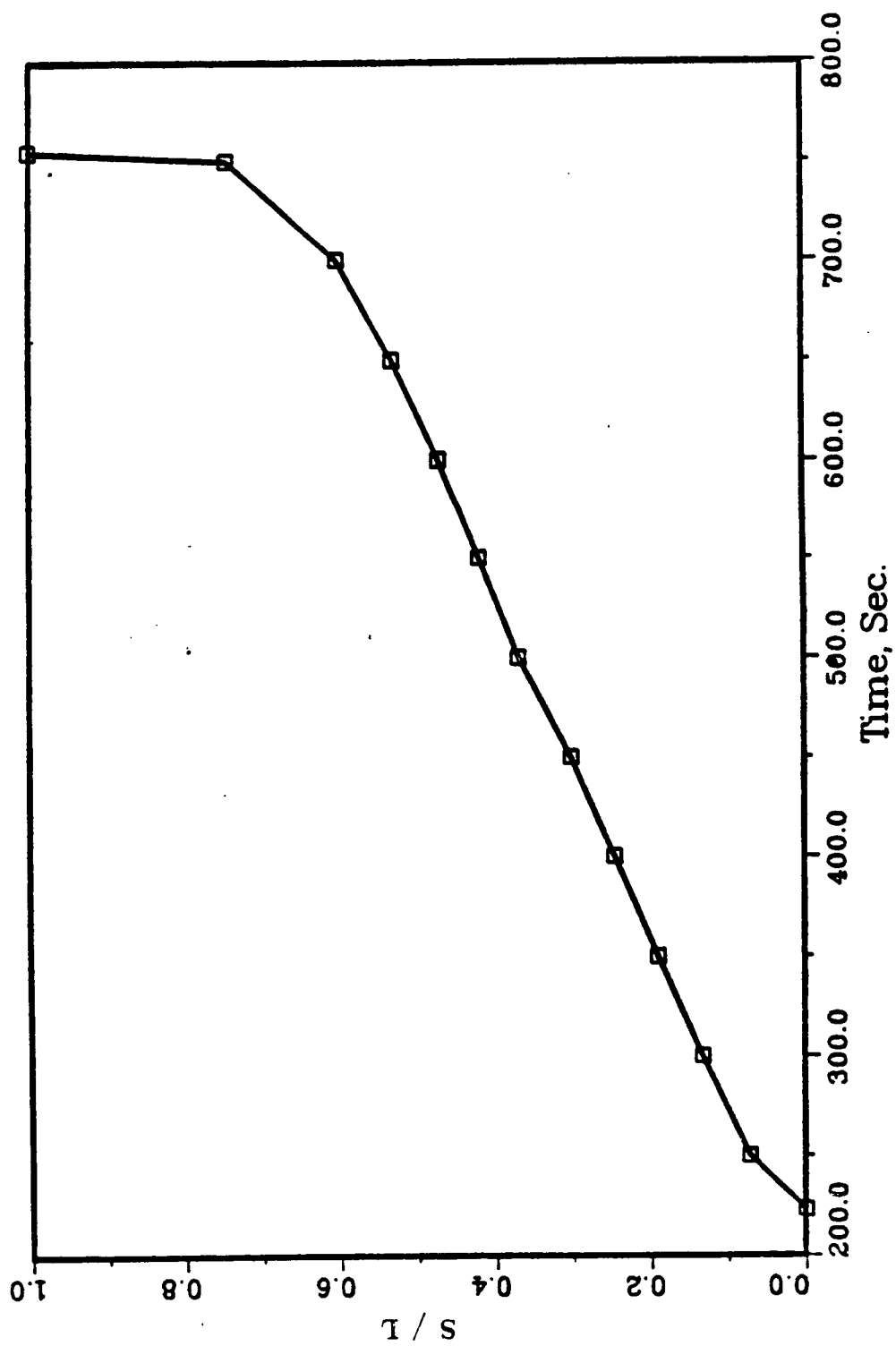


Figure 6.27. Location of phase change of sodium.

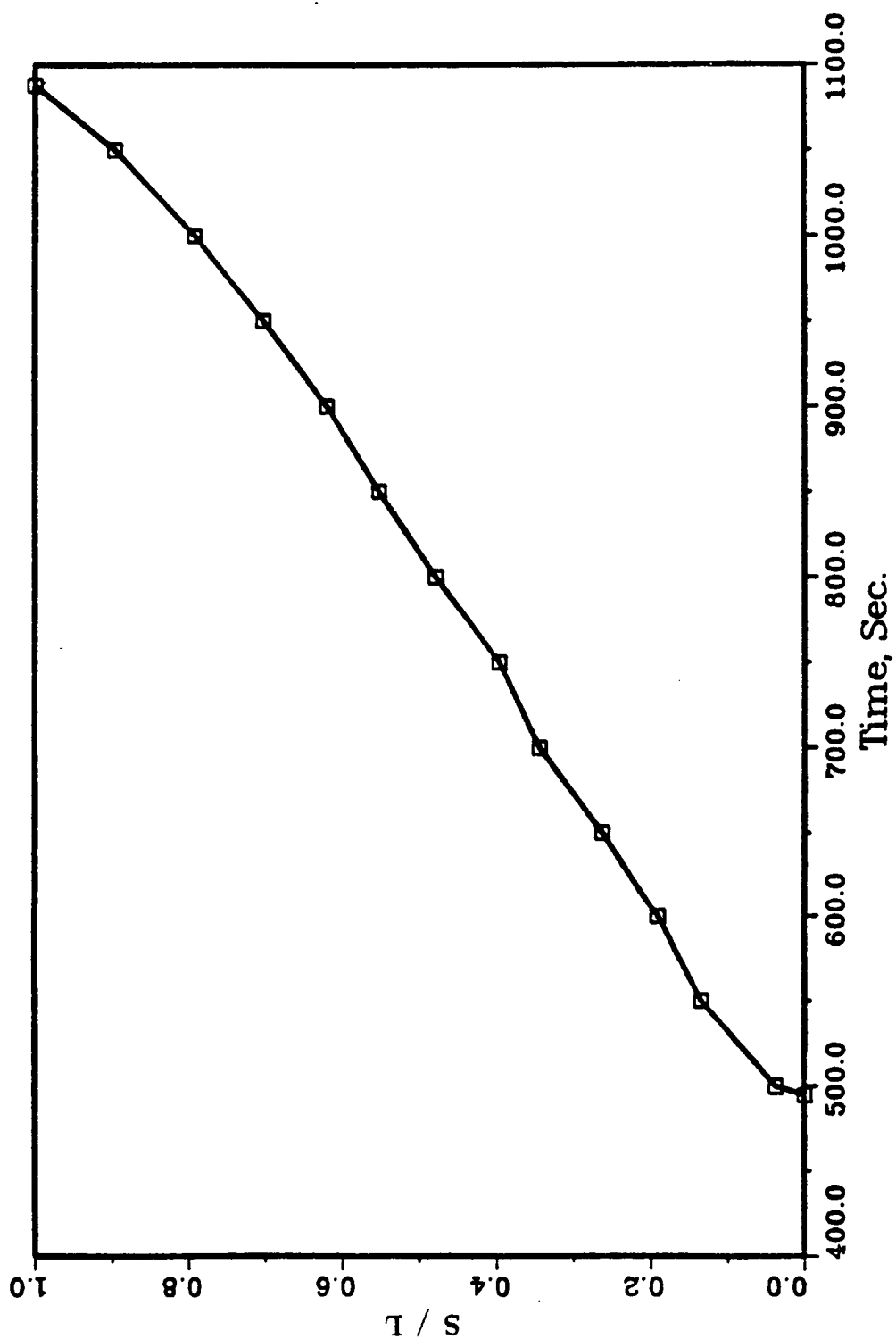


Figure 6.28. Position of continuum flow front.

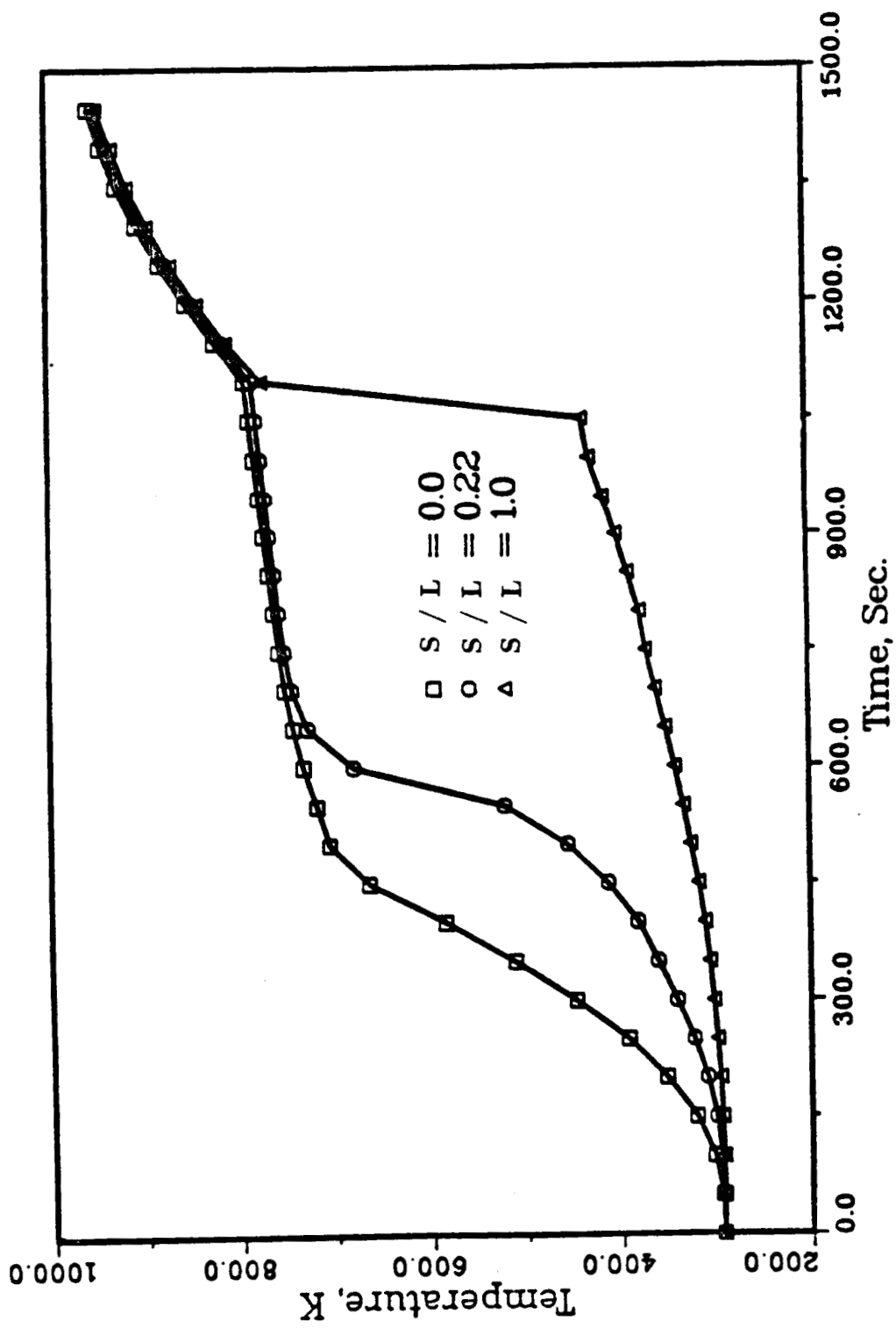


Figure 6.29. Temperature history of three locations in the heat pipe.

ature increases very slowly. As the continuum flow front approaches the end of the heat pipe, the remainder of the vapor space quickly reaches continuum flow. After the entire heat pipe is active, temperatures at all axial locations increase relatively fast, and then tend to change slowly as steady state is reached. Experimental results exhibited steady state at a time of 1500 seconds where the maximum temperature was 883 K. However, the numerical results yield a maximum temperature of 948 K at 1450 seconds. The temperature at 1500 seconds can be estimated to be 958 K, according to the slope of temperature with time. This temperature difference of 77 K may result from using a different emissivity for the heat pipe surface, neglecting natural convection in the numerical calculation, and additional heat loss from the inside surface and end of heat pipe through insulation. These effects increase with temperature. The leading edge test set was coated with a high emissivity ceramic paint to improve heat rejection by radiation, but the emissivity was not specified. For numerical calculations an emissivity of 0.8 is used. The heat loss due to convection is estimated by using the approximation of a horizontal heated plate facing upward. Estimation shows that the operating temperature drop of 35 K may be possible due to convection. Increasing emissivity from 0.8 to 0.9 would reduce the outside temperature about 30 K.

Figure 6.30 shows the temperature distributions at different wall locations. Near the stagnation point, a large temperature difference exists due to intensive heat input while for the rest of the heat pipe the difference is only about 15 K. The figure shows the length of the evaporator, which is not specified initially. Out to a length of about 15 cm, the temperature at the surface is greater than that of the interface, so that this region may be assumed to be the evaporator, and the rest of the length is the condenser section. Figures 6.31 and 32 show detailed temperature distributions obtained by numerical calculation, along the length at the external

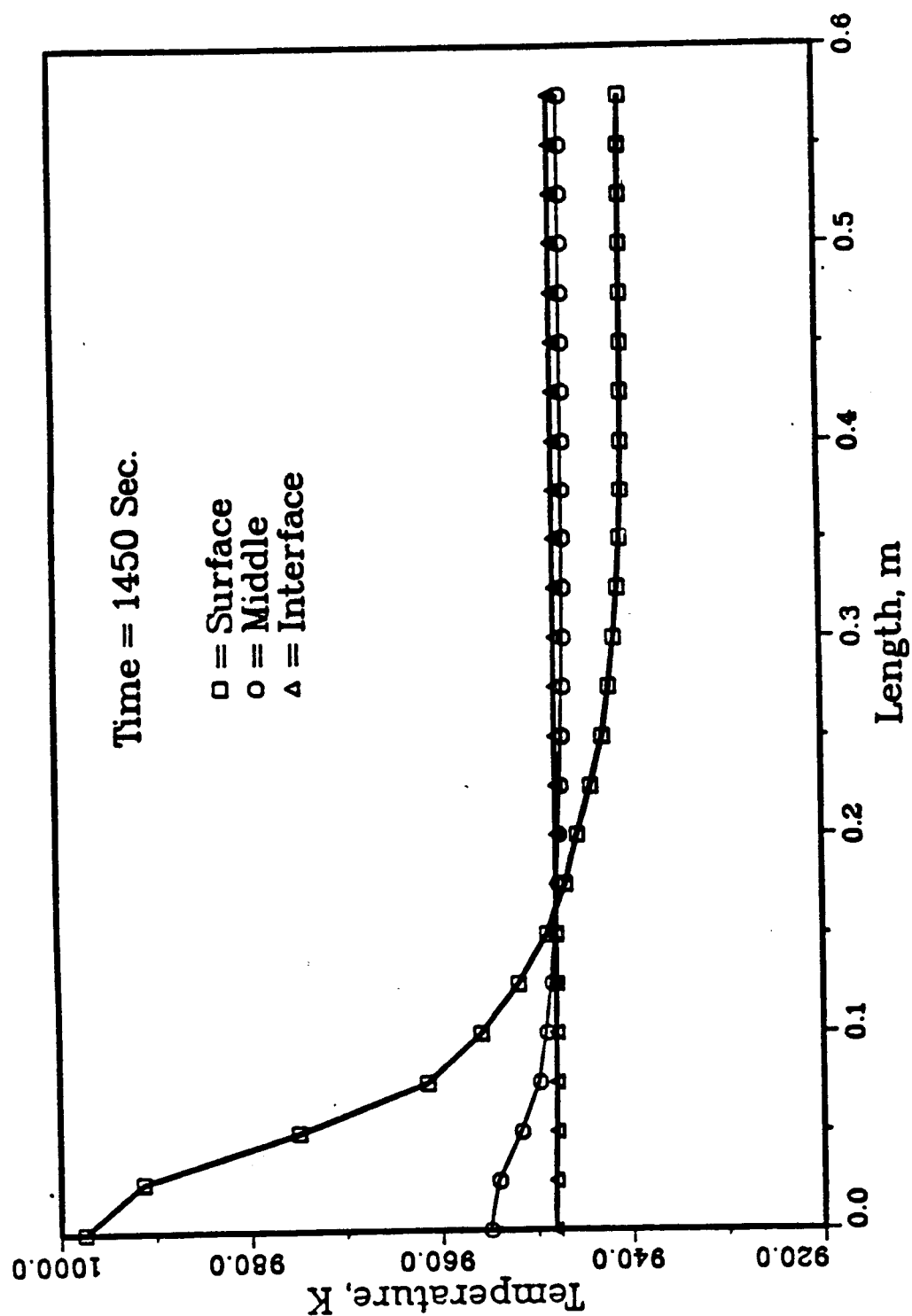


Figure 6.30. Temperature distribution at the different locations in wall.

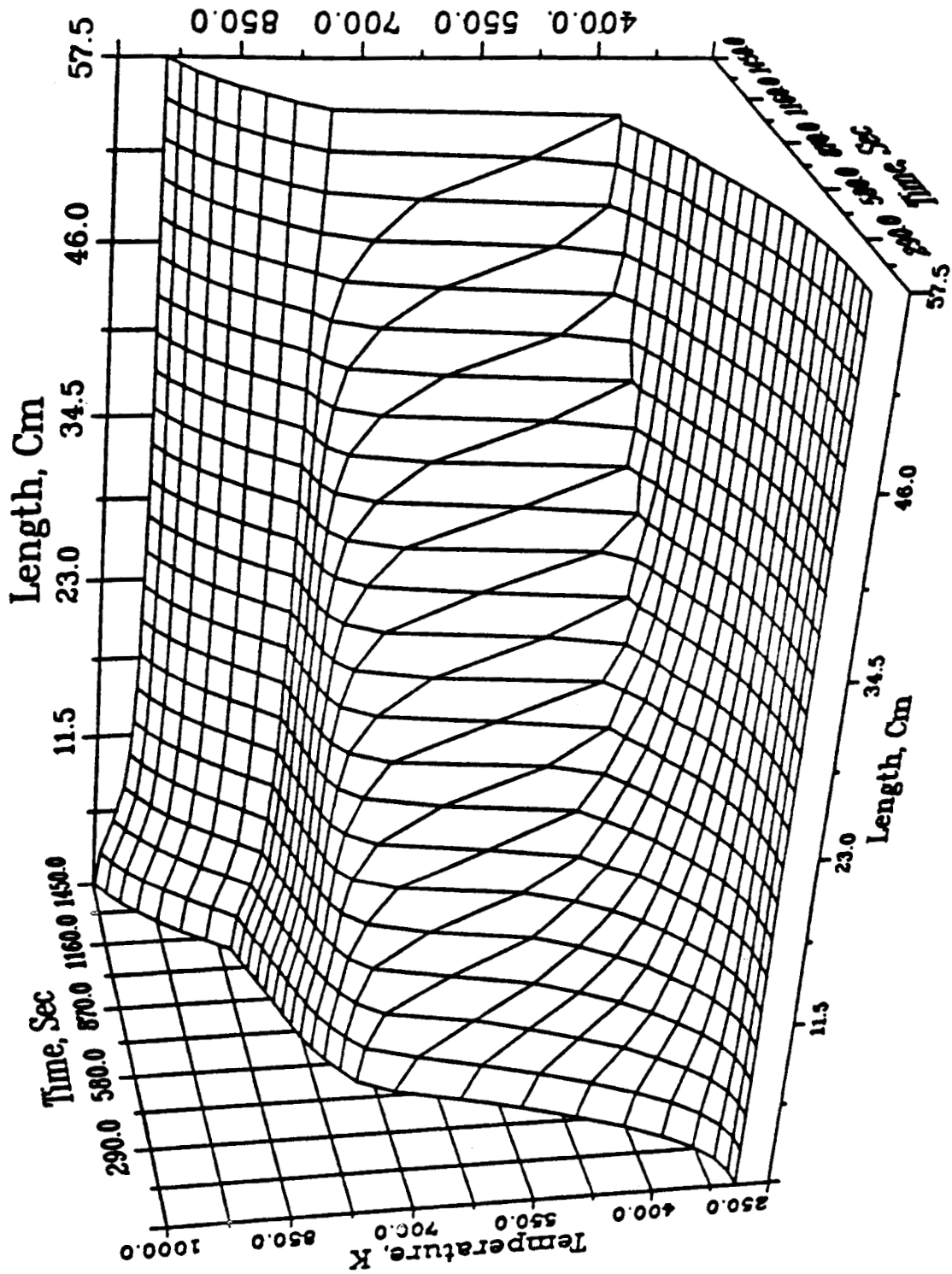


Figure 6.31. Temperature distribution at the surface.

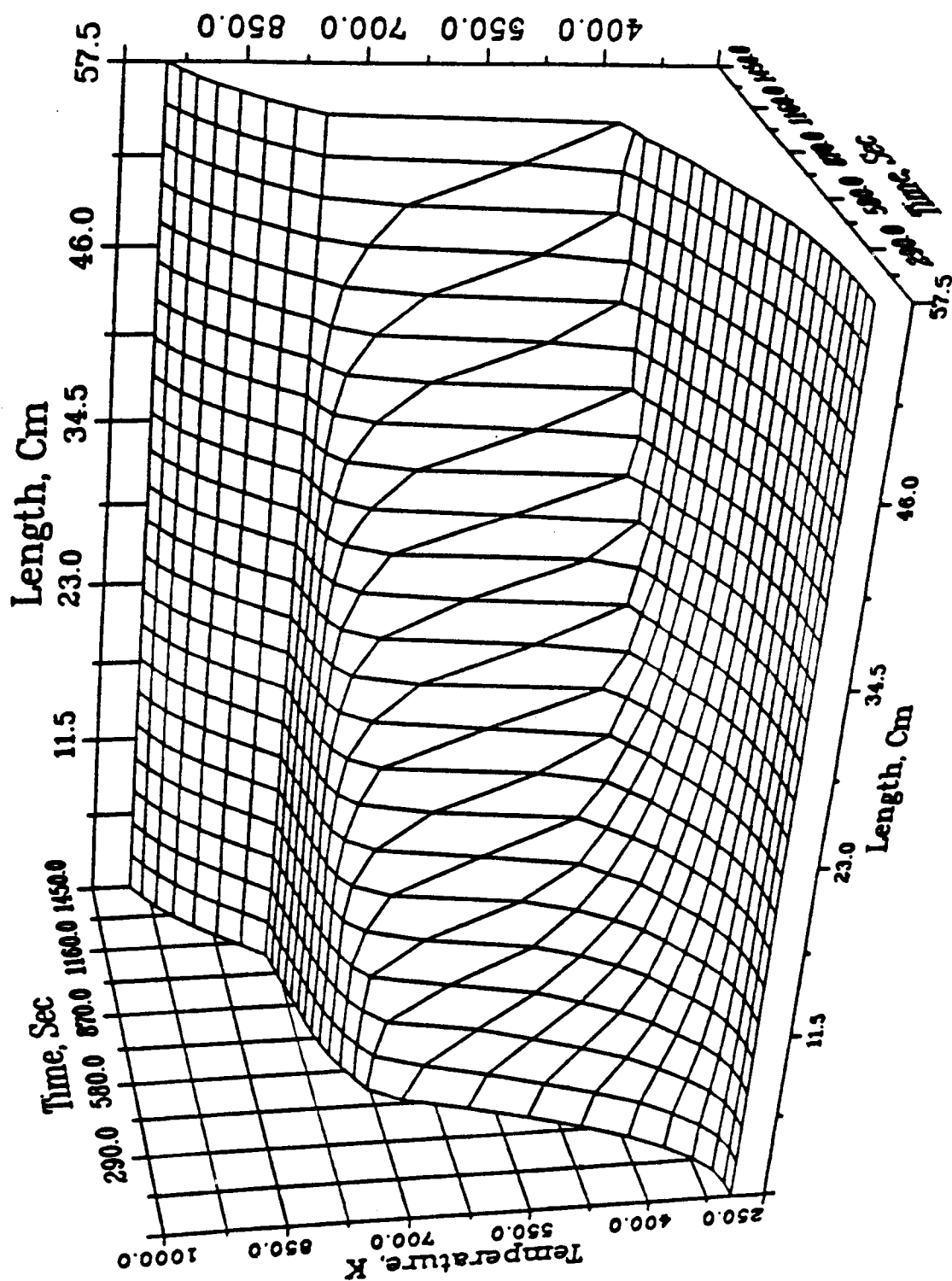


Figure 6.32. Temperature distribution at the interface.

surface and interface between shell and wick structure. respectively, for different times.

Figure 6.33 shows the variation of the average vapor temperature during start-up. Vapor temperature increases corresponding to increasing heat flux. The vapor temperature increases very slowly because most of the heat added in the evaporator is extracted at the interface of the condenser to heat up the adjacent cold zone until the entire vapor space is in the continuum flow regime. Then the vapor temperature rises to approach steady state. Figure 6.34 shows the vapor flow dynamics at a time of 1140 seconds. Even though the sonic limit is not encountered, the velocity of the vapor is about 180 m/s. The temperature drop in the vapor space is about 60 K and pressure is not recovered due to the effect of friction at the interface, so that thermal resistance in the vapor space should be considered.

Even though numerical results do not exactly match experimental results, due to the difference in configuration, material properties and boundary conditions, it is clear that the model does approximately predict the correct startup time and temperature distribution. It is important to note that heat inputs for the model were based on aerodynamic heating computations, which were only approximated in the experiments.

To show the effectiveness of the heat pipe for cooling a leading edge, numerical calculations were executed for the same example problem, except that an adiabatic boundary condition is applied to the liquid-vapor interface during the entire startup. The development of large axial temperature gradients is similar for the cooled and uncooled leading edges, due to the free molecular condition in the entire vapor space during the initial transient heating. However, beyond this stage, peak temperatures are reduced, and temperature gradients disappear when the heat pipe is fully active. Figure 6.35 shows temperature distributions for both cases at a time of 1450 seconds.

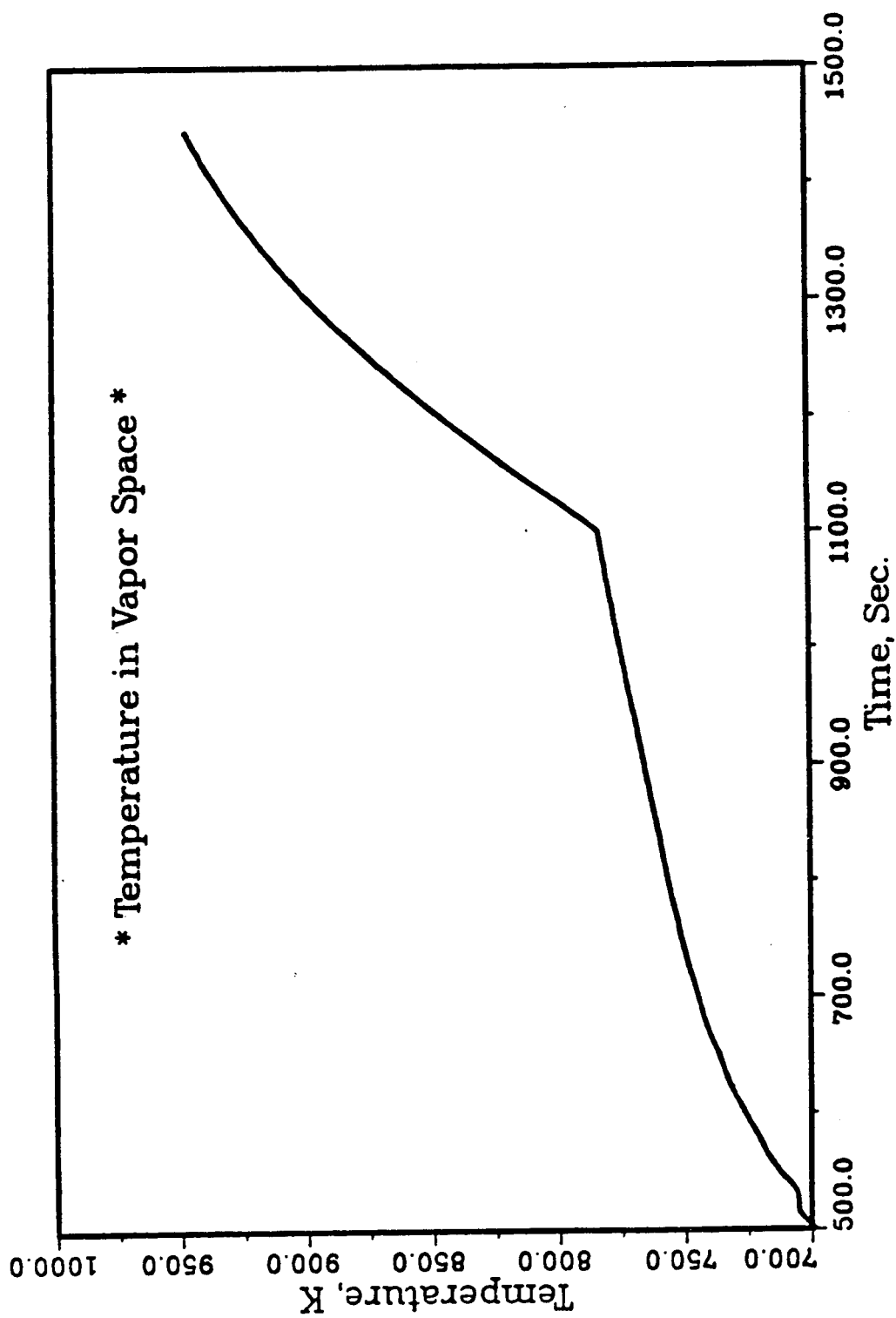


Figure 6.33. Average vapor temperature variation during startup.

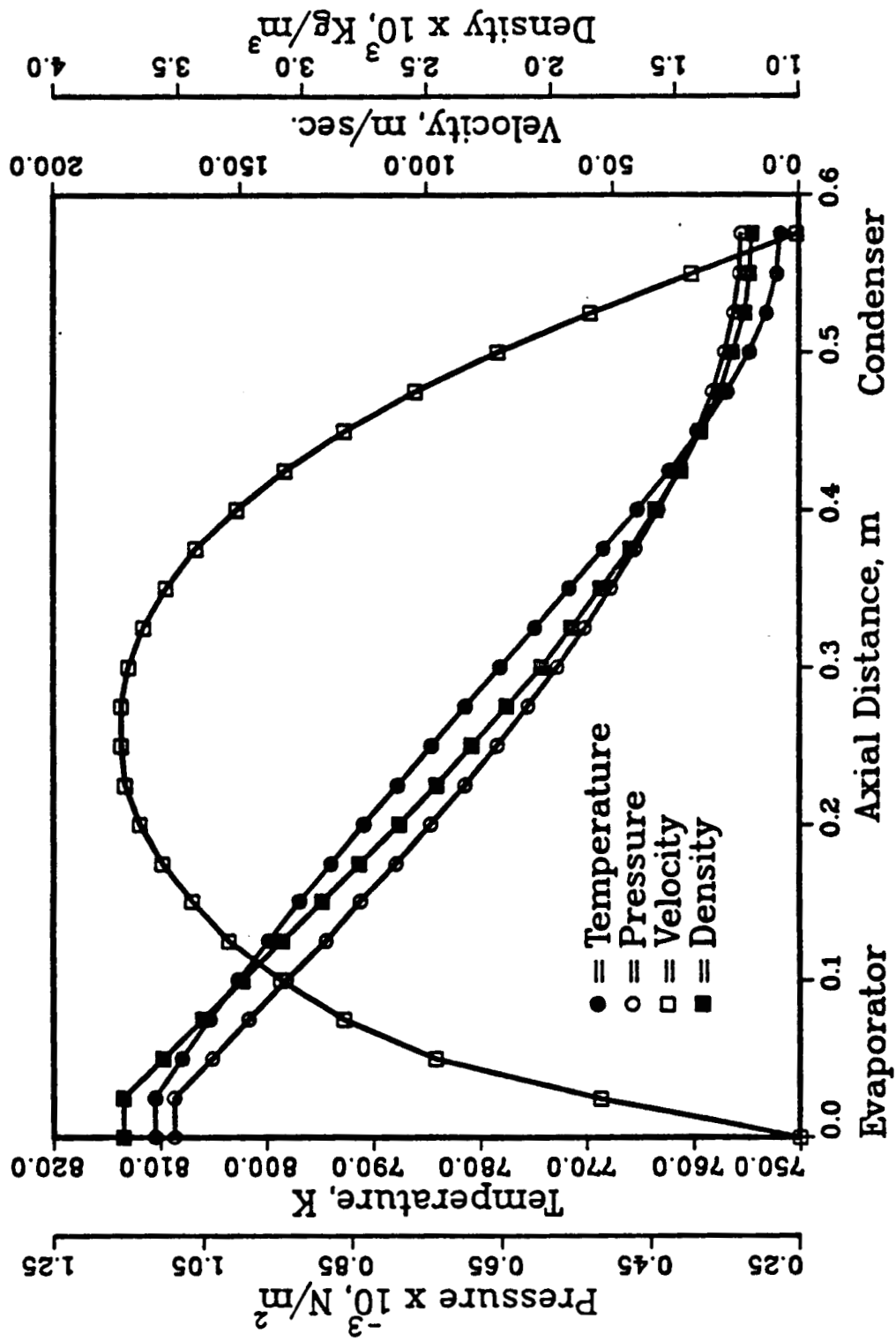


Figure 6.34. Axial variation of vapor temperature, pressure, velocity, and density

at $t = 1140$ sec..

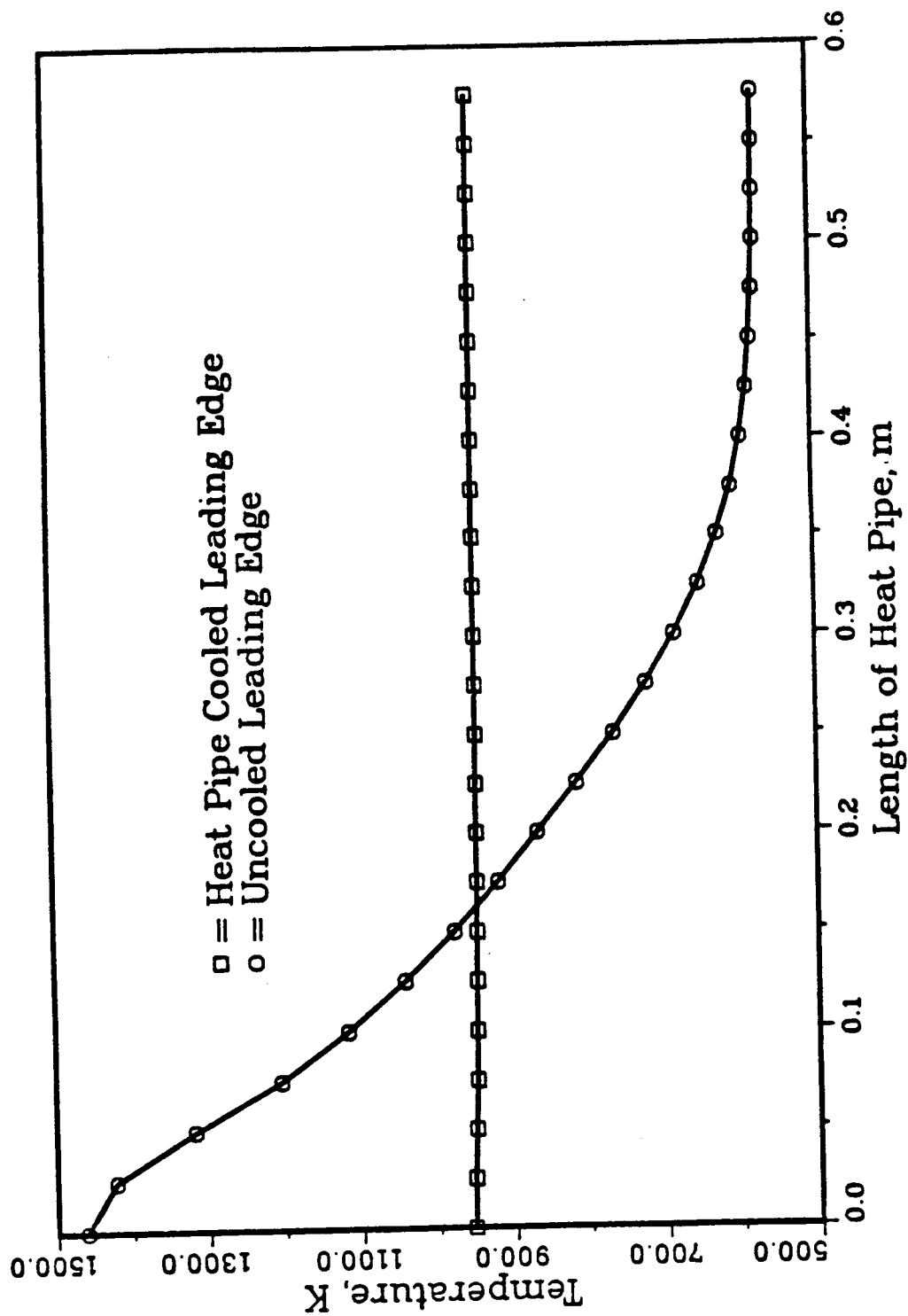


Figure 6.35. Computed temperature distribution for uncooled and cooled leading edge; $t = 1450$ sec..

It is clear that the heat pipe is very effective for reducing peak temperatures near the leading edge and eliminating axial temperature gradients.

6.4 Simulation of reentry heating environment

After the model components were checked against published data, a spacecraft reentry heating environment[30] was simulated to show capability of the present model. The same rectangular cross-section and material of each component were used. Heat input at the stagnation point is much greater than that for the previous test, as shown in Figure 6.36, so that the heating distribution on the heat pipe surface is also much greater as shown in Figure 6.37. Maximum heat flux at the stagnation point is 390 kW/m^2 . A triangular element is used to fit the curved leading edge shape. Figure 6.38 shows the two-dimensional grid system used to represent the leading edge. In order to reduce computational time a relatively small number of elements and nodes was used. Heat input near the stagnation point is very large so that small size elements are used near the stagnation point and large size elements are employed for the rest of the heat pipe. The same numerical procedures as previously described were employed except that an initial time step of 5 seconds was used.

Figure 6.39 shows temperature distributions along the heat pipe from the initial condition to 700 seconds. General behavior is similar to previous results, but due to high heat fluxes the continuum flow region is established early in the vapor space at 230 seconds. Also, as shown in Figures 6.40 and 41, most of the working fluid which is initially in the frozen state is melted at about 350 seconds and the entire vapor space is occupied by continuum flow at 460 seconds. As expected, less time is consumed for the entire heat pipe to become active. At a time of 500 seconds, the heat pipe is nearly isothermal with position, but the temperature increases

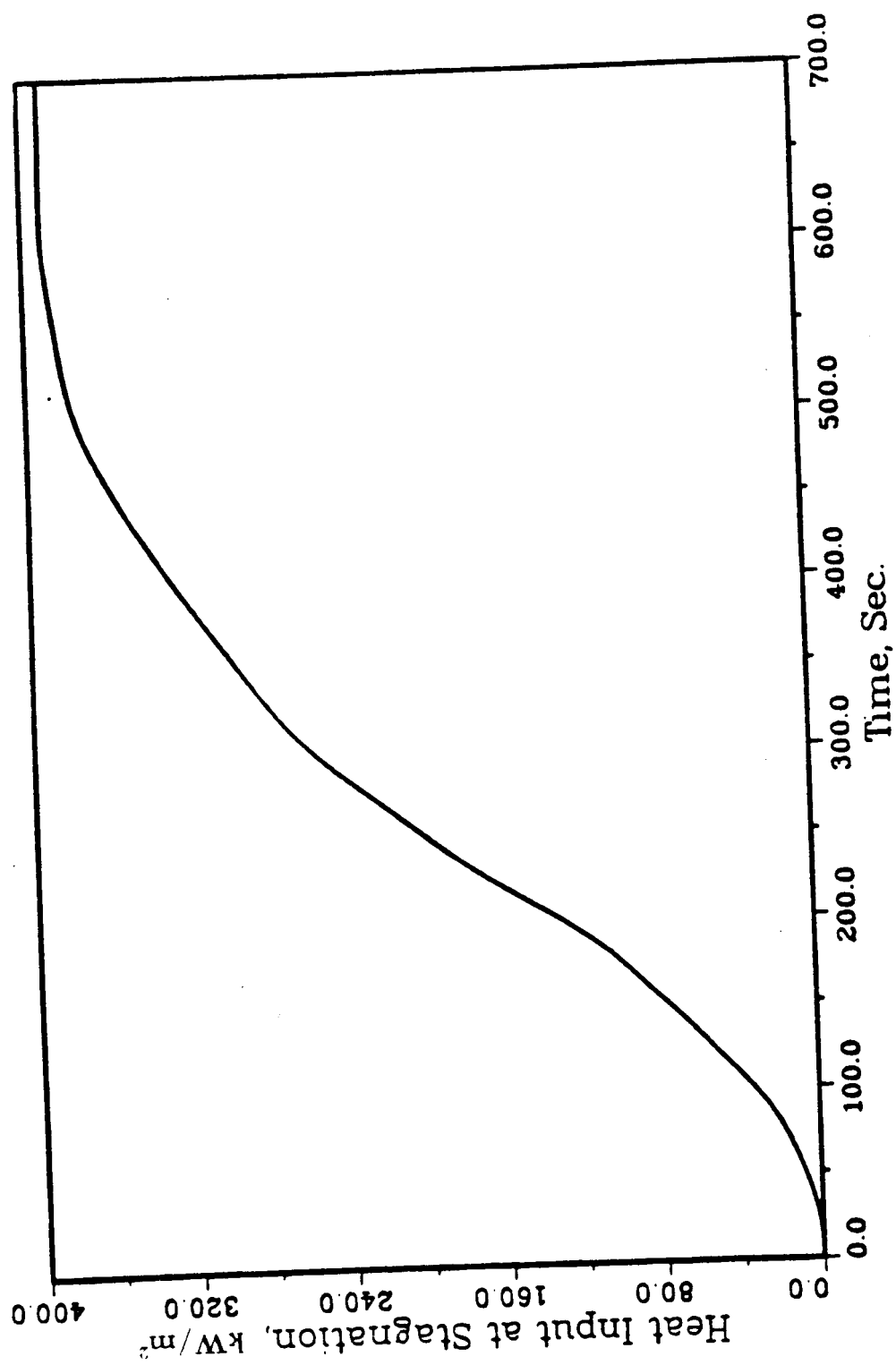


Figure 6.36. Heat input at the stagnation point for reentry simulation.

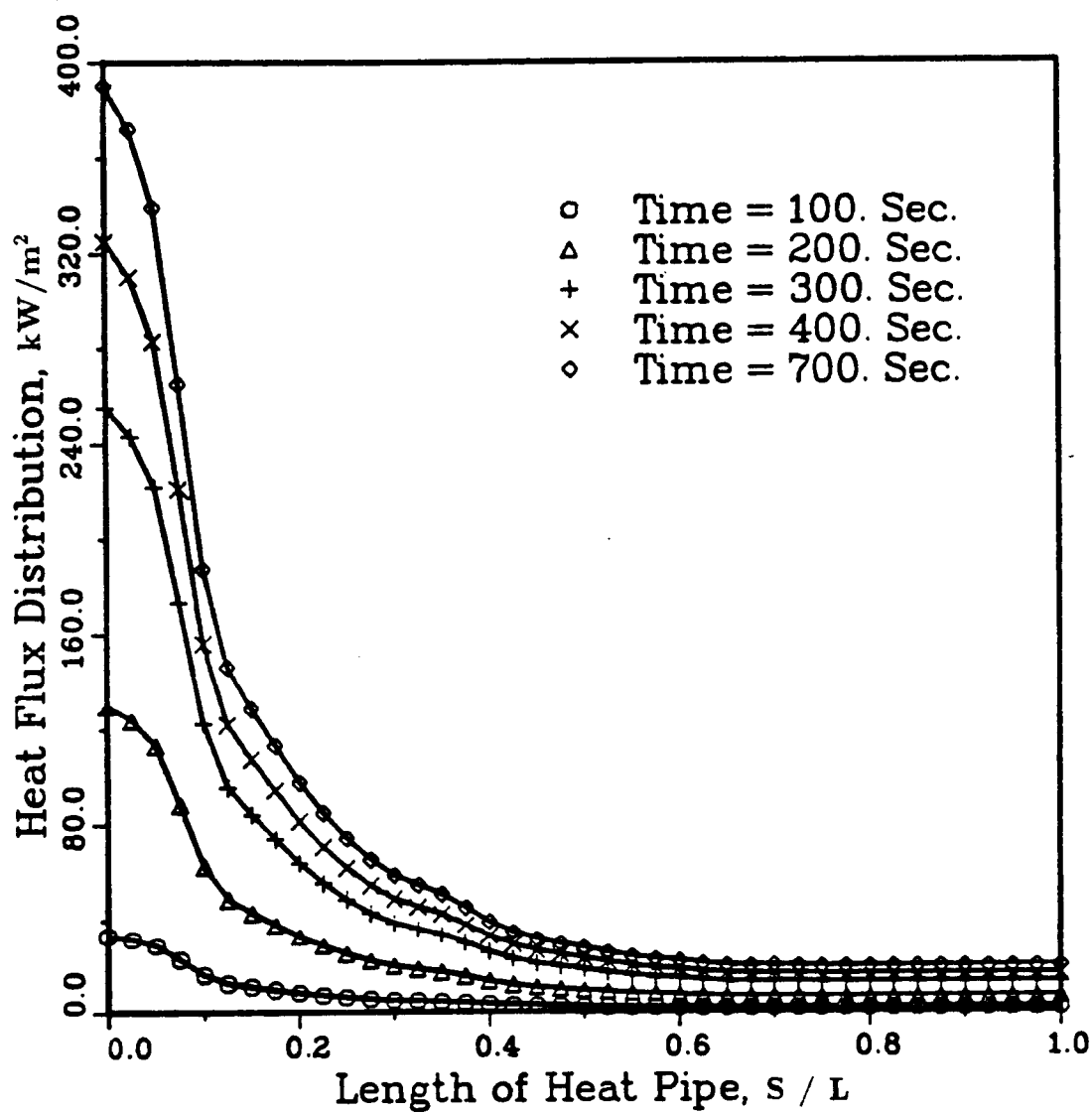


Figure 6.37. Heat flux distribution on a leading edge model for reentry simulation.

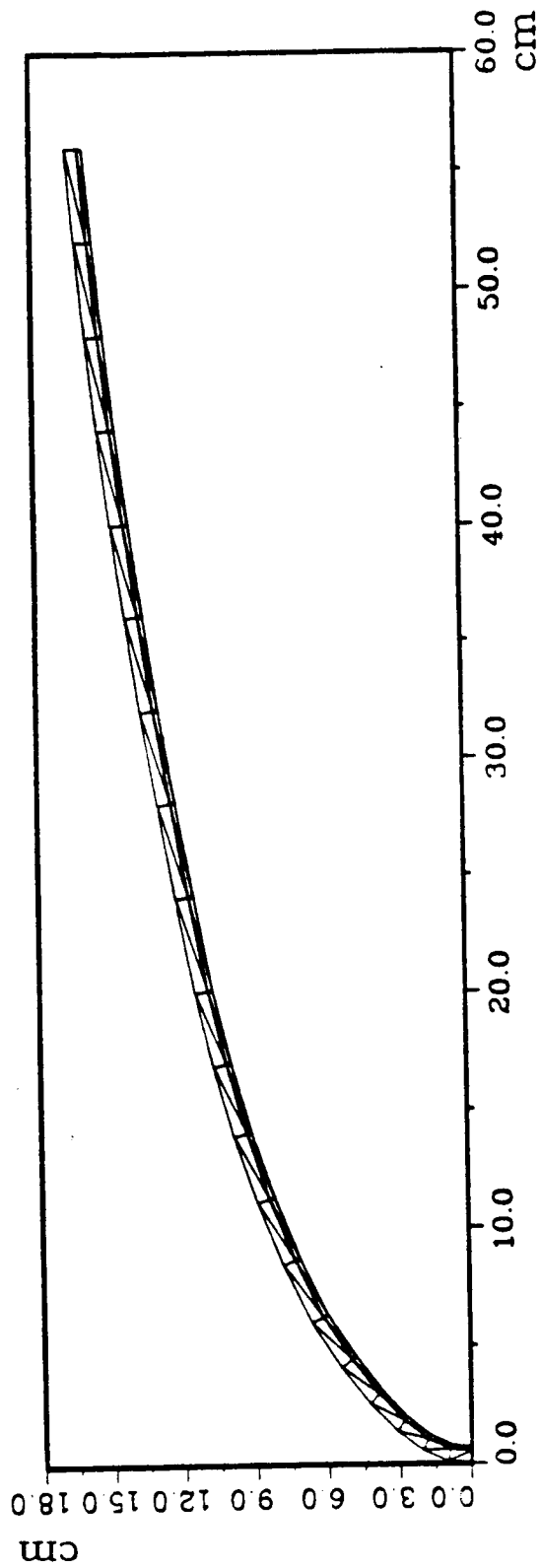


Figure 6.38. Two-dimensional mesh used to represent a heat pipe cooled leading edge for reentry simulation; 80 elements, 63 nodes.

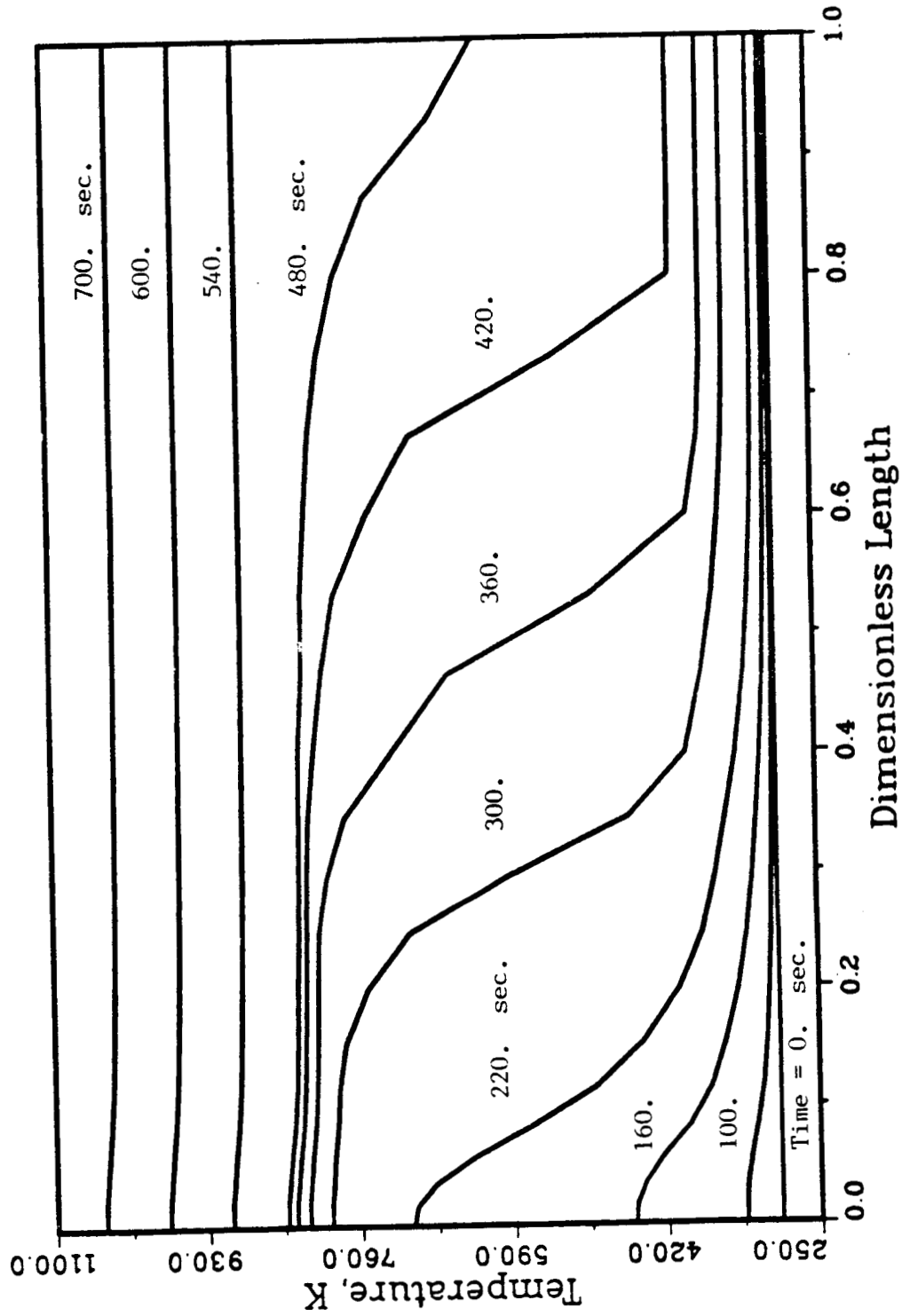


Figure 6.39. Temperature of a heat pipe cooled leading edge for reentry simulation.

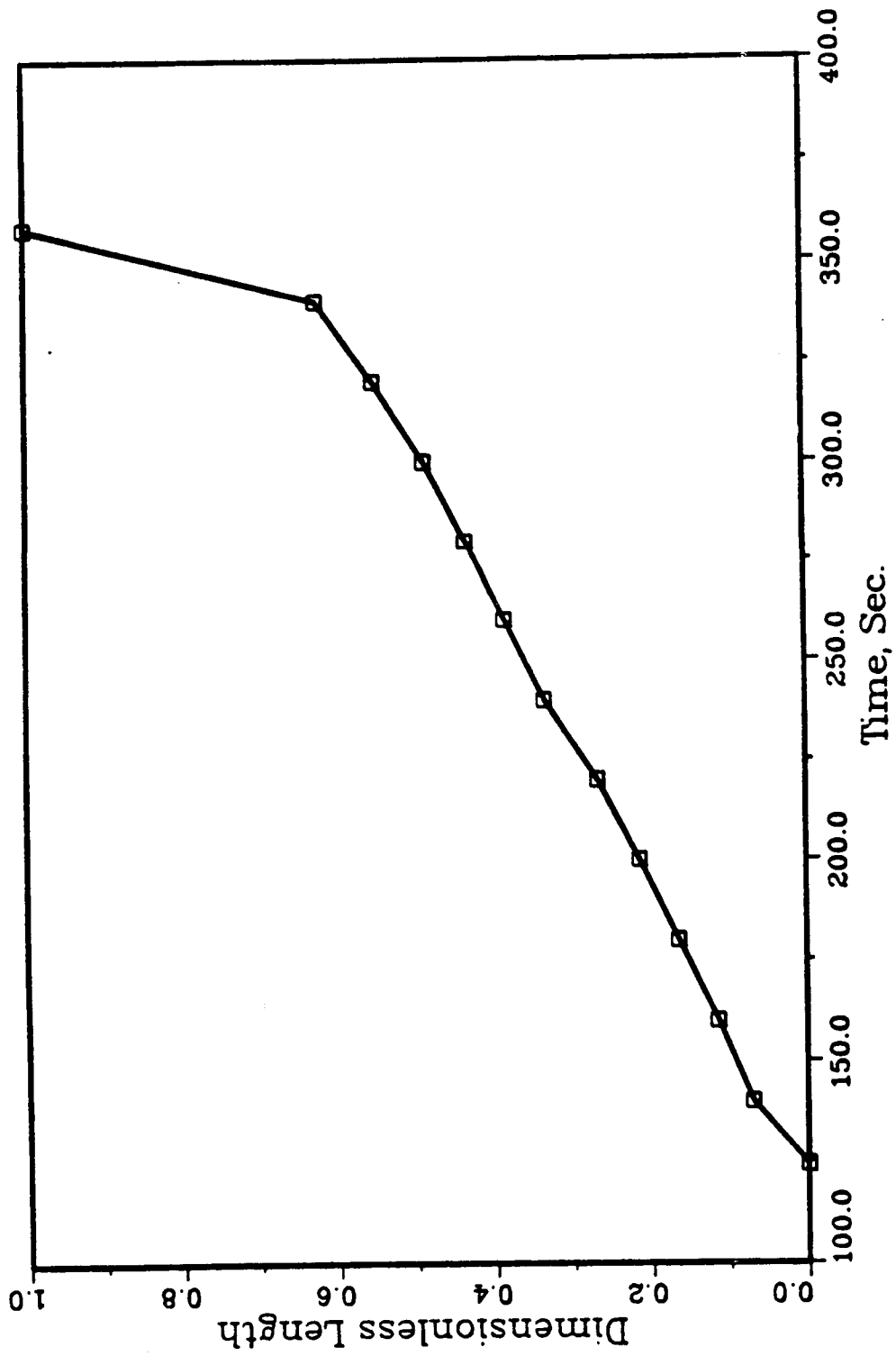


Figure 6.40. Location of phase change of sodium for reentry simulation.

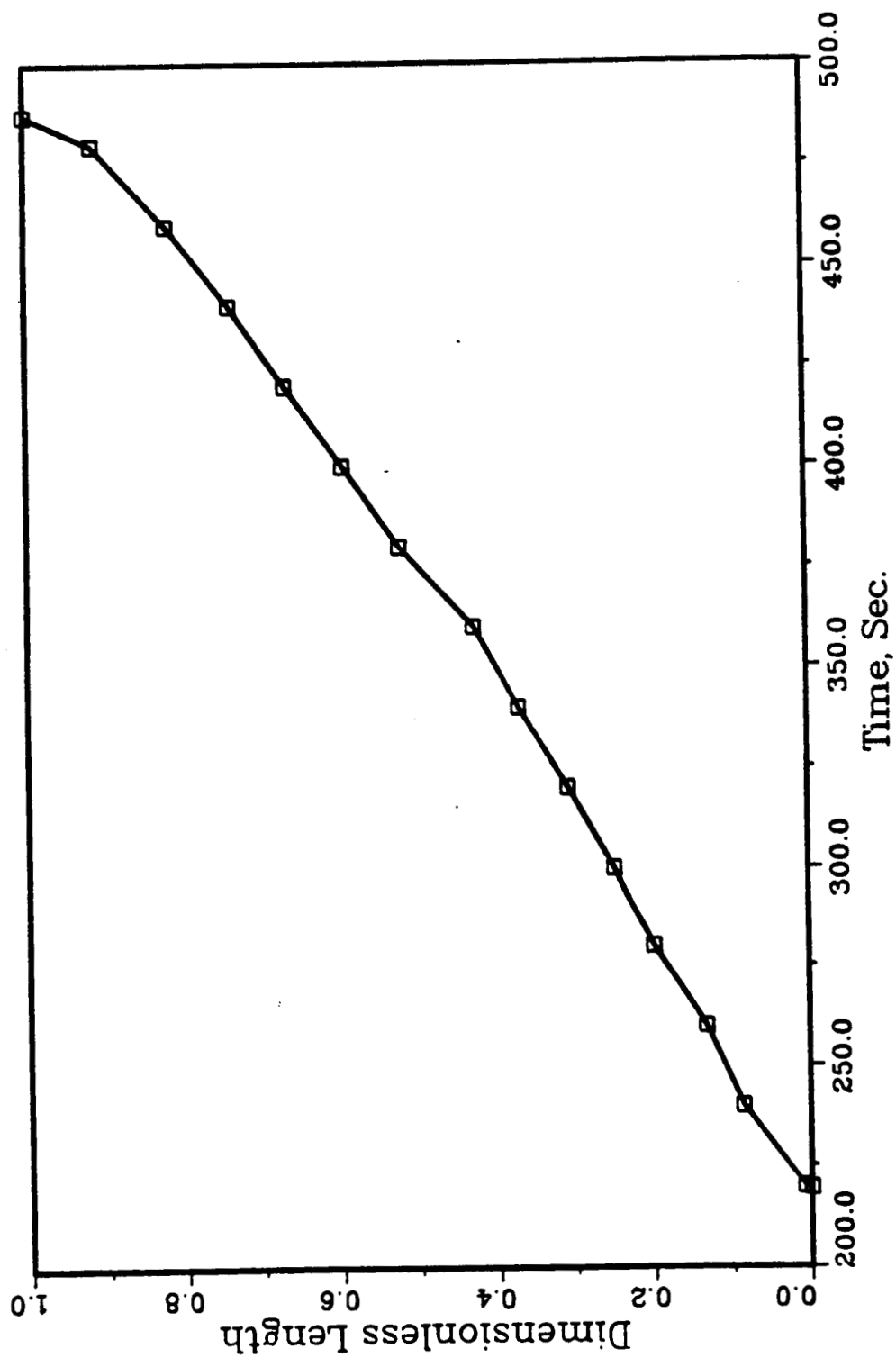


Figure 6.41. Position of continuum flow front for reentry simulation.

uniformly with time until a maximum temperature of 1040 K is achieved at a time of 700 seconds. Figure 6.42 shows the temperature histories of the heat pipe at the stagnation point, end of the heat pipe, and a short distance away from the stagnation point. After the continuum flow region is established, it takes about 280 seconds for the entire vapor space to reach continuum flow. Also Figures 6.43 and 44 show temperature distributions along the length at an interface between shell and wick and at the liquid-vapor interface respectively, from initial time to 700 seconds. Temperature distributions at these sections are shown on Figure 6.45. A maximum temperature difference of 90 K is observed owing to the large heat input at the stagnation point while small differences exist for the rest of the heat pipe.

Variation of the average vapor temperature as shown in Figure 6.46 is similar to that for low heat input. When the entire vapor space reaches the continuum flow regime, vapor temperature increases relatively rapidly and then again slows down to approach steady state. Figure 6.47 shows behavior of the vapor flow at 503 seconds. A temperature drop of 50 K is observed along the length and pressure is not recovered. Since velocity is still large and heat extracted at the beginning of the condenser is small, the effect of friction at the interface is greater than that of inertia. Thus, a maximum velocity of the vapor does not occur at the exit of the evaporator but in the condenser.

As expected, behavior of the heat pipe is similar to the previous results presented except that a higher steady state temperature is achieved and startup is faster due to greater heat input. Figure 6.48 shows temperature distributions for a leading edge with heat pipe cooling and without cooling at 700 seconds into reentry. The heat pipe reduces peak temperature by the 600 K near the stagnation point and the leading edge becomes nearly isothermal. Again, it is obvious that the heat pipe is an effective device for cooling leading edges during reentry.

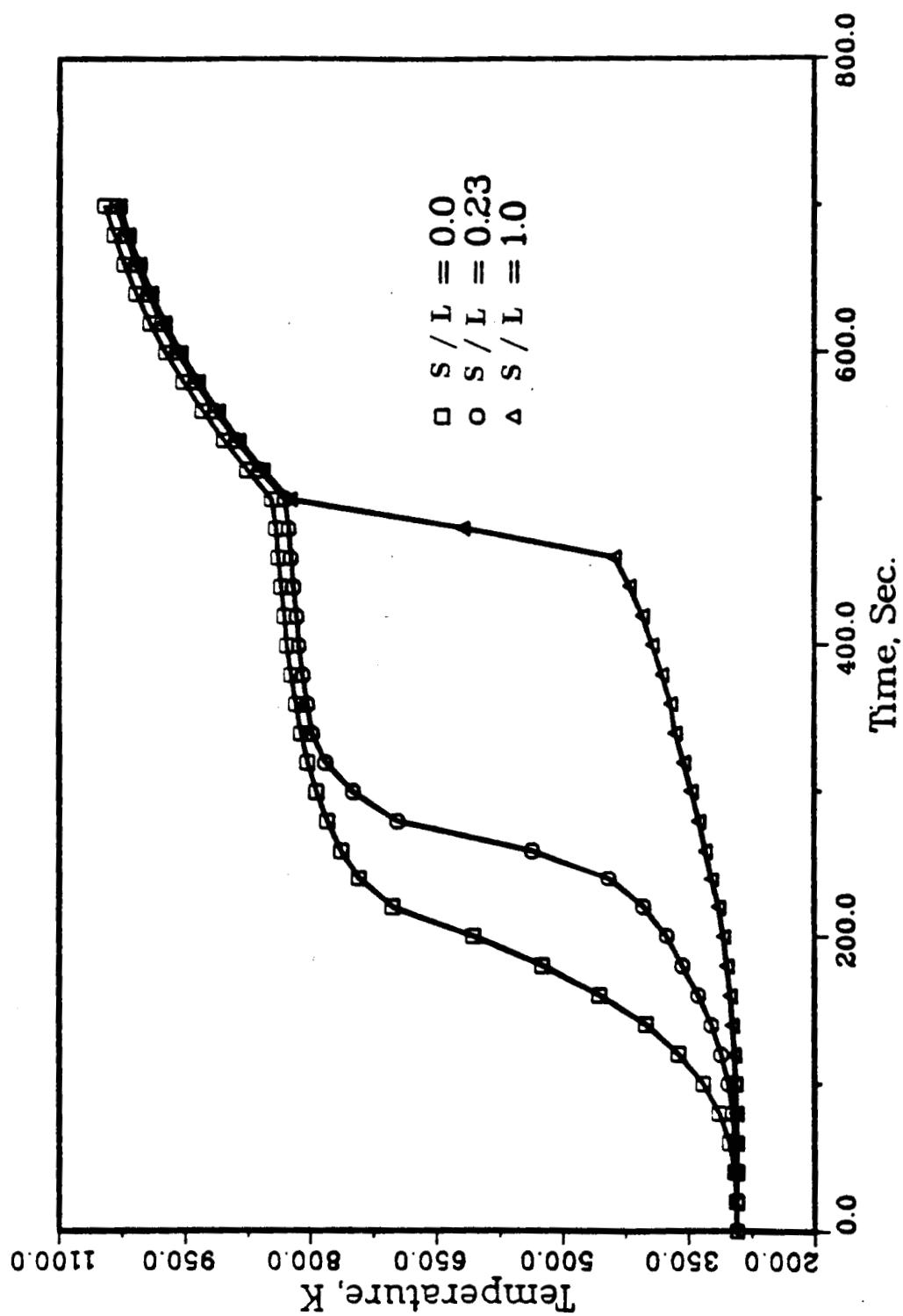


Figure 6.42. Temperature history of three locations in the heat pipe for reentry simulation.

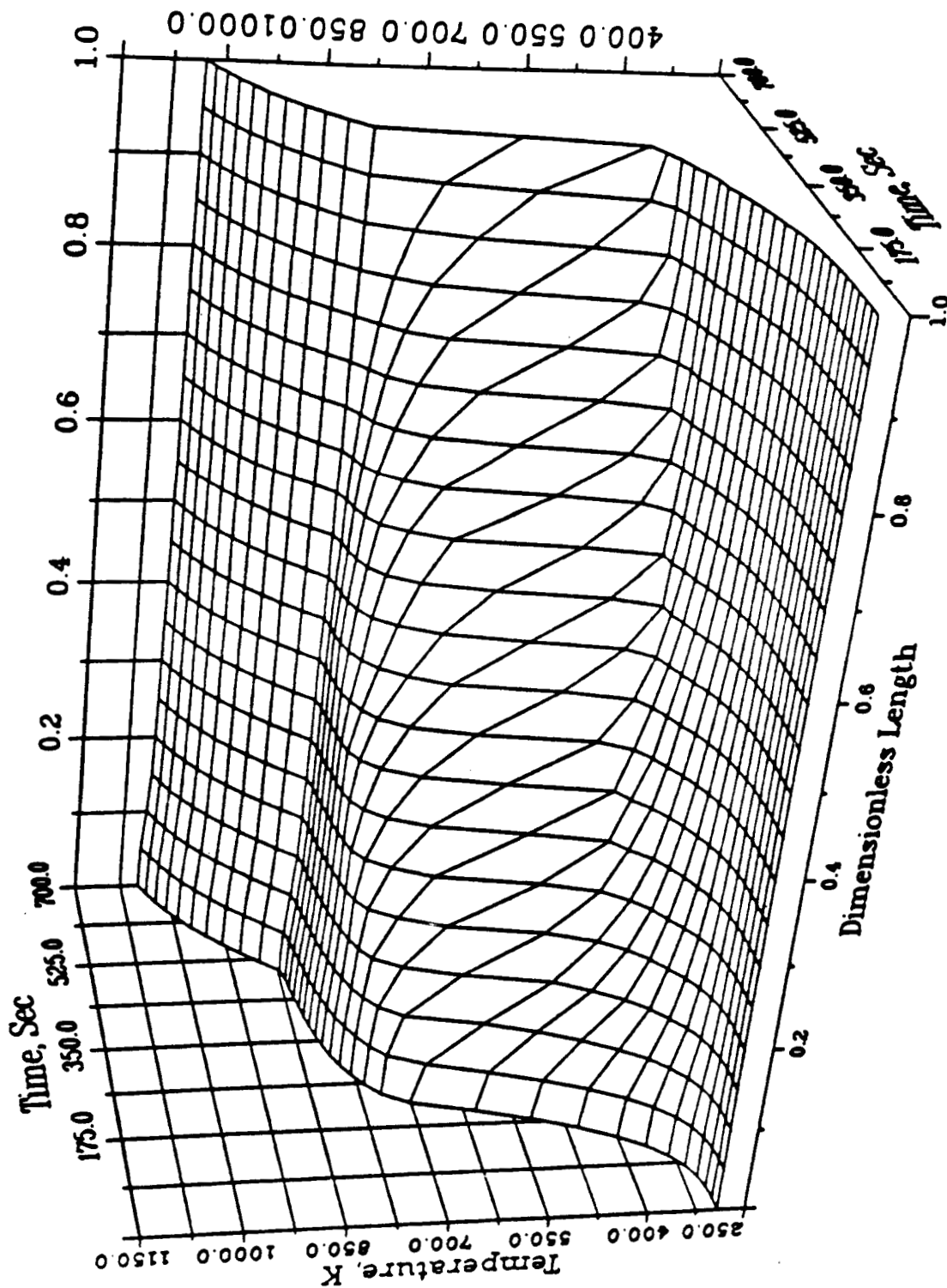


Figure 6.43. Temperature distribution at interface between shell and capillary structure for reentry simulation.

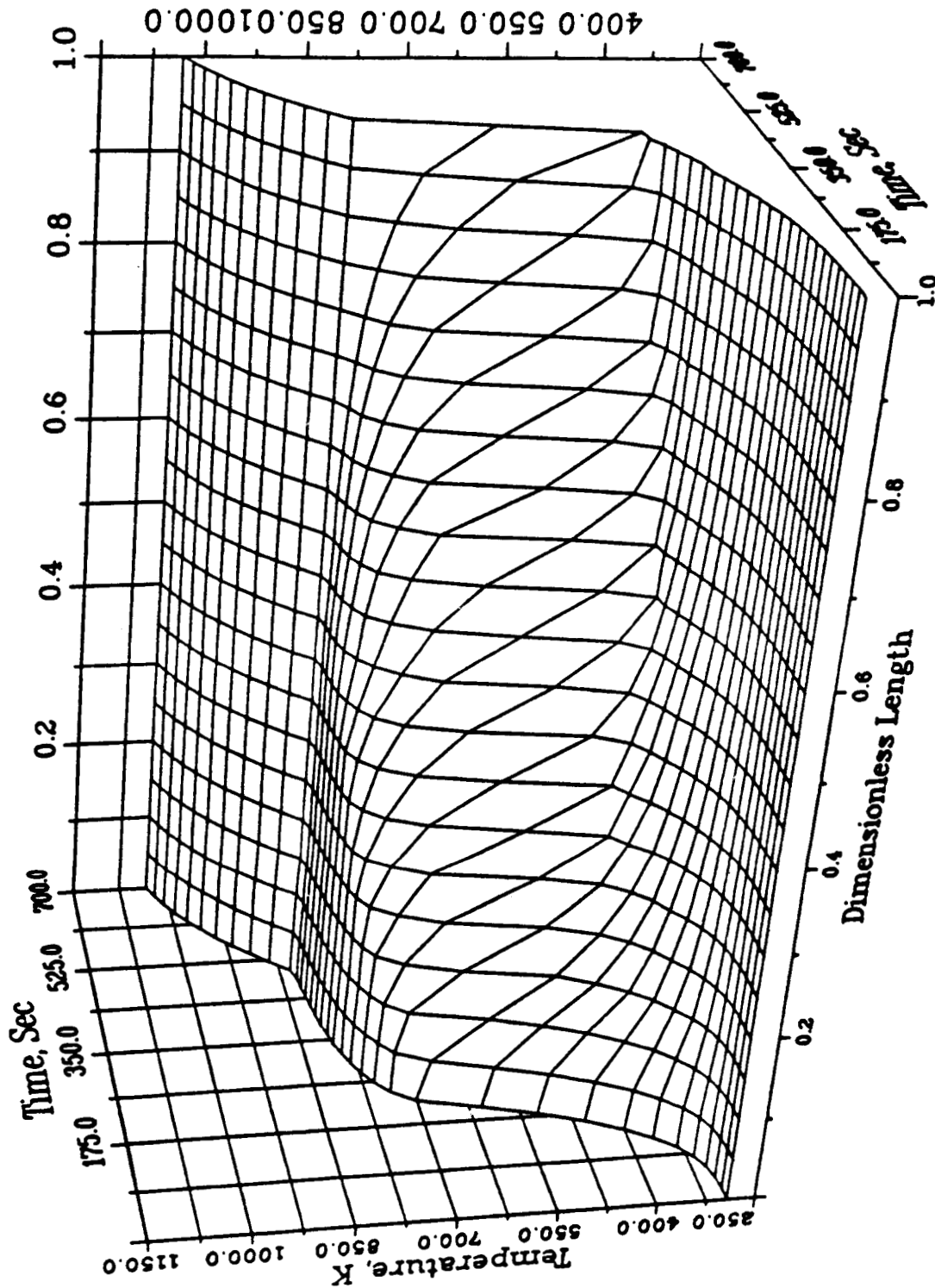


Figure 6.44. Temperature distribution at the interface for reentry simulation.

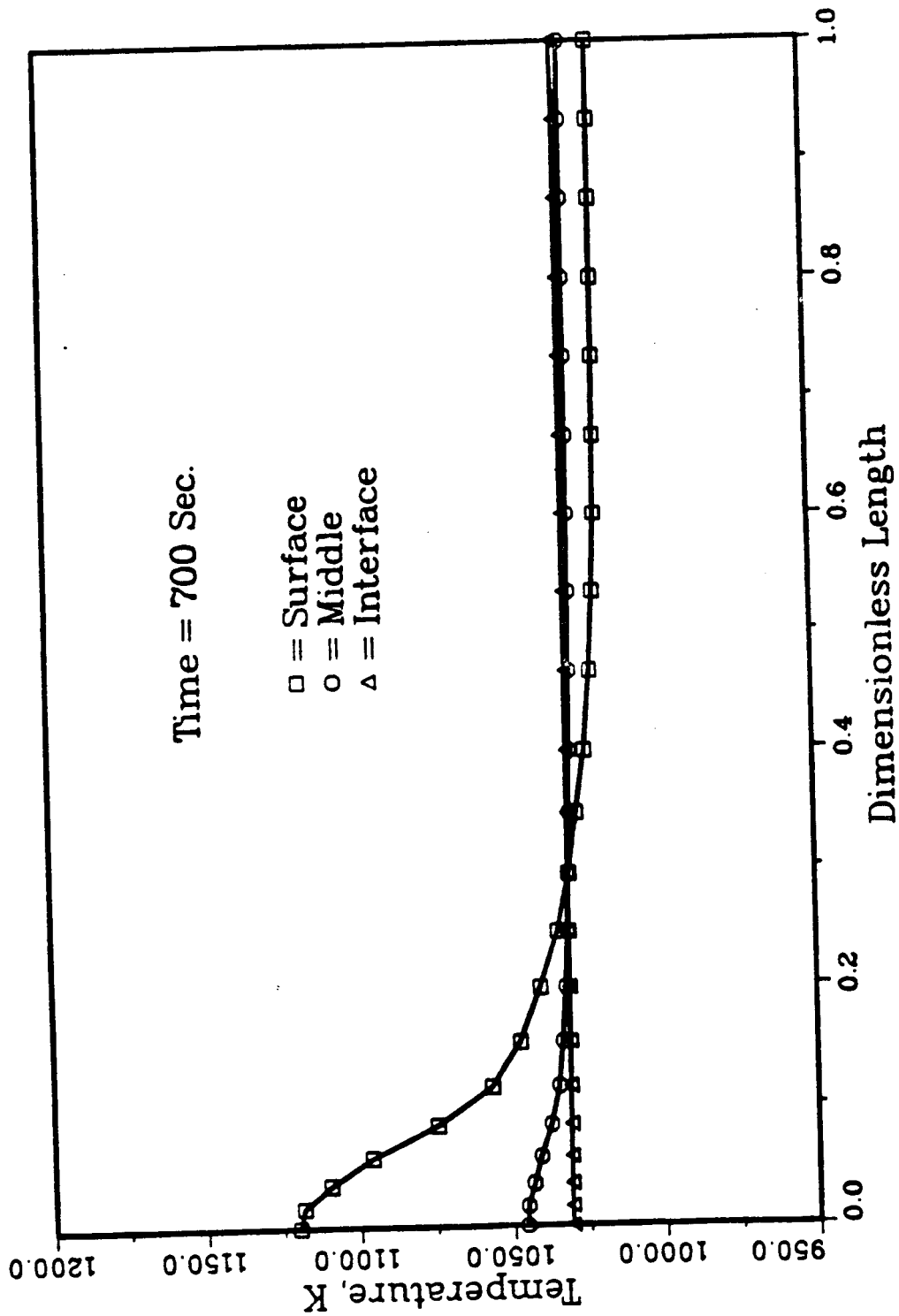


Figure 6.45. Temperature distribution at the different locations in wall for reentry simulation.

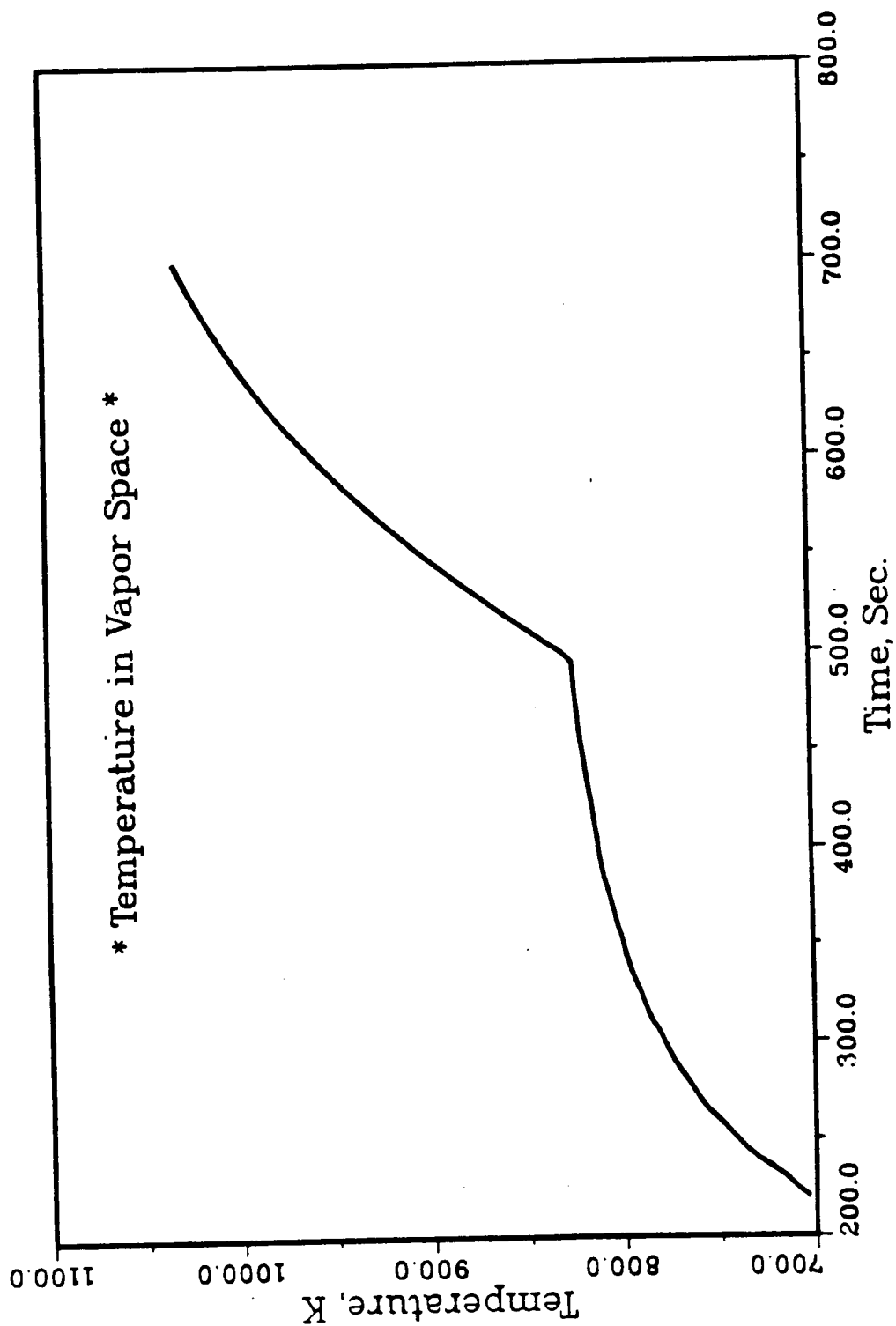


Figure 6.46. Average vapor temperature variation during startup for reentry simulation.

ORIGINAL PAGE IS
OF POOR QUALITY

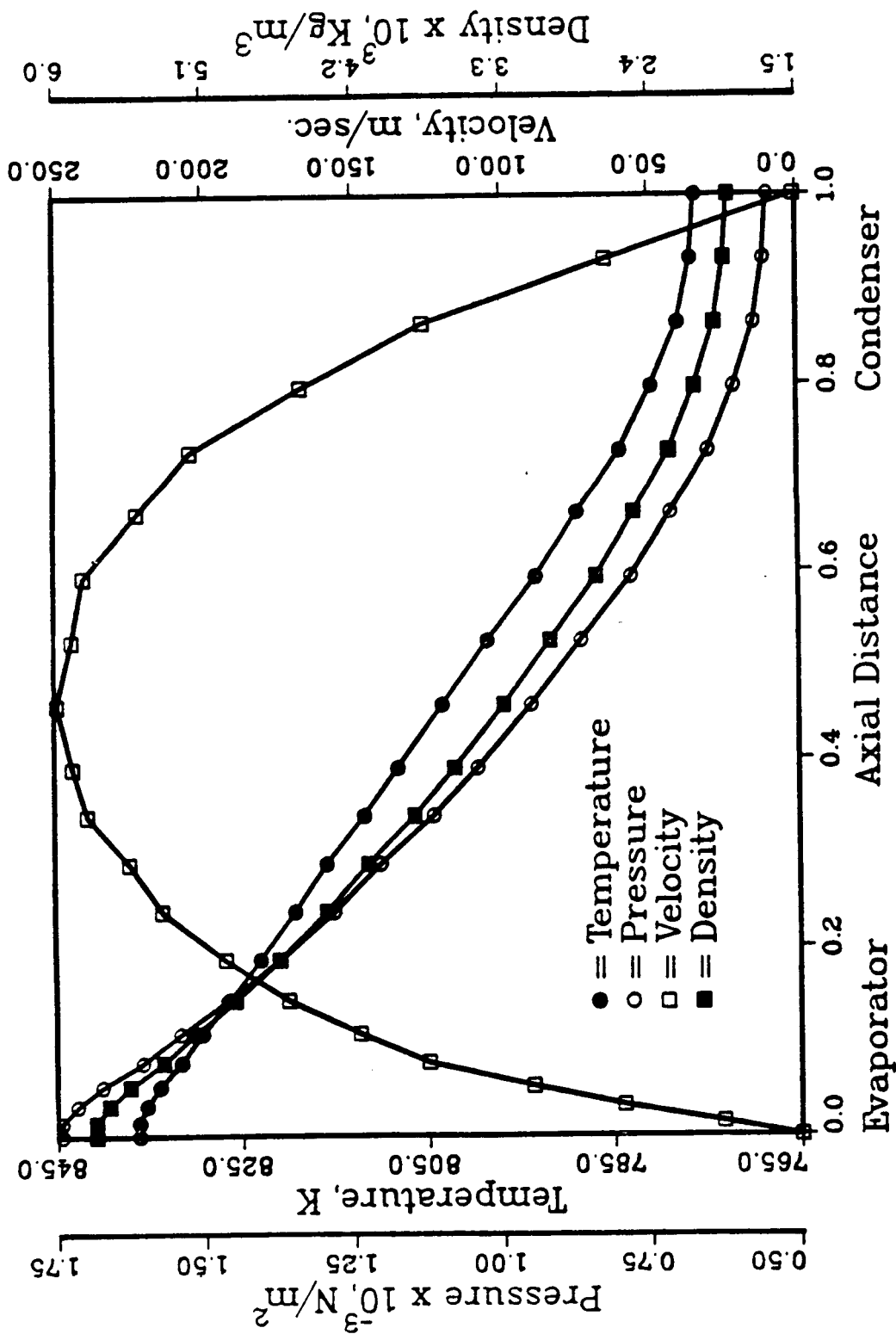


Figure 6.47. Axial variation of vapor temperature, pressure, velocity, and density at $t = 503$ seconds for reentry simulation.

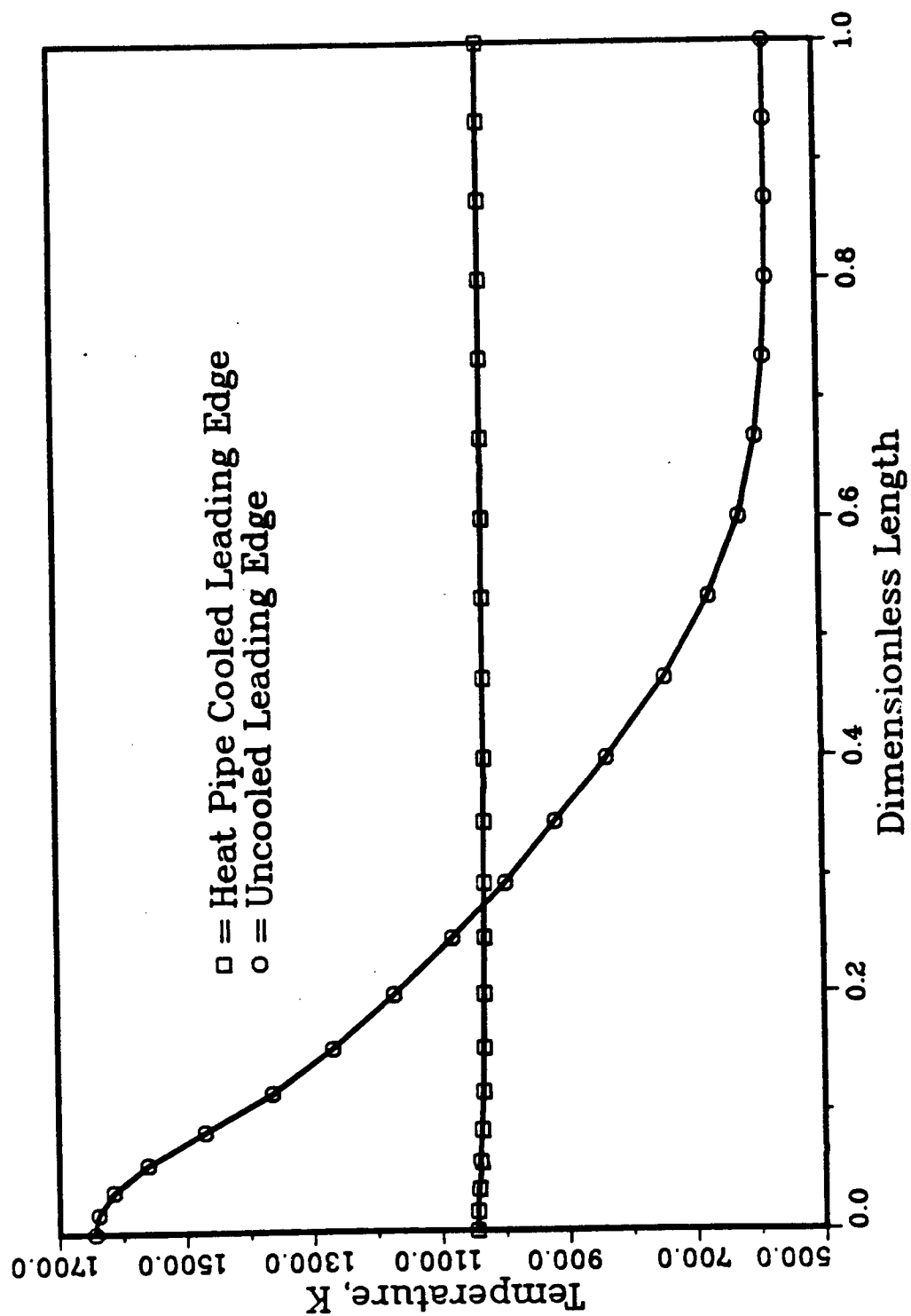


Figure 6.48. Computed temperature distribution for uncooled and cooled leading edge of reentry simulation; $t = 700$ seconds.

CHAPTER VII

CONCLUSIONS AND RECOMMENDATIONS

7.1 Conclusions

This study has been concerned with startup behavior of heat pipes from the frozen state. A mathematical model and associated finite element computational code were developed. Results were compared with published data and a reentry heating environment was simulated to show capability of the model developed. The model approximately predicts the correct startup time and temperature distribution for the reentry problem. Numerical results computed for heat pipe cooled and uncooled leading edges show development of the large chordwise temperature gradients during the initial heating for both cases. After a part of the heat pipe is active, the effectiveness of using the heat pipe is shown clearly. In addition, the following conclusions are derived from numerical results.

1. Temperature near the stagnation point increases rapidly and a large temperature gradient is observed due to the extremely small vapor density during the beginning of startup. Thus, critical design consideration should be given for this period.
2. During the second phase of startup, the sonic vapor limit is encountered due to the large temperature gradient in the vapor space, and temperature increases slowly.
3. When the sonic limit is not present, temperature first increases rapidly and then more slowly as steady state is approached.
4. A large temperature difference exists at all times in the wall and capillary

structure near the stagnation point due to large heat input at this point.

5. Heat pipe cooling of hypersonic wing structures greatly reduces temperature gradients on the skin.
6. Startup behavior of heat pipe cooled leading edges is similar for relatively large and relatively small heat inputs but large inputs cause startup to occur more quickly.

7.2 Recommendations

It is recommended that models and numerical techniques be improved so that more accurate predictions can be made and so that computer costs can be reduced.

1. During startup, the working fluid is only partially melted so that some of the vapor may condense on the surface of the frozen working substance. Drying and rewetting might be incorporated into the model instead of assuming a saturated wick structure.
2. For a better prediction of the vapor flow dynamics, one-dimensional, transient and compressible equations might be developed to take into account supersonic flow of vapor.
3. A better numerical scheme is needed to couple the effect of vapor flow dynamics to governing equations for the heat pipe shell and wick structure.
4. To handle realistic operating conditions, the effects of gravity might be included in the mathematical model.
5. The model should be made fully three dimensional.

6. The computer program should be made user friendly.

APPENDICES

APPENDIX A

ELEMENT MATRICES

A.1 Interpolation function

The spatial domain is discretized into three-node, linear, triangular elements as shown in Figure A.1, since an assemblage of triangles can always represent a two-dimensional domain of any shape. The shape functions are derived by using natural coordinates which range between zero and unity within the element, and whose variation between nodes is linear. Use of these coordinates is advantageous in evaluating the integrals in the element equations[55].

If L_1 , L_2 , and L_3 are selected as the natural coordinates, the location of the point P_0 within the element may be expressed by the following equations

$$X = L_1 X_1 + L_2 X_2 + L_3 X_3 \quad (A.1)$$

$$Y = L_1 Y_1 + L_2 Y_2 + L_3 Y_3 \quad (A.2)$$

$$1 = L_1 + L_2 + L_3 \quad (A.3)$$

From the equations above, natural coordinates are written in terms of cartesian coordinates.

$$L_1 = \frac{1}{2\Delta^{(e)}}(a_1 + b_1 X + c_1 Y) \quad (A.4)$$

ORIGINAL PAGE IS
OF POOR QUALITY

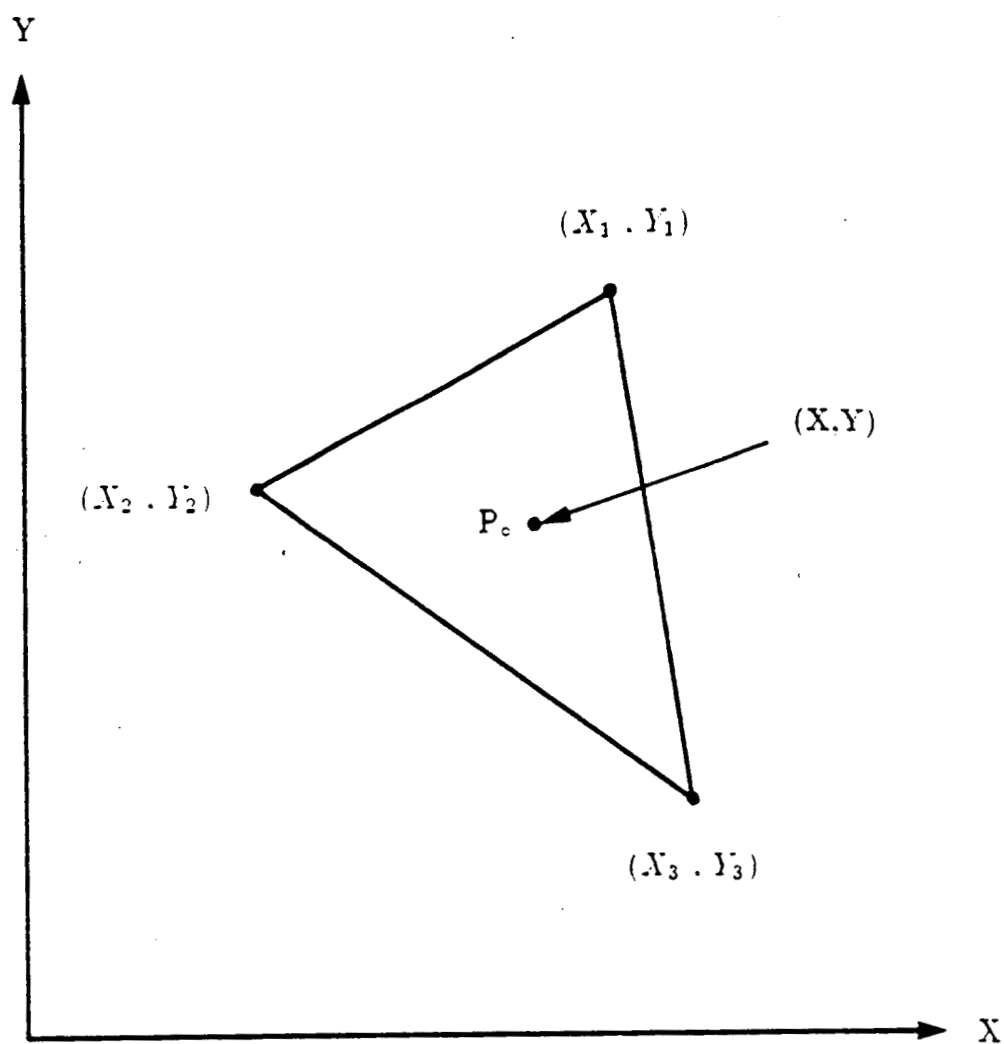


Figure A.1. Three-node, linear, triangular element with global coordinates.

$$L_2 = \frac{1}{2\Delta^{(e)}}(a_2 + b_2X + c_2Y) \quad (A.5)$$

$$L_3 = \frac{1}{2\Delta^{(e)}}(a_3 + b_3X + c_3Y) \quad (A.6)$$

where

$$a_1 = X_2Y_3 - Y_3Y_2, \quad b_1 = Y_2 - Y_3, \quad c_1 = X_3 - X_2$$

$$a_2 = X_3Y_1 - Y_1Y_3, \quad b_2 = Y_3 - Y_1, \quad c_2 = X_1 - X_3$$

$$a_3 = X_1Y_2 - Y_1Y_2, \quad b_3 = Y_1 - Y_2, \quad c_3 = X_2 - X_1$$

$$2\Delta^{(e)} = \begin{vmatrix} 1 & X_1 & Y_1 \\ 1 & X_2 & Y_2 \\ 1 & X_3 & Y_3 \end{vmatrix}$$

These natural coordinates L_1 , L_2 , and L_3 are the linear interpolation functions for a triangle, that is, $N_i = L_i$ for the linear triangle. The interpolation functions are expressed as follows:

$$N_i = \frac{1}{2\Delta^{(e)}}(a_i + b_iX + c_iY) \quad i = 1,2,3 \quad (A.7)$$

$$\frac{\partial N_i}{\partial X} = \frac{b_i}{2\Delta^{(e)}} \quad (A.8)$$

ORIGINAL PAGE IS
OF POOR QUALITY

$$\frac{\partial N_i}{\partial Y} = \frac{c_i}{2\Delta^{(e)}} \quad (A.9)$$

A.2 Two-dimensional element matrices

Thermal conductivity and specific heat are assumed to be constant within an element and are evaluated by using the average temperature. The $[K_e]$ matrices are then expressed by

$$\begin{aligned} [K_e] &= \int_{R^{(e)}} K \left(\frac{\partial N_i}{\partial X} \frac{\partial N_j}{\partial Y} + \frac{\partial N_i}{\partial Y} \frac{\partial N_j}{\partial X} \right) dX dY \\ &= K \left(\frac{b_i}{2\Delta^{(e)}} \frac{b_j}{2\Delta^{(e)}} + \frac{c_i}{2\Delta^{(e)}} \frac{c_j}{2\Delta^{(e)}} \right) \\ &= \frac{K}{4(\Delta^{(e)})^2} (b_i b_j + c_i c_j) \end{aligned} \quad (A.10)$$

where

$$b_i b_j + c_i c_j = \begin{pmatrix} b_1^2 + c_1^2 & b_1 b_2 + c_1 c_2 & b_1 b_3 + c_1 c_3 \\ b_2 b_1 + c_2 c_1 & b_2^2 + c_2^2 & b_2 b_3 + c_2 c_3 \\ b_3 b_1 + c_3 c_1 & b_3 b_2 + c_3 c_2 & b_3^2 + c_3^2 \end{pmatrix}$$

For the element which is not involved in phase change, the $[C]$ matrices are given by

$$\begin{aligned} [C] &= \int_{R^{(e)}} C N_i N_j dX dY \\ &= C \int_{R^{(e)}} \begin{pmatrix} N_1^2 & N_1 N_2 & N_1 N_3 \\ N_2 N_1 & N_2^2 & N_2 N_3 \\ N_3 N_1 & N_3 N_2 & N_3^2 \end{pmatrix} \\ &= C \Delta^{(e)} \begin{pmatrix} 1/6 & 1/12 & 1/12 \\ 1/12 & 1/6 & 1/12 \\ 1/12 & 1/12 & 1/6 \end{pmatrix} \end{aligned} \quad (A.11)$$

ORIGINAL PAGE IS
OF POOR QUALITY

For the matrix contributions of an element having sides coincident with the external boundary of the solution domain, it is assumed that the convective heat transfer coefficient, h_{cr} , heat flux, \ddot{Q} , and radiation coefficient, β_r , are constant along the side of an element. The shape functions for the boundary segment have the same expression of Equation(A.7). For the side of the element shown in Figure A.1 between nodes 1 and 2, coincident with external boundary of the solution domain, the matrix contributions are written as follows:

$$\begin{aligned} [K_h] &= \int_{A_s} h_{cr} N_i N_j dS \\ &= h_{cr} \int_{A_s} \begin{pmatrix} N_1^2 & N_1 N_2 & 0 \\ N_2 N_1 & N_2^2 & 0 \\ 0 & 0 & 0 \end{pmatrix} dS \\ &= \frac{h_{cr} \ell_{12}}{6} \begin{pmatrix} 2 & 1 & 0 \\ 1 & 2 & 0 \\ 0 & 0 & 0 \end{pmatrix} \end{aligned} \quad (A.12)$$

$$\begin{aligned} [K_r] &= \int_{A_s} \beta_r N_i N_j dS \\ &= \frac{\beta_r \ell_{12}}{6} \begin{pmatrix} 2 & 1 & 0 \\ 1 & 2 & 0 \\ 0 & 0 & 0 \end{pmatrix} \end{aligned} \quad (A.13)$$

where ℓ_{12} is the length of the side between nodes 1 and 2 of the element.

Also, the column vectors contributions from surface integrals are

$$\begin{aligned} [F_q] &= \int_{A_s} \ddot{Q} N_i dS \\ &= \ddot{Q} \int_{A_s} \begin{pmatrix} N_1 \\ N_2 \\ 0 \end{pmatrix} dS \\ &= \frac{\ddot{Q} \ell_{12}}{2} \begin{pmatrix} 1 \\ 1 \\ 0 \end{pmatrix} \end{aligned} \quad (A.14)$$

$$\begin{aligned}
[F_h] &= \int_{A_s} h_{cr} N_i T_{cr} dS \\
&= h_{cr} T_{cr} \int_{A_s} \begin{pmatrix} N_1 \\ N_2 \\ 0 \end{pmatrix} dS \\
&= \frac{h_{cr} T_{cr} \ell_{12}}{2} \begin{pmatrix} 1 \\ 1 \\ 0 \end{pmatrix}
\end{aligned} \tag{A.15}$$

$$\begin{aligned}
[F_r] &= \int_{A_4} \beta_r N_i T_r dS \\
&= \beta_r T_r \int_{A_4} \begin{pmatrix} N_1 \\ N_2 \\ 0 \end{pmatrix} dS \\
&= \frac{\beta_r T_r \ell_{12}}{2} \begin{pmatrix} 1 \\ 1 \\ 0 \end{pmatrix}
\end{aligned} \tag{A.16}$$

ORIGINAL PAGE IS
OF POOR QUALITY

APPENDIX B

LISTING OF THE COMPUTER PROGRAM

PROGRAM HPMAIN(INPUT,OUTPUT,TAPE3=INPUT,TAPE4=OUTPUT,HPDAT,
&TAPE5=HPDAT,JANG,TAPE6=JANG,DATA,TAPE7=DATA,RESTA,TAPE8=RESTA,
&DATAV,TAPE2=DATAV)

```
C *****
C * This program solves the startup and transient performance of heat
C * pipe with metallic working fluids by using a finite element method.
C * The temperature is predicted from two-dimensional and transient
C * heat conduction equation, which incorporates the effects of the
C * phase change process in an expression for the volumetric heat cap-
C * pacity by using the enthalpy method. The Galerkin weighted residual
C * method is used to drive finite element formulations.
C * The flow dynamics of the vapor are described by one-D, compress-
C * ible and laminar momentum and energy equations. In one-D model,
C * the variation of velocity at cross section, friction at the liquid-
C * vapor interface, and quality of vapor are considered.
C * Five one-D governing differential equations for vapor are solved
C * by subroutine DVERK which uses Runge-Kutta method. The specified
C * temperature, heat flux, convective, and radiation boundary
C * conditions are applicable. This program can be used to solve pure
C * conduction or phase change problem alone.
C * Implicit or explicit time stepping schemes are used. Since
C * explicit scheme is not self-starting method, implicit scheme is used
C * for first few time steps. For this purpose, set proper number for
C * variable NTS.
C * Grid system can be generated by program HPGRNW. Input data file
C * for program HPMAIN consists of output data file of HPGRNW and
C * general data which specifies some general conditions.
C *
C * To use IMSLIB Library :
C *
C *      AT,IMSLIB/UN=LIBRARY
C *      LIBRARY,IMSLIB
C *
C * To obtain, compile and run program HPMAIN :
C *
C *      GET,HPMAIN,HPDAT,RESTA(Get this RESTA only for restart)
C *      RWF
C *      FTN5,I=HPMAIN,L=0
C *      LGO,,
C *
C *      (PROGRAM WILL PROMPT FOR INPUT DATA)
C *
C * To view results in files JANG, DATA and DATAV:
C *
C *      RWF
C *      C,JANG(Temperature distribution for every time step)
C *      C,DATA(Temp. distribution for particalur time to plot)
C *      C,DATAV(Vapor temperature for every time step)
C *
C *      Created      ; Dec. 9, 1985 by Jong Hoon Jang
C *      Last update ; Dec. 05, 1987 by Jong Hoon Jang
C *****
```

```

14  FORMAT('HOW OFTEN DO YOU WANT TO PRINT, EX = 1,3..?')
    READ(3,*) NFREQ

C .....READ GENERAL DATA.....

    READ(5,*) TEMPI,TMEL,TSTAR,DETP,HRSL,DIST,WIDTH

C          TEMPI = INITIAL TEMPERATURE(TEMP.) [K]
C          TMEL  = MELTING TEMP[K].
C          TSTAR= TRANSIENT TEMP. OF VAPOR [K]
C          DETP  = TEMP. DIFFERENCE FROM TMEL [K]
C          HRSL  = LATENT HEAT OF MELTING(ALWAYS POSITIVE) [J/KG]
C          DIST  = HEIGHT OF VAPOR SPACE [M]
C          WIDTH = ELEMENT THICKNESS [M]
C          TLENG = TOTAL LENGTH OF HEAT PIPE [M]

    READ(5,*) BETA,DELT1,DELTP,MM,NLEM,NTS,NFLUX,NRAD

C          BETA  = 1 FOR FULLY IMPLICIT, .5 FOR CRANK-NIOLSON
C          DELT1 = TIME DIFFERENCE FOR FIRST TIME STEP [SEC.]
C          DELT  = TIME DIFFERENCE BETWEEN EACH TIME STEP [SEC.]
C          MM    = TOTAL NUMBER OF ITERATION FOR EACH TIME STEP
C          MN    = TOTAL NUMBER OF TIME STEP
C          NLEM  = 1 FOR LEMMON METHOD OF ENTHALPY
C                  2 FOR DEL GUIDICE METHOD OF ENTHALPY
C          NFLUX = 1. HEAT FLUX DEPEND ON TIME AND CALL FLUXD
C          NRAD  = 1 RADIATION BOUNDARY CONDITION APPLIED.
C          NTS   = NUMBER OF STEPS OF IMPLICIT

C .....READ ELEMENT DATA PROVIDED FROM GRID2D.....

    READ(5,*) IOPT,LBW,NEL,NP,ICORD,IPROP,INRG,NDIM,IFIN

C          IOPT  = 0 FOR STEADY STATE, 1 FOR TRANSIENT
C          LBW   = BANDWIDTH QUANTITY
C          NEL   = NUMBER OF ELEMENTS
C          NP    = NUMBER OF NODES
C          ICORD = 0 FOR RECTANGULAR COORDINATES
C                  1 FOR CYLINDRICAL COORDINATES
C          IPROP = 0 FOR UNIFORM PROPERTIES THROUGHOUT
C                  1 FOR NON-UNIFORM PROPERTIES
C          INRG  = NUMBER OF REGION
C          NDIM  = 1 FOR ONE DIMENSIONAL PROBLEM
C                  2 FOR TWO DIMENSIONAL PROBLEM
C          IFIN  = 0, NOT A FIN PROBLEM
C                  1, A FIN PROBLEM

    READ(5,*) (IRGN(I),NROW(I),NCOL(I),I=1,INRG)

C          NCOL = NUMBER OF COLUMNS
C          NROW = NUMBER OF ROW

    I = 1
    INRG = INRG/2
    NCOLT = 0

```

ORIGINAL PAGE IS
OF POOR QUALITY

C.....DECLARATION.....

```
COMMON/MATG/ AMC(140,151),RM(140),THETA(140),FLD(140),
&             AM(140,140),BM(140),CIJ(3,3),KIJ(3,3)
& /TEPS/ TEMPR,TEMPI,TMEL,DETP,DELTD,TEMPI(140),THETAG(140),
&         THETAF(140),THETAO(140),THETTO(140),THETAB(70),TEMPO
& /PROC/ HRSL,ALPAR,DIST,BI,KREF,ROUR,SPECR,EMIS,HTC(140,3),
&         BOLT,VOLSPR,WIDTH,QE(140,3),NRESIS,RESIS,IX
& /ELMT/ NEL,NP,GND(140,3),B(140,3),C(140,3),EAREA(140),NPP1,
&         IES(140,2),ESL(140,3),BETA,XC(140,3),YC(140,3),DEFO,
&         NE(140),TLENG,PNO(5,30),EBC(3,3),CM(3,3),GNDB(70)
& /INOUT/TEMPS(70),TEMPV(70),TEMPVS(70),QEI(70),VX(70),
&         GNDI(70),VY1(70),VY2(70),VY3(70),ELSI(30),
&         VY4(70),VY5(70),VY6(70),HFG,TEMPF(70)
& /SPLIN/TIME(3),TIMER(20),QSTAG(20),XP1(25),CP1(4,25),ND1,
&         XP2(60),CP2(4,60),ND2,XP3(25),CP3(4,25),ND3,TS,
&         XP4(25),CP4(4,25),ND4,XP5(15),CP5(4,15),ND5,XP6(15),
&         CP6(4,15),XP7(15),CP7(4,15),ND7,XP8(15),CP8(4,15),
&         ND6,ND8,XP9(15),CP9(4,15),ND9,XP0(15),CP0(4,15),ND0,
&         ELSS(30),TESL(30)
& /OUTPT/MO,IDAY,IYEAR,TITLE,CASE,NUMBER,NO,TEMPCC,HTCC,IOUT,
&         TIMEN,DELT,DELT1,DELT2
DIMENSION X(3),Y(3),RS(70),DUMG(140),DUMC(140),DUMQE(140,3),
&         IRGN(15),NCOL(15),NROW(15),DUMK(140),TEST(140),
&         TEMP(3),TEMPI(3),TEMPB(70),THETAX(140),TA(3,96),
&         AREA(30),QT(70),QEIN(70),DTEMPS(70),TEMPC(140,3)
INTEGER TS,TSM1,TSM2,P,GND,GNDB,GNDI,IOUT,FIRTS,FM1,FP1,PNO
REAL KIJ,KLP,KSN,KFN,KLN,KREF,HRSL,HTC,KEE,MACH,INTVL,MASW,MASWN,
&     JCOB,JCOBI
```

C.....READ IN DATA TO CREATE COVER PAGE.....

```
WRITE(4,5)
5  FORMAT(' INPUT CASE NUMBER?')
   READ(3,*) NO
   WRITE(4,6)
6  FORMAT(' INPUT DATE AS 12 20 1987')
7  FORMAT(I3,I3,I5)
   READ(3,7) MO,IDAY,IYEAR
   WRITE(4,8)
8  FORMAT(' INPUT TITLE WITHIN 27 CHARACTERS')
9  FORMAT(3A9)
   READ(3,9) TITLE,CASE,NUMBER
10 FORMAT(A1)
   WRITE(4,11)
11 FORMAT('RESTART FROM LAST RUN ? (Y/N)')
   READ(3,10) YESNO
   WRITE(4,12)
12 FORMAT(' TIME INTERVAL (SEC.) ?')
   READ(3,*) DELT
   WRITE(4,13)
13 FORMAT(' HOW MANY TIME STEP DO YOU WANT TO RUN?')
   READ(3,*) MN
   WRITE(4,14)
```

```

NROWT = NROW(1) + NROW(INRG+1) - 1
30  NCOLT = NCOLT + NCOL(I)
    IF(I .LT. INRG) THEN
        I = I + 1
        GO TO 30
    END IF
    NCOLT = NCOLT - INRG + 1
    DO 100 I = 1,NEL
        READ(5,*) NE(I), (GND(I,L),L=1,3), (XC(I,L),YC(I,L),L=1,3)

C          NE = NUMBER OF ELEMENT
C          GND = GLOBLE NUMBER OF NODES
C          XC = X-COORDINATE OF NODES [M]
C          YC = Y-COORDINATE OF NODES [M]

        READ(5,*) DUMK(I),DUMG(I),DUMC(I), (IES(I,L),
&          HTC(I,IES(I,L)),TEMPC(I,IES(I,L)),L=1,2),
&          (IES(I,L),QE(I,IES(I,L)),L=1,2)

C          DUMK = THERMAL CONDUCTIVITY [W/(M*K)]
C          DUMG = HEAT GENERATION PER UNIT VOLUME
C          DUMC = SPECIFIC HEAT/DENSITY PRODUCT
C          HTC = HEAT TRANSFER COEFFICIENT [W/(M**2*K)]
C          IES = NUMBER OF SIDE IN EACH ELEMENT
C          QE  = HEAT FLUX ON BOUNDARY SURFACES [W/M**2]
C          TEMP = REFERENCE TEMP. FOR CONVECTIVE HEAT [K]

100  CONTINUE
    IST = 1
    IFN = 6
    40  READ(5,*) (GNDB(I),I = IST,IFN), (TEMPB(I),I=IST,IFN)

C          GNDB = GLOBLE NUMBER OF NODE WHERE IS LOCATED ON
C          THE LIQUID-VAPOR INTERFACE.
C          GNDB = GLOBLE NODE NUMBER OF NODE WHERE IS ON BOUNDARY
C          JFNT = TOTAL NUMBER OF GNDB
C          TEMPB = SPECIFIED BOUNDARY TEMP.

    IF(GNDB(IFN) .GT. 0) THEN
        IST = IST + 6
        IFN = IFN + 6
        GO TO 40
    END IF

C.....READ GLOBAL NODE NUMBER ON LIQUID-VAPOR INTERFACE.....

    JST = 1
    JFN = 6
    50  READ(5,*) (GNDB(I), I = JST, JFN)
    IF(GNDB(JFN) .GT. 0) THEN
        JST = JST + 6
        JFN = JFN + 6
        GO TO 50
    END IF
    JFNT = 0

```

ORIGINAL PAGE IS
OF POOR QUALITY

```
DO 60 I = 1,JFN
  IF(GNDI(I) .GT. 0) THEN
    JFNT = JFNT + 1
  END IF
60 CONTINUE
```

C.....READ DATA FOR RADIATION BOUNDARY CONTITIONS.....

```
IF(NRAD .EQ. 1) THEN
  READ(5,*) TEMPR,EMIS
END IF
```

```
C          TEMPR = REFERENCE TEMP. FOR RADIATION [K]
C          EMIS = EMISSIVITY
```

C.....READ SCALE FACTOR AND HEAT FLUX AT STAGNATION.....

```
15  FORMAT(A20)
    IF(NFLUX .EQ. 1) THEN
      READ(5,15) INPUT1
      READ(5,*) ND1,(XP1(I),CP1(1,I),I=1,ND1)
      READ(5,*) CP1(2,1),CP1(2,ND1)
      CALL SPLINE(ND1-1,XP1,CP1)
      CALL CALCF(ND1-1,XP1,CP1)
      READ(5,15) INPUT2
      READ(5,*) ND2,(XP2(I),CP2(1,I),I=1,ND2)
      READ(5,*) CP2(2,1),CP2(2,ND2)
      CALL SPLINE(ND2-1,XP2,CP2)
      CALL CALCF(ND2-1,XP2,CP2)
    END IF
```

C.....READ CONDUCTIVITY AND SPECIFIC HEAT OF STAINLESS STEEL.....

```
READ(5,15) INPUT3
READ(5,*) ND3,(XP3(I),CP3(1,I),I=1,ND3)
READ(5,*) CP3(2,1),CP3(2,ND3)
CALL SPLINE(ND3-1,XP3,CP3)
CALL CALCF(ND3-1,XP3,CP3)
READ(5,15) INPUT4
READ(5,*) ND4,(XP4(I),CP4(1,I),I=1,ND4)
READ(5,*) CP4(2,1),CP4(2,ND4)
CALL SPLINE(ND4-1,XP4,CP4)
CALL CALCF(ND4-1,XP4,CP4)
```

```
C          ND1,2,3 = NUMBER OF DATA POINTS
C          XP1,2,3 = LOCATION IN X - AXIS
C          CP1,2,3 = COEFFICIENT OF INTERPOLATION EQUATION
```

C.....CONDUCTIVITY ,DENSITY AND SPECIFIC HEAT OF SOLID SODIUM.....

```
READ(5,15) INPUT5
READ(5,*) ND5,(XP5(I),CP5(1,I),I=1,ND5)
READ(5,*) CP5(2,1),CP5(2,ND5)
CALL SPLINE(ND5-1,XP5,CP5)
```



```

CALL CALCF(ND5-1,XP5,CP5)
READ(5,15) INPUT6
READ(5,*) ND6,(XP6(I),CP6(1,I),I=1,ND6)
READ(5,*) CP6(2,1),CP6(2,ND6)
CALL SPLINE(ND6-1,XP6,CP6)
CALL CALCF(ND6-1,XP6,CP6)
READ(5,15) INPUT7
READ(5,*) ND7,(XP7(I),CP7(1,I),I=1,ND7)
READ(5,*) CP7(2,1),CP7(2,ND7)
CALL SPLINE(ND7-1,XP7,CP7)
CALL CALCF(ND7-1,XP7,CP7)

```

C.....CONDUCTIVITY ,DENSITY AND SPECIFIC HEAT OF LIQUID SODIUM.....

```

READ(5,15) INPUT8
READ(5,*) ND8,(XP8(I),CP8(1,I),I=1,ND8)
READ(5,*) CP8(2,1),CP8(2,ND8)
CALL SPLINE(ND8-1,XP8,CP8)
CALL CALCF(ND8-1,XP8,CP8)
READ(5,15) INPUT9
READ(5,*) ND9,(XP9(I),CP9(1,I),I=1,ND9)
READ(5,*) CP9(2,1),CP9(2,ND9)
CALL SPLINE(ND9-1,XP9,CP9)
CALL CALCF(ND9-1,XP9,CP9)
READ(5,15) INPUT0
READ(5,*) ND0,(XP0(I),CP0(1,I),I=1,ND0)
READ(5,*) CP0(2,1),CP0(2,ND0)
CALL SPLINE(ND0-1,XP0,CP0)
CALL CALCF(ND0-1,XP0,CP0)

```

C.....READ NODAL POINT NUMBER TO USE PRINTING TEMP.....

```

READ(5,*) ((PNOD(I,J),J=1,NCOLT),I=1,NROWT)

```

C.....PRINT OUT DATA FOR PLOT.....

```

IF(YESNO .EQ. "N") THEN
  WRITE(7,*) ((GND(I,L),L=1,3),I=1,NEL)
  WRITE(7,*) ((XC(I,L),YC(I,L),L=1,3),I=1,NEL)
END IF

```

C.....SET FIRST GUESS

```

DO 110 I= IST,IFN
  IF(GNDB(I) .GT. -1) THEN
    TEMPG1(GNDB(I)) = TEMPB(I)
  END IF
110 CONTINUE
DO 120 I = 1,NP
  DO 125 J = IST,IFN
    IF(I .NE. GNDB(J)) THEN
      TEMPG1(I) = TEMPI
    ENDIF
125 CONTINUE
120 CONTINUE

```

ORIGINAL PAGE IS
OF POOR QUALITY

CSOME CONSTANT PARAMETER.....

C JNT = NUMBER OF NODES ON INTERFACE FOR PRESENT TIME STEP.
C TS = NUMBER OF TIME STEPS

BOLT = 5.67E-8
FM1 = 1
FIRTS = 1
FP1 = 1
KLP = 72.3
KREF = 141.
VOLSPR = 1.109E6
ALPAR = KREF/(VOLSPR)
DEFO = ALPAR*DELT1/DIST**2
IOUT = 1
JK = 1
JNT = 1
IX = 1
NPP1 = NP + 1
NRESIS = 1
TIMEN = DELT1
TIME(1) = DELT1
TS = 0
TEMPV(2) = 0.

C.....CALCULATE BASIC ELEMENT GEOMETRIC MATRIX.....

DO 200 M = 1,NEL
DO 220 I = 1,3
X(I) = 0.
Y(I) = 0.
X(I) = X(I) + XC(M,I)/DIST
Y(I) = Y(I) + YC(M,I)/DIST
220 CONTINUE
CALL ELMDM(X,Y,M)
200 CONTINUE

C.....CALCULATE LENGTH OF SIDE OF ELEMENT AT INTERFACE.....

K = 2
KM1 = 1
226 DO 225 M = 1,NEL
IF(GND(M,1) .EQ. GNDI(KM1) .AND. GND(M,2) .EQ. GNDI(K)) THEN
ELSI(KM1) = SQRT((XC(M,1) - XC(M,2))**2 +
& (YC(M,1) - YC(M,2))**2)
K = K + 1
KM1 = K - 1
IF(K .LE. JFNT-1) THEN
GO TO 226
END IF
END IF
225 CONTINUE
K = 2

```

      KM1 = 1
      TLENG = 0.0
228 DO 227 M = 1,NEL
      IF(GND(M,3) .EQ. PNOD(1,KM1) .AND. GND(M,2) .EQ.
&      PNOD(1,K)) THEN
      ELSS(KM1) = SQRT((XC(M,2) - XC(M,3))**2 +
&      (YC(M,2) - YC(M,3))**2)
      TLENG = TLENG + ELSS(KM1)
      IF(KM1 .EQ. 1) THEN
      TESL(1) = ELSS(1)
      ELSE
      TESL(KM1) = TESL(KM1 - 1) + ELSS(KM1)
      END IF
      K = K + 1
      KM1 = K - 1
      IF(K .LE. JFNT-1) THEN
      GO TO 228
      END IF
      END IF
227 CONTINUE
      WRITE(7,*) TLENG, (ELSS(I), I=1, JFNT-1)
      WRITE(7,*) (TESL(I), I=1, JFNT-1)
      WRITE(7,*) (ELSI(I), I=1, JFNT-1)
      IF(YESNO .EQ. "Y") THEN
      GO TO 545
      END IF

```

```

C *****
C   TO EVALUATE TEMPERATURE AT FIRST FEW TIME STEPS
C   BY USING IMPLICIT METHOD(BETA = 1.,.5)
C *****

```

C.....SET DIMENSIONLESS BOUNDARY TEMP.....

```

      DO 230 I = 1,IFN
      THETAB(I) = (TEMPB(I) - TMEL)/(TMEL - TEMPI)
230 CONTINUE

```

C.....SET DIMENSIONLESS GUESS TEMP.....

```

      DO 250 I = 1,NP
      THETAG(I) = (TEMPG1(I) - TMEL)/(TMEL - TEMPI)
250 CONTINUE
450 TS = TS + 1
      IF(TS .EQ. 2) THEN
      TIME(2) = TIME(1) + DELT
      ELSE IF(TS .EQ. 3) THEN
      TIME(3) = TIME(2) + DELT
      ELSE IF(TS .GT. 3) THEN
      TIME(1) = TIME(2)
      TIME(2) = TIME(3)
      TIME(3) = TIME(3) + DELT
      END IF
      DO 260 I = 1,NP
      TEMPG1(I) = THETAG(I)*(TMEL - TEMPI) + TMEL

```

ORIGINAL PAGE IS
OF POOR QUALITY

260 CONTINUE
430 P = 0
400 P = P + 1

CSET ARRAYS ZERO.....

```

      DO 310 I = 1,NP
        THETA(I) = 0.
310  CONTINUE
      DO 320 I = 1,NP
        FLD(I) = 0.
        BM(I) = 0.
        RM(I) = 0.
        DO 325 J = 1,NP
          AM(I,J) = 0.
325  CONTINUE
320  CONTINUE
      DO 330 I = 1,NP
        DO 335 J = 1,NPP1
          AMC(I,J) = 0.
335  CONTINUE
330  CONTINUE
      DO 340 M = 1,NEL
        DO 345 I = 1,3
          TEMPG(I) = THETAG(GND(M,I))*(TMEL - TEMPI) + TMEL

```

C.....IMPLICIT TIME STEPPING SCHEME.....

```

      IF(BETA .EQ. 1.) THEN
        TEMP(I) = TEMPG(I)
      ELSE
        TEMP(I) = (TEMPG(I) + TEMPG1(I))*BETA
      END IF
345  CONTINUE

```

C....TO ASSUMBLE ELEMENT MATRIX INTO GLOBAL SYSTEM MATRIX[AMC]....

```

      CALL GLOBMAX(TEMP,TEMPC,M,DUMK,NLEX,NFLUX,NRAD,NTS,P,IFN)
340  CONTINUE

```

C.....APPLY B. C.'S OF FIRST KIND IF APPLICABLE.....

```

      CALL FIRSTBC(IFN)

```

C.....TO EVALUATE RESIDUAL AND THETAG(I) FOR NEXT ITERATION.....

```

      DO 350 I = 1,NP
        THETA(I) = THETAG(I)
        THETAG(I) = 0.
350  CONTINUE
      CALL RESIDUL(RMAX)
      CALL CHLSKY(TS,NTS,THETAX)
      DO 355 I = 1,NP
        THETAG(I) = THETAX(I) + THETA(I)
355  CONTINUE

```

```

C *****
C *CHECK CONVERGENCE CRITERIOR ON DIFFERENCE BETWEEN NEW THETA AND *
C *OLD THETA AT EVERY NODES. IF ONE OF DIFFERENCES IS GREATER THAN *
C *TOLERANCE, THEN ITERATED BY NEWTON-RAPHSON METHOD. IF CRITERION *
C *IS MET, THETA(I) ARE SUBSTITUTED INTO EQUATION TO OBTAIN *
C *THETA(I) AT THE NEXT TIME STEP. *
C *****

```

```

IF(RMAX .LT. .001 .OR. P .GT. MM) THEN
  DO 370 I = 1,NP
    IF(TS .EQ. 1) THEN
      TA(1,I) = THETAG(I)*(TMEL - TEMPI) + TMEL
    ELSE IF(TS .EQ. 2) THEN
      TA(2,I) = THETAG(I)*(TMEL - TEMPI) + TMEL
    ELSE IF(TS .EQ. 3) THEN
      TA(3,I) = THETAG(I)*(TMEL - TEMPI) + TMEL
    ELSE
      TA(1,I) = TA(2,I)
      TA(2,I) = TA(3,I)
      TA(3,I) = THETAG(I)*(TMEL - TEMPI) + TMEL
    END IF
  370 CONTINUE
  NPRINT = JK * NFREQ
  IF(TS .EQ. NPRINT) THEN
    CALL MAINOUT(TA,TSTAR,NTS,MN,NCOLT,NROWT)
    JK = JK + 1
  END IF
  DEFO = (ALPAR/DIST**2)*DELT
  IF(TS .LT. NTS) THEN
    GO TO 450
  ELSE
    IF(NTS .EQ. MN) THEN
      GO TO 540
    ELSE
      GO TO 550
    END IF
  END IF
  ELSE
    GO TO 400
  END IF
540 CONTINUE
GO TO 2

```

```

C *****
C TO EVALUATE TEMPERATURE BY USING EXPLICIT METHOD
C (DUPONT) WITH TEMPERATURES FOR TWO PREVIOUS TIME STEPS
C *****

```

```

545 IF(YESNO .EQ. "Y") THEN
  CALL DATAIN(TA,JK,JNT,TIMEN,FIRTS,TVU,QT,TEMPD)
  FM1 = FIRTS - 1
  FP1 = FIRTS
END IF

```

C.....SET ARRAYS ZERO.....

```

550 TS = TS + 1
    IF(TS .EQ. 2) THEN
        TIME(2) = TIME(1) + DELT
    ELSE IF(TS .EQ. 3) THEN
        TIME(3) = TIME(2) + DELT
    ELSE IF(TS .GT. 3) THEN
        TIME(1) = TIME(2)
        TIME(2) = TIME(3)
        TIME(3) = TIME(3) + DELT
    END IF
530 DO 500 I = 1,NP
    FLD(I) = 0.
    BM(I) = 0.
    DO 510 J=1,NPP1
        AMC(I,J) = 0.0
510 CONTINUE
500 CONTINUE

```

C.....SET INITIAL TEMPERATURE FROM TWO PREVIOUS TIME STEPS.....

```

DO 520 I = 1,NP
    IF(TS .GT. 3) THEN
        THETTO(I) = (TA(2,I) - TMEL)/(TMEL - TEMPI)
        THETAO(I) = (TA(3,I) - TMEL)/(TMEL - TEMPI)
    ELSE
        THETTO(I) = (TA(1,I) - TMEL)/(TMEL - TEMPI)
        THETAO(I) = (TA(2,I) - TMEL)/(TMEL - TEMPI)
    END IF
    DO 525 J = 1,NP
        AM(I,J) = 0.
525 CONTINUE
520 CONTINUE
    DO 600 M = 1,NEL
        DO 610 I = 1,3
            TEMP(I) = THETAO(GND(M,I))*(TMEL - TEMPI) + TMEL
610 CONTINUE

```

C....TO ASSUMBLE ELEMENT MATRIX INTO GLOBAL SYSTEM MATRIX[AMC]....

```

    CALL GLOBMAX(TEMP,TEMPC,M,DUMK,NLEM,NFLUX,NRAD,NTS,P,IFN)
600 CONTINUE

```

C.....APPLY B.C.'S OF FIRST KIND IF APPLICABLE.....

```

    CALL FIRSTBC(IFN)

```

C.....SOLVE MATRIX BY USING CHOLESKY'S DECOMPOSITION.....

```

    CALL CHLSKY(TS,NTS,THETAX)
    DO 646 I = 1,NP
        THETA(I) = THETAX(I)
646 CONTINUE

```

C.....CHECK TEMPERATURES ON LIQUID-VAPOR INTERFACE.....

```

C   GNDI(1)   = GLOBAL NODE NUMBER AT FIRST NODE ON INTERFACE
C   GNDI(JNT) = LAST GLOBAL NODE NUMBER WHOSE TEMPERATURE IS
C               GREATER THAN TSTAR
C   TEMPS     = LIQUID TEMP. AT LIQUID-VAPOR INTERFACE
C   TEMPV     = TEMP. IN VAPOR SPACE
C   TEMPVS    = VAPOR TEMP. AT LIQUID-VAPOR INTERFACE

```

```

DO 660 I = 1,NP
  IF(TS .GT. 3) THEN
    TA(1,I) = TA(2,I)
    TA(2,I) = TA(3,I)
    TA(3,I) = THETA(I)*(TMEL - TEMPI) + TMEL
  ELSE
    TA(1,I) = TA(1,I)
    TA(2,I) = TA(2,I)
    TA(3,I) = THETA(I)*(TMEL - TEMPI) + TMEL
  END IF
660 CONTINUE
  NPRINT = JK * NFREQ
  IF(TS .EQ. NPRINT) THEN
    CALL MAINOUT(TA,TSTAR,NTS,MN,NCOLT,NROWT)
    JK = JK + 1
  END IF
  DO 665 I = 1,JFNT
    TEMPS(I) = 0.
665 CONTINUE
  DO 680 I = 1,2
    JJ = GNDI(I)
    TEMPS(I) = THETA(JJ)*(TMEL - TEMPI) + TMEL
680 CONTINUE

```

C.....ADIABATIC BOUNDARY CONDITION AT LIQUID-VAPOR INTERFACE.....

```

  IF(TEMPS(2) .LT. TSTAR) THEN
    DEFO = (ALPAR/DIST**2)*DELT
    IF(TS .GE. MN) THEN
      GO TO 2000
    ELSE
      DO 910 J = 1,JFNT
        DO 911 I = 1,NEL
          IF(GNDI(J) .EQ. GND(I,1) .AND. GNDI(J+1) .EQ. GND(I,2))
            & THEN
              IES(I,1) = 1
              QE(I,IES(I,1)) = 0.
            END IF
          CONTINUE
611 CONTINUE
910 IF(TEMPS(JFNT) .GT. TSTAR) THEN
      GO TO 2000
    ELSE
      GO TO 550
    END IF
  END IF

```

ORIGINAL PAGE IS
OF POOR QUALITY

ELSE IF(TEMPS(1) .GT. TSTAR .AND. TEMPS(2) .GT. TSTAR) THEN
C.....NO LONGER ADIABATIC CONDITION AT LIQUID-VAPOR INTERFACE.....
C.....HOW MANY NODES ON INTERFACE HAVE GREATER TEMP. THAN TSTAR.....

```

DO 915 I = 1,JFNT
  TEMPS(I) = 0.
915  CONTINUE
  J = 1
920  JG = GNDI(J)
  TEMPS(J) = THETA(JG)*(TMEL - TEMPI) + TMEL
  IF(TEMPS(J) .GT. TSTAR) THEN
    J = J + 1
    IF(J .LT. JFNT) THEN
      GO TO 920
    ELSE
      JNT = JFNT - 1
    END IF
  ELSE
    JNT = J
    TEMPSN = TEMPS(J)
  END IF

```

C.....CALCULATE UNIFORM TEMP. FOR VAPOR SPACE.....

```

TEMPS(JFNT) = THETA(GNDI(JFNT))*(TMEL-TEMPI)+TMEL
DO 922 J = 1,JFNT
  DO 923 I = 1,NEL
    IF(GNDI(J) .EQ. GND(I,1) .AND. GNDI(J+1) .EQ. GND(I,2))
      & THEN
        IES(I,1) = 1
        QE(I,IES(I,1)) = 0.
      END IF
923  CONTINUE
922  CONTINUE
  IF(NRESIS .EQ. 2) THEN
    CALL COUPLE(JNT,QT,TVU,JFNT)
    GO TO 2500
  END IF
  IF(FIRTS .EQ. 1) THEN
    TVU = (TEMPS(1) + TSTAR)/2.
2100  RESD = 0.
    TELSI = 0.
    RESDC = 4.5E6*1.4*.021*2.29E11
    DO 924 I = 1,JNT
      RESDI = ELSI(I)*10.**(-5567./TEMPS(I))/TEMPS(I)
      RESDV = ELSI(I)*10.**(-5567./TVU)/TVU
      RESD = RESD + RESDC*(RESDI - RESDV)
      TELSI = TELSI + ELSI(I)
924  CONTINUE
    JCOB = (1 - 12818.5/TVU)*TELSI
    JCOB = JCOB * 10.**(-5567./TVU)
    JCOB = RESDC*JCOB/(TVU**2)
    TVO = TVU
    TVU = TVO - RESD/JCOB

```



```

      IF (ABS (RESD) .LT. .001) THEN
        CALL INTFLUX (JFNT, JNT, TVU, TEMPV, TEMPS, QEI)
      ELSE
        GO TO 2100
      END IF
    ELSE
2200    RESD = 0.
        TELSI = 0.
        RESDC = 4.5E6*1.4*.021*2.29E11
        DO 928 I = 1, JNT
          RESDI = ELSI(I)*10.**(-5567./TEMPS(I))/TEMPS(I)
          RESDV = ELSI(I)*10.**(-5567./TVU)/TVU
          RESD = RESD + RESDC*(RESDI - RESDV)
          TELSI = TELSI + ELSI(I)
928    CONTINUE
        JCOB = (1 - 12818.5/TVU)*TELSI
        JCOB = JCOB * 10.**(-5567./TVU)
        JCOB = RESDC*JCOB/(TVU**2)
        TVO = TVU
        TVU = TVO - RESD/JCOB
        IF (ABS (RESD) .LT. .001) THEN

```

C.....TO ESTIMATE THE SONIC LIMIT.....

```

      CALL INTFLUX (JFNT, JNT, TVU, TEMPV, TEMPS, QEI)
      VMAX = SQRT (1.4*8314.*TVU/23.)
      PSATT = (2.29E11/SQRT (TVU))*10.**(-5567./TVU)
      DENS = 2.766E-3*PSATT/TVU
      HFGS = 182.*(25474.93 - .9935*TVU)
      QMAX = VMAX*HFGS*DENS*DIST*WIDTH/2.2
      QTAL = 0.
      DO 930 I = 1, JNT
        AREA(I) = 0.
        IF (QEI(I) .GT. 0.) THEN
          QTAL = QTAL + QEI(I)*ELSI(I)*WIDTH
        END IF
930    CONTINUE
      QMAXT = QMAX*.50

```

C.....IF AMOUNT OF HEAT TRANSFER ON EVAPORATOR IS GREATER.....
 C.....THAN THE SONIC LIMIT, IT IS ASSUMED THAT THE SONIC.....
 C.....LIMIT IS ACTUAL HEAT TRANSFER. CALCULATE NEW VAPOR.....
 C.....TEMPERATURE BASE ON SONIC LIMIT.....

```

      IF (QMAX .LE. QTAL .AND. JNT .GE. 4) THEN
2300    RESD = 0
        JCOB = 0.
        DO 931 I = 2, JNT
          IF (TEMPS(I) .GT. TVU) THEN
            JNTL = I
          ELSE IF (TEMPS(I) .LT. TVU .AND. TEMPS(I-1) .GT. TVU)
            THEN
            &      XII = (TEMPS(JNTL) - TVU)*ELSI(I-1)
              XII = XII/(TEMPS(JNTL)-TEMPS(I))
            END IF

```

ORIGINAL PAGE IS
OF POOR QUALITY

```

931      CONTINUE
        RSC1 = 2.29E11*1.5*.021*4.5E6
        RSC2 = 6.34E8*4.5E6*10.26*DIST
        IC = 0
        DO 932 I = 1,JNTL
          IF(QEI(I) .GT. 0.) THEN
            RSC12 = RSC1*ELSI(I)
            IF(I .NE. JNTL) THEN
              RESDI = 10.**(-5567/TEMPS(I))/TEMPS(I)*ELSI(I)*RSC1
              RESDV = 10.**(-5567/TVU)/TVU*RSC12
              JCOBI = RSC1*ELSI(I)
            ELSE
              RESDI = 10.**(-5567/TEMPS(I))/TEMPS(I)*XII*RSC1
              RESDV = 10.**(-5567/TVU)/TVU*(RSC1*XII+RSC2)
              JCOBI = RSC1*XII
            END IF
            RESD = RESD + RESDI - RESDV
            JCOB = JCOB + JCOBI
          ELSE
            IC = IC + 1
          END IF
        CONTINUE
932      JLM1 = JNTL - IC
        JCOB = (JCOB+RSC2)*(1-12818.5/TVU)
        JCOB = JCOB*10.**(-5567./TVU)/(TVU**2)
        TVO = TVU
        TVU = TVO - RESD/JCOB
        IF(ABS(RESD) .LT. .1) THEN

```

C.....CALCULATE HEAT FLUX DISTRIBUTION ON CONDENSER SECTION.....

```

        AREAT = 0.
        DO 933 I = 2,JNT
          IF(TEMPS(I) .LT. TVU .AND. TEMPS(I-1) .GT. TVU)
            THEN
              JNTM = I
              AREA(I) = TEMPS(I) - TVU
              AREA(I) = AREA(I) + (TEMPS(I) - TEMPS(I+1))/2.
              AREA(I) = AREA(I)*ELSI(I)
            ELSE IF(TEMPS(I) .LT. TVU) THEN
              AREA(I) = TEMPS(I) - TVU
              AREA(I) = AREA(I) + (TEMPS(I) - TEMPS(I+1))/2.
              AREA(I) = AREA(I)*ELSI(I)
            END IF
          AREAT = AREAT + AREA(I)
        CONTINUE
933      JNTL = JNTM - 1
        CALL INTFLUX(JFNT,JNTL,TVU,TEMPV,TEMPS,QEI)
        VMAX = SQRT(1.4*8314.*TVU/23.)
        PSATT = (2.29E11/SQRT(TVU))*10.**(-5567/TVU)
        DENS = 2.766E-3*PSATT/TVU
        HFGS = 182.*(25474.93 - .9935*TVU)
        QMAX = VMAX*HFGS*DENS*DIST*WIDTH/2.2
        QTAL = 0.
        DO 935 I = 1,JNTL

```

```

      IF(QEI(I) .GT. 0.) THEN
        IF(I .LT. JNTL) THEN
          QTAL = QTAL + QEI(I)*ELSI(I)*WIDTH
        ELSE
          XII = (TEMPS(JNTL) - TVU)*ELSI(I)
          XII = XII/(TEMPS(JNTL)-TEMPS(JNTM))
          QTAL = QTAL + QEI(I)*XII*WIDTH
        END IF
      END IF
935  CONTINUE
      DO 936 I = JNTM,JNT
        IF(I .EQ. JNTM) THEN
          QEI(I) = - AREA(I) * QMAX/AREAT/ELSI(I)/WIDTH
          IF(TS .GT. 7000) THEN
            END IF
          ELSE
            QEI(I) = - AREA(I)*QMAX/AREAT/ELSI(I)/WIDTH
          END IF
936  CONTINUE
      NRESIS = 1
      ELSE
        GO TO 2300
      END IF
      ELSE IF(QTAL .LE. QMAXT .AND. JNT .GE. JFNT-1) THEN
C.....ARTIFICIAL THERMAL RESISTANCE, WHICH CALCULATED FROM.....
C.....VAPOR FLOW, IS IMPOSED AT LIQUID-VAPOR INTERFACE.....

        CALL COUPLE(JNT,QT,TVU,JFNT)
        NRESIS = 2
      END IF
      ELSE
        GO TO 2200
      END IF
      END IF
2500 IF(TS .EQ. NPRINT) THEN
      WRITE(6,790) TVU
      WRITE(2,775) TVU
    END IF
    DO 945 J = 1,JNT
      DO 946 I = 1,NEL
        IF(GNDI(J) .EQ. GND(I,1) .AND. GNDI(J+1) .EQ. GND(I,2
&      )) THEN
          IES(I,1) = 1
          QE(I,IES(I,1)) = QE(I,IES(I,1)) - QEI(J)
        END IF
946  CONTINUE
945  CONTINUE
      FIRTS = FIRTS + 1
      DEFO = (ALPAR/DIST**2)*DELT
      IF(TS .GE. MN) THEN
        GO TO 2000
      ELSE
        GO TO 550
      END IF

```

ORIGINAL PAGE IS
OF POOR QUALITY

```
ELSE
  DEFO = (ALPAR/DIST**2)*DELT
  IF(TS .GE. MN) THEN
    GO TO 2000
  ELSE
    GO TO 550
  END IF
END IF
```

C.....PRINT UNIFORM VAPOR TEMPERATURE.....

```
2000 CONTINUE
2   FIRTS1 = FIRTS - 1.
775  FORMAT(F8.2)
790  FORMAT(/2X,'TEMPV = ',F8.3,2X,' [K] ')
```

C.....PRINT DATA FOR RESTARTING FROM LAST RUN.....

```
CALL DATAOUT(TA, JK, JNT, TIMEN, FIRTS, TVU, QT, TEMPD)
STOP
END
```

SUBROUTINE ELMDM(X,Y,M)

```
C *****
C * THIS SUBROUTINE CALCULATES ELEMENT DATA SUCH *
C * AS AREA, B(I)B(J) + C(I)C(J), B(I)C(J) - B(J)C(I) *
C * C1(I,J) AND CM(I,J), AND FORMS MATRICES S622, S262 *
C * AND S226 *
C *****
```

```
COMMON/PROC/ HRSL,ALPAR,DIST,BI,KREF,ROUR,SPECR,EMIS,HTC(140,3),
&             BOLT,VOLSPR,WIDTH,QE(140,3),NRESIS,RESIS,IX
&             /ELMT/ NEL,NP,GND(140,3),B(140,3),C(140,3),EAREA(140),NPP1,
&             IES(140,2),ESL(140,3),BETA,XC(140,3),YC(140,3),DEFO,
&             NE(140),TLENG,PNOD(5,30),EBC(3,3),CM(3,3),GNDB(70)
DIMENSION X(3), Y(3)
```

C....TO CALCULATE THE AREA AND BASIC MATRIX OF THE ELEMENT....

```
XY = X(2) * Y(3) - Y(2) * X(3)
YX = X(1) * (Y(2) - Y(3)) + Y(1) * (X(3) - X(2))
XPY = XY + YX
EAREA(M) = .5 * ABS(XPY)
B(M,1) = Y(2) - Y(3)
B(M,2) = Y(3) - Y(1)
B(M,3) = Y(1) - Y(2)
C(M,1) = X(3) - X(2)
C(M,2) = X(1) - X(3)
C(M,3) = X(2) - X(1)
ESL(M,1) = SQRT(B(M,3)**2+C(M,3)**2)
ESL(M,2) = SQRT(B(M,1)**2+C(M,1)**2)
ESL(M,3) = SQRT(B(M,2)**2+C(M,2)**2)
RETURN
```

END

SUBROUTINE CONCP(X,Y,TEMP,M,DUMK,NLEM)

```

C *****
C * THIS IS MAIN SUBROUTINE TO EVALUATE CONDUCTION *
C * AND CAPACITANCE MATRIX FOR EACH ELEMENT *
C *****

```

```

COMMON/MATG/ AMC(140,151),RM(140),THETA(140),FLD(140),
&             AM(140,140),BM(140),CIJ(3,3),KIJ(3,3)
&             /TEPS/ TEMPR,TEMPI,TMEL,DETP,DELTD,TEMPG1(140),THETAG(140),
&             THETAF(140),THETAO(140),THETTO(140),THETAB(70),TEMPD
&             /PROC/ HRSL,ALPAR,DIST,BI,KREF,ROUR,SPECR,EMIS,HTC(140,3),
&             BOLT,VOLSPR,WIDTH,QE(140,3),NRESIS,RESIS,IX
&             /ELMT/ NEL,NP,GND(140,3),B(140,3),C(140,3),EAREA(140),NPP1,
&             IES(140,2),ESL(140,3),BETA,XC(140,3),YC(140,3),DEFO,
&             NE(140),TLENG,PNOB(5,30),EBC(3,3),CM(3,3),GNDB(70)
DIMENSION X(3),Y(3),TEMP(3),KN(3),DUMK(140)
REAL KN

```

```

C TO CALCULATE ELEMENT CONDUCTION [K] AND CAPACITANCE [C]
C MATRIX ON ELEMENT BY ELEMENT BASIS

```

```

C.....TO PROVIDE COMMON MATRIX DATA.....

```

```

IF(DUMK(M) .EQ. 4.) THEN
  CALL FICLAY(TEMP,M)
ELSE

```

```

C....CALCULATE NODAL CONDUCTIVITY AND VOLUMETRIC SPECIFIC HEAT....

```

```

  CALL PROPTY(TEMP,CEE,KN,NLEM,M)

```

```

C....CALCULATE CONDUCTION[KIJ] AND CAPACITANCE[CIJ] MATRIES....

```

```

  CALL CKAN(CEE,KN,TEMP,M)
END IF
RETURN
END

```

SUBROUTINE FICLAY(TEMP,M)

```

C *****
C * THIS SUBROUTINE EVALUATES CONDUCTION AND CAPACITANCE *
C * MATRIX IN FICTITIOUS-LAYER WHICH HAS BEEN ARTIFICIALLY *
C * CREATED TO SMOOTH OUT THE EFFECT OF THE ABRUPT CHANGE *
C * OF TEMPERATURE AT THE BOUNDARY OR FOR HEAT PIPE SHELL. *
C *****

```

```

IMPLICIT REAL (K)
COMMON/MATG/ AMC(140,151),RM(140),THETA(140),FLD(140),
&             AM(140,140),BM(140),CIJ(3,3),KIJ(3,3)
&             /PROC/ HRSL,ALPAR,DIST,BI,KREF,ROUR,SPECR,EMIS,HTC(140,3),
&             BOLT,VOLSPR,WIDTH,QE(140,3),NRESIS,RESIS,IX

```

ORIGINAL PAGE IS
OF POOR QUALITY

```

&      /ELMT/ NEL,NP,GND(140,3),B(140,3),C(140,3),EAREA(140),NPP1,
&      IES(140,2),ESL(140,3),BETA,XC(140,3),YC(140,3),DEFO,
&      NE(140),TLENG,PNOD(5,30),EBC(3,3),CM(3,3),GNDB(70)
      DIMENSION TEMP(3)
      CALL PROSHEL(TEMP,KFIC,CFIC)
      DO 100 I = 1,3
        DO 110 J = 1,3
          EBC(I,J) = (B(M,I)*B(M,J) + C(M,I)*C(M,J))/EAREA(M)
          IF(I.EQ. J) THEN
            CM(I,J) = EAREA(M)/6.
          ELSE
            CM(I,J) = EAREA(M)/12.
          END IF
          KIJ(I,J) = KFIC * EBC(I,J)/4./KREF
          CIJ(I,J) = CFIC * CM(I,J)/VOLSPR
110      CONTINUE
100      CONTINUE
      RETURN
      END

```

SUBROUTINE PROSHEL(TEMP,KFIC,CFIC)

```

C *****
C * SUBROUTINE CALCULATES CONDUCTIVITY AND SPECIFIC HEAT FOR *
C * HEAT PIPE SELL BASED ON AVERAGE TEMPERATURE. *
C *****

```

```

      IMPLICIT REAL (K)
      DIMENSION TEMP(3)

```

C.....CONDUCTIVITY AND SPECIFIC HEAT FOR HASTELLAY X.....

```

      DATA TK1,TK2,TK3,TK4/373.,573.,773.,973./
&      K1 ,K2 ,K3 ,K4 /11.1,14.7,20.6,22.8/
&      CP1,CP2,CP3/498.,582.,699./
&      TC1,TC2,TC3/588.,923.,1143/

      ROU = 8220.
      TAVG = (TEMP(1)+TEMP(2)+TEMP(3))/3.
      IF(TAVG.LT. TK1) THEN
        KFIC = K1
      ELSE IF(TAVG.GE. TK1 .AND. TAVG.LT. TK2) THEN
        KFIC = K1+(K2-K1)*(TAVG-TK1)/(TK2-TK1)
      ELSE IF(TAVG.GE. TK2 .AND. TAVG.LT. TK3) THEN
        KFIC = K2+(K3-K2)*(TAVG-TK2)/(TK3-TK2)
      ELSE IF(TAVG.GE. TK3 .AND. TAVG.LT. TK4) THEN
        KFIC = K3+(K4-K3)*(TAVG-TK3)/(TK4-TK3)
      ELSE
        KFIC = K4
      END IF
      IF(TAVG.LT. TC1) THEN
        CFIC = ROU * CP1
      ELSE IF(TAVG.GE. TC1 .AND. TAVG.LT. TC2) THEN
        CFIC = ROU *(CP1+(CP2-CP1)*(TAVG-TC1)/(TC2-TC1))
      ELSE IF(TAVG.GE. TC2 .AND. TAVG.LT. TC3) THEN

```

```

      CFIC = ROU * (CP2 + (CP3 - CP2) * (TAVG - TC2) / (TC3 - TC2))
    ELSE
      CFIC = ROU * CP3
    END IF
    RETURN
  END

```

```

  SUBROUTINE PROPTY(TEMP,CEE,KN,NLEM,M)

```

```

C *****
C * THIS SUBROUTINE CALCULATES CONDUCTIVITY AND *
C * VOLUMETRIC SPECIFIC HEAT AT NODE IN ELEMENT *
C * WHICH HAS PHASE CHANGE *
C *****

```

```

  IMPLICIT REAL (K)

```

```

  COMMON/TEPS/ TEMPR,TEMPI,TMEL,DETP,DELTD,TEMPI(140),THETAG(140),
&              THETAF(140),THETAO(140),THETTO(140),THETAB(70),TEMPI
&              /PROC/ HRSL,ALPAR,DIST,BI,KREF,ROUR,SPECR,EMIS,HTC(140,3),
&              BOLT,VOLSPR,WIDTH,QE(140,3),NRESIS,RESIS,IX
&              /ELMT/ NEL,NP,GND(140,3),B(140,3),C(140,3),EAREA(140),NPP1,
&              IES(140,2),ESL(140,3),BETA,XC(140,3),YC(140,3),DEFO,
&              NE(140),TLENG,PNOD(5,30),EBC(3,3),CM(3,3),GNDB(70)
&              /SPLIN/TIME(3),TIMER(20),QSTAG(20),XP1(25),CP1(4,25),ND1,
&              XP2(60),CP2(4,60),ND2,XP3(25),CP3(4,25),ND3,TS,
&              XP4(25),CP4(4,25),ND4,XP5(15),CP5(4,15),ND5,XP6(15),
&              CP6(4,15),XP7(15),CP7(4,15),ND7,XP8(15),CP8(4,15),
&              ND6,ND8,XP9(15),CP9(4,15),ND9,XP0(15),CP0(4,15),ND0,
&              ELSS(30),TESL(30)

```

```

  DIMENSION TEMP(3),KN(3),KFN(3),KLN(3),KSN(3),ENTP(3)

```

```

  TMEP = TMEL + DETP

```

```

  TMES = TMEL - DETP

```

```

  DO 50 I = 1,3

```

```

    KFN(I) = 0.

```

```

    KLN(I) = 0.

```

```

    KSN(I) = 0.

```

```

50  CONTINUE

```

```

  DO 100 I = 1,3

```

```

    IF(TEMP(I) .LT. TMES) THEN

```

```

      TEMPS=TEMP(I)

```

```

      KSN(I) = PCUBIC(TEMPS,ND5,XP5,CP5)/KREF

```

```

      CSN = PCUBIC(TEMPS,ND7,XP7,CP7)

```

```

      ROUSN = PCUBIC(TEMPS,ND6,XP6,CP6)

```

```

      ENTP(I) = CSN * ROUSN * TEMP(I)

```

```

    ELSE IF(TEMP(I) .GT. TMEP) THEN

```

```

      TEMPL=TEMP(I)

```

```

      KLN(I) = PCUBIC(TEMPL,ND8,XP8,CP8)/KREF

```

```

      CLN = PCUBIC(TEMPL,ND0,XP0,CP0)

```

```

      ROULN = PCUBIC(TEMPL,ND9,XP9,CP9)

```

```

      CSN = PCUBIC(TMES,ND7,XP7,CP7)

```

```

      ROUSN = PCUBIC(TMES,ND6,XP6,CP6)

```

```

      ENTP(I) = CSN*ROUSN*TMES+HRSL+CLN*ROULN*(TEMP(I) -TMEP)

```

```

    ELSE

```

```

      KSS = PCUBIC(TMES,ND5,XP5,CP5)

```

```

      CSN = PCUBIC(TMES,ND7,XP7,CP7)

```

ORIGINAL PAGE IS
OF POOR QUALITY

```

      ROUSN = PCUBIC(TMES,ND6,XP6,CP6)
      KLP = PCUBIC(TMEP,ND8,XP8,CP8)
      KFN(I) = (KSS + (KLP - KSS)*(TEMP(I) - TMES)/(2.*DETP))/KREF
      ENTP(I) = CSN*ROUSN*TMES + HRSL*(TEMP(I) - TMES)/(2.*DETP)
      END IF
100  CONTINUE
      DETX = 0.
      DETY = 0.
      DO 200 I = 1,3
        DETX = DETX + (B(M,I)*TEMP(I))/(2.*EAREA(M))
        DETY = DETY + (C(M,I)*TEMP(I))/(2.*EAREA(M))
200  CONTINUE
      IF(DETX.NE. 0. .AND. DETY.NE. 0.) THEN
        ENTPX = 0.
        ENTPY = 0.
        DO 300 I = 1,3
          ENTPX = ENTPX + (B(M,I)*ENTP(I))/(2.*EAREA(M))
          ENTPY = ENTPY + (C(M,I)*ENTP(I))/(2.*EAREA(M))
300  CONTINUE
        IF(NLEM.EQ. 1) THEN
          CEE = ((ENTPX**2 + ENTPY**2)/(DETX**2 + DETY**2))/VOLSPR
        ELSE
          CEE = ((ENTPX*DETX + ENTPY*DETY)/(DETX**2 + DETY**2))/VOLSPR
        END IF
      ELSE
        IF(TEMP(1).LT. TMES) THEN
          CEE = CSN*ROUSN/VOLSPR
        ELSE IF(TEMP(1).GT. TMEP) THEN
          CEE = CLN*ROULN/VOLSPR
        END IF
      END IF
      DO 400 I = 1,3
        KN(I) = KFN(I) + KLN(I) + KSN(I)
400  CONTINUE
      RETURN
      END

```

SUBROUTINE CRAN(CEE,KN,TEMP,M)

```

C *****
C * THIS SUBROUTINE CALCULATES CONDUCTION *
C * AND CAPACITANCE MATRICES FOR ELEMENT *
C * WHICH HAS PHASE CHANGE. *
C *****

```

```

      IMPLICIT REAL (K)
      COMMON/MATG/ AMC(140,151),RM(140),THETA(140),FLD(140),
&                AM(140,140),BM(140),CIJ(3,3),KIJ(3,3)
&                /PROC/ HRSL,ALPAR,DIST,BI,KREF,ROUR,SPECR,EMIS,HTC(140,3),
&                BOLT,VOLSPR,WIDTH,QE(140,3),NRESIS,RESIS,IX
&                /ELMT/ NEL,NP,GND(140,3),B(140,3),C(140,3),EAREA(140),NPP1,
&                IES(140,2),ESL(140,3),BETA,XC(140,3),YC(140,3),DEFO,
&                NE(140),TLENG,PNOD(5,30),EBC(3,3),CM(3,3),GNDB(70)
&                /SPLIN/TIME(3),TIMER(20),QSTAG(20),XP1(25),CP1(4,25),ND1,
&                XP2(60),CP2(4,60),ND2,XP3(25),CP3(4,25),ND3,TS,

```



```

&      XP4(25),CP4(4,25),ND4,XP5(15),CP5(4,15),ND5,XP6(15),
&      CP6(4,15),XP7(15),CP7(4,15),ND7,XP8(15),CP8(4,15),
&      ND6,ND8,XP9(15),CP9(4,15),ND9,XP0(15),CP0(4,15),ND0,
&      ELSS(30),TESL(30)
DIMENSION KN(3),TEMP(3)
TAVG = (TEMP(1) + TEMP(2) + TEMP(3))/3.
VOIDF = .684
KSW = PCUBIC(TAVG,ND3,XP3,CP3)
KSW = KSW/KREF
CPSW = PCUBIC(TAVG,ND4,XP4,CP4)
DENSU = 8027.
CPSW = CPSW*DENSU/VOLSPR
KEE = 0.
DO 100 I = 1,3
  KEE = KEE + KN(I)
100 CONTINUE
KEE = KEE/3.
KEE = KEE*((KEE+KSW)-(1-VOIDF)*(KEE-KSW))/
&      ((KEE+KSW)+(1-VOIDF)*(KEE-KSW))
CEE = (VOIDF*CEE)+(1-VOIDF)*CPSW
DO 200 I = 1,3
  DO 210 J = 1,3
    EBC(I,J) = (B(M,I)*B(M,J) + C(M,I)*C(M,J))/EAREA(M)
    IF(I.EQ.J) THEN
      CM(I,J) = EAREA(M)/6.
    ELSE
      CM(I,J) = EAREA(M)/12.
    END IF
    CIJ(I,J) = CEE*CM(I,J)
    KIJ(I,J) = KEE*EBC(I,J)/4.
  210 CONTINUE
200 CONTINUE
RETURN
END

```

SUBROUTINE THIRDB(THETAC,L,CONF,M)

```

C *****
C * THIS SUBROUTINE CALCULATES ELEMENT MATRICES DUE TO SURFACE *
C * INTEGRALS FOR CONVECTIVE BOUNDARY CONDITIONS *
C *****

```

```

IMPLICIT REAL (K)
COMMON/MATG/ AMC(140,151),RM(140),THETA(140),FLD(140),
&      AM(140,140),BM(140),CIJ(3,3),KIJ(3,3)
&      /TEPS/ TEMPR,TEMPI,TMEL,DETP,DELTD,TEMPI1(140),THETAG(140),
&      THETAF(140),THETAO(140),THETTO(140),THETAB(70),TEMPI2
&      /PROC/ HRSL,ALPAR,DIST,BI,KREF,ROUR,SPECR,EMIS,HTC(140,3),
&      BOLT,VOLSPR,WIDTH,QE(140,3),NRESIS,RESIS,IX
&      /ELMT/ NEL,NP,GND(140,3),B(140,3),C(140,3),EAREA(140),NPP1,
&      IES(140,2),ESL(140,3),BETA,XC(140,3),YC(140,3),DEFO,
&      NE(140),TLENG,PNOD(5,30),EBC(3,3),CM(3,3),GNDB(70)
DIMENSION CONF(2,3),CONK(3,3),IE(2)
BI = (DIST/KREF)*HTC(M,IES(M,L))
IF(IES(M,L).EQ.1) THEN

```

```

      IE(L) = 3
    ELSE
      IE(L) = IES(M,L) - 1
    END IF
    DO 100 I = 1,3
      IF(I .EQ. IE(L)) THEN
        CONF(L,I) = 0.
      ELSE
        CONF(L,I) = BI * ESL(M,IES(M,L)) * THETAC/2.
      END IF
    DO 110 J = 1,3
      IF(I .EQ. IE(L) .OR. J .EQ. IE(L)) THEN
        CONK(I,J) = 0.
      ELSE IF(I .EQ. J) THEN
        CONK(I,J) = BI*ESL(M,IES(M,L))/3.
      ELSE
        CONK(I,J) = BI*ESL(M,IES(M,L))/6.
      END IF
    110 CONTINUE
    100 CONTINUE
    DO 200 I = 1,3
      DO 210 J = 1,3
        KIJ(I,J) = KIJ(I,J) + CONK(I,J)
      210 CONTINUE
    200 CONTINUE
    RETURN
  END

```

SUBROUTINE SECNDB(L,QEF,M,NFLUX)

```

C *****
C * THIS SUBROUTINE CALCULATES ELEMENT MATRICES DUE TO SURFACE *
C * INTEGRALS FOR B.C.'S OF SECOND KIND, AND HEAT FLUX(QE) IS *
C * CONSTANT BETWEEN NODES *
C *****

```

IMPLICIT REAL (K)

```

COMMON/TEPS/ TEMPR,TEMPI,TMEL,DETP,DELTD,TEMPI1(140),THETAG(140),
&             THETAF(140),THETAO(140),THETTO(140),THETAB(70),TEMPI2
&             /PROC/ HRSL,ALPAR,DIST,BI,KREF,ROUR,SPECR,EMIS,HTC(140,3),
&             BOLT,VOLSPR,WIDTH,QE(140,3),NRESIS,RESIS,IX
&             /ELMT/ NEL,NP,GND(140,3),B(140,3),C(140,3),EAREA(140),NPP1,
&             IES(140,2),ESL(140,3),BETA,XC(140,3),YC(140,3),DEFO,
&             NE(140),TLENG,PNOD(5,30),EBC(3,3),CM(3,3),GNDB(70)

```

DIMENSION IE(2),QEF(2,3)

INTEGER GND

IF(IES(M,L) .EQ. 1) THEN

IE(L) = 3

ELSE

IE(L) = IES(M,L) - 1

END IF

C.....CONSTANT HEAT FLUX.....

C ESL = LENGTH OF SIDE

C DLQE = DIMENSIONLESS CONSTANT HEAT FLUX ON SIDE OF ELEMENT

```

IF(NFLUX .EQ. 1) THEN
  IF(IES(M,L) .EQ. 1) THEN
    QES = QE(M,IES(M,L))
  ELSE
    QS = QE(M,IES(M,L))
    CALL FLUXD(M,QES)
  END IF
ELSE
  QES = QE(M,IES(M,L))
END IF
DLQE = QES*DIST/(KREF*(TMEL - TEMPI))
IF(IES(M,L) .EQ. 1) THEN
  QEF(L,1)=(ESL(M,IES(M,L))/2.)*DLQE
  QEF(L,2) = QEF(L,1)
  QEF(L,3) = 0.
ELSE IF(IES(M,L) .EQ. 2) THEN
  QEF(L,1) = 0.
  QEF(L,2)=(ESL(M,IES(M,L))/2.)*DLQE
  QEF(L,3) = QEF(L,2)
ELSE
  QEF(L,1)=(ESL(M,IES(M,L))/2.)*DLQE
  QEF(L,2)=0.
  QEF(L,3) = QEF(L,1)
END IF
RETURN
END

```

SUBROUTINE RADB(L,TS,NTS,RADF,M,RADK)

```

C *****
C * THIS SUBROUTINE CALCULATES ELEMENT MATRICES DUE TO SURFACE *
C * INTEGRALS FOR B.C.'S OF RADIATION. *
C *****

```

```

IMPLICIT REAL (K)
COMMON/MATG/ AMC(140,151),RM(140),THETA(140),FLD(140),
&             AM(140,140),BM(140),CIJ(3,3),KIJ(3,3)
&             /TEPS/ TEMPR,TEMPI,TMEL,DETP,DELTD,TEMPI1(140),THETAG(140),
&             THETA(140),THETAO(140),THETTO(140),THETAB(70),TEMPI2
&             /PROC/ HRSL,ALPAR,DIST,BI,KREF,ROUR,SPECR,EMIS,HTC(140,3),
&             BOLT,VOLSPR,WIDTH,QE(140,3),NRESIS,RESIS,IX
&             /ELMT/ NEL,NP,GND(140,3),B(140,3),C(140,3),EAREA(140),NPP1,
&             IES(140,2),ESL(140,3),BETA,XC(140,3),YC(140,3),DEFO,
&             NE(140),TLENG,PNOD(5,30),EBC(3,3),CM(3,3),GNDB(70)
DIMENSION IE(2),RADF(2,3),RADK(3,3)
INTEGER GNDN,GND1,GND2,GND,TS

RADK = (DIST/KREF)*EMIS*BOLT
DELTT = TMEL - TEMPI
IF(IES(M,L) .EQ. 1) THEN
  IE(L) = 3
ELSE
  IE(L) = IES(M,L) - 1

```

ORIGINAL PAGE IS
OF POOR QUALITY

END IF
THETAR = (TEMPR - TMEL)/(TMEL - TEMPI)

C.....CONSTANT BETA.....

```

ETC = ESL(M,IES(M,L))*THETAR
IF(IES(M,L) .EQ. 1) THEN
  GND1 = GND(M,1)
  GND2 = GND(M,2)
ELSE IF(IES(M,L) .EQ. 2) THEN
  GND1 = GND(M,2)
  GND2 = GND(M,3)
ELSE
  GND1 = GND(M,1)
  GND2 = GND(M,3)
END IF
IF(TS .LE. NTS) THEN
  DTHETA = DELTT * (THETAG(GND1) + THETAG(GND2))/2.
ELSE
  DTHETA = DELTT * (THETAO(GND1) + THETAO(GND2))/2.
END IF
RBETAC = RADC * ((DTHETA+TMEL)**2 + TEMPR**2)*(DTHETA+TMEL+TEMPR)
DO 100 I = 1,3
  IF(I .EQ. IE(L)) THEN
    RADF(L,I) = 0.
  ELSE
    RADF(L,I) = ETC * RBETAC /2.
  END IF
DO 110 J = 1,3
  IF(I .EQ. IE(L) .OR. J .EQ. IE(L)) THEN
    RADK(I,J) = 0.
  ELSE IF(I .EQ. J) THEN
    RADK(I,J) = RBETAC*ESL(M,IES(M,L))/3.
  ELSE
    RADK(I,J) = RBETAC*ESL(M,IES(M,L))/6.
  END IF
110 CONTINUE
100 CONTINUE
DO 200 I = 1,3
  DO 250 J = 1,3
    KIJ(I,J) = KIJ(I,J) + RADK(I,J)
  250 CONTINUE
200 CONTINUE
RETURN
END

```

SUBROUTINE FLUXD(M,QES)

```

C *****
C * WHEN HEAT FLUX DEPEND ON TIME, CALCULATE HEAT FLUX ON BOUNDARY *
C * SURFACE BY LINEAR INTERPPLATION. *
C *****

```

```

COMMON/ELMT/ NEL,NP,GND(140,3),B(140,3),C(140,3),EAREA(140),NPP1,
& IES(140,2),ESL(140,3),BETA,XC(140,3),YC(140,3),DEFO,

```

```

&          NE(140), TLENG, PNOD(5,30), EBC(3,3), CM(3,3), GNDB(70)
&          /SPLIN/TIME(3), TIMER(20), QSTAG(20), XP1(25), CP1(4,25), ND1,
&          XP2(60), CP2(4,60), ND2, XP3(25), CP3(4,25), ND3, TS,
&          XP4(25), CP4(4,25), ND4, XP5(15), CP5(4,15), ND5, XP6(15),
&          CP6(4,15), XP7(15), CP7(4,15), ND7, XP8(15), CP8(4,15),
&          ND6, ND8, XP9(15), CP9(4,15), ND9, XP0(15), CP0(4,15), ND0,
&          ELSS(30), TESL(30)
INTEGER NL, NU, NTIME, TS, GND, PNOD, K, KM1, KM2

IF(TS .LT. 3) THEN
  LTS = TS
ELSE
  LTS = 3
END IF
K = 2
KM1 = 1
KM2 = KM1 - 1
50 IF(GND(M,3) .EQ. -PNOD(1,KM1) .AND. GND(M,2) .EQ. PNOD(1,K))
& THEN
  IF(KM1 .EQ. 1) THEN
    XI = TESL(1)/(2.*TLENG)
  ELSE
    XI = (TESL(KM2) + ELSS(KM1)/2.)/TLENG
  END IF
ELSE
  K = K + 1
  KM1 = K - 1
  KM2 = KM1 - 1
  GO TO 50
END IF
QSCALE = PCUBIC(XI, ND1, XP1, CP1)
TMI = TIME(LTS)
QSFLUX = PCUBIC(TMI, ND2, XP2, CP2)
QES = ABS(QSCALE)*QSFLUX
RETURN
END

```

SUBROUTINE SPLINE(N,XI,C)

 * SUBROUTINE SPLINE USES GAUSS ELIMINATION TO CALCULATE C2,I = *
 * SI WITH GIVEN THE NUMBER S C1,I=FI, AND C2,I = S1,C2,N+1=SN+1*

```

DIMENSION XI(60), C(4,60), D(60), DIAG(60)
DATA DIAG(1), D(1)/1., 0./
NP = N+1
DO 10 M = 2, NP
  D(M) = XI(M) - XI(M-1)
  DIAG(M) = (C(1,M) - C(1,M-1))/D(M)
10 CONTINUE
DO 20 M = 2, N
  C(2,M) = 3.*(D(M)*DIAG(M+1) + D(M+1)*DIAG(M))
  DIAG(M) = 2.*(D(M) + D(M+1))
20 CONTINUE

```

```

DO 30 M = 2,N
  G = - D(M+1)/DIAG(M-1)
  DIAG(M) = DIAG(M) + G*D(M-1)
  C(2,M) = C(2,M) + G*C(2,M-1)
30  CONTINUE
DO 40 M = 2,N
  NP = NP - 1
  C(2,NP) = (C(2,NP)-D(NP)*C(2,NP+1))/DIAG(NP)
40  CONTINUE
RETURN
END

```

SUBROUTINE CALCF(N,XI,C)

```

*****
* WITH FI STORED IN C1,I AND SI STORED IN C2,I, SUBROUTINE *
* CALCULATES C3,I, C4,I ,I = 1.....N *
*****

```

```

      DIMENSION XI(60),C(4,60)
      DO 10 I = 1,N
        DX = XI(I+1) - XI(I)
        DIVDF1 = (C(1,I+1) - C(1,I))/DX
        DIVDF3 = C(2,I) + C(2,I+1) - 2.*DIVDF1
        C(3,I) = (DIVDF1 - C(2,I) - DIVDF3)/DX
        C(4,I) = DIVDF3/DX/DX
10    CONTINUE
      RETURN
      END

```

```

      FUNCTION PCUBIC(XBAR,N,XI,C)

      DIMENSION XI(60),C(4,60)
      I = 1
      DX = XBAR - XI(I)
      IF(DX) 10,30,20
10    IF(I .EQ. 1) GO TO 30
      I = I -1
      DX = XBAR - XI(I)
      IF(DX) 10, 30, 30
19    I = I + 1
      DX = DDX
20    IF( I .EQ. N) GO TO 30
      DDX = XBAR - XI(I+1)
      IF(DDX) 30,19,19
30    PCUBIC = C(1,I)+DX*(C(2,I)+DX*(C(3,I)+DX*C(4,I)))
      RETURN
      END

```

SUBROUTINE FORMF(L,CONF,QEF,RADF,M)

```

C *****
C * THIS SUBROUTINE FORMS THE GLOBAL COLUMN VECTORS[FLD] *
C *****

```

```

COMMON/MATG/ AMC(140,151),RM(140),THETA(140),FLD(140),
&             AM(140,140),BM(140),CIJ(3,3),KIJ(3,3)
&             /ELMT/ NEL,NP,GND(140,3),B(140,3),C(140,3),EAREA(140),NPP1,
&             IES(140,2),ESL(140,3),BETA,XC(140,3),YC(140,3),DEFO,
&             NE(140),TLENG,PNOD(5,30),EBC(3,3),CM(3,3),GNDB(70)
DIMENSION CONF(2,3),QEF(2,3),RADF(2,3)
INTEGER GND
DO 100 I = 1,3
  II = GND(M,I)
  FLD(II) = FLD(II) + CONF(L,I) + QEF(L,I) + RADF(L,I)
100 CONTINUE
RETURN
END

```

SUBROUTINE FORMGM(P,TS,NTS,M)

```

C *****
C * FORMS SYSTEM MATRICES AM(I,J) AND BM(I) *
C *****

COMMON/MATG/ AMC(140,151),RM(140),THETA(140),FLD(140),
&             AM(140,140),BM(140),CIJ(3,3),KIJ(3,3)
&             /TEPS/ TEMPR,TEMPI,TMEL,DETP,DELTD,TEMPI(140),THETAG(140),
&             THETAF(140),THETAO(140),THETTO(140),THETAB(70),TEMPD
&             /PROC/ HRSL,ALPAR,DIST,BI,KREF,ROUR,SPECR,EMIS,HTC(140,3),
&             BOLT,VOLSPR,WIDTH,QE(140,3),NRESIS,RESIS,IX
&             /ELMT/ NEL,NP,GND(140,3),B(140,3),C(140,3),EAREA(140),NPP1,
&             IES(140,2),ESL(140,3),BETA,XC(140,3),YC(140,3),DEFO,
&             NE(140),TLENG,PNOD(5,30),EBC(3,3),CM(3,3),GNDB(70)
DIMENSION THETAI(140)
INTEGER GND,P,TS
REAL KIJ
IF(TS .LE. NTS) THEN
DO 100 I = 1,3
  II = GND(M,I)
  THETAI(II) = (TEMPI(II) - TMEL)/(TMEL - TEMPI)
100 CONTINUE
DO 200 I = 1,3
  II = GND(M,I)
DO 210 J = 1,3
  JJ = GND(M,J)
  KIJ(I,J) = KIJ(I,J)*WIDTH/DIST
  CIJ(I,J) = CIJ(I,J)*WIDTH/DIST
  AM(II,JJ) = AM(II,JJ) + (KIJ(I,J)*BETA + CIJ(I,J)/DEFO)
  BM(II) = BM(II)+(CIJ(I,J)/DEFO-(1.-BETA)* KIJ(I,J))*THETAI(JJ)
210 CONTINUE
200 CONTINUE
DO 300 I = 1,NP
  BM(I) = BM(I) + FLD(I)*WIDTH/DIST
300 CONTINUE
ELSE
DO 400 I = 1,3
  II = GND(M,I)
DO 410 J = 1,3

```

ORIGINAL PAGE IS
OF POOR QUALITY

```

      JJ = GND(M,J)
      KIJ(I,J) = KIJ(I,J)*WIDTH/DIST
      CIJ(I,J) = CIJ(I,J)*WIDTH/DIST
      AM(II,JJ) = AM(II,JJ) + 3.*KIJ(I,J)/4. + CIJ(I,J)/DEFO
      BM(II) = BM(II) + (CIJ(I,J)/DEFO)*THETAO(JJ)
&      - KIJ(I,J)*THETTO(JJ)/4.
410  CONTINUE
400  CONTINUE
      DO 420 I = 1,NP
      BM(I) = BM(I) + FLD(I)*WIDTH/DIST
420  CONTINUE
      END IF
      RETURN
      END

      SUBROUTINE GLOBMAX(TEMP,TEMPC,M,DUMK,NLEM,NFLUX,NRAD,NTS,IFN)
C*****
C* THIS SUBROUTINE ASSUMBLE ELEMENT MATRIX AND BOUNDARY CCNDITION *
C* INTO GLOBAL SYSTEM MATRIX[AMC] EXCEPT SPECIFIED TEMPERATURE. *
C*****
      COMMON/MATG/ AMC(140,151),RM(140),THETA(140),FLD(140),
&      AM(140,140),BM(140),CIJ(3,3),KIJ(3,3)
&      /TEPS/ TEMPR,TEMPI,TMEL,DETP,DELTD,TEMPI1(140),THETAG(140),
&      THETA(140),THETAO(140),THETTO(140),THETAB(70),TEMPI2
&      /PROC/ HRSL,ALPAR,DIST,BI,KREF,ROUR,SPECR,EMIS,HTC(140,3),
&      BOLT,VOLSPR,WIDTH,QE(140,3),NRESIS,RESIS,IX
&      /ELMT/ NEL,NP,GND(140,3),B(140,3),C(140,3),EAREA(140),NPP1,
&      IES(140,2),ESL(140,3),BETA,XC(140,3),YC(140,3),DEFO,
&      NE(140),TLENG,PNOD(5,30),EBC(3,3),CM(3,3),GNDB(70)
&      /SPLIN/TIME(3),TIMER(20),QSTAG(20),XP1(25),CP1(4,25),ND1,
&      XP2(60),CP2(4,60),ND2,XP3(25),CP3(4,25),ND3,TS,
&      XP4(25),CP4(4,25),ND4,XP5(15),CP5(4,15),ND5,XP6(15),
&      CP6(4,15),XP7(15),CP7(4,15),ND7,XP8(15),CP8(4,15),
&      ND6,ND8,XP9(15),CP9(4,15),ND9,XP0(15),CP0(4,15),NDO,
&      ELSS(30),TESL(30)
      INTEGER M,NLEM,L,P,IFN,TS
      DIMENSION TEMP(3),DUMK(140),CONK(3,3),RADK(3,3),CONF(2,3),
&      QEF(2,3),RADF(2,3),TEMPC(140,3)

C .....TO OBTAIN ELEMENT DATA.....

      CALL CONCP(X,Y,TEMP,M,DUMK,NLEM)

C*****
C TO EVALUATE SURFACE INTEGRAL(CONVECTION , HEAT FLUX,
C RADIATION BOUNDARY CONDITIONS)
C*****

      DO 100 I = 1,3
      DO 150 J = 1,3
      CONK(I,J) = 0.
      RADK(I,J) = 0.
150  CONTINUE

```



```

100 CONTINUE
DO 200 I = 1,NP
  FLD(I) = .0.0
200 CONTINUE
DO 300 L = 1,2
  DO 350 I = 1,3
    CONF(L,I) = 0.
    QEF(L,I) = 0.
    RADF(L,I) = 0.
350 CONTINUE
IF(HTC(M,IES(M,L)) .GT. 0.) THEN
  THETAC = (TEMPC(M,IES(M,L)) - TMEL)/(TMEL - TEMPI)
  CALL THIRDB(THETAC,L,CONF,M)
END IF
IF(QE(M,IES(M,L)) .NE. 0.) THEN
  CALL SECNDB(L,QEF,M,NFLUX)
END IF
IF(HTC(M,IES(M,L)) .GE. 0. .AND. NRAD .EQ. 1) THEN
  CALL RADB(L,TS,NTS,RADF,M,RADK)
END IF

```

CTO ASSEMBLE THE GLOBAL COLUMN VECTOR[FLD].....

```

  CALL FORMF(L,CONF,QEF,RADF,M)
300 CONTINUE

```

CTO ASSEMBLE ELEMENT MATRIX INTO GLOBAL SYSTEM MATRIX[AMC].....

```

  CALL FORMGM(P,TS,NTS,M)
  RETURN
  END

```

SUBROUTINE FIRSTBC(IFN)

```

C *****
C * THIS SUBROUTINE ENTERS THE SPECIFIED BOUNDARY *
C * TEMPERATURES IN A SYSTEM OF EQUATIONS. *
C *****

```

```

COMMON/MATG/ AMC(140,151),RM(140),THETA(140),FLD(140),
&             AM(140,140),BM(140),CIJ(3,3),KIJ(3,3)
&             /TEPS/ TEMPR,TEMPI,TMEL,DETP,DELTD,TEMPI1(140),THETAG(140),
&             THETAF(140),THETAO(140),THETTO(140),THETAB(70),TEMPI2,
&             /ELMT/ NEL,NP,GND(140,3),B(140,3),C(140,3),EAREA(140),NPP1,
&             IES(140,2),ESL(140,3),BETA,XC(140,3),YC(140,3),DEFO,
&             NE(140),TLENG,PNOD(5,30),EBC(3,3),CM(3,3),GNDB(70)
INTEGER GNDB
DO 100 I = 1,IFN
  II = GNDB(I)
  IF(II .LT. 0) THEN
    GO TO 100
  ELSE
    BM(II) = THETAB(I)
  DO 110 J = 1,NP

```

ORIGINAL PAGE IS
OF POOR QUALITY

```

      IF(II .EQ. J) THEN
        AM(II,J) = 1.
      ELSE
        BM(J) = BM(J) - THETAB(I)*AM(J,II)
        AM(II,J) = 0.
        AM(J,II) = 0.
      END IF
110    CONTINUE
      END IF
100    CONTINUE
      RETURN
      END

```

SUBROUTINE RESIDUL(RMAX)

```

C *****
C * THIS SUBROUTINE CALCULATE RESIDUALS AT EVERY NODES *
C *****

```

```

      COMMON/MATG/ AMC(140,151),RM(140),THETA(140),FLD(140),
&      AM(140,140),BM(140),CIJ(3,3),KIJ(3,3)
&      /TEPS/ TEMPR,TEMPI,TMEL,DETP,DELTD,TEMPG1(140),THETAG(140),
&      THETAF(140),THETAO(140),THETTO(140),THETAB(70),TEMPO
&      /ELMT/ NEL,NP,GND(140,3),B(140,3),C(140,3),EAREA(140),NPP1,
&      IES(140,2),ESL(140,3),BETA,XC(140,3),YC(140,3),DEFO,
&      NE(140),TLENG,PNOD(5,30),EBC(3,3),CM(3,3),GNDB(70)
      DO 100 I = 1,NP
        DO 110 J = 1,NP
          RM(I) = RM(I) + AM(I,J)*THETA(J)
110    CONTINUE
          RM(I) = RM(I) - BM(I)
100    CONTINUE
      RMIN = 10000.
      RMAX = 0.
      DO 200 I = 1,NP
        IF(ABS(RM(I)) .GT. RMAX) THEN
          RMAX = ABS(RM(I))
        END IF
        IF(ABS(RM(I)) .LT. RMIN) THEN
          RMIN = ABS(RM(I))
        END IF
200    CONTINUE
      RETURN
      END

```

SUBROUTINE CHLSKY(TS,NTS,THETAX)

```

C *****
C * THIS SUBROUTINE SOLVES THE SYSTEM OF EQUATION *
C * BY USING CHOLESKY DECOMPOSITION METHOD *
C *****

```

```

      COMMON/MATG/ AMC(140,151),RM(140),THETA(140),FLD(140),

```

```

&          AM(140,140),BM(140),CIJ(3,3),KIJ(3,3)
&      /TEPS/ TEMPR,TEMPI,TMEL,DETP,DELTD,TEMPI1(140),THETAG(140),
&          THETAF(140),THETAO(140),THETTO(140),THETAB(70),TEMPI2(140),
&      /ELMT/ NEL,NP,GND(140,3),B(140,3),C(140,3),EAREA(140),NPP1,
&          IES(140,2),ESL(140,3),BETA,XC(140,3),YC(140,3),DEFO,
&          NE(140),TLENG,PNOD(5,30),EBC(3,3),CM(3,3),GNDB(70)
DIMENSION THETAX(140)
INTEGER TS
DO 100 I = 1,NP
  DO 110 J = 1,NP
    AMC(I,J) = AM(I,J)
110  CONTINUE
100  CONTINUE

```

C...TO SUBSTITUTE RM(I) OR BM(I) INTO THE NPP1TH COLUMN OF MATRIX AMC(NP,NPP1)..

```

DO 120 I = 1,NP
  IF(TS .LE. NTS) THEN
    AMC(I,NPP1) = AMC(I,NPP1) - RM(I)
  ELSE
    AMC(I,NPP1) = AMC(I,NPP1) + BM(I)
  END IF
120 CONTINUE

```

C....TO CALCULATE FIRST ROW OF UPPER UNIT TRIANGULAR MATRIX....

```

DO 200 J = 2,NPP1
  AMC(1,J) = AMC(1,J)/AMC(1,1)
200 CONTINUE

```

C....TO CALCULATE OTHER ELEMENTS OF U AND L MATRICES....

```

DO 300 I = 2,NP
  J = I
  DO 310 II = J,NP
    SUM = 0.
    JM1 = J - 1
    DO 320 K = 1,JM1
      SUM = SUM + AMC(II,K) * AMC(K,J)
320  CONTINUE
    AMC(II,J) = AMC(II,J) - SUM
310  CONTINUE
    IP1 = I + 1
    DO 330 JJ = IP1,NPP1
      SUM = 0.
      IM1 = I - 1
      DO 340 K = 1,IM1
        SUM = SUM + AMC(I,K)*AMC(K,JJ)
340  CONTINUE
      AMC(I,JJ) = (AMC(I,JJ) - SUM)/AMC(I,I)
330  CONTINUE
300  CONTINUE

```

C....TO SOLVE FOR THETAX(I) BY BACK SUBSTITUTION....

ORIGINAL PAGE IS
OF POOR QUALITY

```

      THETAX(NP) = AMC(NP,NPP1)
      L = NP - 1
      DO 400 NN = 1,L
        SUM = 0.
        I = NP - NN
        IP1 = I + 1
        DO 410 J = IP1, NP
          SUM = SUM + AMC(I,J) * THETAX(J)
410      CONTINUE
        THETAX(I) = AMC(I,NPP1) - SUM
400      CONTINUE
      RETURN
      END

```

SUBROUTINE INTFLUX(JFNT,JNT,TVU,TEMPV,TEMPS,QEI)

```

C *****
C * THIS SUBROUTINE CALCULATE HEAT FLUX AT LIQUID - VAPOR INT- *
C * FACE BY USING KINETIC THEORY WITH VAPOR AND INTERFACE TEMP*
C *****

      DIMENSION GNDI(70),TEMPS(70),TEMPV(70),QEI(70),MASW(70)
      INTEGER GNDI
      REAL MASW

      KP = 0
      DO 50 I = 1,JFNT
        QEI(I) = 0.
50      CONTINUE
      DO 100 I = 1,JNT
        TW = TEMPS(I)
        TV = TVU
        CALL NAVPROP(TW,DENV,VISV,HFG,HG,PSATI,KP)
        CALL NAVPROP(TV,DENV,VISV,HFGV,HG,PSATV,KP)
        MASW(I) = (2.*.7*(23./(2.*3.1416*8314.))**.5)*(PSATI/TW**.5
&                - PSATV/TV**.5)
        QEI(I) = MASW(I) * HFG
100     CONTINUE
      RETURN
      END

```

SUBROUTINE COUPLE(JNT,QT,TVU,JFNT)

```

C*****
C* THIS SUBROUTINE CALCULATES THERMAL RESISTANCE IN THE VAPOR *
C* SPACE BY USING KNOWN HEAT FLUX AND EVALUATES NEW HEAT FLUX *
C* AND VAPOR TEMPERATURE *
C*****

      COMMON/MATG/ AMC(140,151),RM(140),THETA(140),FLD(140),
&                AM(140,140),BM(140),CIJ(3,3),KIJ(3,3)
&                /TEPS/ TEMPR,TEMPI,TMEL,DETP,DELTD,TEMPI1(140),THETAG(140),
&                THETAF(140),THETAO(140),THETTO(140),THETAB(70),TEMPI2

```

```

&      /PROC/ HRSL,ALPAR,DIST,BI,KREF,ROUR,SPECR,EMIS,HTC(140,3),
&      BOLT,VOLSPR,WIDTH,QE(140,3),NRESIS,RESIS,IX
&      /ELMT/ NEL,NP,GND(140,3),B(140,3),C(140,3),EAREA(140),NPP1,
&      IES(140,2),ESL(140,3),BETA,XC(140,3),YC(140,3),DEFO,
&      NE(140),TLENG,PNOD(5,30),EBC(3,3),CM(3,3),GNDB(70)
&      /INOUT/TEMPS(70),TEMPV(70),TEMPVS(70),QEI(70),VX(70),
&      GNDI(70),VY1(70),VY2(70),VY3(70),ELSI(30),
&      VY4(70),VY5(70),VY6(70),HFG,TEMPF(70)
&      /SPLIN/TIME(3),TIMER(20),QSTAG(20),XP1(25),CP1(4,25),ND1,
&      XP2(60),CP2(4,60),ND2,XP3(25),CP3(4,25),ND3,TS,
&      XP4(25),CP4(4,25),ND4,XP5(15),CP5(4,15),ND5,XP6(15),
&      CP6(4,15),XP7(15),CP7(4,15),ND7,XP8(15),CP8(4,15),
&      ND6,ND8,XP9(15),CP9(4,15),ND9,XP0(15),CP0(4,15),ND0,
&      ELSS(30),TESL(30)
&      /OUTPT/MO,IDAY,IYEAR,TITLE,CASE,NUMBER,NO,TEMPCC,HTCC,IOUT,
&      TIMEN,DELT,DELT1,DELTP
INTEGER JNT,IX,JNTL,JFNT
REAL JCOB
DIMENSION QT(70)

```

```

C      JNT = NUMBER OF NODE WHOSE TEMPERATURE IS GREATER THAN TSTAR
C      JNTL = NUMBER OF NODE WHOSE TEMPERATURE IS GREATER THAN TVU
C      TEMPD = TEMP. DROP IN VAPOR SPACE [K]
C      RESIS = RESISTANCE IN VAPOR SPACE [K/W]
C      RESISN = ARTIFICIALLY ADDED RESISTANCE AT EACH NODE
C      TEMPF(I) = TEMP. DROP DUE TO NEW RESISTANCE AT INTERFACE

```

```

      QTAL = 0.0
      IF(NRESIS.EQ. 2) THEN
        DO 100 I = 1,JNT
          QEI(I) = QT(I)
100      CONTINUE
        END IF
        NRESIS = 2
        DO 150 I = 1,JNT
          IF(TEMPS(I).GT. TVU) THEN
            JNTL = I
          ELSE IF(TEMPS(I).LT. TVU .AND. TEMPS(I-1).GT. TVU)
            &      THEN
            XII = (TEMPS(JNTL) - TVU)*ELSI(I)
            XII = XII/(TEMPS(JNTL)-TEMPS(I))
          END IF
150      CONTINUE
        DO 200 I = 1,JNT
          IF(QEI(I).GT. 0.) THEN
            QTAL = QTAL + QEI(I)*ELSI(I)*WIDTH
          END IF
200      CONTINUE
        QEI(JFNT) = 0.
        IF(IX.LE. 1) THEN
          CALL HPVAPOR(JNT,TS,DIST,IND,TIME)
          TEMPD = VY4(1) - VY4(JNT)
          RESIS = TEMPD/QTAL
          RESIS = RESIS/23.
        END IF

```

ORIGINAL PAGE IS
OF POOR QUALITY

```

IF(IX .LE. 100) THEN
  IF(TEMPD .LE. 20.) THEN
    RESISN = RESIS
  ELSE
    RESISN = RESIS*IX*.01
  END IF
  IX = IX + 1
  IF(IX .EQ. 100) THEN
    IX = 1
  END IF
END IF
DO 250 I = 1,JNT
  TEMPF(I) = RESISN*QEI(I)*WIDTH*ELSI(I)
  TEMPS(I) = TEMPS(I) - TEMPF(I)
250 CONTINUE
500 RESD = 0.
  TELSI = 0.
  RESDC = 4.5E6*1.4*.021*2.29E11
  DO 260 I = 1,JNT
    RESDI = ELSI(I)*10.**(-5567./TEMPS(I))/TEMPS(I)
    RESDV = ELSI(I)*10.**(-5567./TVU)/TVU
    RESD = RESD + RESDC*(RESDI - RESDV)
    TELSI = TELSI + ELSI(I)
260 CONTINUE
  JCOB = (1 - 12818.5/TVU)*TELSI
  JCOB = JCOB * 10.**(-5567./TVU)
  JCOB = RESDC*JCOB/(TVU**2)
  TVO = TVU
  TVU = TVO - RESD/JCOB
  IF(ABS(RESD) .LT. .01) THEN
    CALL INTFLUX(JFNT,JNT,TVU,TEMPV,TEMPS,QEI)
    DO 270 I = 1,JNT
      QT(I) = QEI(I)
270 CONTINUE
  ELSE
    GO TO 500
  END IF
RETURN
END

```

C.....FOLLOWING SUBROUTINES ARE USED TO CALCULATE PRESSURE, VELOCITY,
C.....DENSITY, TEMPERATURE, AND QUALITY IN VAPOR SPACE.....

SUBROUTINE HPVAPOR(JNTD,TS,DDIST,IND,TIME)

```

C *****
C * THIS PROGRAM CALCULATES THE VAPOR TEMPERATURES, PRESSURES, DENSITIES, *
C * QUALITY, AND VELOCITY WITH CONSIDERATION OF COMPRESSIBILITY BY USING *
C * THE RUNGE-KUTTA METHOD. *
C *****

```

C VARIABLES

```

C
C DIST      HEIGHT OF THE VAPOR SPACE [M]
C INTV      INCREMENT IN AXIAL DIRECTION [M]
C MASW      MASS FLOW AT WALL [KG/M**2]
C TW        WALL TEMPERATURE [K]
C JNT       NUMBER OF POINTS WHERE DATA ARE CALCULATED
C QW        HEAT FLUX [W/M**2]

```

```

COMMON/VAPOR/ REYW(70), II, JNT, DIST, TW, QW, MASW, PSAT, Y1N, Y2N,
&              Y3N, Y4N, Y6N
&      /INOUT/ TEMPS(70), TEMPV(70), TEMPVS(70), QEI(70), VX(70),
&              GNDI(70), VY1(70), VY2(70), VY3(70), ELSI(30),
&              VY4(70), VY5(70), VY6(70), HFG, TEMPF(70)
DIMENSION C(24), W(5,9), TWI(70), Y(6), MACH(70), TIME(3)

```

```

INTEGER II, N, NW, IND, GNDI, TS
REAL MASW, MASWN, INTV, XEND, MACH, JCOB
EXTERNAL FCN1

```

C.....INITIAL PARAMETERS.....

```

C      N      = NUMBER OF DIFFERENTIAL EQUATIONS
C      Y(1)   = PRESSURE OF VAPOR [N/M**2]
C      Y(2)   = VELOCITY [M/SEC.]
C      Y(3)   = DENSITY [KG/M**3]
C      Y(4)   = TEMPERATURE [K]
C      Y(5)   = QUALITY OF VAPOR
C      Y(6)   = SPECIFIC VOLUME [M**3/KG]

```

```

DIST = DDIST
JNT = JNTD
PH = 0.
N = 5
NW = N
IND = 1
TOL = .0001

```

C.....CALAULATE INITIAL VALUES.....

```

CALL INITV
Y(4) = TEMPV(2)
Y(1) = 2.29E11/(Y(4)**.5)*10.**(-5567./Y(4))
Y(3) = 23.*Y(1)/(8314.*Y(4))
Y(5) = 1.
Y(6) = 1./Y(3)
KP = 1
CALL NAVPROP(TEMPV(2), DENV, VISV, HFG, HG, PSATI, KP)
Y(2) = QEI(1)*ELSI(1)/(HFG*DIST*Y(3))

```

C.....SET REFERENCE VALUE TO NORMALIZE.....

```

Y1N = Y(1)
Y2N = Y(2)
Y3N = Y(3)
Y4N = Y(4)

```

ORIGINAL PAGE IS
OF POOR QUALITY

```

Y6N = Y(6)
VX(1) = 0.0
VX(2) = ELSI(1)
VY2(1) = 0.0
VY2(2) = Y(2)
DO 100 I = 1,2
  VY1(I) = Y(1)
  VY3(I) = Y(3)
  VY4(I) = Y(4)
  VY5(I) = Y(5)
  VY6(I) = Y(6)
100 CONTINUE
TWI(1) = TEMPS(1)
TWI(2) = TEMPS(2)

```

C.....CALCULATE P,V,DENSITY,T,QUALITY BY USING DVERK.....

```

DO 200 II = 3,JNT + 1
  IM1 = II - 1
  QW = QEI(IM1)
5  PH = PH + 1
  IF(PH .NE. 1.) THEN
    IND = 1
  END IF
  INTV = ELSI(IM1)
  XEND = VX(II-1) + INTV
  VX(II) = XEND
  X = VX(IM1)

```

C.....NORMALIZE THE DEPENDANT VARIABLES.....

```

Y(1) = VY1(IM1)/Y1N
Y(2) = VY2(IM1)/Y2N
Y(3) = VY3(IM1)/Y3N
Y(4) = VY4(IM1)/Y4N
Y(5) = VY5(IM1)
Y(6) = VY6(IM1)/Y6N
IF(PH .EQ. 1.) THEN
  TW = TEMPS(II)
ELSE
  TW = TWI(II)
END IF
CALL DVERK(N,FCNL,X,Y,XEND,TOL,IND,C,NW,W,IER)
IF(IND .LT. 0 .OR. IER .GT. 0) THEN
  WRITE(4,*) IND,IER
  GO TO 300
END IF
Y1 = Y(1)*Y1N
Y2 = Y(2)*Y2N
Y3 = Y(3)*Y3N
Y4 = Y(4)*Y4N
MASWN = 2.*.7*(23./(2.*3.1416*8314.))**.5*(PSAT/TW**.5
&      - Y1/Y4**.5)
DMAS = (MASW - MASWN)/(MASW)
IF(ABS(DMAS) .LT. .02) THEN

```



```

VY1(II) = Y(1)*Y1N
VY2(II) = Y(2)*Y2N
VY3(II) = Y(3)*Y3N
VY4(II) = Y(4)*Y4N
VY5(II) = Y(5)
VY6(II) = 1./VY3(II)
TEMPV(II) = VY4(II)
TWI(II) = TW
PH = 0.
ELSE
  HFG = 4636437. - 180.82*TW
  RESD = MASW - MASWN
  JCOB = 180.82*QW/(HFG**2)
  JCOB = JCOB - 2.*.7*((23./(2.*3.1416*8314.))**.5)
&      *(2.29E11*(12818.8/TW - 1.)*(10.**(-5567./TW))/TW**2)
  TW = TW - (RESD/JCOB)
  TWI(II) = TW
  GO TO 5
END IF
200 CONTINUE
300 CONTINUE
  IJNT = 2*JNT/3
  WRITE(6,400) TIME(3)
  WRITE(6,410) QW,DIST,INTV,REYW(2),REYW(IJNT)
  WRITE(6,420)
  WRITE(6,430)
  DO 350 II = 1, JNT+1
    MACH(II) = VY2(II)/SQRT(1.4*8314.*VY4(II)/23.)
    WRITE(6,440) VX(II),VY1(II),VY2(II),VY3(II),VY4(II),
&      VY5(II),MACH(II)
350 CONTINUE
400 FORMAT(/2X,83('-')/28X,'**TIME = ',F9.3,2X,'SEC**'/)
410 FORMAT(4X,'HEAT INPUT = ',F8.1,2X,'DIST = ',F6.4,2X,'INTV = ',
& F5.3,3X,'REYNOLD = ',F6.1,2X,F6.1/)
420 FORMAT(8X,'XL(I)',6X,'PRESSURE',4X,'VELOCITY',5X,
& 'DENSITY',5X,'TVAP',6X,'QUAL',5X,'MACH'/)
430 FORMAT(10X,'M',9X,'N/M**2',7X,'M/SEC',6X,'KG/M**3',7X,'K',
& 30X,/2X,83('-')/)
440 FORMAT(5X,E9.2,2X,E11.5,2X,E10.3,3X,E10.4,2X,F7.2,3X,F6.3,3X,F6.3)
  RETURN
  END

```

SUBROUTINE INITV

```

C *****
C * THIS SUBROUTINE CALCULATES INITIAL VAPOR TEMPERARURE. *
C *****

```

```

COMMON/INOUT/ TEMPS(70),TEMPV(70),TEMPVS(70),QEI(70),VX(70),
& GNDI(70),VY1(70),VY2(70),VY3(70),ELSI(30),
& VY4(70),VY5(70),VY6(70),HFG,TEMPF(70)
INTEGER GNDI
REAL MASW,JCOB

```

ORIGINAL PAGE IS
OF POOR QUALITY

```

NN = 0
KP = 0
PHI = 3.1416
UGAS = 8314.
TWI = TEMPS(2)
TVI = TWI - .1
CALL NAVPROP(TWI,DENV,VISV,HFG,HG,PSATW,KP)
100 CALL NAVPROP(TVI,DENV,VISV,HFGV,HG,PSATV,KP)
NN = NN + 1
MASW = 2.*.7*(23./(2.*PHI*UGAS))**.5*(PSATW/TWI**.5
&      - PSATV/TVI**.5)
QEIN = MASW*HFG
DQEI = (QEIN - QEI(1))/QEIN
IF(NN.LT. 5) THEN
IF(ABS(DQEI).LT. .01) THEN
  TEMPV(1) = TVI
  TEMPV(2) = TVI
ELSE
  RESD = QEI(1) - QEIN
  JCOB = 2.*.7*HFG*(23./(2.*PHI*UGAS))**.5
  JCOB = JCOB * 2.29E11*10.**(-5567./TVI)/(TVI**2)
  JCOB = JCOB*(12818.5/TVI-1.)
  TVI = TVI - RESD/JCOB
  GO TO 100
END IF
END IF
RETURN
END

```

SUBROUTINE FCN1(N,X,Y,YPR)

```

C *****
C * THIS SUBROUTINE PROVIDE DERIVATIVE OF GOVERNING EQUATIONS *
C *****

COMMON/VAPOR/ REYW(70),II,JNT,DIST,TW,QW,MASW,PSAT,Y1N,Y2N,
&              Y3N,Y4N,Y6N
&      /INOUT/ TEMPS(70),TEMPV(70),TEMPVS(70),QEI(70),VX(70),
&              GNDI(70),VY1(70),VY2(70),VY3(70),ELSI(30),
&              VY4(70),VY5(70),VY6(70),HFG,TEMPF(70)
DIMENSION YPR(5),Y(6)
REAL MASW

IM1 = II - 1
Y(6) = VY6(IM1)
KP = 0
CALL NAVPROP(TW,DENW,VISW,HFG,HGW,PSAT,KP)
MASW = QW/HFG
VW = MASW/(DENW)
REYW(IM1) = - DENW*VW*DIST/VISW
HCP = 904.

```

C.....THIS SUBROUTINE CALCULATES ALPAR,BETA,F2P0, AND F2P1.....

CALL FACTOR(ALPAR,BETA,F2P0,F2P1)

C.....THIS SUBROUTINE CALCULATES THE PROPERTIES OF SODIUM.....

```

TEMPK = Y(4)*Y4N
KP = 1
CALL NAVPROP(TEMPK,DDEN,VISV,HFGV,HG,DPAST,KP)
Y1 = Y(1)*Y1N
Y2 = Y(2)*Y2N
Y3 = Y(3)*Y3N
Y4 = Y(4)*Y4N
Y6 = Y(6)
RSTA = 8314./23.
SPEV = 1./Y3
SPEVF = 1./((.927 - .238E-3*(Y4 - 373))*1000.)
IF(Y(5) .LE. 0.) THEN
    SPEVG = 0.
ELSE IF(Y(5) .GT. 1.) THEN
    Y(5) = 1.
    SPEVG = SPEV
    SPEVF = 0.
ELSE
    SPEVG = (SPEV - SPEVF)/Y(5) + SPEVF
END IF
SPERI = (SPEVG - SPEVF)/SPEV
RTH = (1. - RSTA*Y4/HFGV)
FIC = 8.*VISV*(F2P0 - F2P1)/(Y3*DIST*Y2)
PY1 = ALPAR*MASW/(BETA*Y2*DIST)
PY2 = 2.*HFGV
PY3 = SPERI*(HGW-HG+(BETA*Y2**2)/2.+(VW**2)/2.)
PY4 = HFGV/(BETA*SPEV)
PY5 = SPERI/SPEV*Y2**2
PY6 = - PY1*(PY2 + PY3)
PY7 = PY6 - (PY4+PY5)*FIC/(8.*DIST)
PY8 = ALPAR*HFGV*Y(5)*SPEVG*RTH/(BETA*Y1*SPEV**2)
PY9 = ALPAR*SPERI*HCP*RSTA*Y4**2/(BETA*SPEV*HFGV*Y1)
PY10 = SPERI + HFGV/(BETA*Y2**2) - PY8 - PY9
PY = PY7/PY10
YPR(1) = PY/Y1N

```

C.....CALCULATE THE DERIVITIVE OF QUALITY.....

```

QUAL1 = (Y2**2)*Y(5)*SPEVG*RTH/(Y1*SPEV**2)
QUAL2 = (-1./ALPAR + QUAL1)*PY
QUAL3 = FIC*Y2**2/(8.*DIST*SPEV*ALPAR)
QUAL4 = SPERI*Y2**2/SPEV
QUAL5 = (QUAL2 - QUAL3)/QUAL4
QUAL6 = 2.*MASW*SPEV/(Y2*DIST*SPERI)
QUAL = QUAL5 - QUAL6
YPR(5) = QUAL

```

C.....CALCULATE THE DERIVITIVE OF VELOCITY.....

```

VEL1 = MASW*SPEV/DIST
VEL2 = Y2*SPERI*QUAL
VEL3 = Y2*Y(5)*SPEVG*(-RTH)*PY/(Y1*SPEV)

```

ORIGINAL PAGE IS
OF POOR QUALITY

VEL = VEL1 + VEL2 + VEL3
YPR(2) = VEL/Y2N

C.....CALCULATE THE DERIVITIVE OF DENSITY.....

ROU1 = SPERI*QUAL/SPEV
ROU2 = SPEVG*Y(5)*RTH*PY/(Y1*SPEV**2)
ROU = -ROU1 + ROU2
YPR(3) = ROU/Y3N
TY = PY*RSTA*Y4**2/(Y1*HFGV)
YPR(4) = TY/Y4N
RETURN
END

SUBROUTINE NAVPROP(TEMPK,DENV,VISV,HFG,HG,PSAT,KP)

C *****
C * THIS SUBROUTINE CALCULATES THE PROPERTIES OF THE SODIUM SUCH AS *
C * THE SATURATION PRESSURE, THE DENSITY, THE VISCOSITY, THE LATENT *
C * HEAT OF VAPORIZATION, AND THE ENTHALPY. *
C *****

T = TEMPK
IF(KP .EQ. 0) THEN
PSAT = (2.29E11/T**.5)*10.**(-5567./T)
ELSE
PSAT = 0.
END IF
DENV = 2.766E-3*PSAT/T
VISV = 6.083E-9*T + 1.2606E-5
HF = 98.973 + 1.4367 * (T - 273.16)
HF = HF - 2.902E-4*(T - 273.16)**2
HF = 1000.*(HF + 2.4E4*EXP(-1.36E4/T))
HFG = 182.*(25474.93 - .9935*T)
HG = HF + HFG
RETURN
END

SUBROUTINE FACTOR(ALPAR,BETA,F2P0,F2P1)

C *****
C * THIS SUBROUTINE PROVIDES THE VALUES OF ALPAR,BETA,F2P0, *
C * AND F2P1 CORRESPONDING TO THE GIVEN REYNOLDS NUMBERS. *
C *****

COMMON/VAPOR/ REYW(70),II,JNT,DIST,TW,QW,MASW,PSAT,Y1N,Y2N,
& Y3N,Y4N,Y6N
REYW1 = REYW(II-1)
REYW2 = REYW1**2
IF(REYW1 .LT. 2. .AND. REYW1 .GT. -30.) THEN
F2P0 = 6.0995 - .42198*REYW1 - 3.8013E-3 * REYW2
F2P1 = - 5.6405 - .2349*REYW1 - 5.2913E-3*REYW2
ALPAR = 1.2049 - 1.0386E-3*REYW1

```

      BETA = 1.5574 - 3.1837E-3*REYW1
      ELSE IF(REYW1 .GE. 2.) THEN
        F2P0 = 6.0995 - .42198*REYW1 - 3.8013E-3 * REYW2
        F2P1 = -6.548 - .1417*REYW1 - .1233*REYW2
        ALPAR = 1.22 - 1.5082E-2 * REYW1 + 2.6689E-3*REYW2
        BETA = 1.612 - 5.0904E-2 * REYW1 + 8.6570E-3*REYW2
      ELSE IF(REYW1 .LE. -30.) THEN
        F2P0 = 15.34 - .223*(REYW1 + 30)
        F2P1 = - 3.06
        ALPAR = 1.227
        BETA = 1.63
      END IF
      RETURN
      END

```

SUBROUTINE NEWRA(JNT,KN,QEI,QEIN,TEMPS,TEMPV,QW)

```

C *****
C * CALCULATE NEW WALL TEMPERATURE BY USING NEWTON-RAPHSON *
C * METHOD FOR NEXT ITERATION. *
C *****

```

```

      DIMENSION TEMPS(70),TEMPV(70),QEI(70),QEIN(70)
      REAL MASW,MASWN,JCOB

```

```

      DO 100 I = 2,JNT+1
        TW = TEMPS(I)
        TV = TEMPV(I)
        MASW = QEI(I)
        MASWN = QEIN(I)
        RESD = MASW - MASWN
        JCOB = -364.*.7*(SQRT(23./(2.*3.1416*8314.)))
&      *((2.29E11*(10.**(-5567./TW))/TW)
&      *(-.9935 + (25474.93 - .9935*TW)*((12818.5-TW)/TW**2))
&      + .9935*(2.29E11/TV)*10.**(-5567./TV))
        TW = TW - RESD/JCOB
100    CONTINUE
      RETURN
      END

```

```

&      SUBROUTINE DATAIN(TA,JK,JNT,TIMEN,
&      FIRTS,TVU,QT,TEMPD)

```

```

C*****
C* THIS SUBROUTINE READS IN INTERMEDIATE DATA FOR RESTARTING OF *
C* MAIN PROGRAM FROM LAST RUN *
C*****

```

```

      COMMON/PROC/ HRSL,ALPAR,DIST,BI,KREF,ROUR,SPECR,EMIS,HTC(140,3),
&      BOLT,VOLSPR,WIDTH,QE(140,3),NRESIS,RESIS,IX
&      /ELMT/ NEL,NP,GND(140,3),B(140,3),C(140,3),EAREA(140),NPP1,
&      IES(140,2),ESL(140,3),BETA,XC(140,3),YC(140,3),DEFO,
&      NE(140),TLENG,PNOD(5,30),EBC(3,3),CM(3,3),GNDB(70)
&      /INOUT/ TEMPS(70),TEMPV(70),TEMPVS(70),QEI(70),VX(70),

```

```
&          GNDI(70),VY1(70),VY2(70),VY3(70),ELSI(30),
&          VY4(70),VY5(70),VY6(70),HFG,TEMPF(70)
&      /SPLIN/TIME(3),TIMER(20),QSTAG(20),XP1(25),CP1(4,25),ND1,
&          XP2(60),CP2(4,60),ND2,XP3(25),CP3(4,25),ND3,TS,
&          XP4(25),CP4(4,25),ND4,XP5(15),CP5(4,15),ND5,XP6(15),
&          CP6(4,15),XP7(15),CP7(4,15),ND7,XP8(15),CP8(4,15),
&          ND6,ND8,XP9(15),CP9(4,15),ND9,XPO(15),CPO(4,15),ND0,
&          ELSS(30),TESL(30)
```

```
DIMENSION TA(3,96),QT(70)
INTEGER TS,JK,JNT,NPP1,FIRTS
REWIND 8
READ(8,*) TS,FIRTS,JK,JNT,NRESIS,IX
READ(8,*) NPP1,TIMEN,RESIS,TEMPD
IF(TS .LE. 3) THEN
    LTS = TS
ELSE
    LTS = 3
END IF
READ(8,*) (TIME(I),I=1,LTS),TVU,DEFO
READ(8,*) ((TA(I,J),I=2,3),J=1,NP)
IF(FIRTS .GT. 1) THEN
    READ(8,*) ((QE(I,J),J=1,2),I=1,NEL)
    READ(8,*) (QT(I),I=1,JNT)
END IF
RETURN
END
```

```
      SUBROUTINE DATAOUT(TA,JK,JNT,TIMEN,
&          FIRTS,TVU,QT,TEMPD)
```

```
C*****
C* THIS SUBROUTINE WRITES INTERMEDIATE DATA FOR RESTARTING OF *
C* MAIN PROGRAM FROM LAST RUN *
C*****
```

```
COMMON/PROC/ HRSL,ALPAR,DIST,BI,KREF,ROUR,SPECR,EMIS,HTC(140,3),
&          BOLT,VOLSPR,WIDTH,QE(140,3),NRESIS,RESIS,IX
&      /ELMT/ NEL,NP,GND(140,3),B(140,3),C(140,3),EAREA(140),NPP1,
&          IES(140,2),ESL(140,3),BETA,XC(140,3),YC(140,3),DEFO,
&          NE(140),TLENG,PNOD(5,30),EBC(3,3),CM(3,3),GNDB(70)
&      /INOUT/TEMPS(70),TEMPV(70),TEMPVS(70),QEI(70),VX(70),
&          GNDI(70),VY1(70),VY2(70),VY3(70),ELSI(30),
&          VY4(70),VY5(70),VY6(70),HFG,TEMPF(70)
&      /SPLIN/TIME(3),TIMER(20),QSTAG(20),XP1(25),CP1(4,25),ND1,
&          XP2(60),CP2(4,60),ND2,XP3(25),CP3(4,25),ND3,TS,
&          XP4(25),CP4(4,25),ND4,XP5(15),CP5(4,15),ND5,XP6(15),
&          CP6(4,15),XP7(15),CP7(4,15),ND7,XP8(15),CP8(4,15),
&          ND6,ND8,XP9(15),CP9(4,15),ND9,XPO(15),CPO(4,15),ND0,
&          ELSS(30),TESL(30)
DIMENSION TA(3,96),QT(70)
INTEGER TS,JK,JNT,NPP1,FIRTS
REWIND 8
IF(TS .LE. 3) THEN
    LTS = TS
ELSE
```

```

      LTS = 3
END IF
WRITE(8,*) TS,FIRTS,JK,JNT,NRESIS,IX
WRITE(8,*) NPP1,TIMEN,RESIS,TEMPD
WRITE(8,*) (TIME(I),I=1,LTS),TVU,DEFO
WRITE(8,*) ((TA(I,J),I=2,3),J=1,NP)
IF(FIRTS .GT. 1) THEN
  WRITE(8,*) ((QE(I,J),J=1,2),I=1,NEL)
  WRITE(8,*) (QT(I),I=1,JNT)
END IF
RETURN
END

```

SUBROUTINE MAINOUT(TA,TSTAR,NTS,MN,NCOLT,NROWT)

```

C *****
C * THIS SUBROUTINE PRINT OUT TEMPERATURES FOR HEAT PIPE SHELL *
C * AND WICK *
C *****

```

```

COMMON/MATG/ AMC(140,151),RM(140),THETA(140),FLD(140),
&             AM(140,140),BM(140),CIJ(3,3),KIJ(3,3)
& /TEPS/ TEMPR,TEMPI,TMEL,DETP,DELTD,TEMPG1(140),THETAG(140),
&          THETAF(140),THETAO(140),THETTO(140),THETAB(70),TEMPD
& /PROC/ HRSL,ALPAR,DIST,BI,KREF,ROUR,SPECR,EMIS,HTC(140,3),
&          BOLT,VOLSPR,WIDTH,QE(140,3),NRESIS,RESIS,IX
& /ELMT/ NEL,NP,GND(140,3),B(140,3),C(140,3),EAREA(140),NPP1,
&          IES(140,2),ESL(140,3),BETA,XC(140,3),YC(140,3),DEFO,
&          NE(140),TLENG,PNOD(5,30),EBC(3,3),CM(3,3),GNDB(70)
& /INOUT/ TEMPS(70),TEMPV(70),TEMPVS(70),QEI(70),VX(70),
&          GNDI(70),VY1(70),VY2(70),VY3(70),ELSI(30),
&          VY4(70),VY5(70),VY6(70),HFG,TEMPF(70)
& /SPLIN/ TIME(3),TIMER(20),QSTAG(20),XP1(25),CP1(4,25),ND1,
&          XP2(60),CP2(4,60),ND2,XP3(25),CP3(4,25),ND3,TS,
&          XP4(25),CP4(4,25),ND4,XP5(15),CP5(4,15),ND5,XP6(15),
&          CP6(4,15),XP7(15),CP7(4,15),ND7,XP8(15),CP8(4,15),
&          ND6,ND8,XP9(15),CP9(4,15),ND9,XPO(15),CP0(4,15),ND0,
&          ELSS(30),TESL(30)
& /OUTPT/ MO,IDAY,IYEAR,TITLE,CASE,NUMBER,NO,TEMPCC,HTCC,IOUT,
&          TIMEN,DELT,DELT1,DELTP
INTEGER TS,PNOD,IT,IOUT
DIMENSION TA(3,96)

```

C.....PRINT BASIC DATA ON FILE JANG.....

```

IF(IOUT .EQ. 1) THEN
  WRITE(6,100) MO,IDAY,IYEAR
  WRITE(6,110) TITLE,CASE,NUMBER
  WRITE(6,120) NO
  WRITE(6,130) TLENG,DIST
  WRITE(6,140) WIDTH,ELSI(15)
  WRITE(6,150) TEMPI,TSTAR
  WRITE(6,160) TMEL,DETP,HRSL
  WRITE(6,170) TEMPCC,HTCC
  WRITE(6,180) TEMPR,EMIS

```

ORIGINAL PAGE IS
OF POOR QUALITY

```

WRITE(6,190) DELT,BETA,NTS,MN
WRITE(6,200) NEL,NP
WRITE(6,210)
WRITE(6,220)
WRITE(6,230)
WRITE(6,240)
WRITE(6,250)
IOUT = 2
END IF

```

C.....PRINT TEMPERATURE DISTRIBUTIONS.....

```

IF(TS .LT. 3) THEN
  IT = TS
ELSE
  IT = 3
END IF
WRITE(6,300) TIME(IT)
WRITE(6,310)
DO 400 I = 1,NROWT
  WRITE(6,320) (TA(IT,PNOI(I,J)),J=1,11)
400 CONTINUE
WRITE(6,330)
DO 420 I = 1,NROWT
  WRITE(6,320) (TA(IT,PNOI(I,J)),J=12,NCOLT)
420 CONTINUE

```

C.....PRINT TEMPERATURE DISTRIBUTIONS FOR PLOT.....

```

TMN = TIME(IT) - TIMEN
IF(TIME(IT) .EQ. TIMEN .OR. ABS(TMN) .LT. DELT/1000.) THEN
  WRITE(7,340) TIME(IT)
  WRITE(7,350) (TA(IT,J),J=1,NP)
  IF(TIMEN .EQ. DELT1) THEN
    TIMEN = DELTP
  ELSE
    TIMEN = TIMEN + DELTP
  END IF
END IF
100 FORMAT(///20X,37('*')/20X,'*',10X,'PROGRAM - HPMAIN',9X,'*/20X,
& '*',9X,'INPUT FILE - HPDAT',8X,'*/20X,'*',11X,'OUTPUT - JANG',
& 11X,'*/20X,'*',7X,'OUTPUT FOR PLOT - DATA',6X,'*/20X,'*',
& 8X,'FOR RESTART - RESTA',8X,'*/20X,
& '*',8X,'DATE : ',I3,'/',I3,'/',I5,7X,'*/20X,37('*')/)
110 FORMAT(/20X,37('-')//20X,'***',6X,3A9,'***//20X,37('-')/)
120 FORMAT(/24X,'** CASE NUMBER ',I6,' **//72('-')/)
130 FORMAT(3X,'TOTAL LENGTH OF HEAT PIPE(TLENG)',6X,E10.3,4X,'M'/
& 3X,'HEIGHT OF VAPOR SPACE(DIST)',11X,E10.3,4X,'M')
140 FORMAT(3X,'ELEMENT THICKNESS(WIDTH)',14X,E10.3,4X,'M'/
& 3X,'DISTANCE BETWEEN NODES(ELSI)',10X,E10.3,4X,'M'/)
150 FORMAT(3X,'INITIAL TEMP. (TEMPI)',18X,F10.3,4X,'K'/
& 3X,'TRANSIENT TEMP. OF VAPOR(TSTAR)',7X,F10.3,4X,'K')
160 FORMAT(3X,'PHASE CHANGE TEMP. (TMEL)',14X,F10.3,4X,'K'/
& 3X,'TEMP. DIFFERENCE FROM TMEL(DETP)',6X,F10.3,4X,'K'/
& 3X,'LATENT HEAT OF PHASE CHANGE(HRSL)',5X,E10.3,4X,'J/KG'/)

```



```
170 FORMAT(3X,'REF. TEMP. FOR CONVECTION(TEMPC)',6X,F10.3,4X,'K'/  
& 3X,'HEAT TRANSFER COEF.(HTC)',14X,F10.3,4X,'W/M**2*K')  
180 FORMAT(3X,'REF. TEMP. FOR RADIATION(TEMPR)',7X,F10.3,4X,'K'/  
& 3X,'EMISSIVITY',28X,F10.3,4X/)  
190 FORMAT(3X,'TIME STEP(DELT)',23X,F10.3,4X,'SECOND'/  
& 3X,'IMPLICIT TIME SCHEME(BETA)',12X,F10.3,4X/  
& 3X,'NUMBER OF STEP FOR IMPLICIT(NTS)',6X,I10,4X/  
& 3X,'TOTAL NUMBER OF TIME STEP(MN)',9X,I10,4X/)  
200 FORMAT(3X,'NUMBER OF ELEMENT(NEL)',16X,I10,4X/  
& 3X,'NUMBER OF NODAL POINT(NP)',13X,I10,4X)  
210 FORMAT(/3X,'INITIAL TIME',40X,'SECOND')  
220 FORMAT(3X,'FINAL TIME',42X,'SECOND')  
230 FORMAT(/3X,'SRU')  
240 FORMAT(3X,'CPU TIME',44X,'SECOND')  
250 FORMAT(3X,'EXPENSE',45X,'DOLLARS'//72('-')////)  
300 FORMAT(2X,83('-')/26X,'** TIME = ',2X,F9.3,2X,'SECONDS**'/)  
310 FORMAT(5X,'LEADING EDGE(EVAPORATOR)'/)  
320 FORMAT(1X,12F8.2)  
330 FORMAT(/55X,'TRAILING EDGE(CONDENSER)'/)  
340 FORMAT(F9.3)  
350 FORMAT(10(F8.2,1X))  
RETURN  
END
```

ORIGINAL PAGE IS
OF POOR QUALITY

APPENDIX C

SAMPLE INPUT DATA

Input data are needed for initial and boundary conditions, dimensions of the heat pipe, information on nodal points and elements, properties, and operating conditions of the program. Input file (HPDAT) has all these data. A grid generation program, which was written by Dr. J. G. Hartley, was used to generate data for the element grid. A sample for input data file HPDAT is listed in the following pages.

293.,371.,700.,1.,1.045E8,.0044,.0127

1.,10.,.025,100,2,10,1,1

0 6 138 96 0 1 6 2 0

1 2 3

2 2 5

3 2 18

4 3 18

5 3 5

6 3 3

| | | | | | | | | | |
|---|-----------|----|----|-----------|-----------|-----------------------------|-------|-------|-------|
| 1 | 90 | 86 | 87 | .0000 | .0000 | .0250 | .0000 | .0250 | .0020 |
| | .5000E+01 | | | .0000E+00 | .0000E+00 | 1 -1. 0. 2 -1. 0. 1 0. 2 0. | | | |
| 2 | 90 | 87 | 91 | .0000 | .0000 | .0250 | .0020 | .0000 | .0020 |
| | .5000E+01 | | | .0000E+00 | .0000E+00 | 1 -1. 0. 2 -1. 0. 1 0. 2 0. | | | |
| 3 | 86 | 82 | 83 | .0250 | .0000 | .0500 | .0000 | .0500 | .0020 |
| | .5000E+01 | | | .0000E+00 | .0000E+00 | 1 -1. 0. 2 -1. 0. 1 0. 2 0. | | | |
| 4 | 86 | 83 | 87 | .0250 | .0000 | .0500 | .0020 | .0250 | .0020 |
| | .5000E+01 | | | .0000E+00 | .0000E+00 | 1 -1. 0. 2 -1. 0. 1 0. 2 0. | | | |
| 5 | 82 | 78 | 79 | .0500 | .0000 | .0750 | .0000 | .0750 | .0020 |
| | .5000E+01 | | | .0000E+00 | .0000E+00 | 1 -1. 0. 2 -1. 0. 1 0. 2 0. | | | |
| 6 | 82 | 79 | 83 | .0500 | .0000 | .0750 | .0020 | .0500 | .0020 |
| | .5000E+01 | | | .0000E+00 | .0000E+00 | 1 -1. 0. 2 -1. 0. 1 0. 2 0. | | | |

.

.

.

.

.

.

.

.

| | | | | | | | | | |
|-----|-----------|----|----|-----------|-----------|-----------------------------|-------|-------|-------|
| 135 | 91 | 87 | 92 | .0000 | .0020 | .0250 | .0020 | .0250 | .0047 |
| | .4000E+01 | | | .0000E+00 | .0000E+00 | 1 -1. 0. 2 -1. 0. 1 0. 2 0. | | | |
| 136 | 91 | 92 | 94 | .0000 | .0020 | .0250 | .0047 | .0000 | .0047 |
| | .4000E+01 | | | .0000E+00 | .0000E+00 | 1 -1. 0. 2 -1. 0. 1 0. 2 0. | | | |
| 137 | 87 | 83 | 88 | .0250 | .0020 | .0500 | .0020 | .0500 | .0047 |
| | .4000E+01 | | | .0000E+00 | .0000E+00 | 1 -1. 0. 2 -1. 0. 1 0. 2 0. | | | |
| 138 | 87 | 88 | 92 | .0250 | .0020 | .0500 | .0047 | .0250 | .0047 |
| | .4000E+01 | | | .0000E+00 | .0000E+00 | 1 -1. 0. 2 -1. 0. 1 0. 2 0. | | | |
| -1 | -1 | -1 | -1 | -1 | -1 | 0. 0. 0. 0. 0. 0. | | | |

90 86 82 78 74 70

66 62 58 54 50 46

42 38 34 30 26 22

18 14 10 6 2 3

0 0 0 0 0 0

293. .8

SCALE FACTOR

| | | | | | | | |
|------|------|-----|------|----|------|-----|------|
| 21 | | | | | | | |
| .0 | 1. | .05 | .87 | .1 | .48 | .15 | .33 |
| .2 | .25 | .25 | .19 | .3 | .15 | .35 | .13 |
| .4 | .1 | .45 | .08 | .5 | .07 | .55 | .06 |
| .6 | .055 | .65 | .05 | .7 | .05 | .75 | .049 |
| .8 | .049 | .85 | .049 | .9 | .049 | .95 | .049 |
| 1. | .049 | | | | | | |
| -2.6 | 0.0 | | | | | | |

HEAT FLUX

| | | | | | | | |
|-------|--------|-------|--------|-------|--------|-------|--------|
| 19 | | | | | | | |
| 0.0 | 0. | 120. | 10.E3 | 240. | 30.E3 | 360. | 50.E3 |
| 450. | 75.E3 | 600. | 100.E3 | 720. | 120.E3 | 840. | 140.E3 |
| 1250. | 230.E3 | 1300. | 236.E3 | 1350. | 238.E3 | 1375. | 239.E3 |
| 1400. | 240.E3 | 1430. | 240.E3 | 1450. | 240.E3 | 1500. | 240.E3 |
| 1650. | 240.E3 | 1800. | 240.E3 | 2000. | 240.E3 | | |
| 0.0 | 0.0 | | | | | | |

APPENDIX D

THERMAL PROPERTIES OF SODIUM

The properties of sodium in the vapor state are expressed in terms of temperatures, which are in degree Kelvin in the following property equations:

Saturation vapor pressure[60] [N/m²]:

$$P = 2.29 \times 10^{11} \times \frac{1}{T^{0.5}} \times 10^{\frac{-5567}{T}}$$

Density of sodium vapor[60] [kg/m³]:

$$\rho = 6.335 \times 10^8 \times \frac{1}{T^{1.5}} \times 10^{\frac{-5567}{T}}$$

Viscosity of sodium vapor[61] [N-S/m²]:

$$\mu = 6.083 \times 10^{-9} \times T + 1.2606 \times 10^{-5}$$

Enthalpy of sodium vapor[60] [J/kg]:

$$h_f = 271,831. - 1,595.3 \times T - 0.29024 \times T^2 + 2.4 \times 10^6 \times \exp \frac{-13,600.}{T}$$

$$h_{fg} = 4,636,437.26 - 180.817 \times T$$

Thermal properties of sodium in the solid and liquid state[62,63] are tabulated as follows:

Density of solid sodium

| T[K] | ρ [kg/m ³] | T[K] | ρ [kg/m ³] |
|------|-----------------------------|------|-----------------------------|
| 273. | 972.5 | 283. | 970.5 |
| 293. | 968.4 | 303. | 966.3 |
| 313. | 964.2 | 323. | 962.1 |
| 333. | 959.9 | 343. | 957.7 |
| 353. | 955.5 | 363. | 953.2 |
| 371. | 951.4 | | |

Specific heat of solid sodium

| T[K] | c_p [J/kg-K] | T[K] | c_p [J/kg-K] |
|------|----------------|------|----------------|
| 273. | 1200. | 298. | 1223. |
| 323. | 1256. | 348. | 1308. |
| 371. | 1364. | | |

Conductivity of solid sodium

| T[K] | K[W/m-K] | T[K] | K[W/m-K] |
|------|----------|------|----------|
| 100. | 136. | 150. | 140. |
| 200. | 142. | 250. | 143. |
| 371. | 141. | | |

Density of liquid sodium

| T[K] | ρ [kg/m ³] | T[K] | ρ [kg/m ³] |
|------|-----------------------------|-------|-----------------------------|
| 373. | 927. | 473. | 904. |
| 573. | 882. | 673. | 859. |
| 773. | 834. | 873. | 809. |
| 973. | 783. | 1073. | 757. |

Specific heat of liquid sodium

| T[K] | c_p [J/kg-K] | T[K] | c_p [J/kg-K] |
|-------|----------------|-------|----------------|
| 371. | 1385. | 373. | 1384. |
| 473. | 1340. | 573. | 1305. |
| 673. | 1279. | 773. | 1262. |
| 873. | 1255. | 973. | 1255. |
| 1073. | 1269. | 1173. | 1289. |

Conductivity of liquid sodium

| T[K] | K[W/m-K] | T[K] | K[W/m-K] |
|-------|----------|------|----------|
| 473. | 81.5 | 573. | 75.7 |
| 673. | 71.0 | 773. | 67.2 |
| 873. | 63.9 | 973. | 61.0 |
| 1073. | 58.3 | | |

APPENDIX E

THERMAL PROPERTIES OF HASTELLOY X
AND STAINLESS STEEL

Thermal properties of hastelloy x[64] for heat pipe shell and type 316 stainless steel[64] for wick screen are tabulated as follow:

Conductivity of hastelloy x

| T[K] | K[W/m-K] |
|------|----------|
| 373. | 11.1 |
| 573. | 14.7 |
| 773. | 20.6 |
| 973. | 22.8 |

Specific heat of hastelloy x

| T[K] | c_p [J/kg-K] |
|-------|----------------|
| 588. | 498. |
| 923. | 582. |
| 1143. | 699. |

Conductivity of stainless steel

| T[K] | K[W/m-K] | T[K] | K[W/m-K] |
|--------|----------|-------|----------|
| 80.4 | 8.3 | 107.6 | 9.7 |
| 154.8 | 11.5 | 195.2 | 12.8 |
| 247.3 | 14.2 | 299.3 | 15.2 |
| 379.1 | 16.5 | 442.5 | 17.5 |
| 516.5 | 18.4 | 611.1 | 19.8 |
| 687.8 | 20.8 | 763.7 | 21.7 |
| 855.7 | 22.8 | 980.9 | 24.7 |
| 1182.1 | 26.9 | | |

Specific heat of stainless steel

| T[K] | c_p [J/kg-K] | T[K] | c_p [J/kg-K] |
|--------|----------------|--------|----------------|
| 71.8 | 286.5 | 114.0 | 329.7 |
| 162.9 | 367.0 | 197.9 | 392.3 |
| 270.0 | 433.4 | 337.3 | 465.0 |
| 435.1 | 500.7 | 587.6 | 540.7 |
| 736.5 | 561.8 | 967.7 | 604.5 |
| 1231.1 | 648.2 | 1468.5 | 690.2 |

REFERENCES

1. R. S. Gaugler, "Heat Transfer Device," *US Patent 2350348*, Dec. 1942.
2. G. M. Grover, "Evaporation - Condensation Heat Transfer Device," *US Patent 3229759*, Dec. 1963.
3. W. S. Chang, "Heat Pipe Startup from the Supercritical State," *Ph. D. Dissertation*, Georgia Institute of Technology, March 1981.
4. G. T. Colwell and W. S. Chang, "Measurement of the Transient Behavior of a Capillary Structure Under Heavy Thermal Loading," *Int. J. Heat Mass Transfer*, Vol. 27, No. 4, 1984, PP. 541 - 551.
5. W. S. Chang and G. T. Colwell, "Mathematical Modeling of the Transient Operating Characteristics of Low-Temperature Heat Pipe," *Numerical Heat Transfer*, Vol. 8, 1985, PP. 169 - 186.
6. P. Dunn, and D. A. Reay, *Heat Pipes*, 3rd edition, Pergamon Press, 1982, PP. 45 - 48.
7. G. M. Grover, T. P. Cotter, and G. F. Erickson, "Structures of Very High Thermal Conductance," *J. Appl. Phys.*, Vol. 35, PP. 1990 - 1991, 1964.
8. J. E. Deverall and J. K. Kemme, "High Thermal Conductance Devices Utilizing the Boiling of Lithium or Silver," *LA - 3211*, April 1965.
9. J. E. Deverall and J. E. Kemme, "Satellite Heat Pipe," *LA - 3278 -MS*, April 1965.
10. T. P. Cotter, "Theory of Heat Pipes," *LA - 3246 - MS*, Feb. 1965.
11. M. N. Ivanovskii, V. P. Sorokin, and I. V. Yagodkin, *The Physical Principles of Heat Pipes*, Clarendon Press, Oxford, 1982.
12. S. W. Chi, *Heat Pipe Theory and Practice*, McGraw - Hill Book Co., 1976, PP. 79 - 89.
13. C. A. Busse, "Pressure Drop in the Vapor Phase of Long Heat Pipes," *Proceedings of the 1967 Thermionic Conversion Specialist Conference*, 1967, PP. 391 - 398.
14. E. K. Levy, "Effect of Friction on the Sonic Velocity Limit in Sodium Heat Pipes," *AIAA Paper No. 71 - 407*, 1971.
15. E. K. Levy, "Theoretical Investigation of Heat Pipes," *Proc. Aviation and Space Conference*, Beverly Hills, Calif., 1968, PP. 671 - 676.

16. Y. M. Brovalsky, P. I. Bystrov, and M. V. Melkinov, "The Method of Calculation and Investigation of High-Temperature Heat Pipe Characteristics Taking into Account the Vapor Flow Compressibility, Friction, and Velocity Profile," *2nd International Heat Pipe Conf.*, 1976, PP. 113 - 122.
17. C. A. Bankston and H. J. Smith, "Incompressible Laminar Vapor Flow in Cylindrical Heat Pipes," *ASME Paper No. 71 - WA/HT - 15*, 1972.
18. C. L. Tien and A. R. Rohani, "Analysis of the Effects of Vapor Pressure Drop on Heat Pipe Performance," *Int. J. Heat Mass Transfer*, Vol. 17, 1974, PP. 61 - 67.
19. H. V. Ooijen and C. J. Hoogendoorn, "Vapor Flow Calculations in a Flat-Plate Heat Pipe," *AIAA J.*, Vol. 17, No. 11, Nov. 1979, PP. 1251 - 1259.
20. K. A. R. Ismail and N. Murcia, "Combined Liquid Vapor Flow in Cylindrical Heat Pipes with Modified Internal Geometry," *Advances in Heat pipe Technology*, Pergamon Press, Oxford, 1982, PP. 349 - 358.
21. D. W. Demichele, "A Numerical Solution to Axial Symmetric Compressible Flow with Mass Injection and Its Application to Heat Pipes," *Ph.D. Thesis*, Univ. of Arizona, June, 1970.
22. W. J. Bowman, "Simulated Heat Pipe Vapor Dynamics," *Ph. D. Dissertation*, Air Force Institute of Technology, May 1987.
23. K. H. Sun and C. L. Tien, "Simple Conduction Model for Theoretical Steady-State Heat Pipe Performance," *AIAA Journal*, Vol. 10, No. 8, August 1972, PP. 363 - 380.
24. K. H. Sun and C. L. Tien, "Thermal Performance Characteristics of Heat Pipes," *Int. J. Heat Mass Transfer*, Vol 18., 1975, PP. 363 - 380.
25. M. Kuramae, "Transient Heat Transfer Characteristics of Heat Pipes," *6th International Heat Pipe Conf.*, Grenoble, France, May 1987, PP. 29 - 35.
26. T. P. Cotter, "Heat Pipe Startup Dynamics," *Proc. IEEE Thermionic Conversion Specialist Conference*, Palo Alto, Calif, Oct. 1967, PP. 344 - 348.
27. L. G. Neal, "An Analytical and Experimental Study of Heat Pipes," *TRW Systems Rept. No. 99900 - 6114 - R000*, Jan. 1967.
28. A. P. Shlosinger, "Heat Pipe Devices for Space Suit Temperature Control," *TRW Systems Rept. No. 06462 - 6005 - R000*, Nov. 1968.
29. J. E. Deverall, J. E. Kemme, and L. W. Florschuetz, "Sonic Limitations and Startup Problems of Heat Pipes," *LA - 4518*, 1970.

30. C. J. Camarda, "Analysis and Radiant Heating Tests of a Heat-Pipe-Cooled Leading Edge," *NASA TN - 8486*, Aug. 1977.
31. C. C. Silverstein, "A Feasibility Study of Heat-Pipe-Cooled Leading Edges for Hypersonic Cruise Aircraft," *NASA CR - 1857*, Nov. 1971.
32. M. A. Merrigan, E. S. Keddy, and J. T. Sena, "Transient Heat Pipe Investigations for Space Power Systems," *LA - UR - 85 - 3341*, 1985.
33. E. R. G. Eckert and R. M. Drake, *Analysis of Heat and Mass Transfer*, McGraw - Hill Book Co., New York, 1972, PP. 470 - 471.
34. N. Hattori, "Emissivity of Liquid Sodium," *Heat Transfer Japanese Research*, Vol. 13, No. 1, 1984, PP. 30 - 40.
35. S. P. Sukhatme and W. M. Rohsenow, "Heat Transfer During Film Condensation of a Liquid Metal Vapor," *J. of Heat Transfer*, Feb. 1966, PP. 19 - 28.
36. J. G. Collier, *Convective Boiling and Condensation*, McGraw - Hill Book Co., New York, 1981.
37. J. E. Kemme, "Ultimate Heat-Pipe Performance," *IEEE Trans. Electron Devices*, Vol. ED - 16, No. 8, Aug. 1969, PP. 717 - 723.
38. M. N. Ozisik, *Heat Conduction*, John Wiley and Sons, 1980, PP. 410 - 415.
39. O. C. Zienkiewicz and Y. K. Cheung, "Finite Elements in the Solution of Field Problems," *The Engineer*, Vol. 220, 1965, PP. 507 - 510.
40. T. Dupont, G. Fairweather, and J. Johnson, "Three-Level Galerkin Methods for Parabolic Equations," *SIAM J. Num. Analysis*, Vol. 11, 1974, PP. 392 - 410.
41. M. Lees, "A Linear Three-Level Difference Scheme for Quasilinear Parabolic Equations," *Maths. Comp.*, Vol. 20, 1966, PP. 516 - 522.
42. G. Comini, S. Del-Guidice, R. W. Lewis, and O. C. Zienkiewicz, "Finite Element Solution of Non-Linear Heat Conduction Problems with Special Reference to Phase Change," *Int. J. Num. Method Engng.*, Vol. 8, 1974, PP. 613 - 624.
43. G. Comini and R. W. Lewis, "A Numerical Solution of Two-dimensional Problems Involving Heat and Mass Transfer," *Int. J. Heat Mass Trans.*, Vol. 19, 1976, PP. 1387 - 1392.
44. G. Comini and S. Del-Giudice, "Thermal Aspects of Cryosurgery," *J. Heat Trans.*, Vol. 98, 1976, PP. 543 - 549.

45. P. E. Frivik, E. Thorbergsen, S. Del-Giudice, and G. Comini, "Thermal Design of Pavement Structures in Seasonal Frost Areas," *J. Heat Trans.*, Vol. 99, 1977, PP. 533 - 540.
46. P. E. Frivik and G. Comini. "Seepage and Heat Flow in Soil Freezing," *J. Heat Trans.*, Vol. 104, 1982, PP. 323 - 328.
47. K. Morgan, R. W. Lewis, and O. C. Zienkiewicz, "An Improved Algorithm for Heat Conduction Problems with Phase Change," *Int. J. Num. Method Engng.*, Vol. 12, 1978, PP. 1191 - 1195.
48. M. A. Hogge, "A Comparison of Two- and Three-Level Integration Schemes for Non-Linear Heat Conduction," *Num. Meth. Heat Trans.*, R. W. Lewis et al. eds., John Wiley and Sons, 1981, PP. 75 - 90.
49. B. G. Thomas, I. V. Samarasekera, and J. K. Brimacombe, "Comparison of Numerical Modeling Techniques for Complex, Two-Dimensional, Transient Heat Conduction Problems," *Metallurgical Transaction B*, Vol. 15b, No. 2, 1984, PP. 307 - 318.
50. N. Shamsundar and E. M. Sparrow, "Analysis of Multidimensional Conduction Phase Change Via the Enthalpy Model," *J. Heat Transfer*, August 1975, PP. 333 - 340.
51. S. Del-Giudice, G. Comini, and R. Lewis, "Finite Element Simulation of Freezing Processes in Solid," *Int. J. Numerical and Analytical Methods Geomechanics*, Vol. 2, 1978, PP. 223 - 235.
52. C. L. Tien, "Fluid Mechanics of Heat Pipes," *Annual Review of Fluid Mechanics*, Vol. 7, 1975, PP. 167 - 185.
53. P. L. Donoughe, "Analysis of Laminar Incompressible Flow in Semiporous Channels," *NACA TN - 3759*, August 1956.
54. E. R. G. Eckert, P. L. Donoughe, and B. J. Moore, "Velocity and Friction Characteristics of Laminar Viscous Boundary-Layer and Channel Flow over Surfaces with Ejection or Suction," *NACA TN - 4102*, Dec. 1957.
55. K. H. Huebner and E. A. Thornton, *The Finite Element Method for Engineers*, John Wiley and Sons, New York, 1977.
56. M. L. James, G. M. Smith, and J. C. Wolford, *Applied Numerical Methods for Digital Computation*, Harper and Row Publisher, New York, 1977.
57. A. V. Luikov, *Analytical Heat Diffusion Theory*, Academic press, 1968.
58. A. H. Sheikh and E. M. Sparrow, "The Solution of Heat Conduction Problems by Probability Methods," *J. Heat Transfer*, Vol. 89, 1967, PP. 121 - 131.

59. K. A. Rathjen and L. M. Jiji, "Heat Conduction with Melting or Freezing in a Corner," *J. Heat Transfer*, Feb. 1971, PP. 101 - 109.
60. G. H. Golden and J. V. Tokar, *Thermophysical Properties of Sodium*, Argonne National Laboratory, August, 1967.
61. M. Makansi, W. A. Selke, and C. F. Bonilla, "Thermodynamic Properties of Sodium," *J. Chemical and Engineering Data*, Vol. 5, No. 1, January 1960, PP. 441 - 452.
62. Atomic Energy Commission, *Liquid - Metals Handbooks*, June 1955.
63. W. M. Rohsenow, J. P. Hartnett, and E. N. Ganic, ed. *Handbook of Heat Transfer Fundamentals*, 2nd edition, McGraw-Hill Book Co., 1986.
64. American Society for Metals, *Metals Handbook*, 9th Ed., Vol. 3.
65. J.H. Jang, "An Analysis of Startup from the Frozen State and Transient Performance of Heat Pipes," Ph.D. Dissertation, Georgia Institute of Technology, March 1988.